

NASA Contractor Report NAS3-26664

Modeling of Thermal Barrier  
Coatings

**Final Report**

B.L. Ferguson, G.J. Petrus, and T.M. Krauss  
Deformation Control Technology, Inc.  
Cleveland, OH 44130

November 12, 1992

Prepared for  
Lewis Research Center  
Under Contract NAS3-26664

## FOREWORD

This Final Report covers activities performed under NASA Contract NAS3-26664, "Modeling of Thermal Barrier Coatings". The objective of this work was to examine the effects of interface geometry and material properties on the thermo-mechanical response of a thermal barrier coating system to a typical burner rig thermal cycle using the finite element method. The study was conducted by Mr. T.M. Krauss, Mr. G.J. Petrus and Dr. B.L. Ferguson of Deformation Control Technology, Inc. Dr. Ferguson was the Principal Investigator.

Special thanks are due to Dr. A. Freed and Dr. W. Brindley of NASA Lewis Research Center for their valued input during technical discussions and their sharing of relevant data and information concerning the complex subject of thermal barrier coatings.

# TABLE OF CONTENTS

<u>Section</u>	<u>Page</u>
1.0 SUMMARY . . . . .	1
2.0 INTRODUCTION . . . . .	2
3.0 FINITE ELEMENT MODEL DEVELOPMENT . . . . .	4
3.1 Model Geometry . . . . .	4
3.2 Model Boundary Conditions. . . . .	4
3.3 Steady State Creep Model . . . . .	5
3.4 Material Property Data . . . . .	7
4.0 FEA RESULTS . . . . .	10
4.1 SINE_1 Interface Geometry. . . . .	10
4.1.1 Bond Coat Creep, Elastic TBC and Core . . . . .	10
4.1.2 High CTE in Bond Coat, Elastic TBC and Core. . . . .	12
4.1.3 Baseline Creep. . . . .	14
4.1.4 Baseline Creep, High CTE in Bond Coat . . . . .	15
4.1.5 Higher Creep Coefficient in Bond Coat . . . . .	17
4.1.6 Lower Creep Exponent in Ceramic . . . . .	18
4.2 SINE_2 Interface Geometry: 1.5X Amplitude. . . . .	18
4.2.1 Baseline Creep. . . . .	18
4.3 SINE_3 Interface Geometry: Twice Frequency . . . . .	20
4.3.1 Baseline Creep. . . . .	20
4.3.2 Baseline Creep, High CTE in Bond Coat . . . . .	21
4.4 Smooth Interface Geometry. . . . .	22
4.4.1 Baseline Creep. . . . .	22
5.0 DISCUSSION. . . . .	23
5.1 Thermal-Elastic Behavior vs. Baseline Creep in TBC. . . . .	23
5.2 Effect of Bond Coat CTE . . . . .	24
5.3 Effect of Bond Coat Creep Resistance. . . . .	27
5.4 Effect of Interface Geometry. . . . .	27
6.0 CONCLUSIONS . . . . .	30
REFERENCES . . . . .	32
APPENDICES . . . . .	86
A Creep Models Implemented in NIKE2D . . . . .	86
B ISLAND - Adaptive Solution Control for NIKE2D. . . . .	89
C Auxiliary FEA Model Results. . . . .	90

## LIST OF ILLUSTRATIONS

<u>Figure</u>	<u>Title</u>	<u>Page</u>
3.1.1.	Schematic of Models.....	34
3.2.1.	Schematic of Basic Model with Dimensions.....	35
3.2.2.	Temperature - Time Curve for Burner Rig Test.....	36
4.1.	Nodes and Elements Referenced in Figures.....	37
4.1.1.	SINE_1 Interface, Axial Stress (350 sec).....	38
4.1.2.	SINE_1 Interface, Axial Strain (350 sec).....	39
4.1.3.	SINE_1 Interface, Axial Stress (600 sec).....	40
4.1.4.	SINE_1 Interface, Axial Strain (600 sec).....	41
4.1.5.	SINE_1 Interface, Time History Axial Stress.....	42
4.1.6.	SINE_1 Interface, Time History Axial Strain.....	43
4.1.7.	SINE_1 Interface, Time History Radial Stress.....	44
4.1.8.	SINE_1 Interface, Time History Radial Strain.....	45
4.1.9.	SINE_1 Interface, Time History Axial Stress.....	46
4.1.10.	SINE_1 Interface, Time History Axial Strain.....	47
4.1.11.	SINE_1 Interface, Time History Radial Stress.....	48
4.1.12.	SINE_1 Interface, Time History Radial Strain.....	49
4.1.13.	SINE_1 Interface, Time History Effective Stress....	50
4.1.14.	SINE_1 Interface, Time History Effective Strain....	51
4.1.15.	SINE_1 Interface, Time History Axial Stress.....	52
4.1.16.	SINE_1 Interface, Time History Axial Strain.....	53
4.1.17.	SINE_1 Interface, Time History Radial Stress.....	54
4.1.18.	SINE_1 Interface, Time History Radial Strain.....	55
4.1.19.	SINE_1 Interface, Time History Effective Stress....	56
4.1.20.	SINE_1 Interface, Time History Effective Strain....	57
4.1.21.	SINE_1 Interface, Time History Axial Stress.....	58
4.1.22.	SINE_1 Interface, Time History Axial Strain.....	59
4.1.23.	SINE_1 Interface, Time History Radial Stress.....	60
4.1.24.	SINE_1 Interface, Time History Radial Strain.....	61
4.1.25.	SINE_1 Interface, Time History Effective Stress....	62
4.1.26.	SINE_1 Interface, Time History Effective Strain....	63
4.1.27.	SINE_1 Interface, Time History Axial Stress.....	64
4.1.28.	SINE_1 Interface, Time History Axial Strain.....	65
4.1.29.	SINE_1 Interface, Time History Radial Stress.....	66
4.1.30.	SINE_1 Interface, Time History Radial Strain.....	67
4.1.31.	SINE_1 Interface, Time History Axial Stress.....	68
4.1.32.	SINE_1 Interface, Time History Axial Strain.....	69
4.1.33.	SINE_1 Interface, Time History Radial Stress.....	70
4.1.34.	SINE_1 Interface, Time History Radial Strain.....	71
4.2.1.	SINE_2 Interface, Axial Stress.....	72
4.2.2.	SINE_2 Interface, Axial Strain.....	73
4.2.3.	SINE_2 Interface, Time History Axial Stress.....	74
4.2.4.	SINE_2 Interface, Time History Axial Strain.....	75
4.2.5.	SINE_2 Interface, Time History Radial Stress.....	76
4.2.6.	SINE_2 Interface, Time History Radial Strain.....	77

LIST OF ILLUSTRATIONS (continued)

<u>Figure</u>	<u>Title</u>	<u>Page</u>
4.3.1.	SINE_3 Interface, Axial Stress.....	78
4.3.2.	SINE_3 Interface, Axial Strain.....	79
4.3.3.	SINE_3 Interface, Time History Axial Stress.....	80
4.3.4.	SINE_3 Interface, Time History Axial Strain.....	81
4.3.5.	SINE_3 Interface, Time History Axial Stress.....	82
4.3.6.	SINE_3 Interface, Time History Axial Strain.....	83
4.4.1.	Smooth Interface Model - Radial Stress History Plot	84
4.4.2.	Smooth Interface Model - Radial Strain History Plot	85

LIST OF TABLES

<u>Table</u>	<u>Title</u>	<u>Page</u>
3.3.1.	Candidate Values of Creep Coefficient & Exponent..	7
3.3.2.	Creep Properties for Ni-16%Cr-6%Al-0.3%Y.....	7
3.4.1.	Ceramic Material Properties.....	8
3.4.2.	Bond Coat Material Properties.....	8
3.4.3.	Superalloy Material Properties.....	9
5.1.	Comparison of Stress & Strain Behavior (1).....	24
5.2.	Comparison of Stress & Strain Behavior (2).....	26
5.3.	Interface Pressure.....	28

## 1.0 SUMMARY

This project examined the effectiveness of studying the creep behavior of a thermal barrier coating system through the use of a general purpose, large strain finite element program, NIKE2D. Constitutive models implemented in this code were applied to simulate thermal-elastic and creep behavior.

Four separate ceramic - bond coat interface geometries have been examined in combination with a variety of constitutive models and material properties. The reason for focusing attention on the ceramic - bond coat interface is that prior studies have shown that cracking occurs in the ceramic near interface features which act as stress concentration points. The model conditions examined include: i) two bond coat coefficient of thermal expansion curves; ii) the creep coefficient and creep exponent of the bond coat for steady state creep; iii) the interface geometry; and iv) the material model employed to represent the bond coat, ceramic, and superalloy base.

It is concluded that the stress and strain states of thermal barrier coating systems can be effectively modeled by the use of finite element programs such as NIKE2D, that the relative effects and interactions of constitutive model parameters can be used to investigate material behavior, and that computer modeling is a tool that can be used to augment physical experimentation.

More specifically, creep of bond coat materials during thermal cycling has a pronounced impact on stress and strain state of the ceramic top coat. For the burner rig cycle modeled, cool down seems to be a more aggravating portion of the burner rig cycle than heat up. This is most likely due to stress reduction mechanisms of microcracking and creep that are available during heat up but not during cool down. Increased roughness of the bond coat - ceramic interface is associated with increased stress concentration and higher potential for interface separation. The effect of bond coat CTE on TBC performance is in part dependent on fatigue strength of the bond coat. A higher CTE subjects the bond coat to a higher strain cycle during burner rig testing, and this strain cycle may induce fatigue in the bond coat. A higher bond coat creep strength should give better TBC performance. Model results showed that lower creep resistance caused more creep in the bond coat without decreasing the peak stress in the ceramic. Stress concentration sites identified by the models were at peaks in the interface, with highest stresses in the adjacent ceramic material. These locations match cracking locations identified by other experimenters.

## 2.0 INTRODUCTION

The application of a thermal barrier coating (TBC) provides a method for improving turbine efficiency by allowing the engine to operate at higher temperatures. By coating the surface of a turbine blade with a ceramic material having a low thermal conductivity, such as yttria stabilized zirconia, the maximum temperature in the blade can be maintained below a critical level as the combustion temperature is increased. However, three problems have hindered the use of this technology in commercial practice. First, thermal stresses due to the difference in the coefficients of thermal expansion of the blade and the coating may be large enough to crack and spall the brittle coating. Research has shown that the use of a compliant bond coat material increases coating life by reducing the effects of thermal expansion mismatch. Second, the effectiveness of the bond coat is dependent to a large measure on its corrosion resistance. The ceramic outer coating does not offer corrosion resistance to the bond coat material, and the growth of corrosion product at the bond coat - ceramic interface aids spalling of the ceramic to reduce the effectiveness of the TBC system. The third hindrance to the development and implementation of this technology has been the lack of design guidelines that relate TBC performance to bond coat and ceramic properties. The primary reasons for this is the difficulty associated with the physical experiments and the complexity of the interrelationships between thermal and mechanical properties and performance. This project focuses on this third area.

Typically, the bond coat is a high density layer 130 to 200  $\mu\text{m}$  (5 to 8 mils) in thickness applied by a plasma spray process. A porous ceramic top coat is then deposited over the bond coat, again by a plasma spray process, to complete the TBC system. The bond coat has been shown to improve TBC life by enhancing the adherence of the ceramic to the substrate and by protecting the substrate from oxidation. (Hillery88, DeMasi89) Bond coat thickness has also been shown to affect TBC life, with a minimum thickness needed for acceptable life. Bond coat materials with higher creep strength have been found to produce longer TBC life. (Hillery88) The achievement of enhanced life through use of a bond coat is dependent on the development of a tight yet compliant bond between the ceramic top coat and the bond layer. Since the actual bond between the ceramic and the bond coat is more mechanical than chemical in nature, the bond coat must provide mechanical locking sites (a rough surface). Because the ceramic top coat is weak in tension, the bond coat must minimize thermally induced stress in the ceramic top coat during cyclic heating and cooling.

The roughness of the bond coat - ceramic interface is a result of the plasma spray process variables and the starting powder size. The interface roughness provides sites for the needed mechanical bonding between the ceramic top coat and the bond layer; unfortunately, the roughness also provides a series of stress concentration sites which have been shown to promote ceramic failure. The roughness also affects the bond coat surface area available for oxidation, which in turn degrades TBC life. The nature of the interface is therefore one of the primary variables that affects TBC life.

Delamination and subsequent spalling of the ceramic top coat has been linked to the formation of cracks in the ceramic near high points or peaks in the bond coat. Information on the magnitude and concentration of stresses in the ceramic coat as a function of bond coat geometry, i.e. thickness and roughness, and material properties is clearly necessary to develop adequate lifetime prediction models and to improve the manufacture and processing of TBC systems. Chang and Phucharoen (Chang87) used the finite element method to analyze the influence of interface geometry on stress in the TBC system. Their analysis assumed elastic - plastic behavior and examined the influences of elastic modulus and CTE on thermal stress level for a sinusoidal interface geometry.

The principal objectives of this work were:

- to examine the effects of interface geometry and material properties on the thermo-mechanical response of a thermal barrier coating system to a typical burner rig thermal cycle using the finite element method;
- to develop some initial guidelines for design of thermal barrier coating systems; and
- to evaluate the use of computer-based experiments as a means of augmenting physical experiments.

To achieve these objectives, a series of two dimensional finite element models were developed to examine the effects of interface geometry, the CTE of the bond coat, and the creep strength of the bond coat on stress in the TBC system. The geometries and material properties used in these models are described in Section 3 of this report. The results are presented in Section 4 and discussed in Section 5. Section 6 contains conclusions for this study.

### 3.0 FINITE ELEMENT MODEL DEVELOPMENT

The finite element computer code used for this modeling study was a derivative of NIKE2D, a large deformation stress modeler. This computer program was developed originally at Lawrence Livermore National Laboratories and has been ported by DCT to operate on 80486 class PC's. A steady state creep model was used to examine the time dependent effects of the thermal cycle on stress and deformation in the TBC system.

#### 3.1 Model Geometry

A thin slice of a typical burner rig test bar was selected as the geometry to model. The bond coat and ceramic outer coat were applied to the outer surface of the bar. Since axisymmetry was assumed by this geometry, a single radial cross section was used to develop the finite element mesh. The basic radial dimensions for the various cross sections were:

- superalloy bar radius: 0.0127 m (0.5 in)
- average bond coat thickness: 130  $\mu\text{m}$  (5.1 mils)
- average ceramic coat thickness: 250  $\mu\text{m}$  (9.8 mils)

The coating thicknesses correspond to typical TBC system thicknesses.

The geometry of the bond coat - ceramic interface was modeled as a sinewave to simulate surface roughness along the axis of the test bar. A smooth or featureless interface was also modeled for comparison. Specific model interface geometries are shown in Figure 3.1.1. The baseline sinusoidal interface is designated by the term SINE\_1. SINE\_2 geometry used a wave amplitude 1.5 times that of SINE\_1 geometry, and SINE\_3 geometry has a wavelength 0.5 times that of SINE\_1 geometry. In simulating roughness, the effect of increasing the amplitude is to increase the surface roughness. The effect of decreasing the wavelength (increasing the frequency) is to reduce the roughness spacing. By keeping the wave amplitude in the SINE\_3 condition the same as the baseline SINE\_1 amplitude, the effect is to increase the stress concentration at the peak due to the smaller radius of curvature. For SINE\_2 geometry, the increase in amplitude over a constant period also increases the stress concentration at the wave peak. Using the radius of curvature at the wave peak as a measure of stress concentration, it is expected that SINE\_3 geometry has the highest stress concentration and SINE\_1 has the lowest.

#### 3.2 Model Boundary Conditions

As mentioned, axisymmetry was assumed. A general schematic

of this model is shown in Figure 3.2.1. Because the superalloy base material, the bond coat and the ceramic top coat have different CTE values, both radial and axial expansion and contraction occur with heating and cooling. The bottom surface of the model shown in Figure 3.2.1 is fixed axially and allowed to move radially. The top surface in Figure 3.2.1 is assigned nodal constraints so that it can move both radially and axially. However, the nodal constraint balances the allowed axial movement across the three different materials. The result is that the top surface remains planar as it expands and contracts.

The thermal profile of Figure 3.2.2 was imposed uniformly on the entire body for each of the models in this study. This profile closely follows that in (DeMasi89) and (Hillery88).

### 3.3 Steady State Creep Model

A power law creep model resident in the NIKE2D code was used. The basic relationship in this creep model is summarized by equation (1):

$$\dot{\epsilon} \text{ creep rate} = A \cdot (\sigma_{\text{effective}})^B \quad \text{eq. (1)}$$

where A is the creep coefficient, and  
B is the power law creep exponent.

As implemented, A and B are functions of temperature. This model has been implemented into the NIKE2D code and is discussed in more detail in Krieg77.

In comparing the simplified creep model presented in Eq.(1) to a more complex phenomenological model proposed by Frost and Ashby (Frost82) for power law creep at high temperatures (above  $0.5 \cdot T_{\text{melting}}$ ), the creep coefficient A is of the form:

$$A \propto (D_v \cdot G \cdot b) / (R \cdot T) \quad \text{eq. (2)}$$

where  $D_v$  is the bulk or lattice diffusion coefficient,  
G is the shear modulus of the material,  
b is the magnitude of the Burger's vector,  
R is the universal gas constant, and  
T is the absolute temperature.

Since

$$D_v = D_o \cdot \exp[-Q_v / (R \cdot T)]$$

the coefficient A incorporates the activation energy for diffusion, which is directly related to the activation energy for creep.

Freed, et al. (Freed92) determined that a phenomenological

model of creep rate having the form shown in Eq.(3) gave good agreement with experimental data for copper and a LiF-22%Ca<sub>2</sub>F salt. Here,

$$\dot{\epsilon}_{\text{creep rate}} = C \cdot \theta \cdot \sinh^n(\sigma/\sigma_b) \quad \text{eq. (3)}$$

where C is the creep coefficient,  
 $\sigma_b$  is the stress at power law breakdown,  
 n is the power law creep exponent (B in Eq.(1)), and

$$\theta = \begin{cases} \exp[-Q_c/(R \cdot T)] & \text{for } T_t \leq T \leq T_{\text{melting}} \\ \exp[-Q_c/(R \cdot T_t) \cdot (\ln(T_t/T) + 1)] & \text{for } 0 \leq T \leq T_t \end{cases}$$

and

$$T_t = 0.5 \cdot T_{\text{melting}}$$

For stresses below the power law breakdown stress,  $\sigma_b$ , Eq.(3) reduces to the form of Eq. (1). From the  $\theta$  term in Eq.(3), it is apparent that the related creep coefficient term A in Eq.(1) will decrease linearly as temperature decreases below the transition temperature,  $T_t$ . For temperatures above  $T_t$ ,  $\theta$  is constant, meaning that the creep coefficient A in Eq.(1) becomes relatively insensitive to temperature.

The power law exponent, B, is a measure of the strain rate sensitivity of the material. High numerical values for B indicate low rate sensitivity, and since most materials exhibit low rate sensitivity at low temperatures, it is expected that low temperature values of B would be large. For example, experimental data for superalloy materials at temperatures below  $T_t$  have B values of 25 to 50. At temperatures where power law creep is active, the B values are typically in the range 3 to 6, depending on the active deformation mechanism.

Impacting the selection of A and B values are considerations of computer calculations and model implementation. These are not trivial considerations. For example, if the real creep rate of a material is  $2.0e-6/s$ , any A and B values that satisfy Eq.(1) may seem to be satisfactory property selections. Table 3.3.1 contains some candidate pairs of A and B values, and these pairs show the possible large variation in numerical values for the creep coefficient A and the creep exponent B. Stress relaxation curves were used to determine some representative A and B values over a range of temperatures for Ni-16%Cr-6%Al-0.3%Y bond coat material; the data are reported in Table 3.3.2. (Brindley92) Clearly, the creep coefficient A is nearly zero at room temperature and the creep exponent B is a large number. As temperature is raised, A increases to values of about  $1e-14$ .

Table 3.3.1.  
Candidate Values of Creep Coefficient and Creep Exponent  
to Produce a Creep Rate of  $2.0e-6/s$

<u>Effective Stress, MPa</u>	<u>A</u>	<u>B</u>
100	1.0e-99	46.65
100	1.0e-50	22.15
100	1.0e-10	2.15
300	1.0e-99	37.67
300	1.0e-50	17.88
300	1.0e-10	1.74

Table 3.3.2.\*  
Creep Properties for Ni-16Cr-6Al-0.3Y

<u>Temperature, °C</u>	<u>ln( A )</u>	<u>B</u>
22	-349	48
500	-595	83
700 ( $\sigma < 900$ MPa)	-55.7	7.4
700 ( $\sigma > 900$ MPa)	-23.7	2.5
800 ( $\sigma < 90$ MPa)	-24.7	3.6
800 ( $\sigma > 90$ MPa)	-19.0	2.3
900 ( $\sigma < 60$ MPa)	-21.4	3.7
900 ( $\sigma > 60$ MPa)	-15.5	2.1
1000 ( $\sigma > 10$ MPa)	-14.0	2.3

\* derived from curves reported in Brindley92.

Correspondingly, B decreases to values of 2 to 3.

The actual values used as model data for parameters A and B of Eq.(1) are presented in the following section.

### 3.4 Material Property Data

The ceramic top coat material modeled in this study was yttria stabilized zirconia,  $ZrO_2 - 8\%Y_2O_3$ . The properties employed are listed in Table 3.4.1.

The bond coat properties are listed in Table 3.4.2. These properties are similar to properties for Ni-16%Cr-6%Al-0.3%Y and Ni-35%Cr-6%Al-0.95%Y bond coat materials. The cases examined the effects of a slightly less creep resistant material (slightly higher A value) and different bond coat CTE on TBC stress and

Table 3.4.1.  
Material Property Data for Ceramic Material in Models

Temperature	10°C	500°C	600°C	760°C	1150°C	1250°C
Poisson's ratio	0.15	0.3	0.31	0.32	0.3	0.3
E, MPa	48000	32000	29500	26000	20000	17000
G, MPa	20870	11830	10605	9775	7650	6500
K, MPa	22855	27195	25928	25490	16700	13500
CTE, /°C						
A	0.76E-5	0.98E-5	1.02E-5	1.09E-5	1.23E-5	1.27e-5
B	1.0e-40	1.0e-37	1.0e-34	1.0e-28	1.0e-13	1.0e-12
c, J/kg·°C	16.0	15.5	15.0	10.0	2.0	1.5
k, W/m·K	580					603
	0.635					0.665

Table 3.4.2.  
Material Property Data for Bond Coat Materials

Baseline Material Data

Temperature	10°C	500°C	600°C	760°C	1150°C	1250°C
G, MPa	80500	73000	71000	67200	50000	46700
K, MPa	149000	135000	130000	124000	100000	90600
CTE, /°C						
A	1.20E-5	1.44E-5	1.48E-5	1.55E-5	1.83e-5	1.93E-5
B	4.85e-36	1.0e-34	1.06e-31	3.65e-23	1.0e-9	1.0e-12
c, J/kg·°C	16.0	15.5	15.0	10.0	3.0	6.0
k, W/m·K	628.0					712.0
	17.40					34.50

Slightly Higher Creep Coefficient A

Temperature	10°C	500°C	600°C	760°C	1150°C	1250°C
G, MPa	80500	73000	71000	67200	50000	46700
K, MPa	149000	135000	130000	124000	100000	90600
CTE, /°C						
A	1.20E-5	1.44E-5	1.48E-5	1.55E-5	1.83e-5	1.93E-5
B	4.85e-36	1.0e-34	1.06e-31	3.65e-22	1.0e-8	1.0e-10
c, J/kg·°C	16.0	15.5	15.0	10.0	3.0	6.0
k, W/m·K	628.0					712.0
	17.40					34.50

Higher CTE in Bond Coat

Temperature	10°C	500°C	600°C	760°C	1150°C	1250°C
G, MPa	80500	73000	71000	67200	50000	46700
K, MPa	149000	135000	130000	124000	100000	90600
CTE, /°C						
A	1.15E-5	1.26E-5	1.31E-5	1.40E-5	2.00e-5	2.15E-5
B	4.85e-36	1.0e-34	1.06e-31	3.65e-23	1.0e-9	1.0e-12
c, J/kg·°C	16.0	15.5	15.0	10.0	3.0	6.0
k, W/m·K	628.0					712.0
	17.40					34.50

Table 3.4.3.  
Material Property Data for Superalloy Material in Models

Temperature	10°C	500°C	600°C	760°C	1150°C	1250°C
Poisson's ratio	0.3	0.3	0.3	0.3	0.3	0.3
E, MPa	208000	183000	178500	106000	110000	85000
G, MPa	80500	73000	71000	67200	50000	46700
K, MPa	149000	135000	130000	124000	100000	90600
CTE, /°C	1.20E-5	1.44E-5	1.48E-5	1.55E-5	1.83e-5	1.93E-5
A	4.85e-36	1.0e-34	1.06e-31	3.65e-24	5.0e-9	5.0e-12
B	16.0	15.5	15.0	10.0	3.0	6.0
c, J/kg·°C	628.0					6.0
k, W/m·K	17.40					712.0
						34.50

strain. The CTE's of the cases identified as "baseline" and "higher CTE" reflects the difference in CTE between Ni-16Cr-6Al-0.3Y and Ni-35Cr-6Al-0.9Y bond coat materials, respectively. The CTE of the latter material is lower at low temperatures, but higher at temperatures above 900°C than that of the Ni-16Cr-6Al-0.3Y material. The assignment of "higher" CTE for the Ni-35Cr-6Al-0.9Y material is therefore somewhat of a misnomer.

A superalloy base material was modeled in all the cases, using typical Ni-based superalloy properties listed in Table 3.4.3.

During model execution, the FEA program performs a linear interpolation to calculate properties at temperatures between those defined in the data tables. The data reflect the significance of 760°C as the approximate transition temperature above which rate dependency is more pronounced and creep is expected to be more active.

The data were assembled mainly from references (Hillery88) and (DeMasi89) and reflect modification after discussions with A.D. Freed and W.J. Brindley of Lewis Research Center. Additional modification of the creep coefficient and creep exponent values proved to be necessary in light of numerical considerations for the actual creep model implementation.

## 4.0 FEA RESULTS

The results of the finite element models are presented in this section. As with any analysis of this type, the amount of data generated is overwhelming, even when presented graphically. To minimize the length of this section, only a few of the many possible stress and strain figures are presented. Appendix C contains other graphical model results for review.

Figure 4.1 shows element and nodal locations used in the history plots. These positions are referred to as "peak" (elements 120 & 445 and node 130) and "valley" (elements 12 & 229 and node 13) locations at the bond coat - ceramic interface.

### 4.1 Sine\_1 Interface Geometry

The interface geometry in this model was SINE\_1 type, and the material properties were the baseline values in Table 3.4.1. Uniform heating and cooling was assumed, so no thermal gradients were present.

#### 4.1.1 Bond Coat Creep, Elastic TBC and Core

The material properties applied to this model were thermo-elastic for the ceramic and superalloy substrate and the baseline creep data for the bond coat.

Figure 4.1.1 shows a contour map of axial stress near the end of the high temperature hold period (350 sec). From the contour lines, it is clear that changes in stress occur around the interface area. The very tip of the bond coat peak in the ceramic is the point of highest axial stress, with a tensile value of 384 MPa. The stress drops off rapidly in the bond coat valleys to a level around 60 MPa. The bond coat is in moderate compression.

Figure 4.1.2 shows contours of axial strain at the same time. The maximum strain appears near the peak in the bond coat.

Contours of axial stress at the end of the thermal cycle are shown in Figure 4.1.3. The highest tensile stress of about 94 MPa is in the ceramic at the interface peak. The bond coat just opposite this location is in compression (-37 MPa). In the ceramic, the stress is strongly compressive in the valley, at a level of -169 MPa. Away from the interface, the ceramic is generally in zero to very slight tension.

Axial strain contours corresponding to the previous figure

indicate maximum positive strain in the bond coat at the interface peak, Figure 4.1.4. The adjacent ceramic shows a slight positive strain which rapidly decreases and becomes negative as the distance from the bond coat peak increases. The ceramic in the valley has the most negative axial strain, at a value of  $-0.004$ .

The axial stress history plot, Figure 4.1.5, shows that bond coat element 12 in the interface valley assumes a slightly compressive state throughout heat-up and hold. During cool down, the bond coat material becomes stressed in tension (100 MPa) and then relaxes to a final level of about 20 MPa. The peak bond coat element 120, after an initial tensile stress fluctuation, settles into a near zero axial stress state until the cool down, at which time it is driven into compression and finally levels out near  $-10$  MPa at cycle end. The ceramic near the valley, element 229, initially assumes a moderate level of tension, and then seems to stabilize around 55 to 60 MPa for the duration of the hold. Cool down forces element 229 into steadily increasing compression, leveling off at  $-148$  MPa by cycle end. The ceramic near the bond coat peak, element 445, exhibits the most dramatic swing in axial stress state, rising rapidly to 348 MPa in tension, holding fairly steady until cool down, and then dropping even more rapidly to a final tensile stress near 65 to 70 MPa.

Figure 4.1.6 shows the axial strain history plot. The elements on either side of the interface valley end up in a compressive axial strain state, while the elements around the interface peak are axially strained in tension. Because creep has occurred, the presence of tensile or compressive final strain does not necessarily indicate the presence of final tensile or compressive stress. Comparison of Figures 4.1.5 and 4.1.6 illustrate this point, where elements 12 and 229 have opposite stress directions and yet both have final compressive strains. It maybe more helpful to think of strain in terms of difference from original location as opposed to associating total local strain with local stress.

Radial stress and strain history plots appear in Figures 4.1.7 and 4.1.8, respectively. After an initial compressive spike and recovery, element 120 in the bond coat at the interface peak assumes a compressive radial stress of  $-20$  MPa. This level decreases slightly during the hold period. During cool down, this element is driven into radial tension, peaking at a value of 96 MPa, and relaxing slightly to about 93 MPa. The strain plot shows that element 120 ends the cycle with a moderate compressive strain of  $-0.002$ . The adjacent ceramic material, element 445, generally assumes a radial tensile stress during heat-up and hold, and the stress level continues to rise somewhat during hold. During cool down, element 445 is rapidly stressed

in radial tension, peaking at 107 MPa, before relaxing to the same level as element 120, about 93 MPa.

#### 4.1.2 High CTE in Bond Coat, Elastic TBC and Core

The material properties applied to this model were thermo-elastic for the TBC and superalloy substrate and the higher CTE creep model for the bond coat found in Tables 3.4.1, 3.4.2 and 3.4.3.

The axial stress history plot in Figure 4.1.9 shows that the axial stress state in valley element 12 of the bond coat changes from initial tension to compression during heat-up, and gradually becomes slightly tensile by the end of the hold. Cool down drives element 12 into axial compression of about -90 MPa, which relaxes to a final level of about -45 MPa. The ceramic near the valley, element 229, is also driven into initial tension that then relaxes somewhat more slowly than the bond coat to a steady tensile stress of approximately 40 MPa. The ceramic near the bond coat peak, element 445, exhibits the most dramatic swing in axial stress state as in the previous model, rising rapidly to near 360 MPa in tension during heating, holding fairly steady during the soak, and then dropping even more rapidly during cool down to a final tensile stress near 75 MPa.

In comparing Figure 4.1.9 with Figure 4.1.5 for the baseline CTE case, the axial stress in the ceramic elements 229 and 445 is similar in behavior, but the axial stress in the bond coat is far different. The thermal cycle for the baseline CTE ended with the valley bond coat element 12 being in mild tension of about 22 MPa and the peak being low compression of 10 MPa. For this CTE case, both the bond coat valley and peak areas are in axial compression of about -40 to -50 MPa.

Figure 4.1.10 shows the axial strain history plot. This model is similar to the previous model in that the valley region has been axially compressed during the cycle while the peak region has been axially stretched at the cycle end. The amount of stretching is slightly higher for this CTE case than the baseline CTE (see Figure 4.1.6), with the respective axial strains in element 120 being about 0.0327 and 0.0310 at the end of the hold period, and about 0.0026 and 0.0025 at the end of the cycle.

From the comparisons made for axial stress and strain in the preceding two paragraphs, it appears that creep of the bond coat was higher in this case than in the baseline CTE case.

Radial stress and strain history plots are found in Figures 4.1.11 and 4.1.12, respectively. During heat-up and hold, the

ceramic at both the interface peak and valley, elements 445 and 229, follow similar stress state paths, exhibiting tension in the 10-18 MPa range during the hold. However, the radial stress at the valley in the ceramic is decreasing while the stress at the peak location is rising during the hold. Upon cool down, these locations are stressed oppositely, with the ceramic in the peak region being in tension and the valley being in compression. On the other hand, the bond coat material in the peak, element 120, is under compression of about -35 MPa that relaxes during the hold to about -29 MPa. In general, the final radial stress pattern after cool down is similar to the previous case, with the peak being in radial tension and the valley being in radial compression. In the valley, the compressive stress in both the bond coat and ceramic appears to decay at a decreasing rate, rather than rapidly assuming some level and holding steady as in Figure 4.1.1.7. The material near the interface peak, elements 120 and 445, both are subjected to a rapid rise in tensile stress during the cool down, followed by a general lessening of tension as the cooling rate decreases. In this model, the difference in bond coat CTE has resulted in a wider difference in radial stress between the bond coat and ceramic than in the previous model.

A comparison of radial strain histories between this model, Figure 4.1.12, and the previous model with baseline CTE, Figure 4.1.8, shows that the radial strain in bond coat elements 12 and 120 covers a greater range in this model. For example, at the end of the hold period, the radial strains in element 12 for this model and the previous model are 0.0375 and 0.0244, respectively. The strain at the end of the thermal cycle is about the same in both models, 0.002. The strain range in this case is therefore more than 0.013 greater than the baseline case for this element.

Figure 4.1.13 is a history plot of effective stress, and the corresponding plot of effective strain is shown in Figure 4.1.14. The bond coat elements 12 and 120 both exhibit an initial sharp rise in stress, a sudden drop, and then a more gradual gain during the heating period of 120 seconds. During the hold period, 120 second to 360 seconds, there is a gradual decrease in effective stress. The effective stress in the ceramic is highest in the peak element 445, which has values similar to the axial stress levels reported above. The final effective strain in the bond coat peak element 120 of about 0.003 reflects the high stress in the neighboring ceramic element. It appears creep in the bond coat has been highest at the peak, and as a result of bond coat creep, the final stress and strain states are not zero, as an all elastic case would have been.

### 4.1.3 Baseline Creep

The results presented in this section are based on the SINE\_1 interface geometry and the baseline creep properties listed in Table 3.4.1. History plots for the peak and valley elements are described. Appendix C contains selected contour maps of stress and strain at the end of the soak period (350 seconds) and at the end of the thermal cycle (600 seconds).

Figure 4.1.15 shows the axial stress history. Initially, the ceramic elements 229 and 445 are stressed in axial tension, and a stress drop occurs after a value of 105 MPa has been reached. At the same time, the peak element in the bond coat, 120, experiences a stress drop at 20 MPa. Element 12 in the valley is initially stressed in compression and then tension. Once temperature has nearly maximized, after 120 seconds, both valley elements and the bond coat peak element 120 experience stress reduction. The axial stress in peak element 120 of the bond coat decreases to nearly zero, while the stress in the valley element 12 of the bond coat becomes compressive. Element 229 at the valley in the ceramic relaxes from a stress of 80 MPa to less than 50 MPa during the high temperature hold. The stress in 445 of the ceramic continues to increase throughout the heating portion of the thermal cycle, reaching a peak value of 149 MPa. Upon cooling, elements 229 and 445 in the ceramic are under axial compression. Element 12 in the bond coat is stressed in tension at 40 MPa, while element 120 is in axial compression of nearly 40 MPa.

The axial strain history in Figure 4.1.16 shows that the peak elements continue to elongate axially throughout the heating portion of the cycle. The valley elements are elongated axially during heating, but they contract slightly during the hold period. At the end of the thermal cycle, the valley elements are in compression, while the peak elements end in an axial tensile strain state.

Radial stress histories for the four peak and valley elements are given in Figure 4.1.17. As heating begins, valley elements 12 and 229 are stressed in tension. The same type of stress drop as described for axial stress at about 10 seconds is present. After 75 seconds, the stress in 12 and 229 has started a steady decline that lasts up to 360 seconds. The bond coat is undergoing stress relaxation in element 12, and the stress in the adjacent ceramic element 229 is also relaxing. In fact, element 12 drops from low radial tension into low compression; element 229 stays in radial tension. Upon cooling, these two elements are stressed radially in compression. Elements 120 and 445 at the peak of the interface behave somewhat differently. During the heating stage, they immediately go into radial compression.

At 10 seconds, a sharp change in stress state occurs, and they become nearly stress free. With continued heating, the bond coat element 120 is subjected to low radial tension that transitions into low radial compression, and element 445 is subjected to low radial compression. During the soak period, element 445 in the ceramic transitions from compression to radial tension. Element 120 remains in relatively low compression. After cooling, both elements are in radial tension, with ceramic at -58 MPa and the bond coat at -40 MPa.

Figure 4.1.18 shows radial strain history. Looking at elements at the interface peak, numbers 120 in the bond coat and 445 in the ceramic, one sees an opposite effect. Element 120 is strained in tension while element 445 is strained in compression. Notice that over the high temperature soak period, roughly 120 to 360 seconds, the level of radial strain decreases in element 120. Correspondingly, the level of compressive strain in element 445 decreases. After cooling, these elements are both strained compressively. The tensile strain in element 12 increases continually during the heating period, and then decreases during cooling. Element 12 is still in a radially elongated condition after cooling. The tensile strain in 229 increases, but at a much lower rate. After cooling, 229 is under compressive strain.

History plots of effective stress and strain for the peak and valley elements are shown in Figures 4.1.19 and 4.1.20. While, the shape of the effective stress and strain histories indicate the presence of creep, it is not directly clear from the figures exactly what is creeping. Examination of the numerical values provides some insight. For example, the stress peak at about 10 seconds is over 150 MPa in element 445 of the ceramic. Using the steady state creep properties, the effective creep rate is estimated to be  $9.0e-4/s$  for the ceramic. For the bond coat, the effective stress at the load drop is about 75 MPa. The creep rate is estimated to be  $2.0e-5/s$  in the bond coat. At effective stress levels pertinent to the soak period, e.g. 125 MPa in element 445 of the ceramic and 80 MPa for element 120 of the bond coat, the estimated creep rates are  $1.6e-9/s$  and  $5.0e-4/s$  respectively. From these estimates, it seems that the ceramic is responsible for the initial load drop; the values selected for the creep coefficient A and the creep exponent B at 10°C in Table 3.4.1 are not proper for the stress experienced in the ceramic during heating. This stress is purely due to CTE differences and the stress concentrating effect of the interface geometry.

#### 4.1.4 Baseline Creep, High CTE in Bond Coat

The history plot of axial stress for this model, Figure 4.1.21, shows that all of the interface elements begin to experience axial tension and then a sharp stress reduction.

During the heating cycle until cool down begins, element 445 in the ceramic returns to a high tensile stress and holds while element 120 in the bond coat becomes compressively stressed and then relaxes somewhat. Element 12 stays around 0 and element 229 is tensile and relaxes slightly. During rapid cooling all the elements drop into axial compression and element 12 returns to the lowest magnitude of compressive stress of -38 MPa. Element 120 also shows this reduction in compressive stress magnitude. The stresses in elements 229 and 445 in the ceramic meanwhile increase compressively until the end of the cooling cycle.

The axial strain plot, Figure 4.1.22, shows that all of the elements increase in length axially, and then reduce during cool down. The peak elements experience about twice the amount of strain as the valley elements. The peak elements retain about twice the amount of residual strain as the valley elements due to creep.

Figure 4.1.23, the radial stress plot, shows that the peak elements are compressed radially upon heating, then stress relax during the hold period, and are then stressed in tension during cooling. The bond coat material exhibits a higher magnitude of stress through the cycle than the ceramic. The valley elements are stressed radially in tension upon heating, stress relax during the hold period, and suffer radial compression during cool down. Element 120 in the bond coat retains the highest amount of radial compression (about 29 MPa), but this is much less than the axial compression reported above.

The plot of radial strain, Figure 4.1.24, shows that elements 12, 229, and 120 are stretched radially, with 12 having the highest radial strain, followed by 120. Element 445 is compressed radially upon heat up. On cooling, the bond coat elements 12 and 120 contract back to nearly 0 strain while the ceramic elements 229 and 445 show a radial shrink.

A plot of effective stress, Figure 4.1.25 shows that the larger stresses throughout the cycle are experienced in the ceramic material. The ceramic also retains much more residual stress at the end of the thermal cycle than the bond coat. The peak elements also show a larger stress than their valley counterparts of the same material.

A plot of effective strain, Figure 4.1.26, shows that peak element 445 in the ceramic has the highest amount of strain upon heating, followed by bond coat element 12 which has about half the amount of strain on heating. It is interesting that element 445 decreases in effective strain slightly during the hold period, while the other elements continue to increase in effective strain, albeit at a low rate. Elements 229 and 120

experience the lowest amount of strain during heating. Upon cooling, the ceramic elements show a higher residual strain than the bond coat elements which return nearly to zero.

#### 4.1.5 Higher Creep Coefficient in Bond Coat

In this model, the bond coat material has a higher creep coefficient at temperatures above 760°C than the baseline creep case. Again, the higher creep coefficient listed in Table 3.4.2 indicates lower creep strength.

Figure 4.1.27 shows axial stress as a function of time. Element 12 in the bond coat is held in axial compression throughout heat-up and hold, and then in tension during cool down. Element 229 in the ceramic, complimentary to 12, is tensile during heat-up and hold; it relaxes noticeably during the hold, and then is stressed sharply into compression during cool down. Element 120 is stressed in low tension during the initial heat-up, goes to zero during the hold, and then becomes moderately compressive during cool down. Element 445 is stressed strongly in tension to a level of 160 MPa upon initial heating and soaking, and then is compressively stressed to nearly -125 MPa during cool down.

Figure 4.1.28 shows axial strain as a function of time. The pair of peak elements, 120 and 445, are elongated during heating and contract during cooling; the final strain state for these elements is a slight positive extension. The pair of elements at the valley are also elongated axially during heating, as expected. However, upon cooling, these elements return to an axially compressed state.

Figure 4.1.29 shows the radial stress in selected elements as a function of time. The valley elements 12 and 229, after being initially stressed in radial tension, are in states of low radial compression at the end of the high temperature hold. Cool down drives both elements sharply into deeper compression, which relaxes as the cooling rate decreases. Element 229 is apparently able to reduce its tensile state during heat-up and hold due to bond coat creep at element 12. During heat-up and hold, element 120 in the bond coat follows a path similar to that of 229 in the ceramic, but is noticeably more compressive. During cool down, however, element 120 goes sharply tensile. Element 445 in the ceramic undergoes a sharp compressive spike and then is stressed in tension and remains so for the duration of the cycle, exhibiting a more tensile jump during cool down.

Figure 4.1.30 shows the radial strain history for these same four elements. Element 12 is radially strained in tension and

remains in a tensile strain state after cool down. Elements 229 and 120 are strained in tension during heating, and they transition to compressive strain upon cool down. Element 445 at the peak in the ceramic is compressed radially and remains in a compressive strain state after cool down.

#### 4.1.6 Lower B in the Ceramic

A plot of the axial stress in Figure 4.1.31 shows that the ceramic elements upon heating go into axial tension with 445 being about four times higher than valley element 229. Element 120 stays nearly 0 in axial stress during heating while element 12 goes into a small axial compression. On cooling, element 12 in the bond coat is subjected to tension of about 50 MPa while element 120 is stressed to about -40 MPa in compression. In the ceramic, elements 229 and 445 swing to a large axial compression of about -185 and -130 MPa, respectively.

A plot of axial strain in Figure 4.1.32 shows that the peak elements experience a large positive strain during heating and the valley elements experience about half of that strain value. On cooling the peak elements retain a moderate amount of positive axial strain while the valley elements contract to a small negative strain.

The radial stress plot in Figure 4.1.33 shows that the peak elements experience a much larger stress than the valley elements during heat up. Upon cool down, the stresses in the peak elements in both the ceramic and the bond coat are stressed radially in tension and the valley elements are stressed in compression; the values are nearly balanced.

A plot of the radial strain in Figure 4.1.34 shows that on heating element 12 in the bond coat experiences a large positive radial strain of 0.0239, and then contracts during cooling to a final strain of 0.0027. Elements 120 and 229 experience a small positive radial strain during heat up, and then contract to final negative strains of -0.0023 and -0.0041, respectively. Element 445 fluctuates at the beginning of the cycle, and after contracting radially ends up around 0 at the end of the hold. At the end of the thermal cycle, element 445 has been radially strained to -0.0054.

## 4.2 SINE\_2 Interface Geometry: 1.5X Amplitude

### 4.2.1 Baseline Creep

The interface geometry in this model was SINE\_2 type; this geometry has the same period as SINE\_1 but 1.5 times the

amplitude. The material properties applied were the baseline values in Table 3.4.1 and 3.4.2. As above, uniform heating and cooling was assumed, so no thermal gradients were present.

Figure 4.2.1 shows the axial stress contour at 350 seconds, near the end of the hold. The lowest axial stress is compressive (-23 MPa) and is located in the bond coat near the valley. The presence of this compressive stress is due to the CTE difference between the bond coat and ceramic. The bulk of the bond coat is at a near 0 MPa axial stress value. The ceramic, on the other hand, is highly stressed, with a maximum value of over 180 MPa right at the interface peak. The bulk of the ceramic is in high axial tension of over 100 MPa due to the higher CTE of the bond coat and the nodal constraint boundary condition which forces the ceramic to move with the massive superalloy body.

Figure 4.2.2 contains axial strain contours. All of the axial deformation at this time is tensile, with the maximum being in the bond coat at the interface peak.

Figure 4.2.3 shows the axial stress history for the peak and valley elements. Stress reduction is evident during the high temperature hold period in elements 12 and 120 of the bond coat, and in element 229 of the ceramic. As element 12 crept, the resultant stress in 229 was lowered. The stress in element 445 of the ceramic continued to increase throughout the heating cycle.

The axial strain history in Figure 4.2.4 shows that the peak elements continued to strain in tension throughout the heating portion of the cycle, while the valley elements strained in tension and then relaxed somewhat. At the end of the thermal cycle, the valley elements have been compressed axially, while the peak elements have been axially stretched.

Radial stress histories are given in Figure 4.2.5. As heating begins, valley elements 12 and 229 are stressed in tension. After 100 seconds, the stress in 12 and 229 has settled down. Element 12 drops from low compression to slightly lower compression; element 229 stays in slight radial tension. Upon cooling, these two elements are stressed radially in compression. Elements 120 and 445, the peak elements, behave somewhat differently. During the heating stage, they go into radial compression, and then during the soak time, element 445 transitions from compression to radial tension. Element 120 remains in relatively low compression. After cooling, both elements are in radial tension.

Figure 4.2.6 shows radial strain history. Looking at the peak elements, numbers 120 in the bond coat and 445 in the ceramic, one sees a mirror effect. Element 120 is strained in

tension while element 445 is strained in compression. This reflects the difference in CTE between the two materials. Notice that over the high temperature soak period, roughly 120 to 360 seconds, the level of radial strain decreases slightly in element 120. Correspondingly, the level of compressive strain in element 445 decreases. This suggests creep in the bond coat at the peak region during the high temperature hold. After cooling, these elements are both strained compressively. The behavior of the valley elements 12 and 229 also suggest creep. The tensile strain in 12 increases continually during the heating period, and then decreases during cooling. Element 12 is still under tensile radial strain after cooling. The tensile radial strain in element 229 also increases, but at a much lower rate. After cooling, element 229 is under compressive radial strain.

The results presented are similar to the SINE\_1 interface geometry model in Section 4.1.3. The effect of increasing the amplitude is to increase the spread in stress and the magnitude.

#### 4.3 SINE\_3 Interface Geometry: Twice Frequency

The following paragraphs report the results for models that incorporate an interface geometry with the same amplitude as the baseline SINE\_1 case, but twice the frequency. This geometry is designated as SINE\_3 geometry in Figure 3.1.1.

##### 4.3.1 **Baseline Creep**

Baseline creep properties listed in Tables 3.4.1, 3.4.2 and 3.4.3 were applied in this model. As Figure 4.3.1 shows, the interface geometry for this model is considerably 'sharper' due to the increased frequency and same amplitude as the SINE\_1 condition. This figure contains a contour plot of radial stress after the high temperature hold portion of the thermal cycle. Note that the maximum radial stress is located in the ceramic a small distance outward from the interface peak. The maximum value of 35 MPa for this time of 350 seconds is greater than the maximum radial stress values for SINE\_1 (19 MPa) and for SINE\_2 (31 MPa). This reflects the greater stress concentration due to the small radius of curvature of this interface. Away from the interface, the magnitude of radial stress drops to zero.

The corresponding contour map of radial strain is shown in Figure 4.3.2 for the same model time of 350 seconds. The strain at the interface peak is radially compressive in the ceramic and tensile in the bond coat.

Figure 4.3.3 contains the axial stress history for the peak and valley elements of the bond coat and the ceramic. After the load drop, now associated with low temperature behavior of the

ceramic, the valley elements reach a peak as soak time starts, and the axial stress decreases from this peak. For element 12, this means that axial compression is increasing. Element 120 in the bond coat follows similar behavior, in that a peak stress is reached and then the level of axial tension falls during soak. Element 445, the peak element in the ceramic, however, is subjected to increasing axial tension during the soak period, reaching a maximum value of 140 MPa. Upon cooling, this element is subjected to axial compression of 175 MPa. Element 229 in the ceramic is also placed under axial compression, as is element 120 of the bond coat. Element 12 in the bond coat is in axial tension. The decrease in stress during high temperature soaking, and the changes during cooling are indicative of relaxation due to creep.

The interesting features of the radial stress histories in Figure 4.3.4 are:

- the rise in radial tension in element 445 during the soak period;
- the final compressive radial stress states of elements 12 and 445 of about -15 MPa;
- the final radial compression of -70 MPa in element 229 of the ceramic and radial tension of 75 MPa in element 120 of the bond coat; and
- the decrease in radial stress during soaking and cooling.

These features indicate creep at work.

#### 4.3.2 Baseline Creep, High CTE in Bond Coat

Figure 4.3.5 shows the axial stress as a function of time for the model with different CTE behavior in the bond coat. First, all of the elements are stressed in tension initially during heating, and the low temperature load drop due to the ceramic behavior is shown. The axial stress in the peak element 445 of the ceramic is stressed in tension during the heating period, and finishes the hold at a stress of nearly 160 MPa. This element experiences a reversal of stress state to finish the cool down in axial compression. The other elements plotted in this figure show stress change during the hold period, with the valley element in the bond coat changing from low compression to low tension. Interestingly, all of the elements finish the thermal cycle in axial compression.

Figure 4.3.6 shows the radial stress in the selected elements as a function of time. Bond coat material near the valley, element 120, goes to a compressive state during the high temperature hold, and after final cool down in under radial

tension of 32 MPa. The other elements are mainly tensile during heating and soaking, with the slopes of the curves during the soak period indicating the presence of creep. At the end of the thermal cycle, the ceramic is under radial compression and the bond coat is under radial tension at both peak and valley locations.

#### 4.4 Smooth Interface Model

The purpose of the smooth interface model was to provide a contrast for interface geometry effects. This model assumed uniform heating and cooling and used the baseline material properties found in Tables 3.4.1, 3.4.2 and 3.4.3.

##### 4.4.1 Baseline Creep

Figure 4.4.1 shows a history plot of radial stress at the interface peak; these are elements 120 in the bond coat and 445 in the ceramic. During heating, these elements are in low radial compression of about -2 MPa. Upon cooling, radial tension is imposed, but again at a low level of 3 MPa. The corresponding radial strain history for these elements is shown in Figure 4.4.2. Element 120 in the bond coat undergoes a radial strain slightly in excess of 0.018 during heating and then contracts to its original position. Element 445 in the ceramic is radially strained to a value of 0.002 during heating, and then contracts to a final radial strain of -0.004.

The axial stress history for these same elements is shown in Figure 4.4.3. During heating, element 120 in the bond coat is axially stressed at a tension value of 20 MPa that then decreases down to 0 during the hold period. Then, during the cooling portion of the cycle, this element is placed in low axial compression, with the value increasing to nearly zero as cooling progresses. Element 445 in the ceramic, on the other hand, is subjected to high tensile stress as the bond coat tries to expand axially during heating more than the ceramic. Upon cooling, the ceramic interface element is placed into high axial compression of -141 MPa.

## 5.0 DISCUSSION

Because cracking of the thermal barrier coating has been associated with regions in the ceramic near aspartities in the bond coat, most of the points of discussion focus on the regions in the ceramic at the peak and valley locations. It is most encouraging to note that the points of high stress concentration identified in Section 4 coincide with cracking sites observed by experimenters with these materials.

### 5.1 Thermal-Elastic Behavior vs. Baseline Creep Behavior in TBC

Since the creep properties in the ceramic were educated guesses rather than extracted from actual experimental data, it is interesting to compare the effects of thermal-elastic behavior in the ceramic against ceramic defined with creep properties. To reiterate, normally ceramics are not considered to be materials that creep. However, yttria containing zirconia has been reported to undergo high temperature creep. (DeMasi89) Speculation on this behavior has to include microcracking as a source of compliance and relaxation of tensile stresses. From Section 4.1.3, the baseline modeling results did reveal low temperature creep in the ceramic, and this was attributed to the selection of the creep parameters.

A comparison of the bond coat - ceramic interface at 350 seconds and at the end of the thermal cycle shows a considerable difference in stress and strain between these models. Table 5.1 is compiled from history plots from Section 4.1.1 for the case of thermal-elastic behavior in the ceramic, and from Section 4.1.3 for the baseline creep behavior. The provision for compliance of the ceramic dropped the axial stress from 348 to 143 MPa in peak element 445. Upon cool down, this element was in tension for the elastic case, and axial compression for the compliant case.

From the data in Table 5.1, it is clear that compliance in the ceramic produces lower stresses throughout the thermal cycle. This compliance, modeled here as creep at low temperatures, may be considered a reflection of microcracking/sintering phenomena or microplasticity.

Table 5.1.  
Comparison of Stress and Strain Behavior

Cycle Time: 350 sec.					
Interface Geometry	TBC	element	radial stress MPa	axial stress MPa	axial strain
Sine_1	elastic	445	22	348	0.027
"	"	229	2	50	0.014
Sine_1	creep	445	10	143	0.029
"	"	229	4	55	0.017
Cycle Time: 600 sec.					
Interface Geometry	TBC	element	radial stress MPa	axial stress MPa	axial strain
Sine_1	elastic	445	95	65	0.001
"	"	229	-70	-148	-0.003
Sine_1	creep	445	40	-125	0.002
"	"	229	-57	-148	-0.002

## 5.2 Effect of Bond Coat CTE

The effect of bond coat CTE on stress and strain in the ceramic was examined by using CTE values for Ni-16Cr-6Al-0.3Y as baseline and Ni-35Cr-6Al-0.9Y as the "high" CTE material. As mentioned, the data in Table 3.4.2 show that the CTE curves cross. The Ni-35Cr-6Al-0.9Y alloy has lower CTE at temperatures up to 900°C, so it is only at the top of the thermal cycle temperature range that this alloy actually has a higher CTE. This means that at low temperatures, the CTE difference between the bond coat and ceramic is lower for the Ni-35Cr-6Al-0.9Y material than the baseline material. However, examination of axial stress histories for these two materials in Figures 4.1.5 and 4.1.9 shows little difference in stress rise in the ceramic during heating. At temperature, Table 5.2 shows that the high CTE bond coat material generates slightly higher axial stress than baseline material, but the difference is negligible.

No striking difference is apparent in the ceramic response reported in Table 5.2 for the two CTE curves. The main difference seems to be in the bond coat itself. Comparing Figures 4.1.1 and 4.1.9 for the case of thermal-elastic ceramic

behavior, the axial stress in the bond coat is compressive at both the peak and valley regions along the interface in the higher CTE case (4.1.9). As Figure 4.1.10 shows, the axial strain at the end of the thermal cycle is compressive as well for the bond coat. The extra creep caused by the higher thermal stress during heating is responsible for the higher compression in the bond coat. As mentioned in Section 4.1.2, the total strain cycle for the bond coat is greater for the case of high CTE at high temperature.

For the case of a compliant ceramic, Table 5.2 again shows little difference in the ceramic due to bond coat CTE differences. After the thermal soak, the axial stresses in the ceramic are similar for the two bond coat materials. The change in sign for the radial stress from tensile for the baseline condition to compressive for the "high" CTE condition is due to greater bond coat creep. The plots of effective strain in Figure 4.1.20 for the baseline case, and Figure 4.1.26 for the high CTE case indicate a large difference in strain behavior at element 12 in the bond coat. Again, it seems that the major effect of the CTE difference has been to cause more creep in the bond coat, particularly at the interface valley.

The small difference in CTE in these models has not lead to a completely clear position on the effect of CTE. In this case, the lower CTE at low temperatures and higher CTE at high temperatures for the Ni-35Cr-6Al-0.9Y bond coat resulted in more creep of the bond coat and little difference in stress in the ceramic. Since the bond coat is subjected to creep fatigue during actual burner rig testing, the fatigue resistance of the bond coat plays an important role in determining bond coat life.

In general terms, a consistently higher CTE in the bond coat will impose higher thermal stress during heating and cooling. If the bond coat creep strength is very high and the CTE is high, then the ceramic will experience very high stresses on heating and will most likely crack. If the bond coat creep strength is low, a high CTE will induce more creep during heating. Then, the cooling cycle will cause the ceramic to become compressively stressed. These ideas should be examined more thoroughly.

Table 5.2.  
Comparison of Stress and Strain Behavior

Cycle Time: 350 sec.						
Interface Geometry	TBC	C T E*	element	radial stress MPa	axial stress MPa	axial strain
Sine_1	elastic	n	445	22	348	0.027
"	"	n	229	2	50	0.014
Sine_1	elastic	h	445	15	360	0.030
"	"	h	229	11	26	0.013
Sine_1	creep	n	445	10	143	0.029
"	"	n	229	4	55	0.017
Sine_1	creep	h	445	-7	137	0.030
"	"	h	229	18	25	0.016
Sine_3	creep	n	445	28	142	-
"	"	n	229	-1	25	-
Sine_3	creep	h	445	17	159	-
"	"	h	229	33	-13	-
Cycle Time: 600 sec.						
Interface Geometry	TBC		element	radial stress MPa	axial stress MPa	axial strain
Sine_1	elastic	n	445	95	65	0.001
"	"	n	229	-70	-148	-0.003
Sine_1	elastic	h	445	65	75	0.001
"	"	h	229	-55	-118	-0.002
Sine_1	creep	n	445	40	-125	0.002
"	"	n	229	-57	-148	-0.002
Sine_1	creep	h	445	14	-144	0.001
"	"	h	229	-27	-132	0.000
Sine_3	creep	n	445	-11	-175	-
"	"	n	229	-72	-113	-
Sine_3	creep	h	445	-17	-173	-
"	"	h	229	-33	-110	-

\* n: CTE for Ni-16Cr-6Al-0.3Y  
h: CTE for Ni-35Cr-6Al-0.9Y (the "high" CTE material)

### 5.3 Effect of Bond Coat Creep Resistance

The effect of increasing the creep coefficient of the bond coat at high temperatures (see Table 3.4.2) was to increase the tensile stress in the ceramic at the interface peak by about 20 MPa, and to decrease the axial stress in the other interface elements by about that amount. The peak in the ceramic remained the highest axial strain position, but the corresponding strain in the bond coat increased from 0.027 (Figure 4.1.16) to 0.028 (Figure 4.1.28). Therefore, raising the creep coefficient, A, in the bond coat had the expected effect of increasing the strain level in the bond coat. This gives a wider spread in final axial strain values in terms of differences between the peak and valley locations and in strain across the interface. Based on these results, a bond coat with higher creep strength (lower creep coefficient) should give better performance than a bond coat with lower creep strength.

### 5.4 Effect of Interface Geometry

The effect of surface roughness can be assessed by comparing the baseline SINE\_1 interface and the SINE\_2 and SINE\_3 geometries. A summary of interface pressure at one specific interface node is tabulated in Table 5.3. Examination of normal pressure distribution along the interface has shown that the valley region becomes tensile at the end of the thermal cycle.

An examination of Table 5.3 shows that during cool down, the interface pressure in the valley of the bond coat is negative, meaning that a tensile state exists across the bond coat - ceramic interface. The magnitude of the interface pressure is a function of the geometry and the amount of creep that takes place. Using SINE\_1 geometry as baseline, the stress across the interface is reported to be -45 MPa. Reducing the roughness spacing (wave period) increases the tension across the bond line to 72 MPa, as shown by the SINE\_3 data in Table 5.3. Increasing the roughness (wave amplitude) increases the tension across the interface to 57 MPa, as seen in the SINE\_2 data. Clearly, models with greater surface roughness produce higher tensile stresses across the interface.

The effect of a change in bond coat - ceramic interface geometry may be seen by comparing the results of the baseline case SINE\_1 geometry, Section 4.1.3, with the SINE\_3 geometry (Section 4.3.1) and SINE\_2 geometry, Section 4.2.1. During heat-up and hold, the radial stresses generated in the peak region of the ceramic are nearly 87% higher for the SINE\_3 model than for the SINE\_1 model, compare Figures 4.1.17 and 4.3.4. In contrast, the radial stress values in the valley are similar between the two models, and therefore a much larger radial stress gradient

exists in the SINE<sub>3</sub> model. At the end of the thermal cycle, the ceramic adjacent to the bond coat valley in model SINE<sub>3</sub> the stress state is some 24% more tensile than the baseline case. From the larger stress differential between the peak and valley, as well as from the fact that the peaks and valleys are much closer spatially in the SINE<sub>3</sub> model, the stress concentration is higher in the SINE<sub>3</sub> model than in the SINE<sub>1</sub> model.

In comparing the effect of roughness (wave amplitude), the SINE<sub>2</sub> model has a roughness of 1.5 times the baseline SINE<sub>1</sub> model. The axial strain histories in Figures 4.1.16 for SINE<sub>1</sub> and Figure 4.2.4 for SINE<sub>2</sub> show that peak strains are higher and the final strain state has a wider spread for the "rougher" SINE<sub>2</sub> geometry.

In summary, an increase in roughness magnitude (SINE<sub>2</sub>) increases the creep in the bond coat and the tendency to separate along the critical interface. Increasing the roughness spacing (SINE<sub>3</sub>) increases the stress concentration effect at the

Table 5.3.  
Interface Pressure for Several Models  
Node 13 - Bond Coat Valley

Time	S0	S1	S2	Sh0	Sa0
0	0	0	0	0	0
50	19	-10	12	17	10
100	22	5	12	35	16
150	18	12	10	28	12
200	14	15	8	12	6
250	12	15	7	5	3
300	10	14	6	-3	0
350	9	13	6	-7	-2
400	-28	-96	-27	-46	-30
450	-41	-72	-43	-65	-52
500	-44	-69	-45	-73	-55
550	-44	-67	-43	-69	-58
600	-45	-65	-45	-72	-57

Key:

- S0 - SINE<sub>1</sub> geometry - baseline case
- S1 - SINE<sub>1</sub> geometry - higher CTE in bond coat
- S2 - SINE<sub>1</sub> geometry - higher A values in bond coat
- Sh0 - SINE<sub>3</sub> geometry - sine wave frequency = 2x baseline
- Sa0 - SINE<sub>2</sub> geometry - sine wave amplitude = 1.5x baseline

interface peaks and increases creep of the bond coat. The gradient between peak and valley positions is intensified because the peak-to-peak spacing has been made smaller. The result is more constraint across the interface and a higher potential for cracking problems.

Both roughness spacing and roughness magnitude have an impact on stress and creep near the interface. Since roughness is needed for mechanical bond strength, uniformity of the roughness is important, meaning that consistent deposition be achieved. Large asparities in the interface geometry, as might be caused by variation in starting powder size or local build-up, will degrade the ceramic performance by providing debonding sites. It is also important to determine an optimum roughness. Mechanical bonding and stress concentration are competing effects, and there should exist some range of roughness below which the mechanical bond strength is reduced, and above which the stress concentration reduces TBC performance.

## 6.0 CONCLUSIONS

1. The use of an elastic-plastic constitutive model as opposed to a creep model gives different results for stress and strain in the TBC system. An all-elastic model was not run, but such a model would have no retained stress or strain upon completion of the thermal cycle. The presence of both retained stress and strain at the completion of the thermal cycle for these models which allow creep deformation shows the necessity of including creep effects.
2. From these analyses, cool down generates more aggravating stress conditions than heating during the burner rig test. Thermal stress is generated during heating, but there are two outlets for this stress. First, microcracking of the ceramic relieves tensile stress. Second, at higher temperatures, the bond coat creeps and stresses are relaxed. During cooling, thermal stresses are reintroduced, but there are no effective mechanisms for relieving stress. Even though the overall stress in the ceramic may be compressive, local stress concentrations at the bond coat - ceramic interface promote separation along the interface.
3. Interface geometry has a pronounced effect on stress at the interface. Increased roughness and decreased roughness spacing increase the stress concentration associated with peak and valley locations. Creep of the bond coat relieves stress during high temperature portions of the burner rig cycle, but tensile stress across the interface is generated during the cool down portion of the cycle.
4. A definitive position on the effect of bond coat CTE on TBC performance was not established by this project due to the complexity of interactions. However, in comparing different CTE behaviors such as Ni-16Cr-6Al-0.3Y and Ni-35Cr-6Al-0.9Y materials, some preliminary differences can be noted. The latter material has a higher CTE only at temperatures above 900°C. Little difference in stress state in the ceramic was seen. However, the higher CTE at high temperature resulted in more creep of the bond coat and a greater strain cycle during the thermal cycle. The fatigue resistance of the bond coat is therefore an important consideration in assessing the effect of CTE.
5. A higher bond coat creep strength should give better TBC performance. Model results showed that lower creep resistance caused more creep in the bond coat without decreasing the peak stress in the ceramic.
6. The use of a steady state creep model in the finite element

program NIKE2D proved to be an effective method for examining TBC stresses in a typical burner rig test cycle. The data produced by these models seems to agree at least qualitatively with reported TBC experiments.

## REFERENCES

- W.J. Brindley and R.A. Miller, "TBC's for Better Engine Efficiency", Advanced Materials & Processes, pp 29-33, August 1989.
- W.J. Brindley and J.D. Whittenberger, "Stress Relaxation of Low Pressure Plasma Sprayed NiCrAlY Alloys", to be published.
- G.C. Chang and W. Phucharoen, "Finite Element Thermal Stress Solutions for Thermal Barrier Coatings", Surface and Coatings Technology, v. 32, pp 307-325, 1987.
- J.T. DeMasi, et al., "Thermal Barrier Coating Life Prediction Model Development: Phase 1 Final report", NASA Contract Report 182230, December 1989.
- A.D. Freed, S.V. Raj and K.P. Walker, "Stress Versus Temperature Dependence of Activation Energies for Creep", Trans. of the ASME, vol. 114, pp 46-50, January 1992.
- H.J. Frost and M.F. Ashby, Deformation-Mechanism Maps, Pergamon Press, 1982.
- R.V. Hillery, et al., "Thermal Barrier Coating Life Prediction Model Development", NASA Contract Report 180807, November 1988.
- R.D. Krieg, "Numerical Integration of Some New Unified Plasticity-Creep Formulations", SMiRT-4, M6/4, 1977.
- W. Phucharoen, "Development of an Analytical-Experimental Methodology for Predicting the Life and Mechanical Behavior of Thermal Barrier Coatings", Ph.D. Thesis, Cleveland State University, August 1990.

**FIGURES**

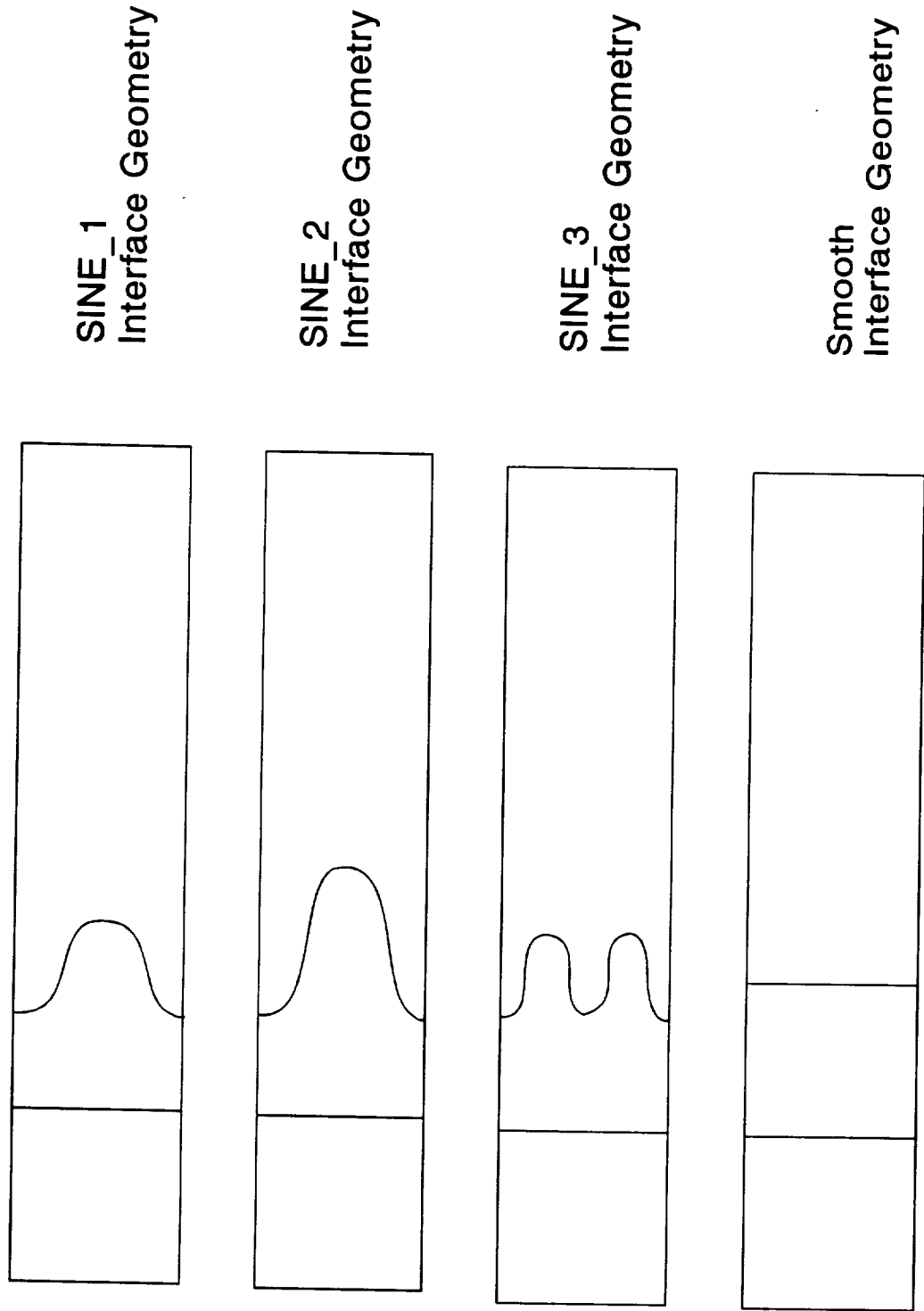


Figure 3.1.1.1. Schematic of Models.

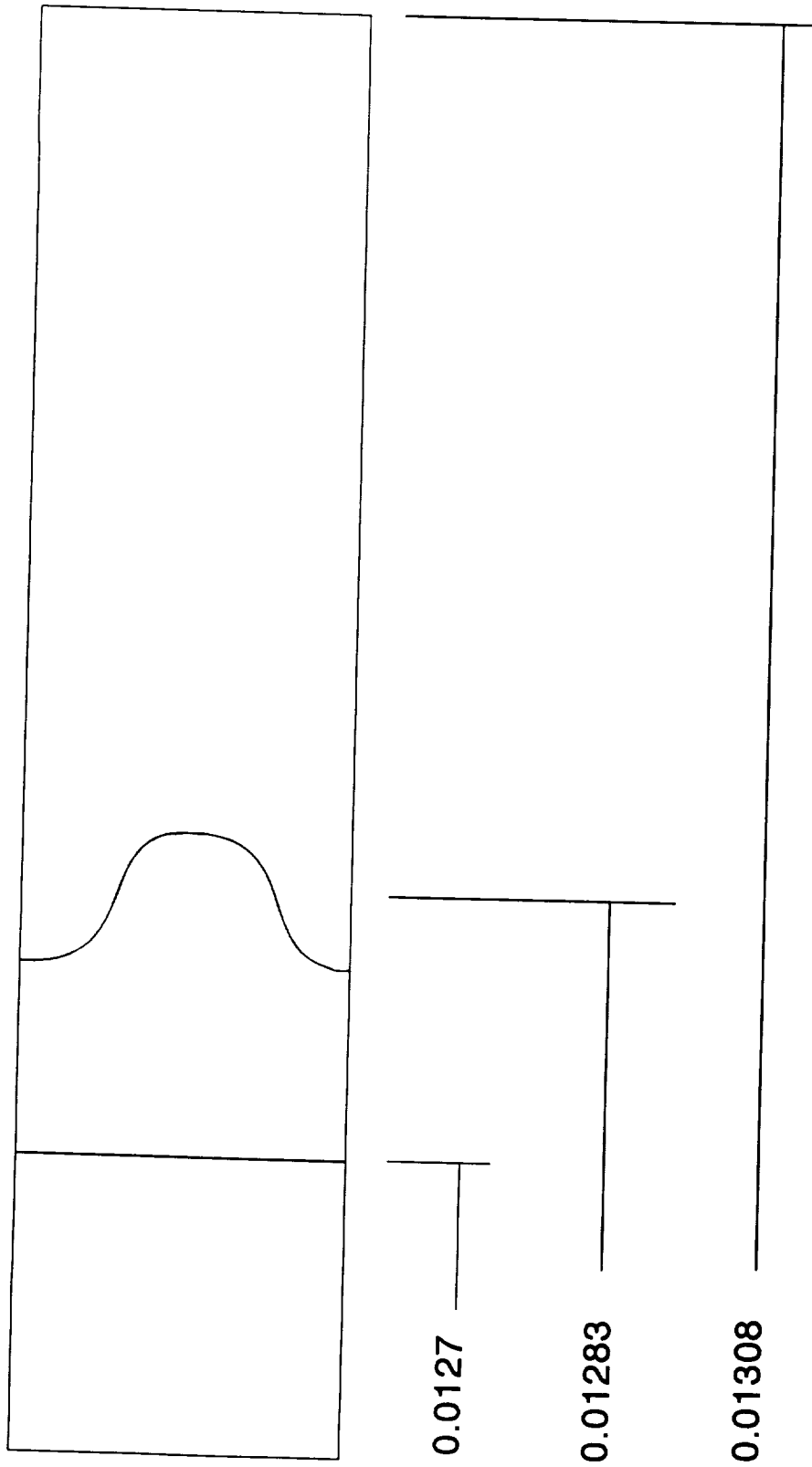


Figure 3.2.1. Schematic with Nominal Dimensions (meters).

Topaz Model: T&C Coasting

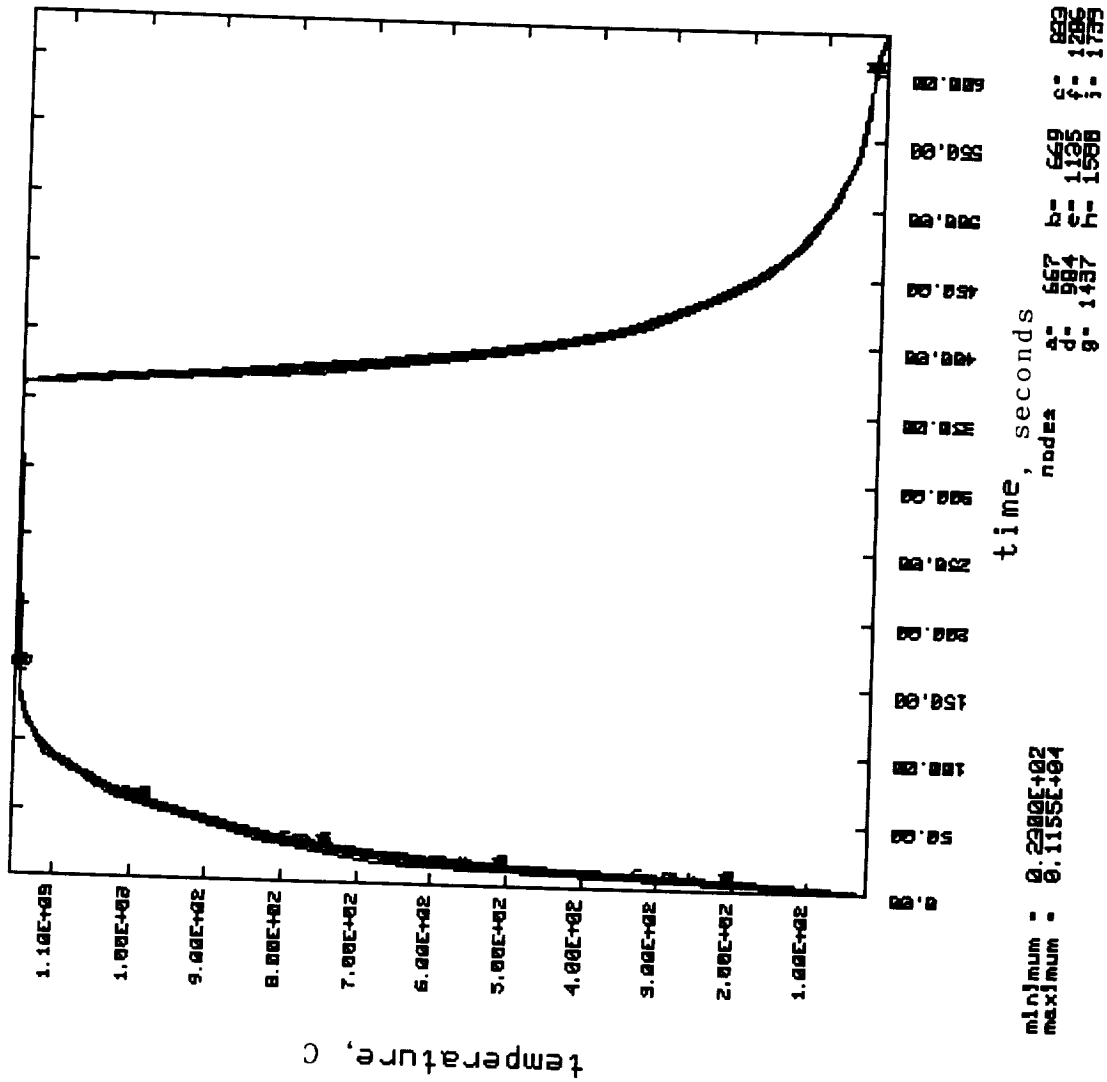


Figure 3.2.2. Temperature - Time Curve for Burner Rig Test.



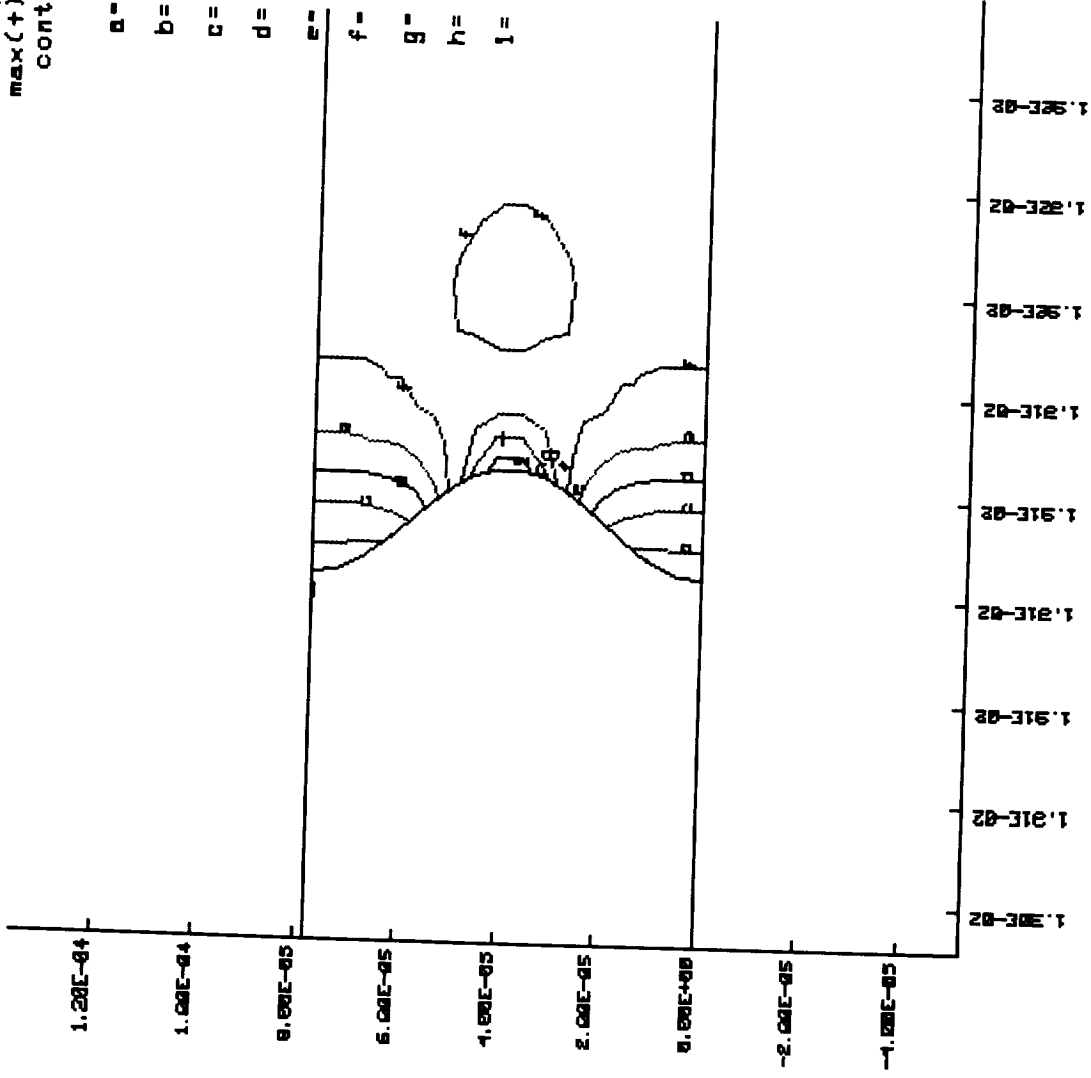
SINE\_1 Interface: Base Bond Materials, Elastic TBC & Core  
 contours of axial stress

time= 0.35000E+03

min(-)=-0.16634E+02  
 max(+)= 0.38419E+03  
 contour levels

MPa

- a= 0.23450E+02
- b= 0.63530E+02
- c= 0.10400E+03
- d= 0.14400E+03
- e= 0.18400E+03
- f= 0.22400E+03
- g= 0.26400E+03
- h= 0.30400E+03
- i= 0.34400E+03



SINE\_1 Interface Geometry with Base Case Bond Material, Elastic TBC and Core -  
 Contour Map of Axial Stress at the Bond Coat/Ceramic Interface.

Figure 4.1.1



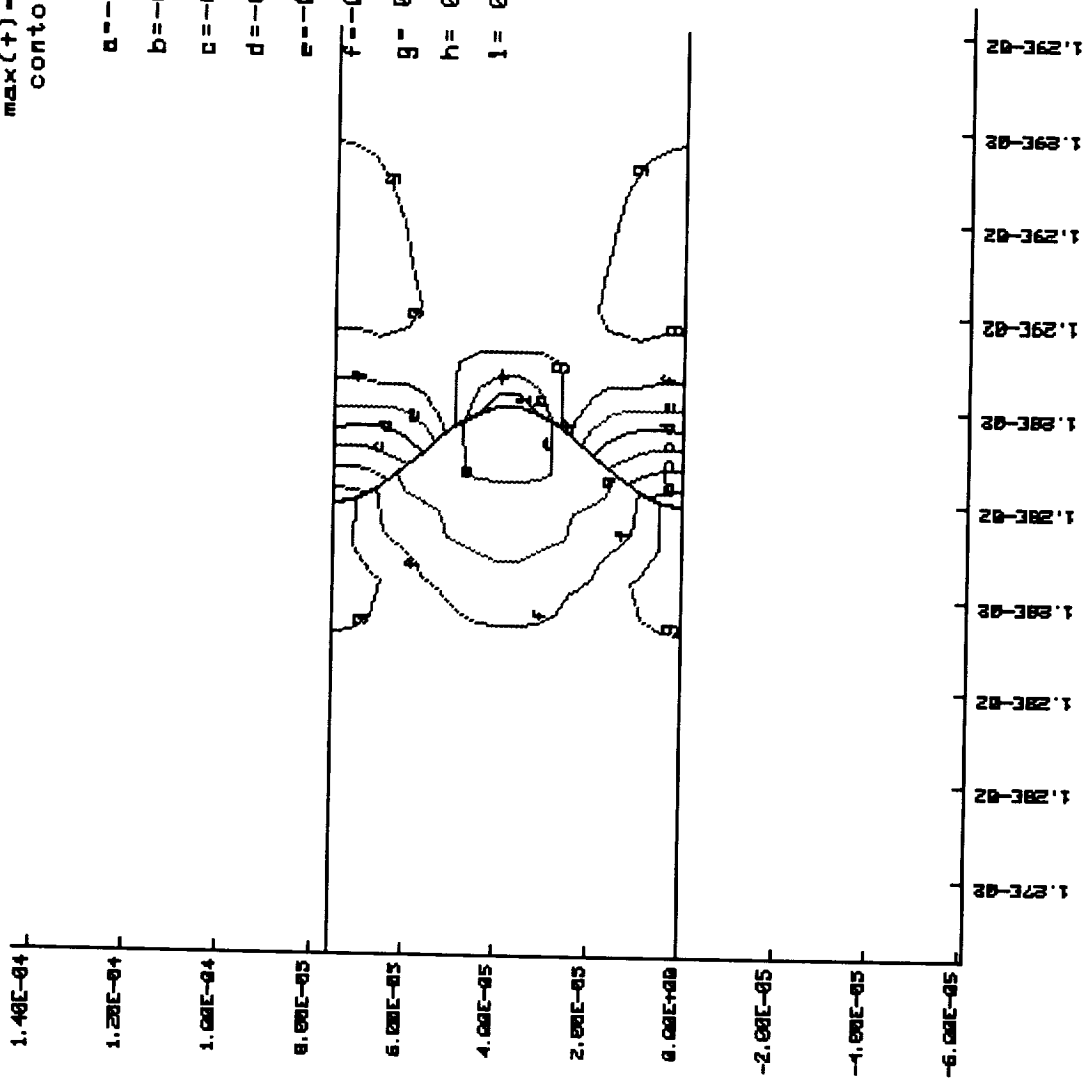
SINE\_1 Interface: Base Bond Materials, Elastic TBC & Core  
 Contours of axial stress

time= 0.600000E+03

min(-)=-0.16882E+03  
 max(+)= 0.93889E+02  
 contour levels

MPa

- a=-0.14300E+03
- b=-0.11600E+03
- c=-0.90010E+02
- d=-0.63740E+02
- e=-0.37470E+02
- f=-0.11200E+02
- g= 0.15070E+02
- h= 0.41350E+02
- i= 0.67620E+02



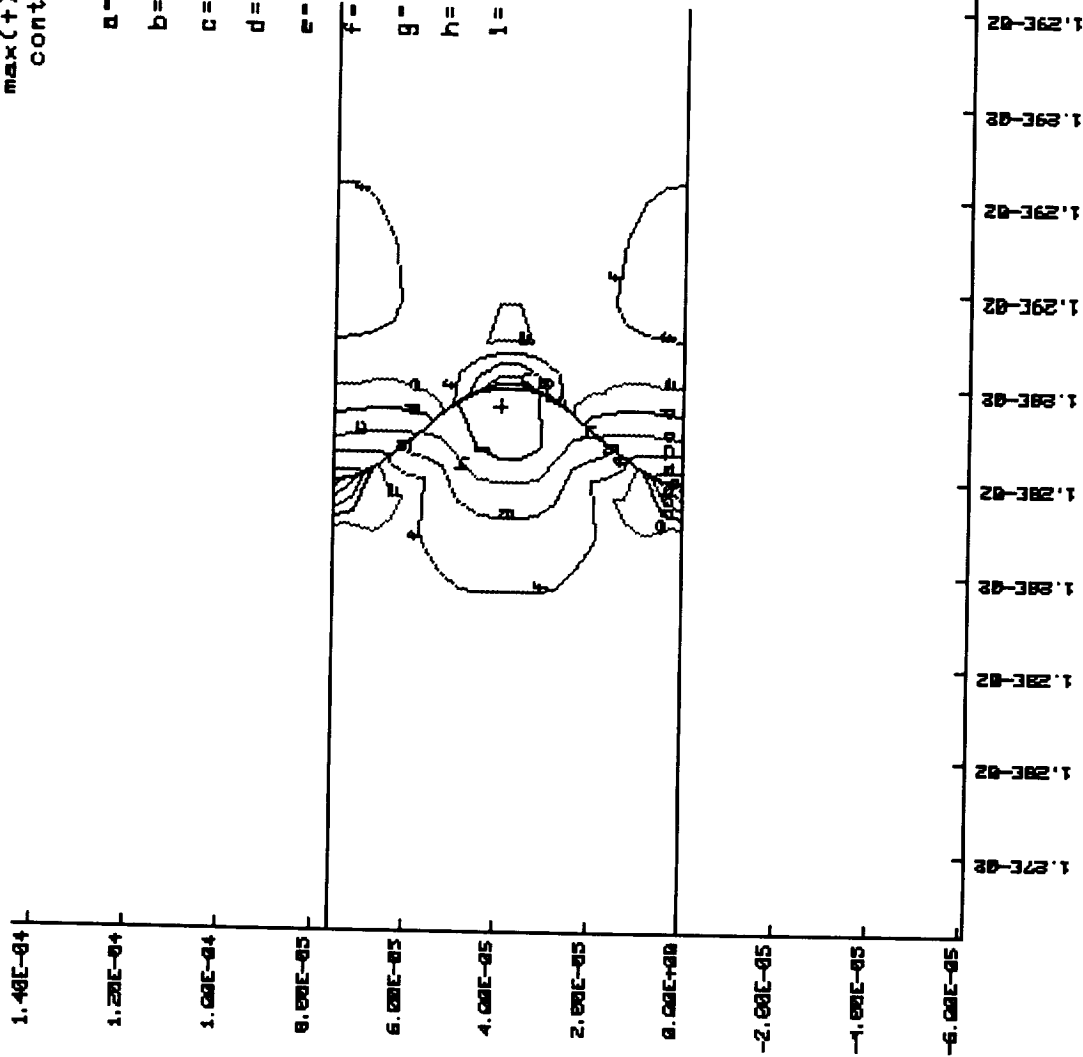
SINE\_1 Interface Geometry with Base Case Bond Material, Elastic TBC and Core-  
 Contour Map of Axial Stress at the Bond Coat/Ceramic Interface.

Figure 4.1.3

SINE\_1 Interface: Base Bond Materials, Elastic TBC & Core  
 contours of axial strain  
 ( InfIntmax )

time = 0.600000E+03  
 min(-) = -0.40271E-02  
 max(+) = 0.29297E-02  
 contour levels

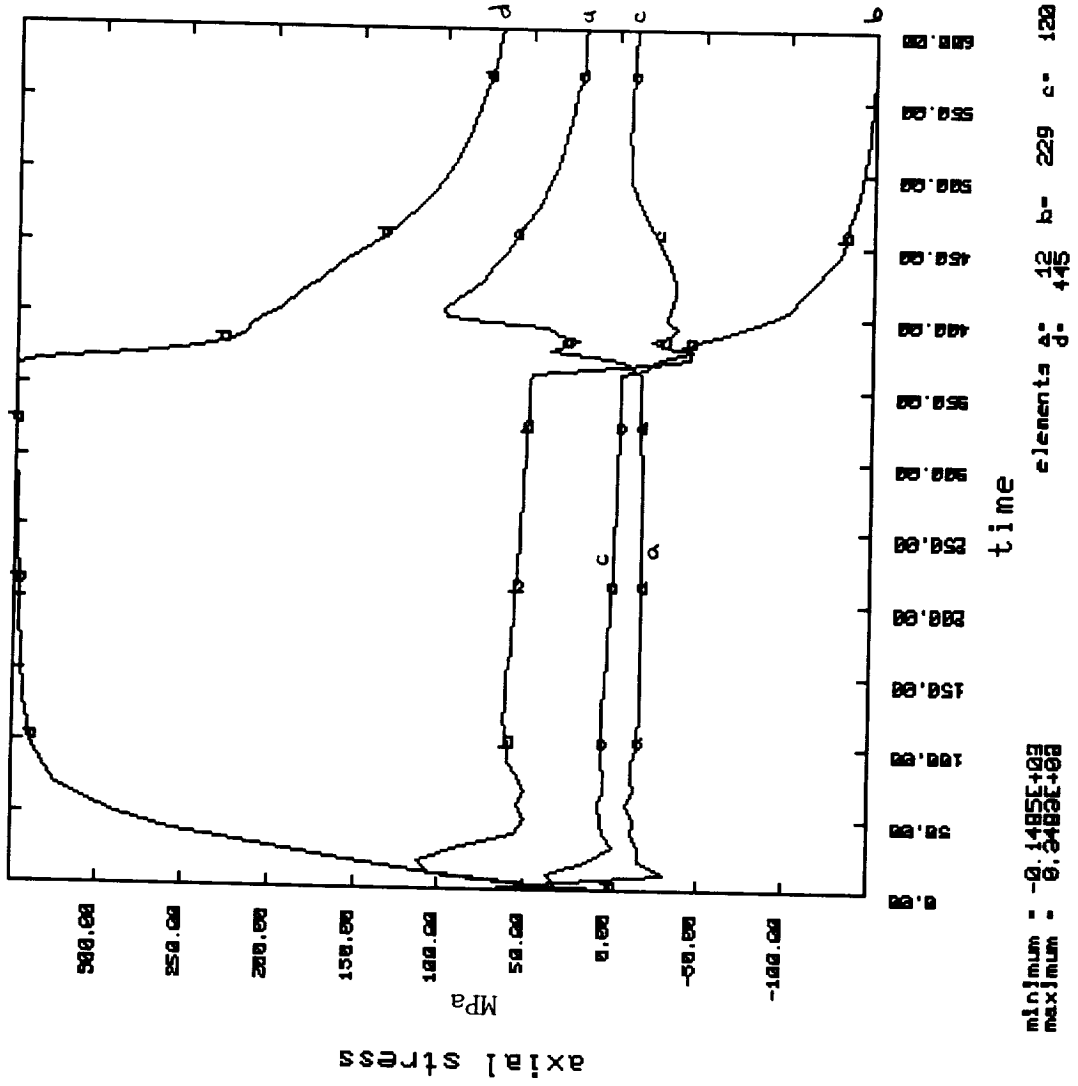
- a = -0.33310E-02
- b = -0.26360E-02
- c = -0.19400E-02
- d = -0.12440E-02
- e = -0.54900E-03
- f = 0.14700E-03
- g = 0.84300E-03
- h = 0.15380E-02
- i = 0.22340E-02



SINE\_1 Interface Geometry with Base Case Bond Material, Elastic TBC and Core -  
 Contour Map of Axial Strain at the Bond Coat/Ceramic Interface.

Figure 4.1.4

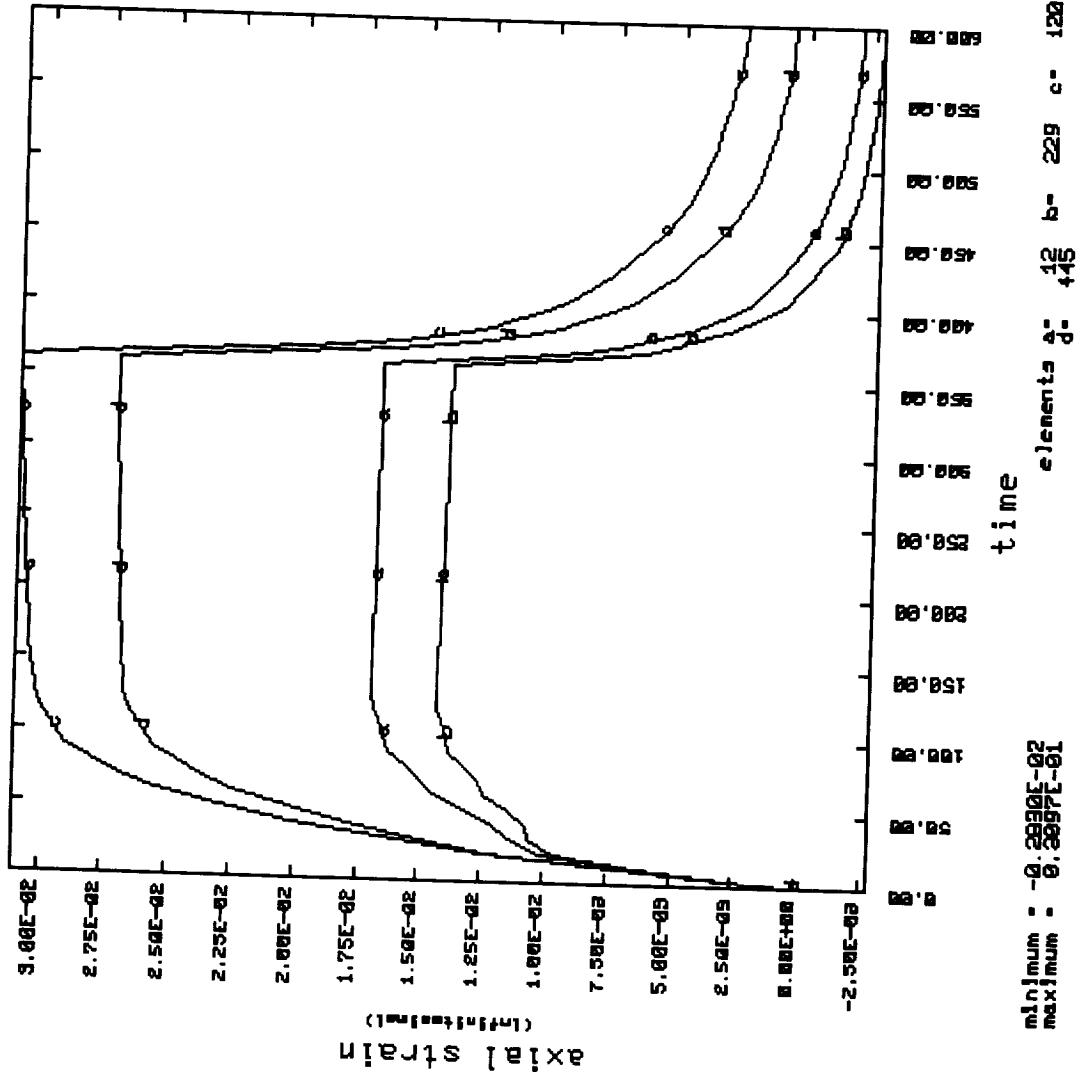
SINE\_1 Interface: Base Bond Materials, Elastic TBC & Core



SINE\_1 Interface Geometry with Base Case Bond Material, Elastic TBC and Core - Axial Stress History Plot.

Figure 4.1.5

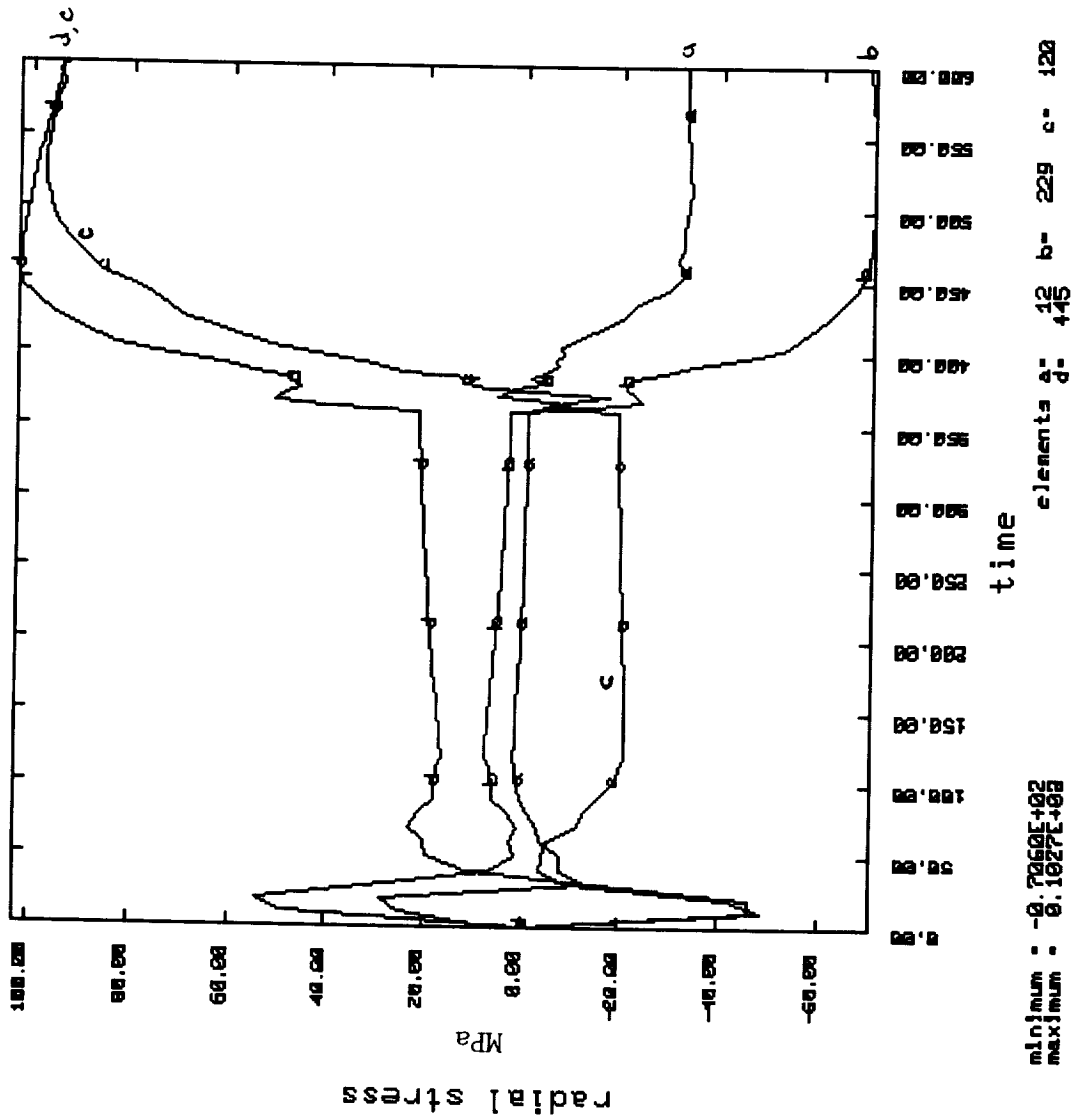
SINE\_1 Interface: Base Bond Materials, Elastic TBC & Core



SINE\_1 Interface Geometry with Base Case Bond Material, Elastic TBC and Core - Axial Strain History Plot.

Figure 4.1.6

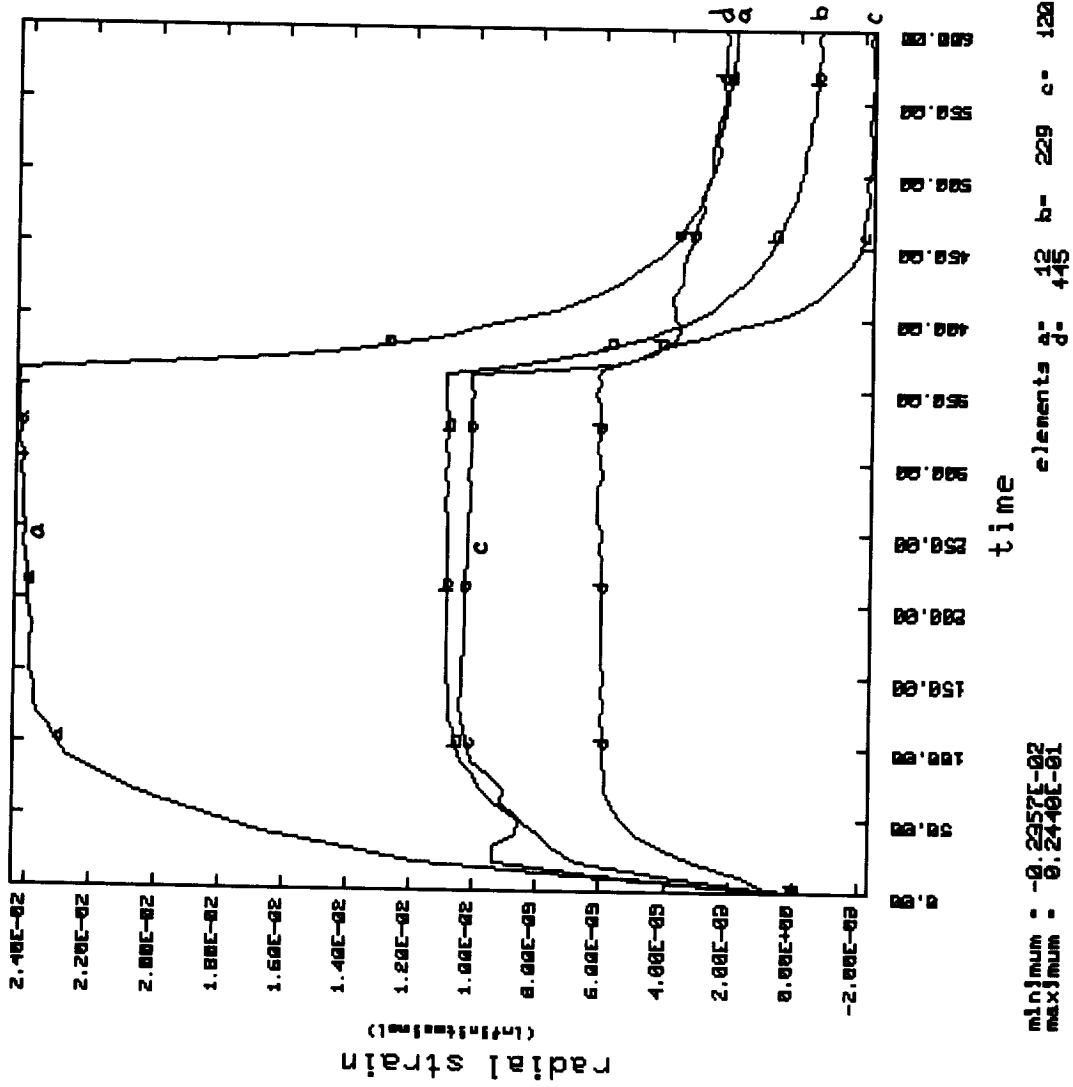
SINE\_1 Interface: Base Bond Materials, Elastic TBC & Core



SINE\_1 Interface Geometry with Base Case Bond Material, Elastic TBC and Core -  
Radial Stress History Plot.

Figure 4.1.7

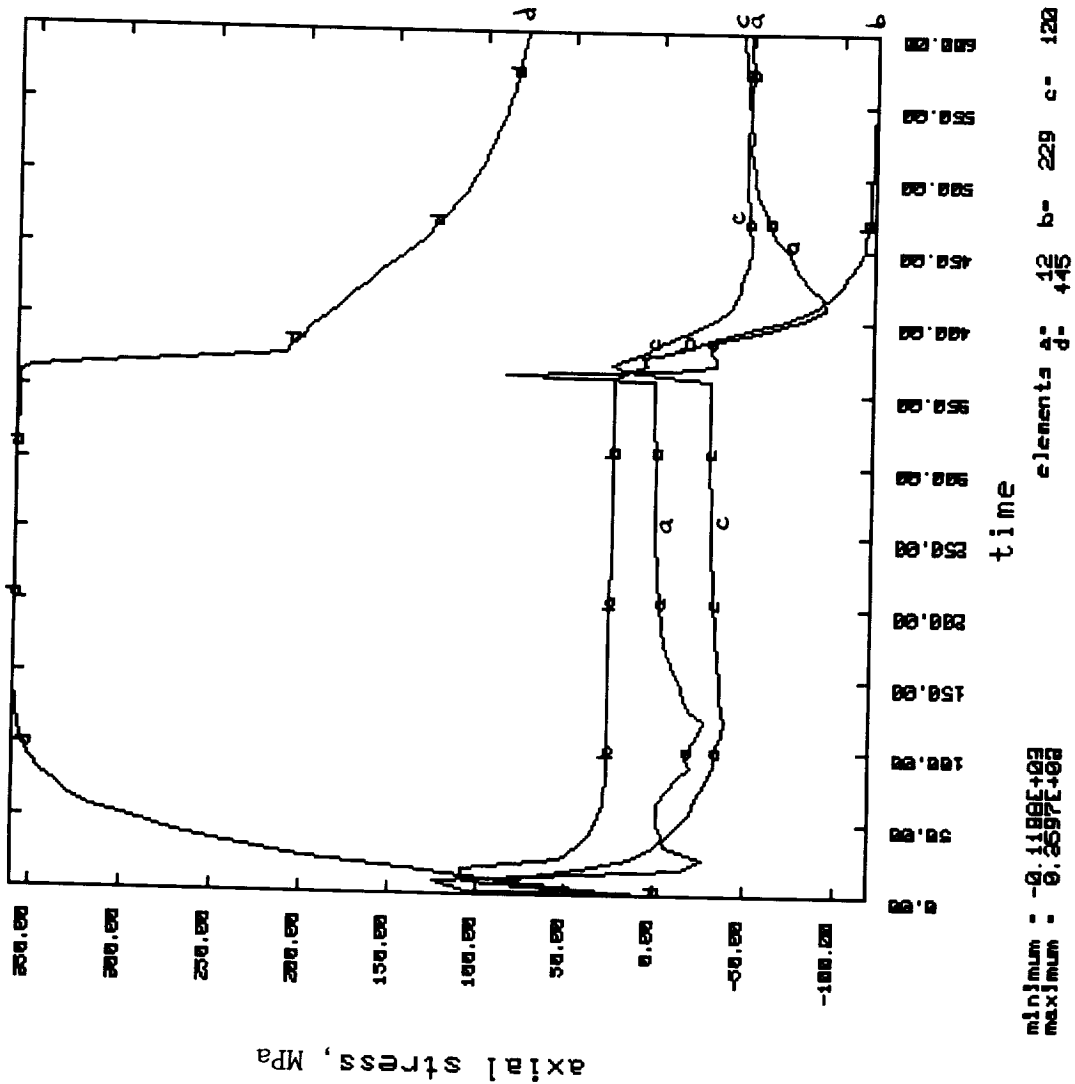
SINE\_1 Interface: Base Bond Materials, Elastic TBC & Core



SINE\_1 Interface Geometry with Base Case Bond Material, Elastic TBC and Core - Radial Strain History Plot.

Figure 4.1.8

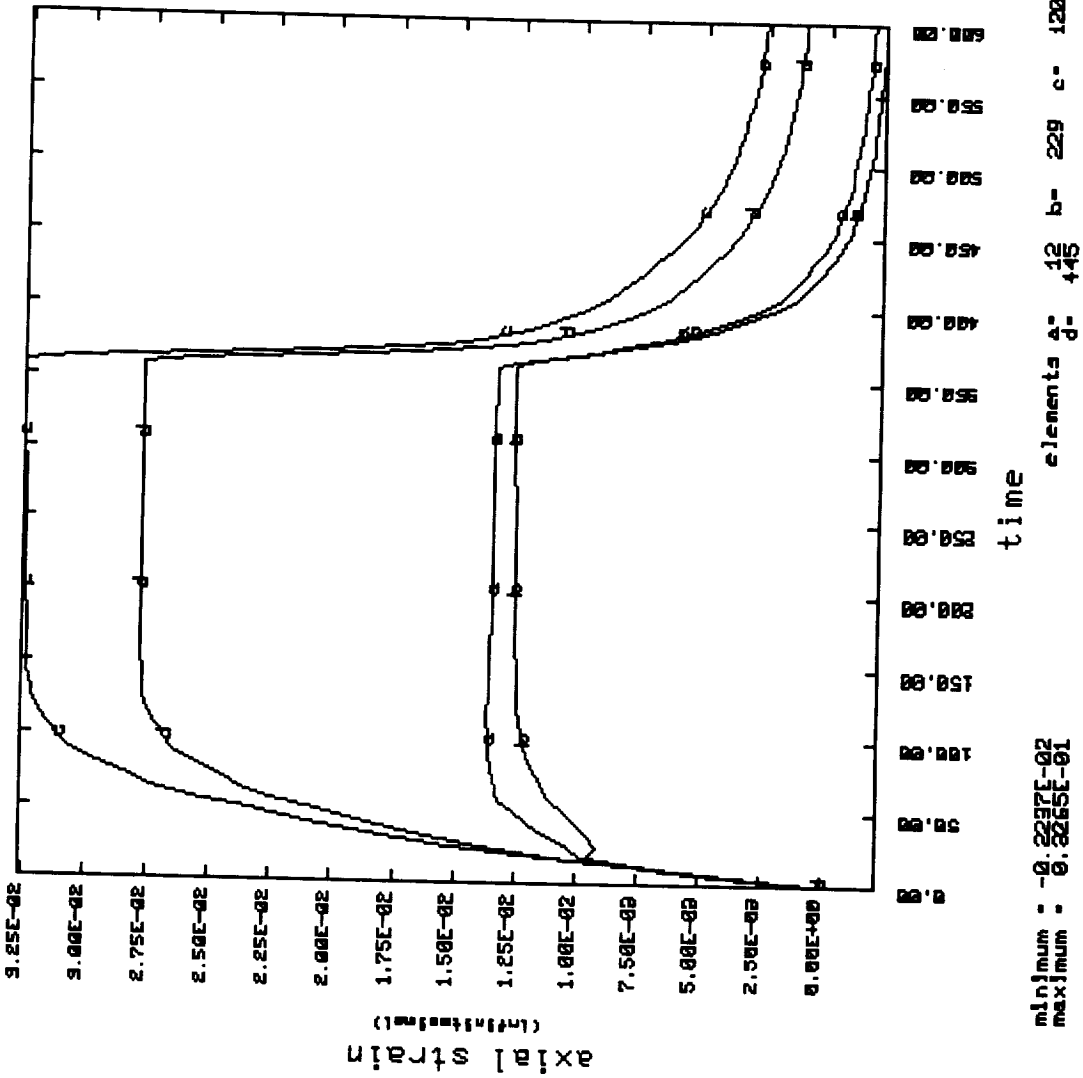
SINE\_1 Interface: Higher Bond Coat CTE, Elastic TBC & Core



SINE\_1 Interface Geometry with Higher Bond Coat CTE, Elastic TBC & Core:  
Axial Stress History Plot.

Figure 4.1.9

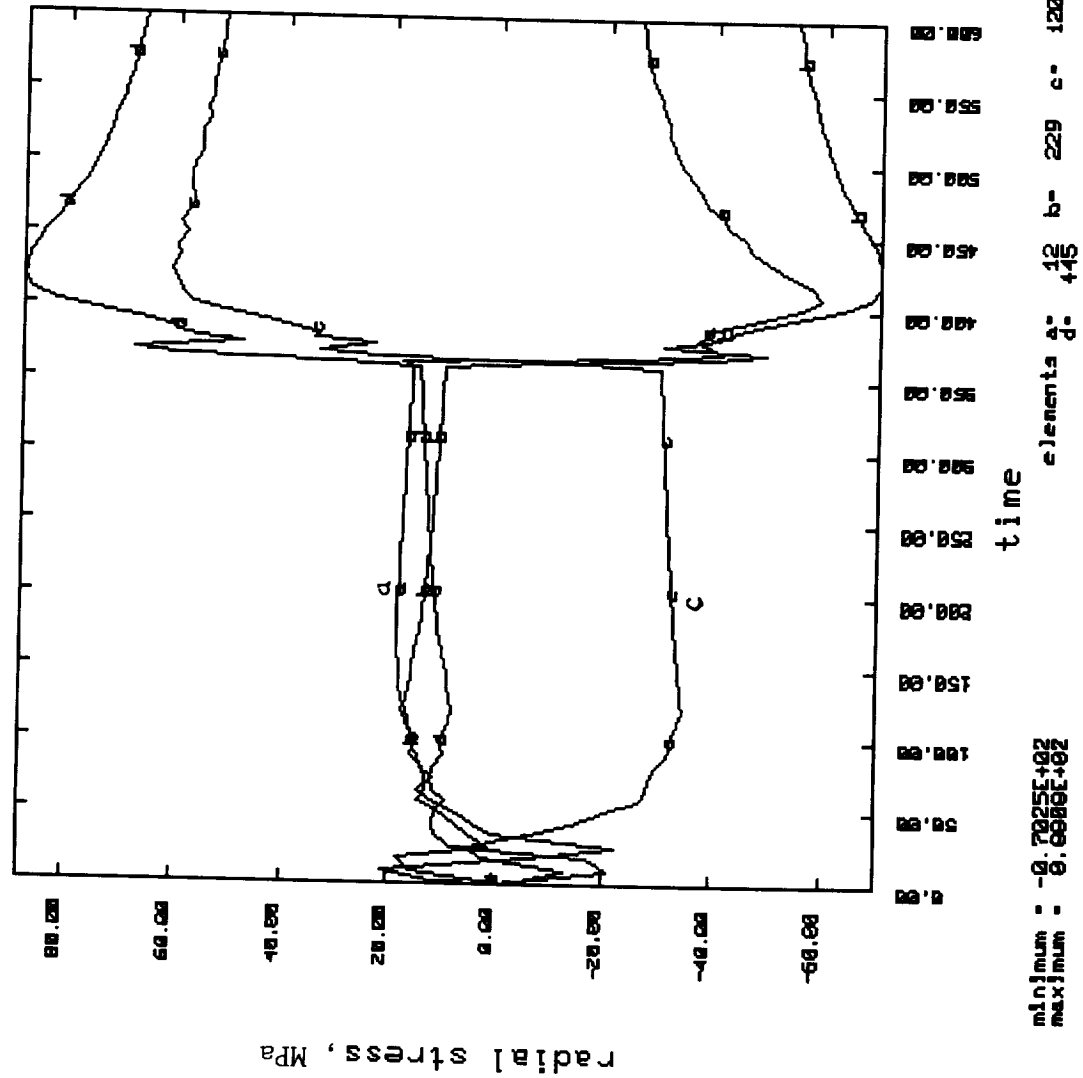
SINE\_1 Interface: Higher Bond Coat CTE, Elastic TBC & Core



Axial Strain History Plot.

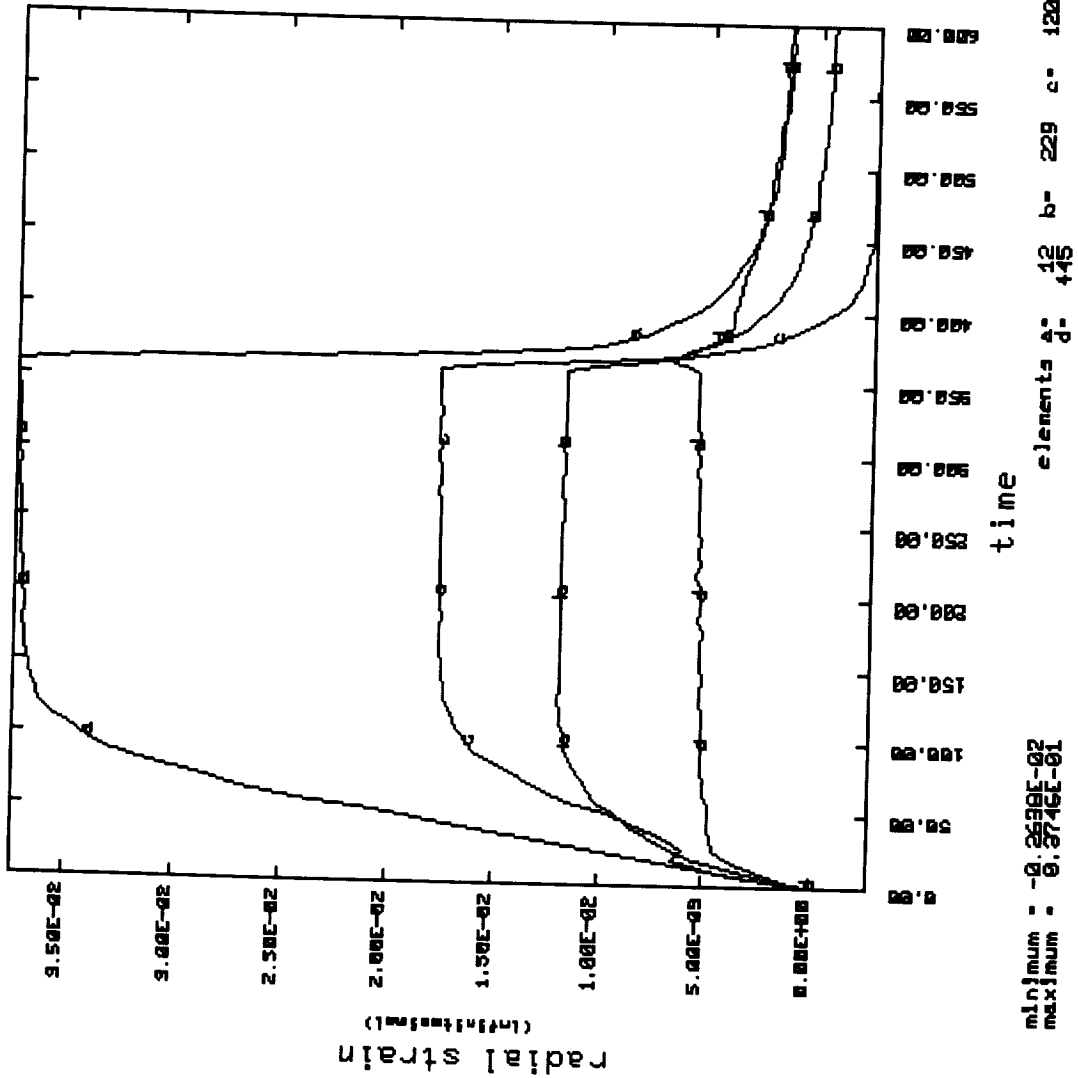
Figure 4.1.10

SINE\_1 Interface: Higher Bond Coat CTE, Elastic TBC & Core



Radial Stress History Plot.  
Figure 4.1.11

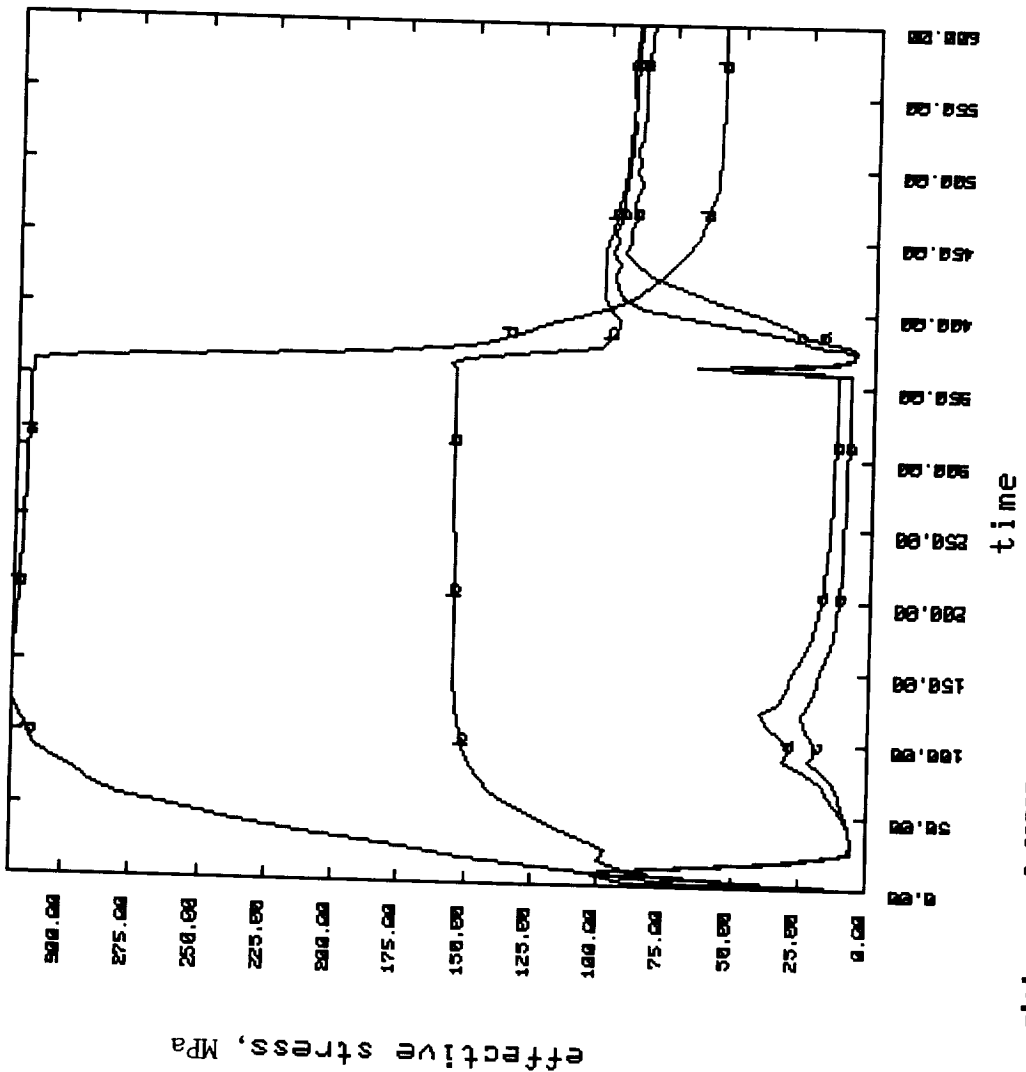
SINE\_1 Interface: Higher Bond Coat CTE, Elastic TBC & Core



Radial Strain History Plot.

Figure 4.1.12

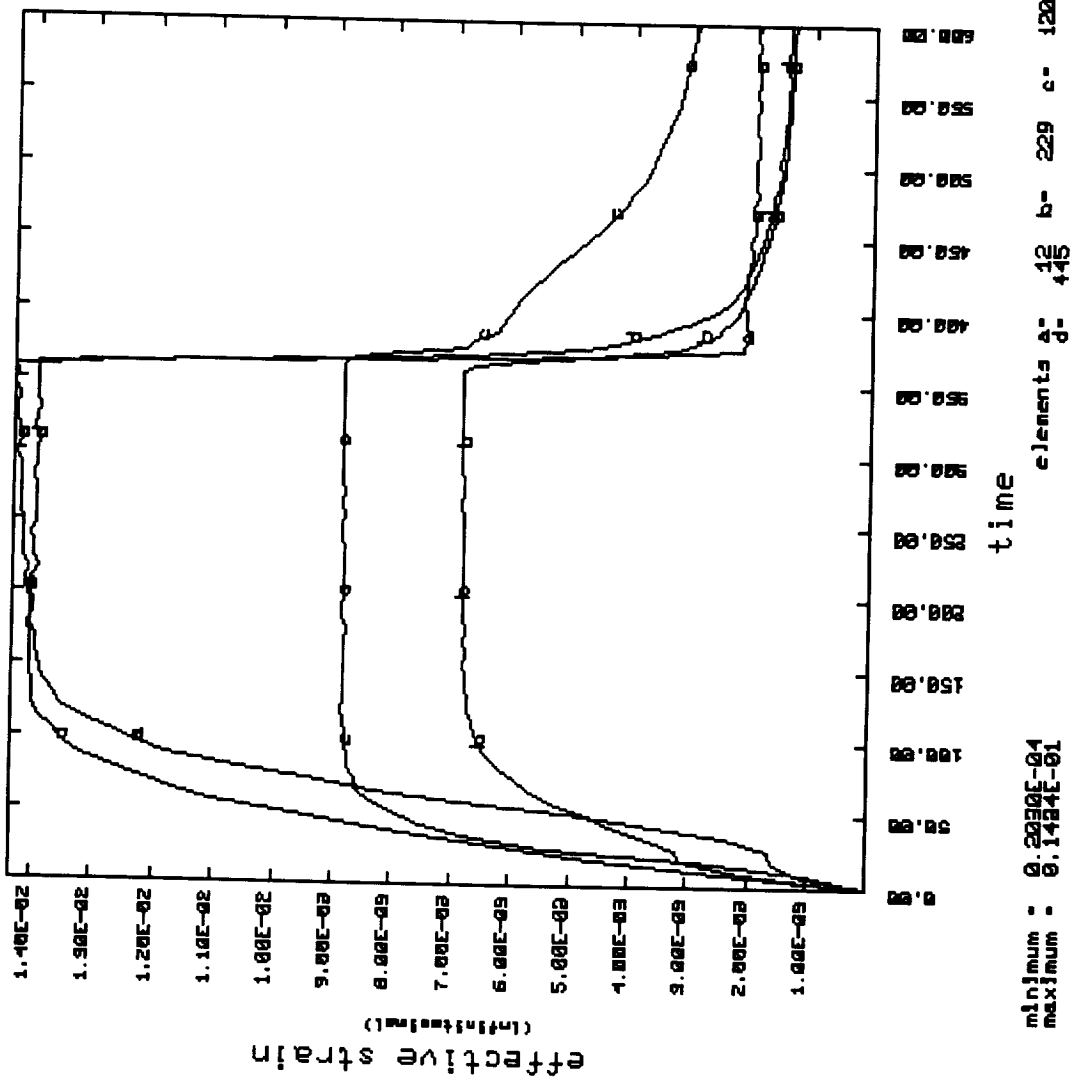
SINE\_1 Interface: Higher Bond Coat CTE, Elastic TBC & Core



Effective Stress History Plot.

Figure 4.1.13

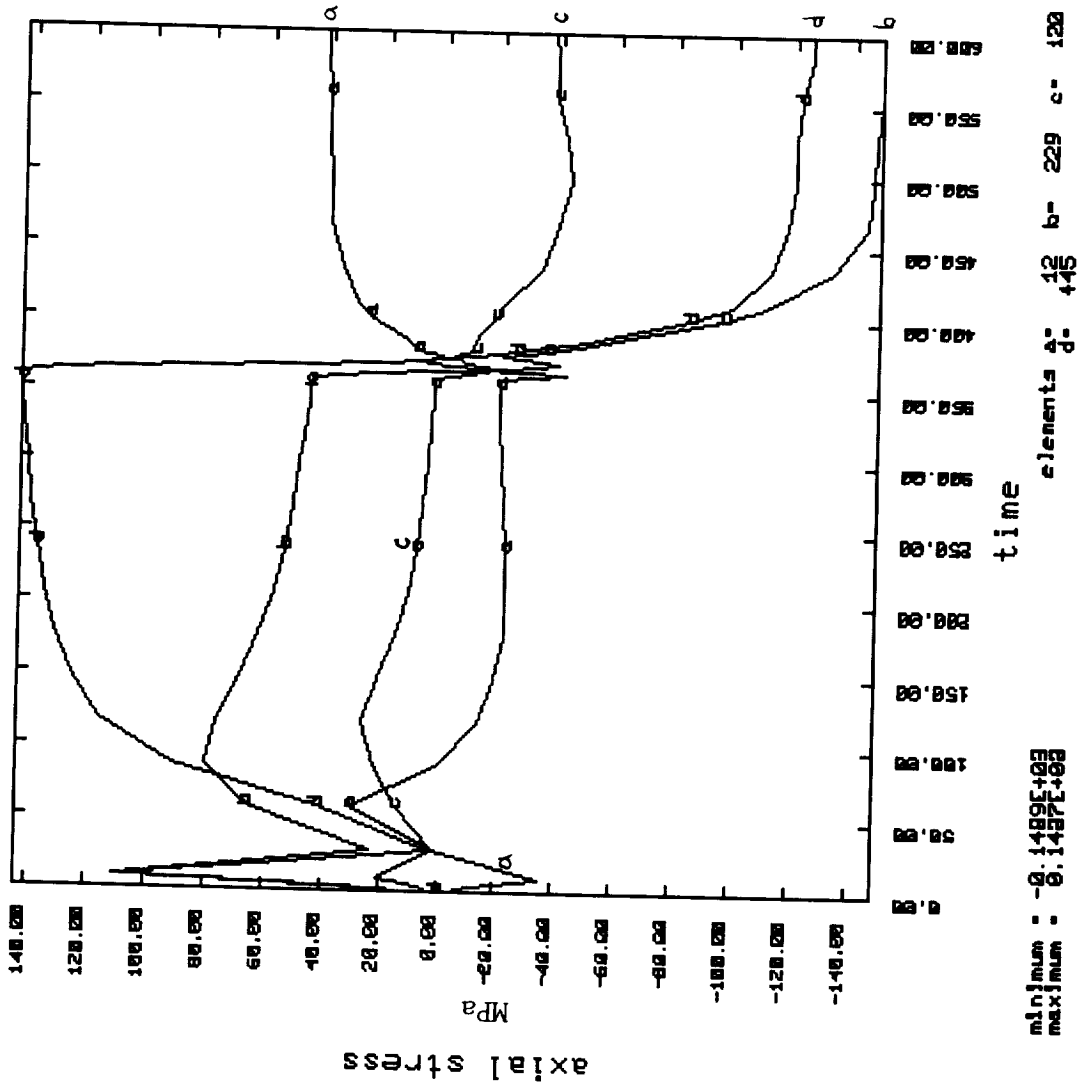
SINE\_1 Interface: Higher Bond Coat CTE, Elastic TBC & Core



Effective Strain History Plot.

Figure 4.1.14

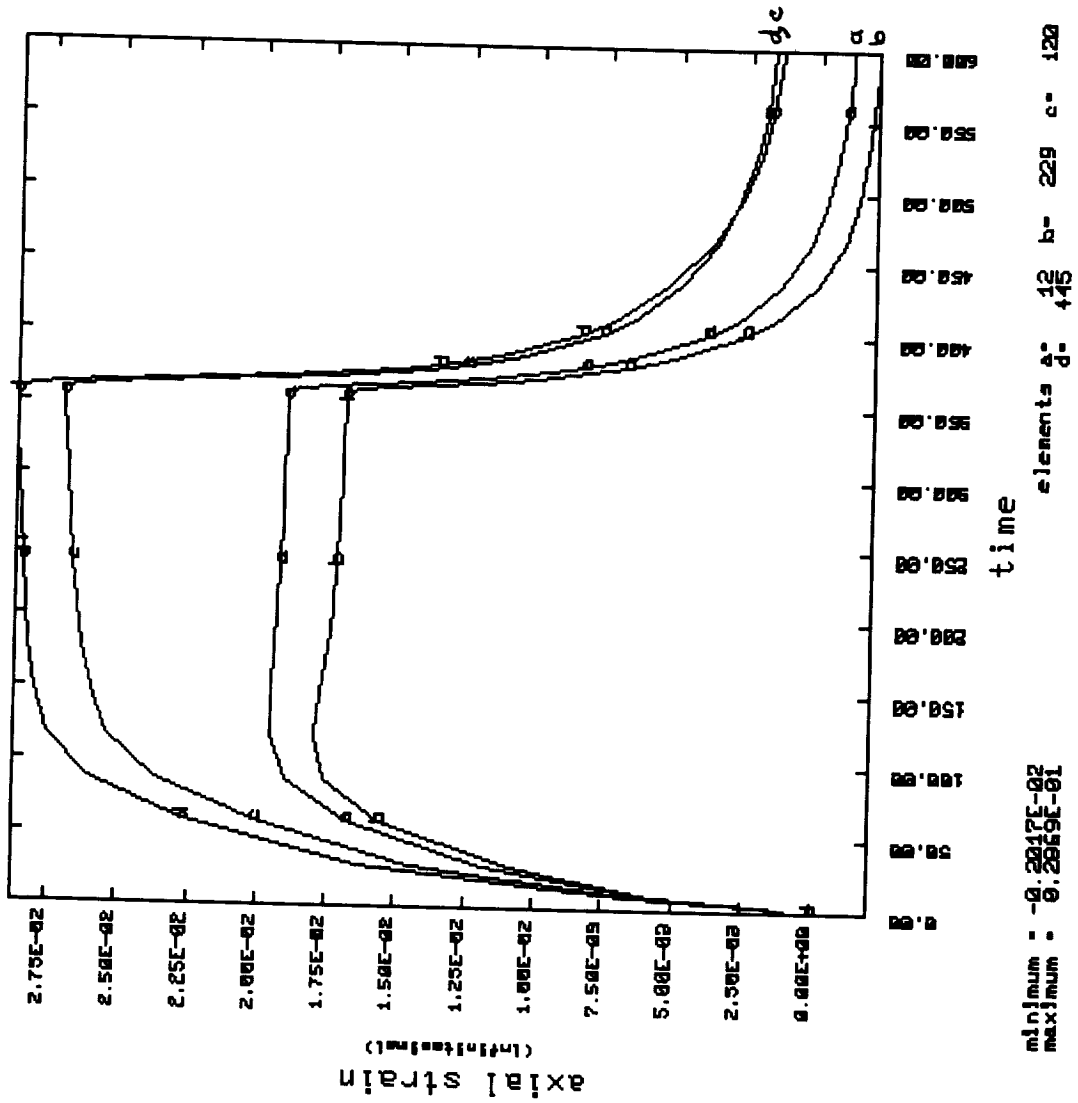
SINE\_1 Interface Geometry



SINE\_1 Interface Baseline Case -  
Axial Stress History Plot.

Figure 4.1.15

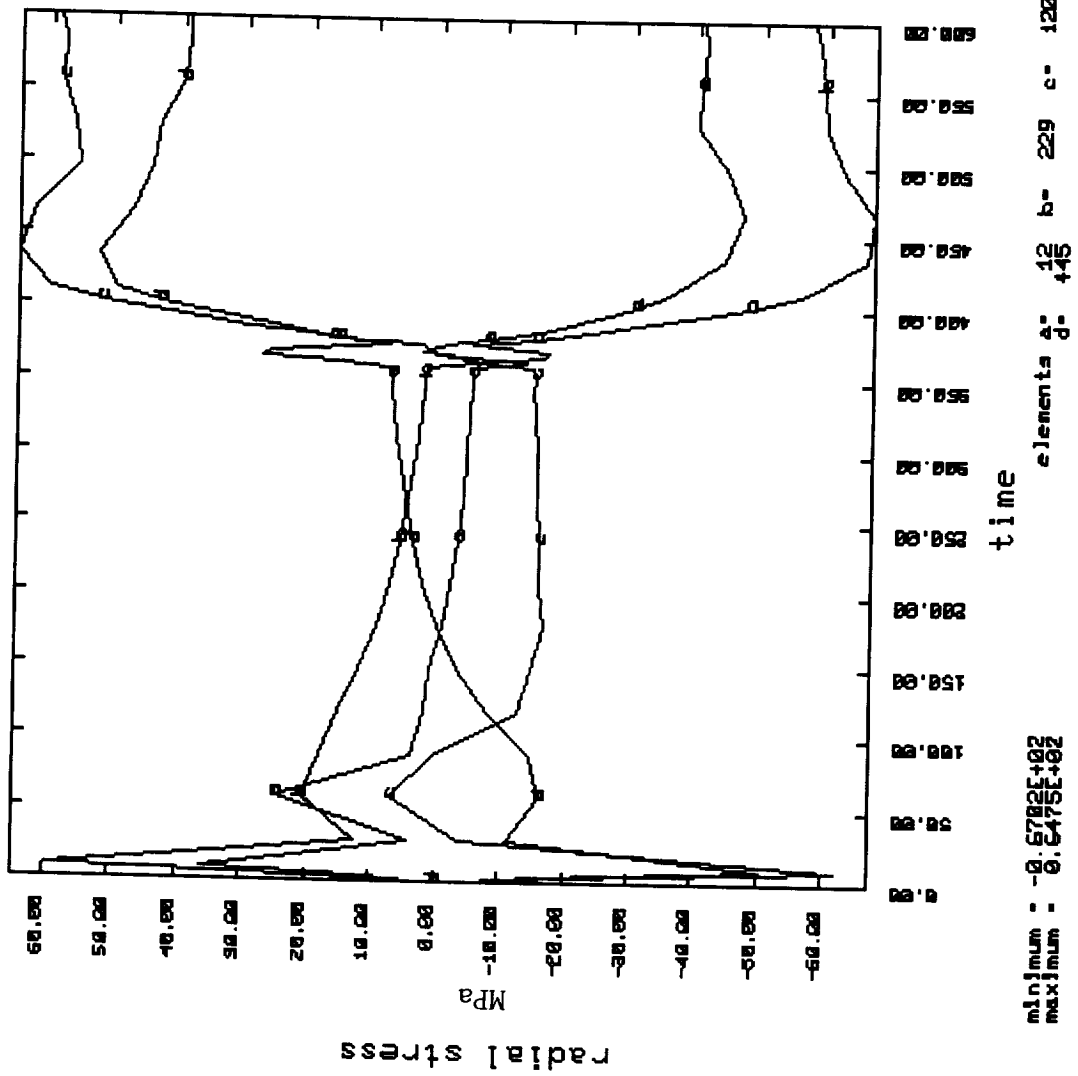
SINE\_1 Interface Geometry



SINE\_1 Interface Baseline Case -  
 Axial Strain History Plot.

Figure 4.1.16

SINE\_1 Interface Geometry

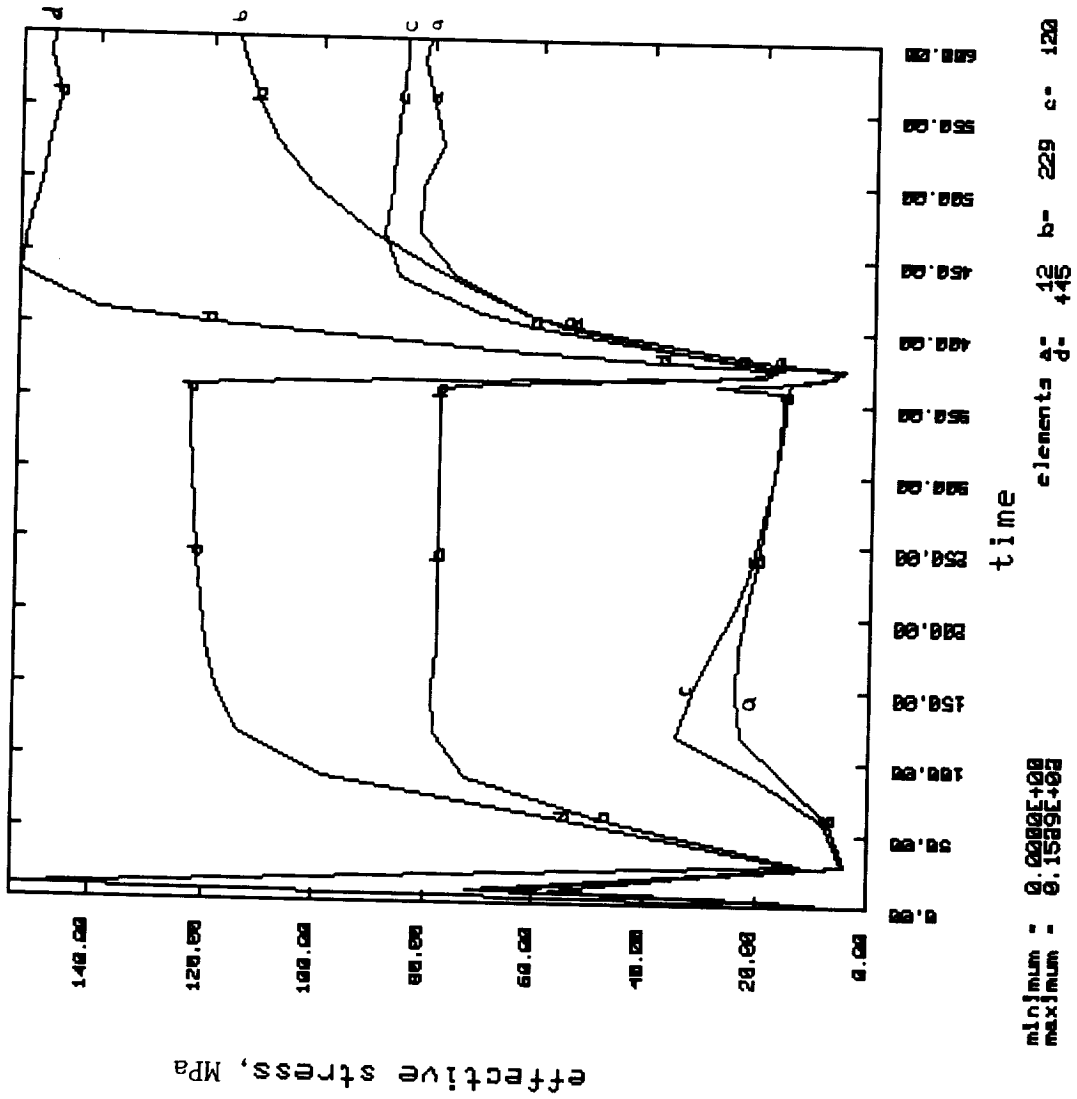


SINE\_1 Interface Baseline Case -  
Radial Stress History Plot.

Figure 4.1.17



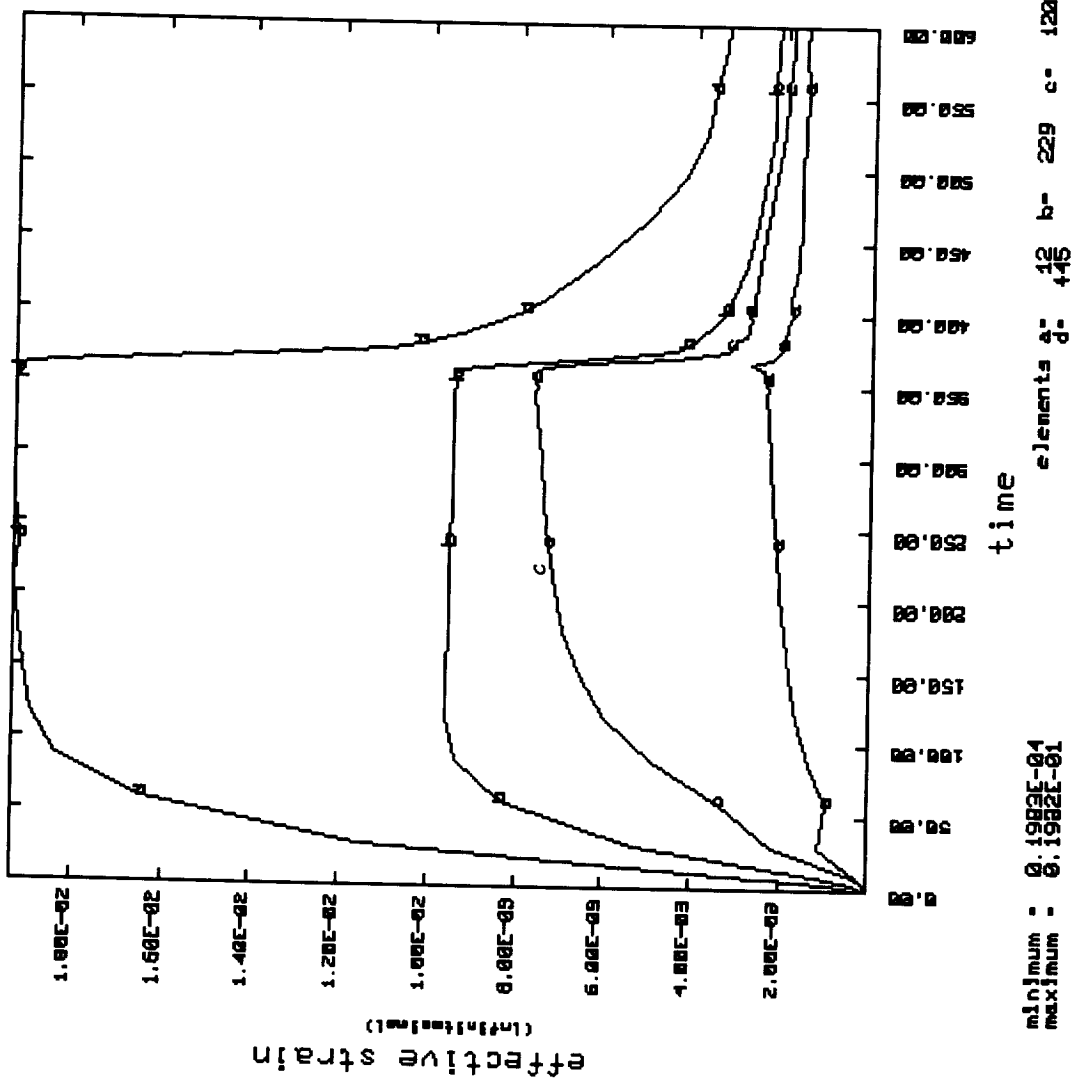
SINE\_1 Interface Geometry:



Effective Stress History Plot.

Figure 4.1.19

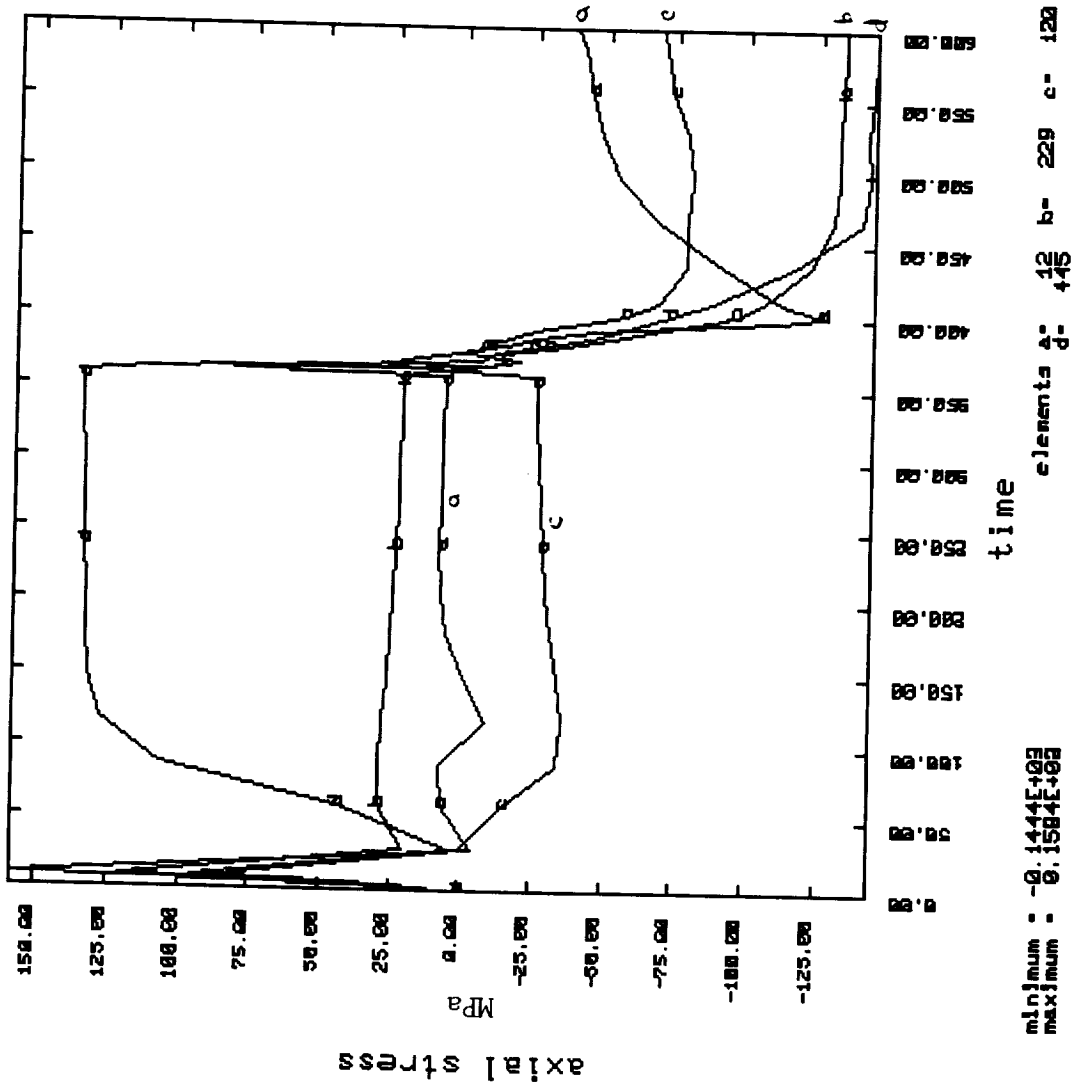
SINE\_1 Interface Geometry:



Effective Strain History Plot.

Figure 4.1.20

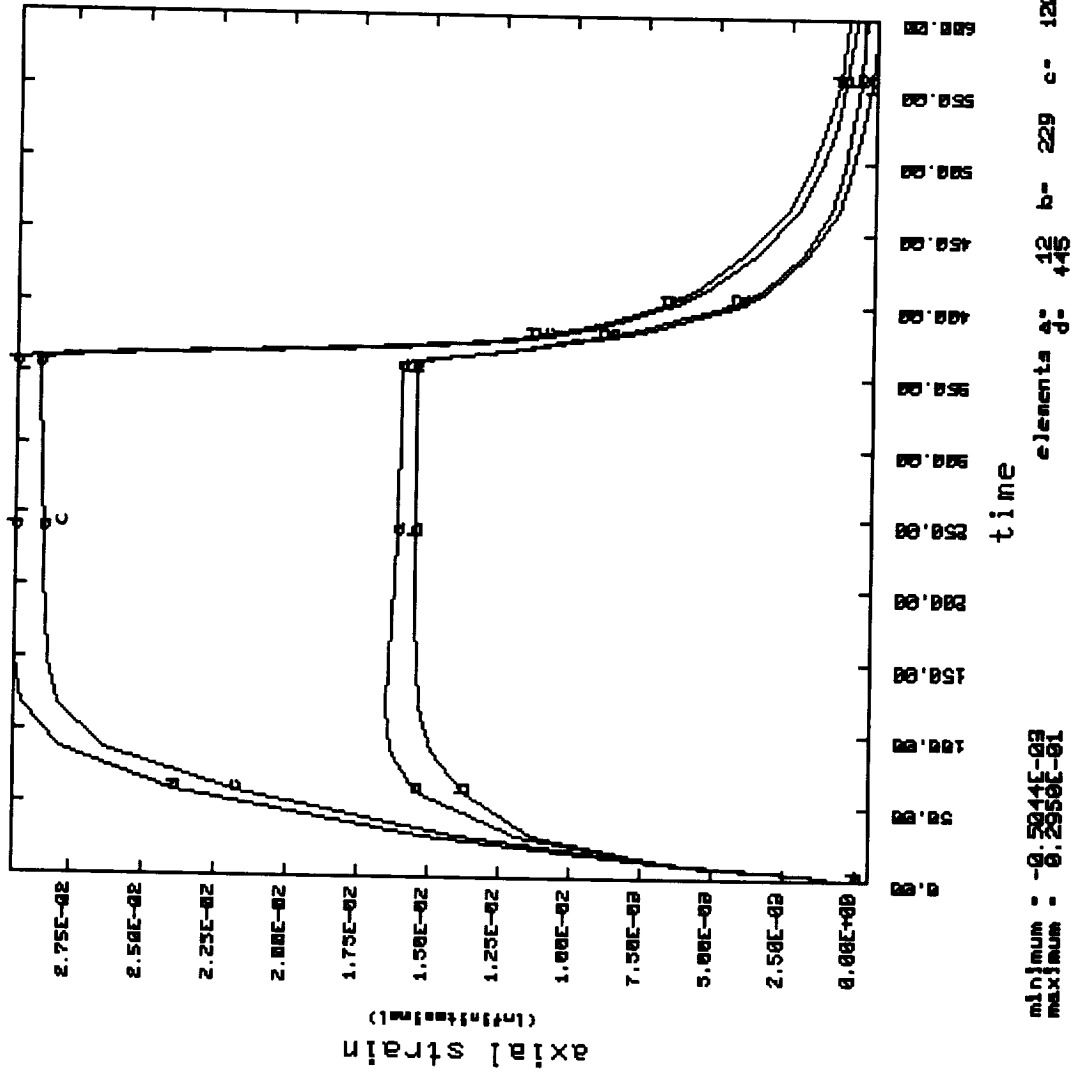
SINE\_1 Geometry, Higher CTE in Bond Coat



SINE\_1 Interface Model with Higher CTE in Bond Coat - Axial Stress History Plot.

Figure 4.1.21

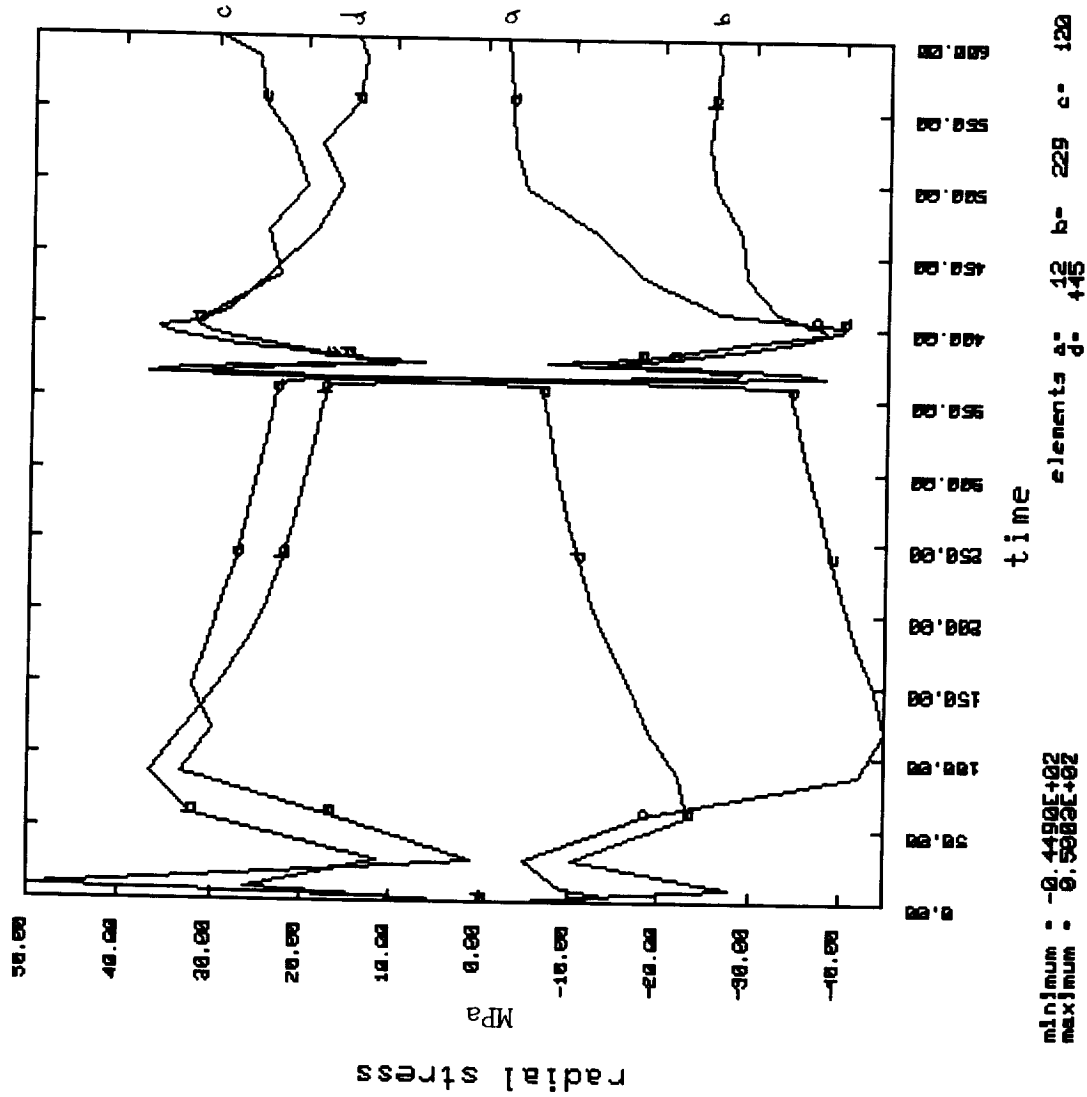
SINE\_1 Geometry, Higher CTE in Bond Coat



SINE\_1 Interface Model with Higher CTE in Bond Coat - Axial Strain History Plot.

Figure 4.1.22

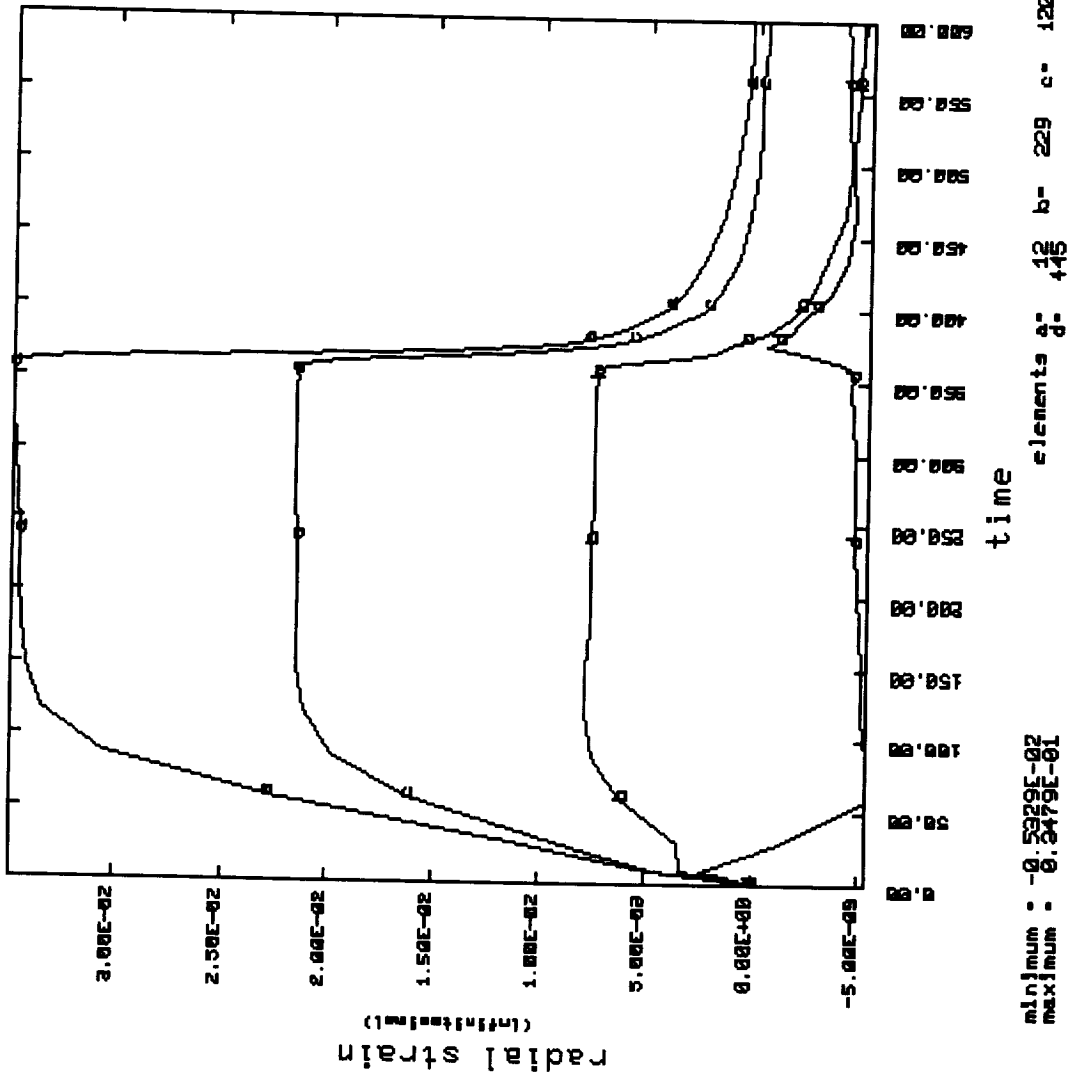
SINE\_1 Geometry, Higher CTE in Bond Coat



SINE\_1 Interface Model with Higher CTE in Bond Coat -  
Radial Stress History Plot.

Figure 4.1.23

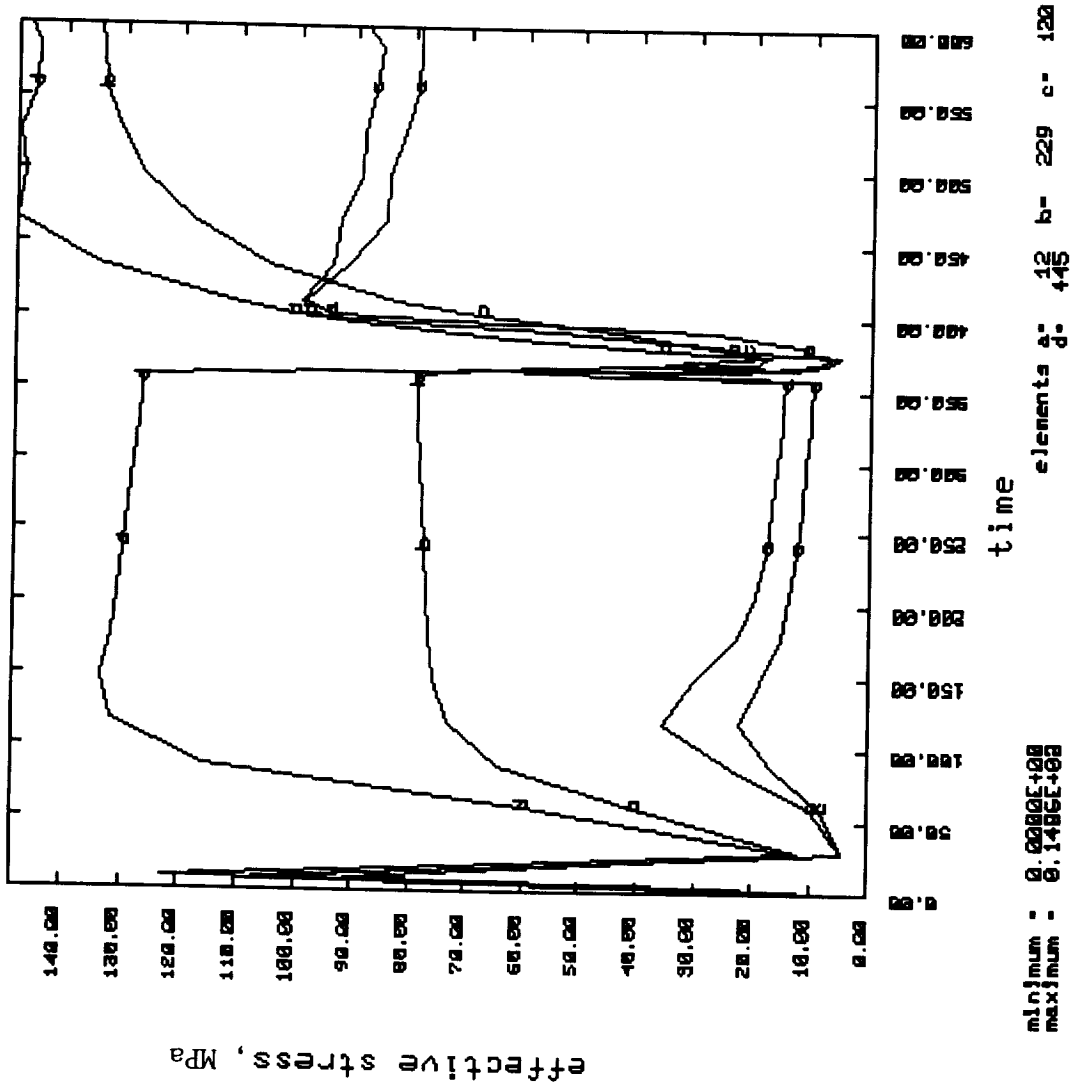
SINE\_1 Geometry, Higher CTE in Bond Coat



SINE\_1 Interface Model with Higher CTE in Bond Coat -  
 Radial Strain History Plot.

Figure 4.1.24

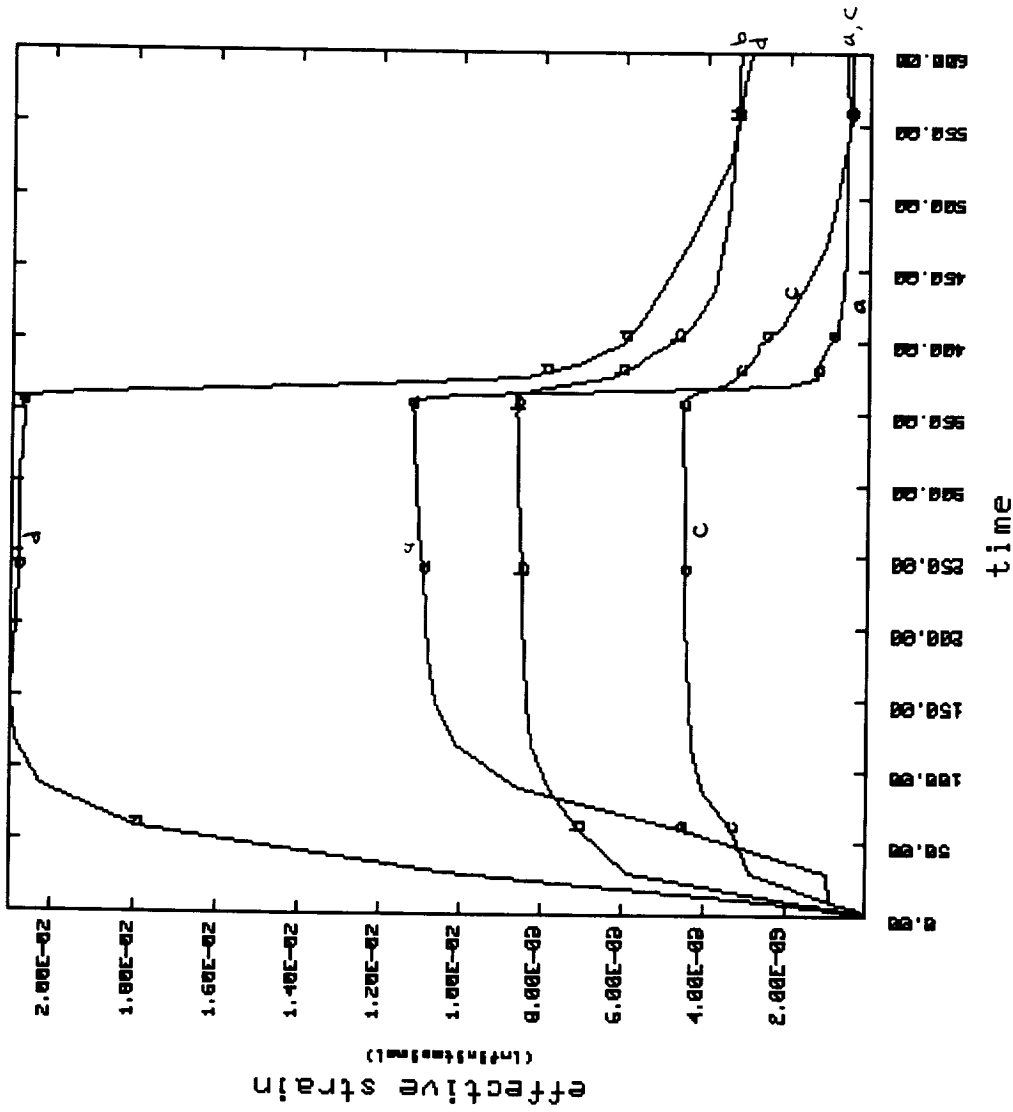
SINE\_1 Interface: Higher CTE in Bond Coat



Effective Stress History Plot.

Figure 4.1.25

SINE\_1 Interface: Higher CTE in Bond Coat



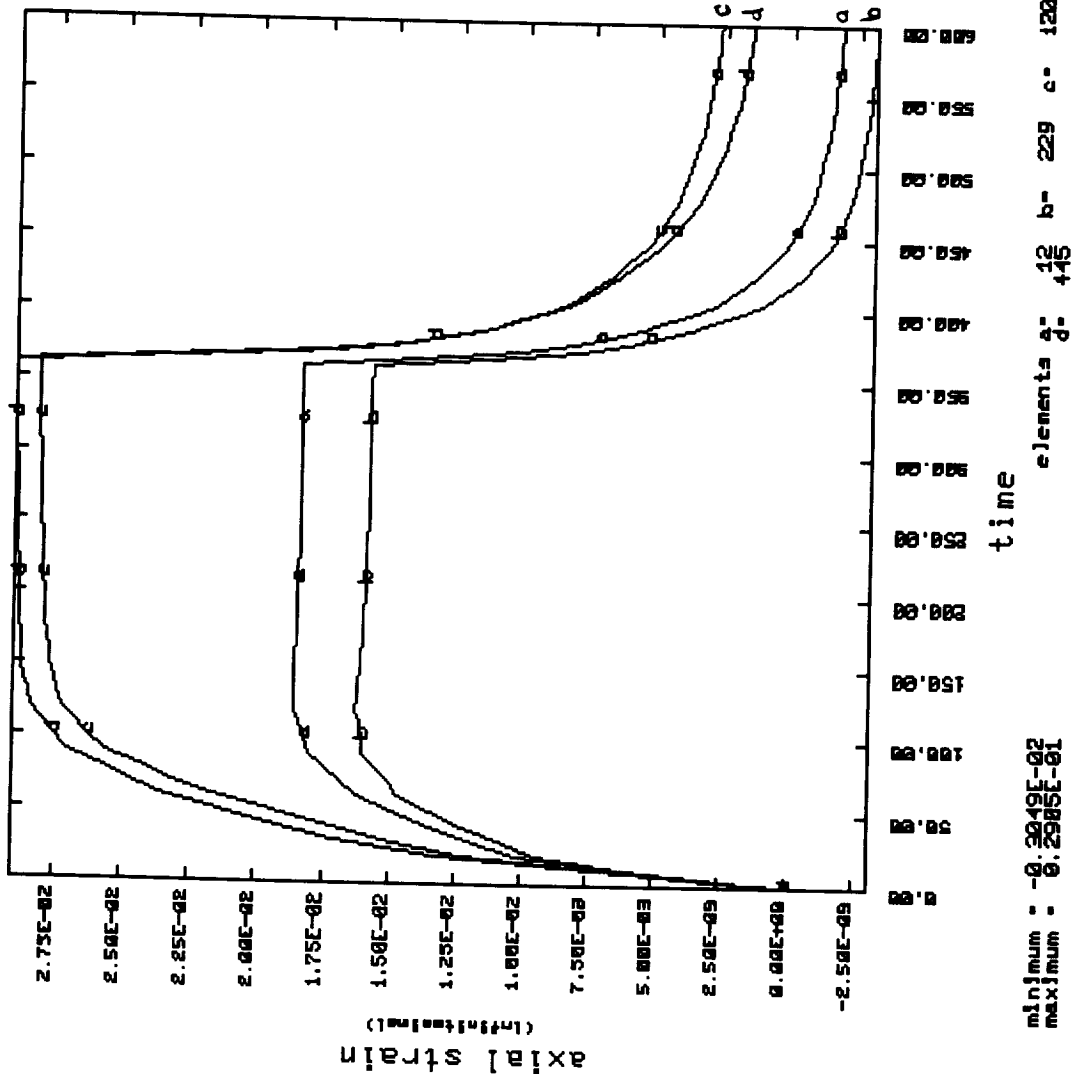
minimum : 0.2030E-04  
 maximum : 0.2180E-01  
 elements a= 12 b= 229 c= 120  
 d= 445

Effective Strain History Plot.

Figure 4.1.26



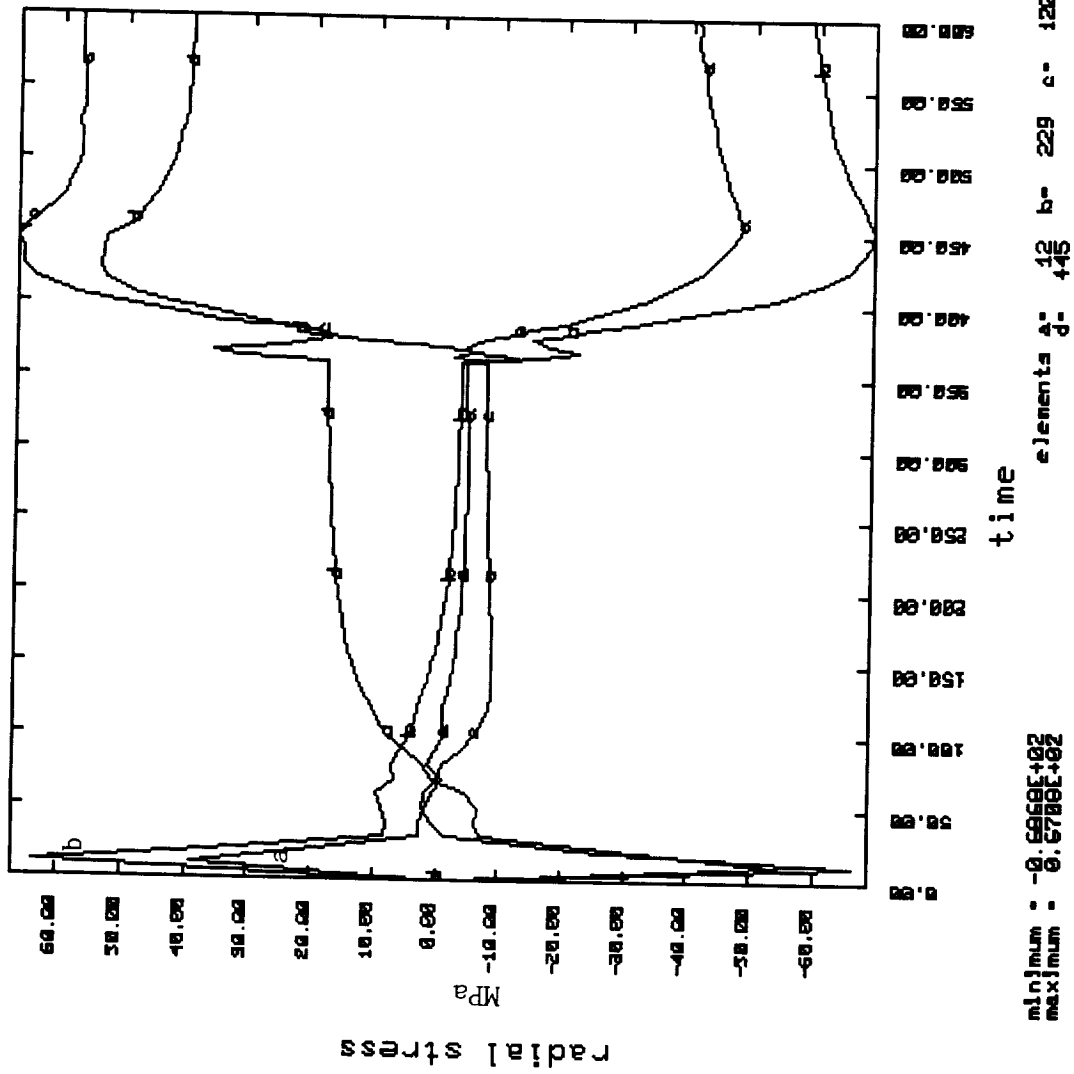
SINE\_1 Interface: Higher Creep Coefficient



SINE\_1 Interface Model with Higher Creep Coefficients - Axial Strain History Plot.

Figure 4.1.28

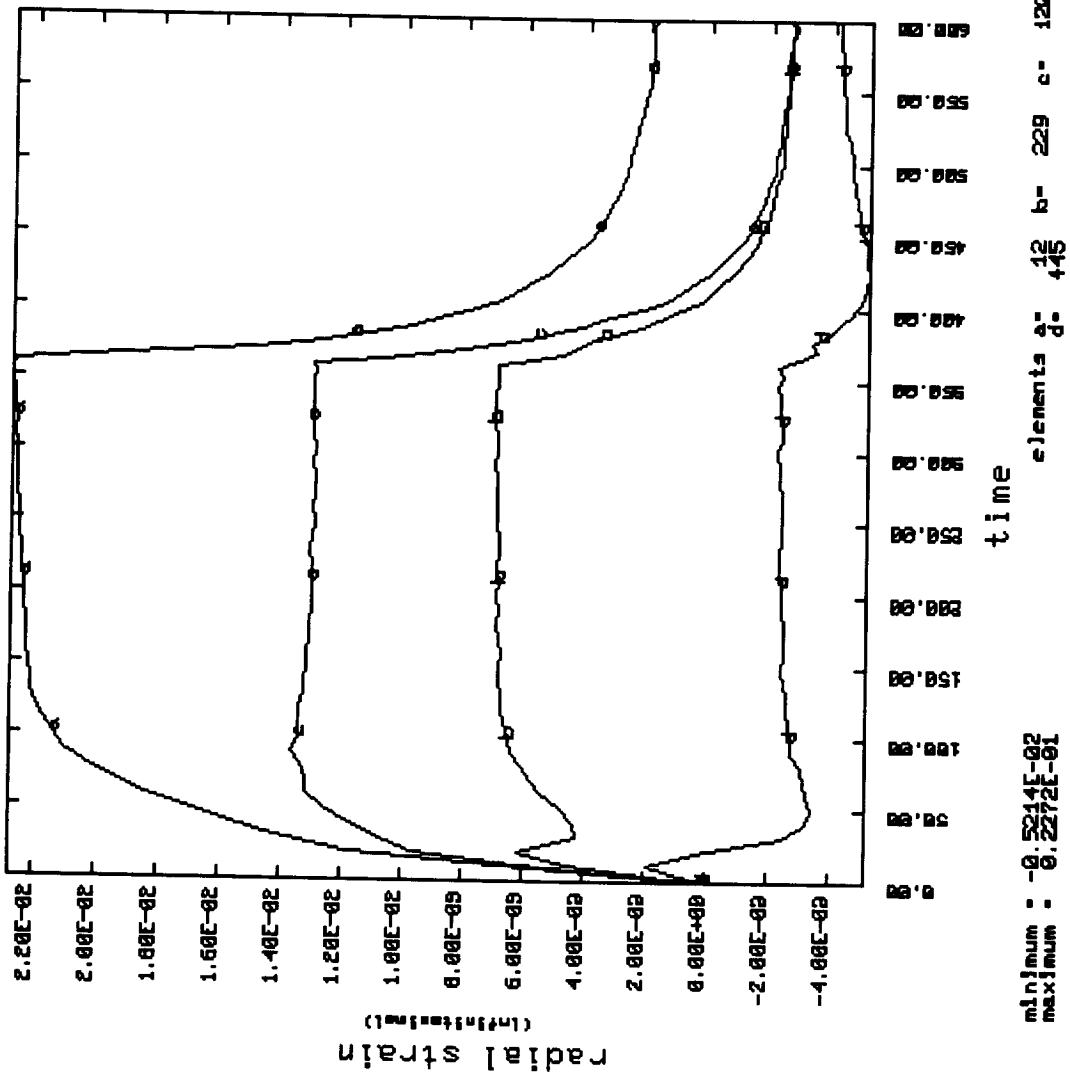
SINE\_1 Interface: Higher Creep Coefficient



SINE\_1 Interface Model with Higher Creep Coefficients -  
Radial Stress History Plot.

Figure 4.1.29

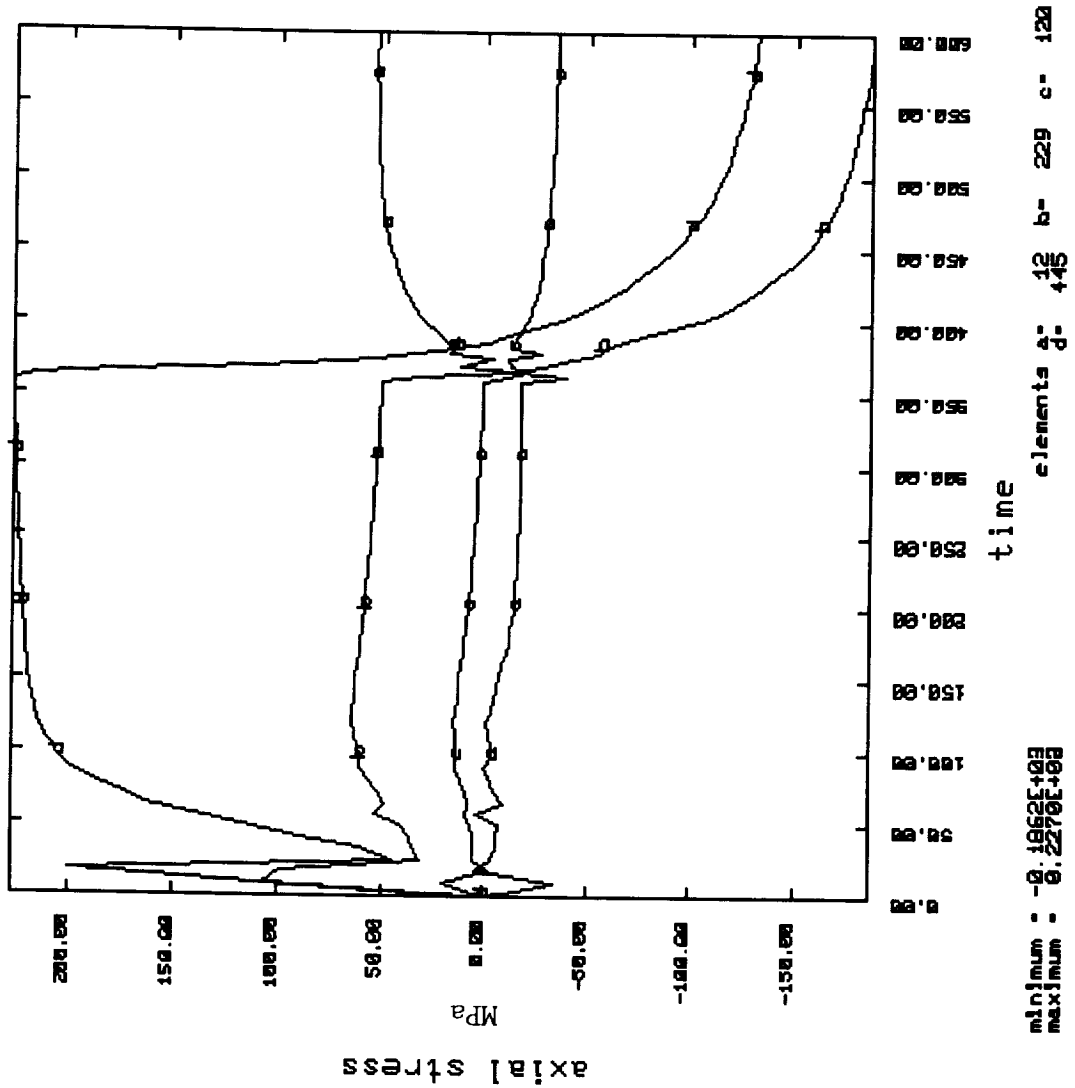
SINE\_1 Interface: Higher Creep Coefficient



SINE\_1 Interface Model with Higher Creep Coefficients -  
 Radial Strain History Plot.

Figure 4.1.30

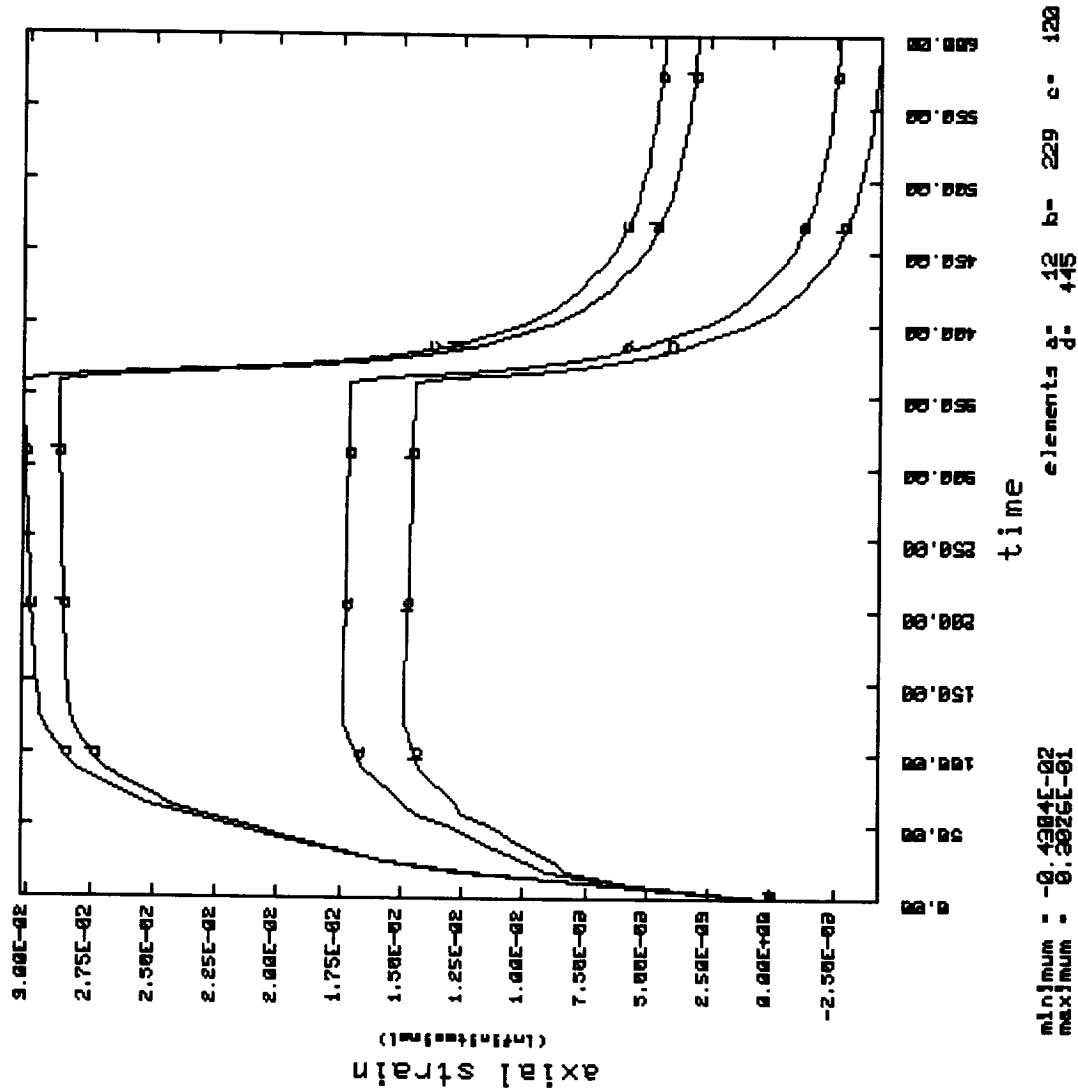
SINE\_1 Interface: Lower B in TBC



SINE\_1 Geometry with Lower B in TBC - Axial Stress History Plot.

Figure 4.1.31

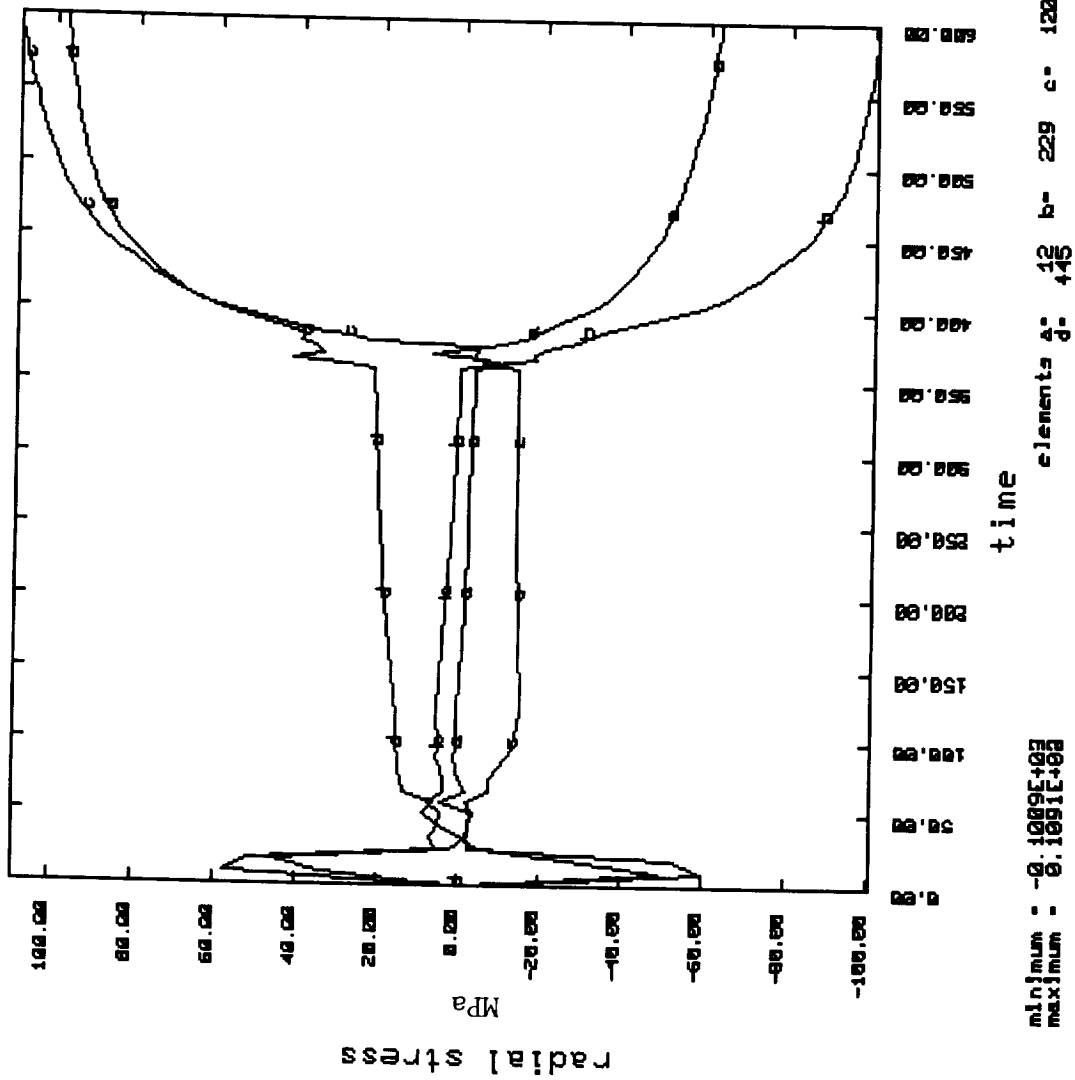
SINE\_1 Interface: Lower B in TBC



SINE\_1 Interface Geometry with Lower B in TBC - Axial Strain History Plot.

Figure 4.1.32

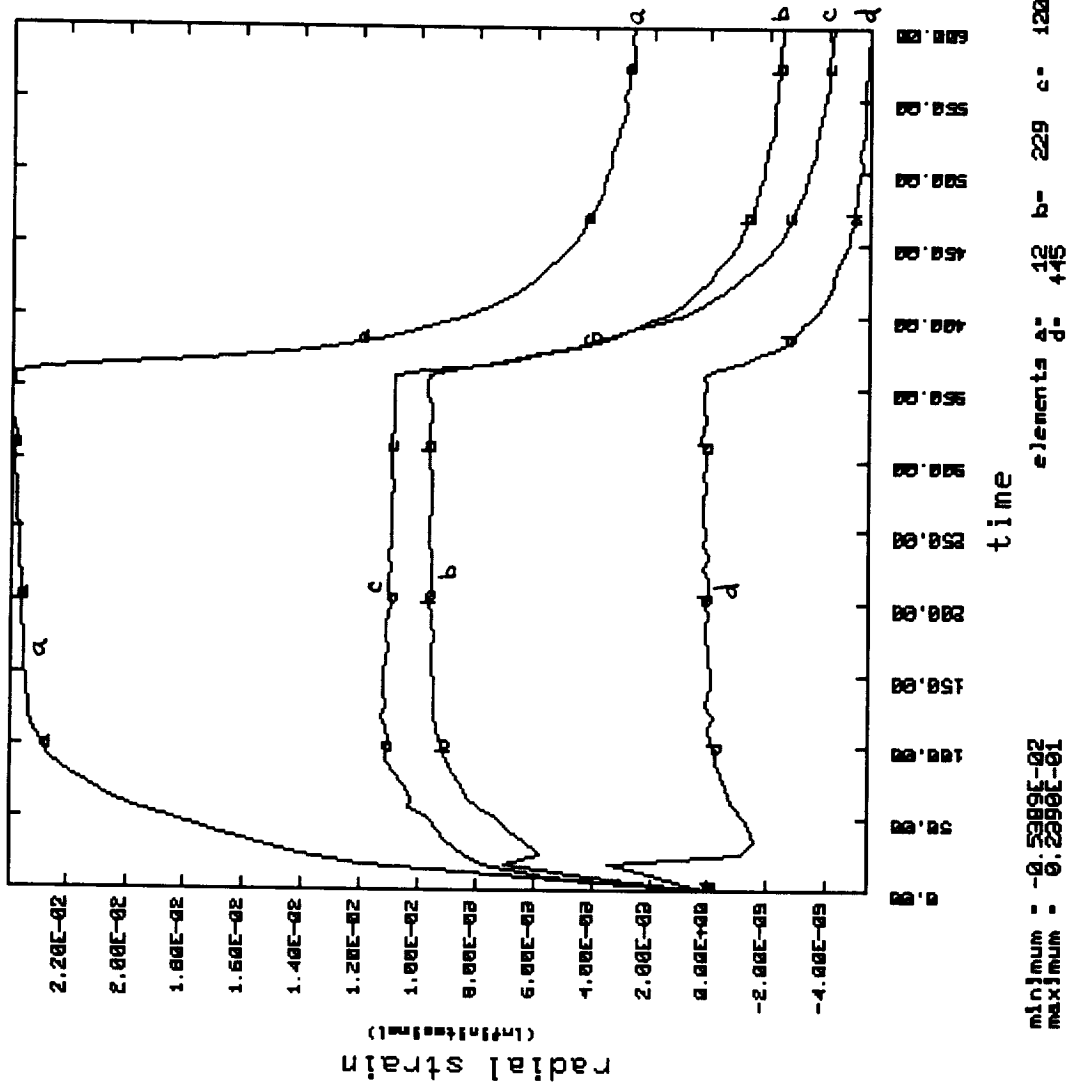
SINE\_1 Interface: Lower B in TBC



SINE\_1 Interface Geometry Model with Lower B in TBC -  
Radial Stress History Plot.

Figure 4.1.33

SINE\_1 Interface: Lower B in TBC



SINE\_1 Interface Geometry Model with Lower B in TBC -  
Radial Strain History Plot.

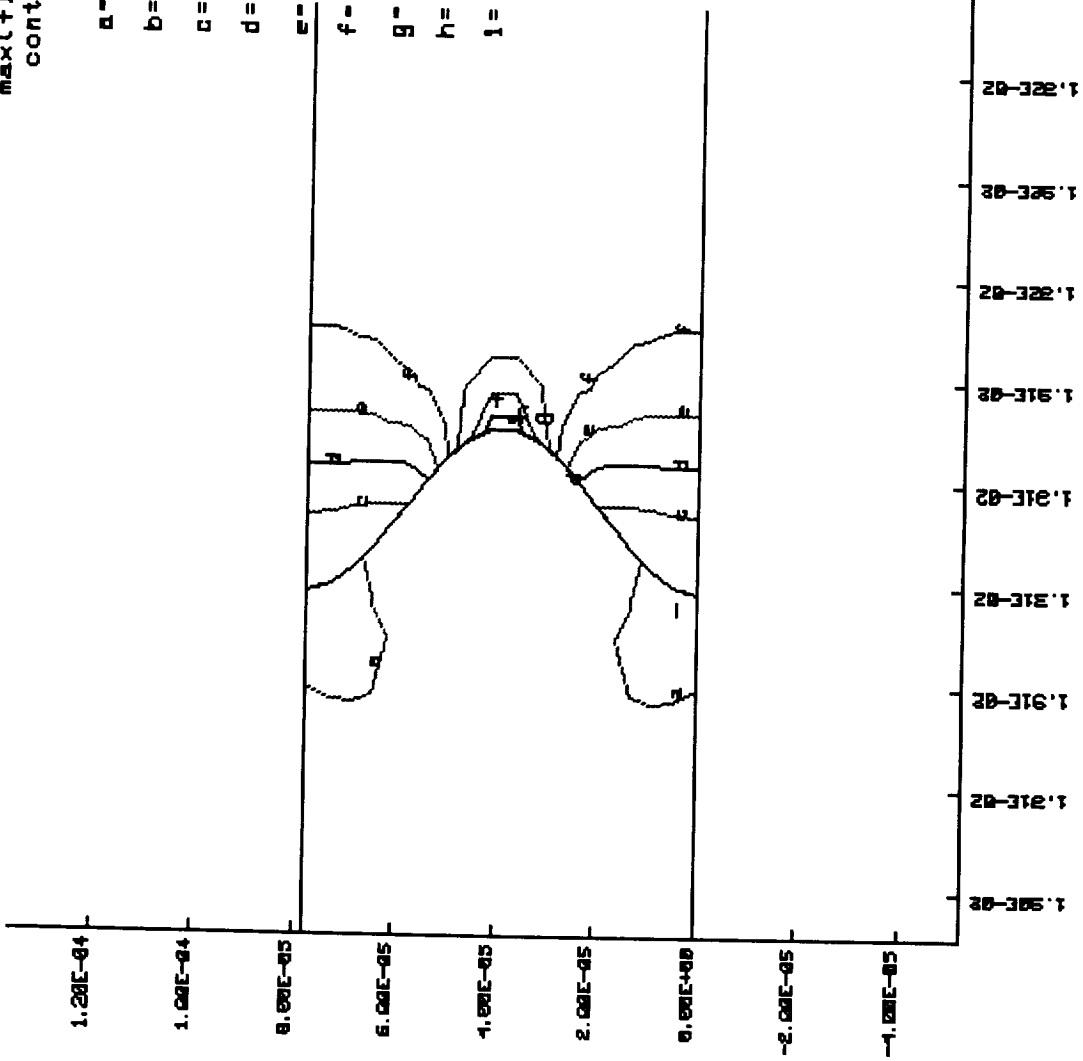
Figure 4.1.34

SINE\_2 Interface: Base Materials, 1.5x amplitude  
 contours of axial stress

time= 0.350000E+03

min(-)=-0.23166E+02  
 max(+)= 0.18276E+03  
 contour levels

- MPa
- a= -0.25700E+01
  - b= 0.18020E+02
  - c= 0.38610E+02
  - d= 0.59210E+02
  - e= 0.79800E+02
  - f= 0.10000E+03
  - g= 0.12100E+03
  - h= 0.14200E+03
  - i= 0.16200E+03



SINE\_2 Interface Geometry Model with Base Materials and 1.5x Amplitude  
 Contour Map of Axial Stress at the Bond Coat/Ceramic Interface.

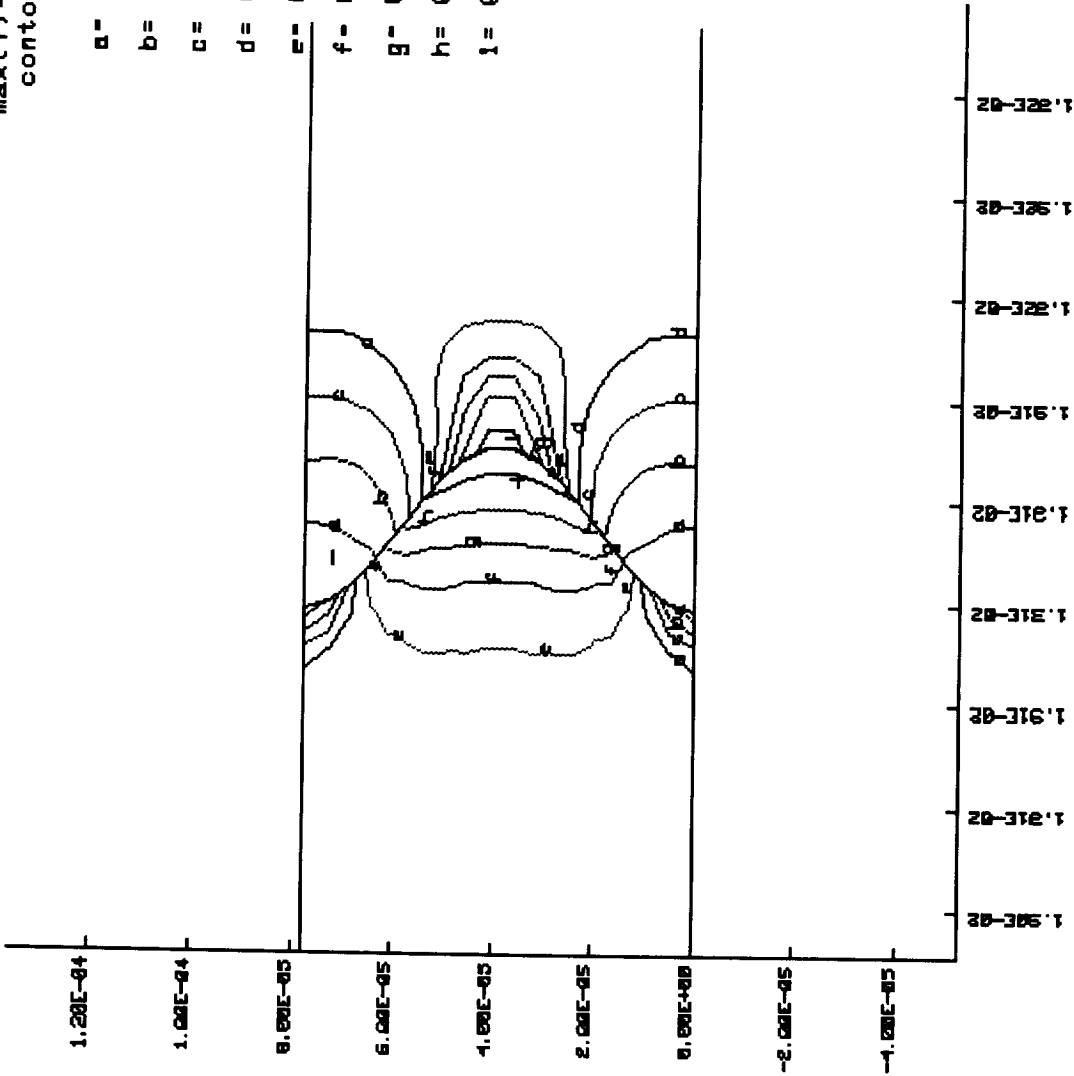
Figure 4.2.1

SINE\_2 Interface: Base Materials, 1.5x amplitude  
 contour of axial strain  
 ( infintimes )

time= 0.35000E+03

min(-) = 0.13566E-01  
 max(+) = 0.32572E-01  
 contour levels

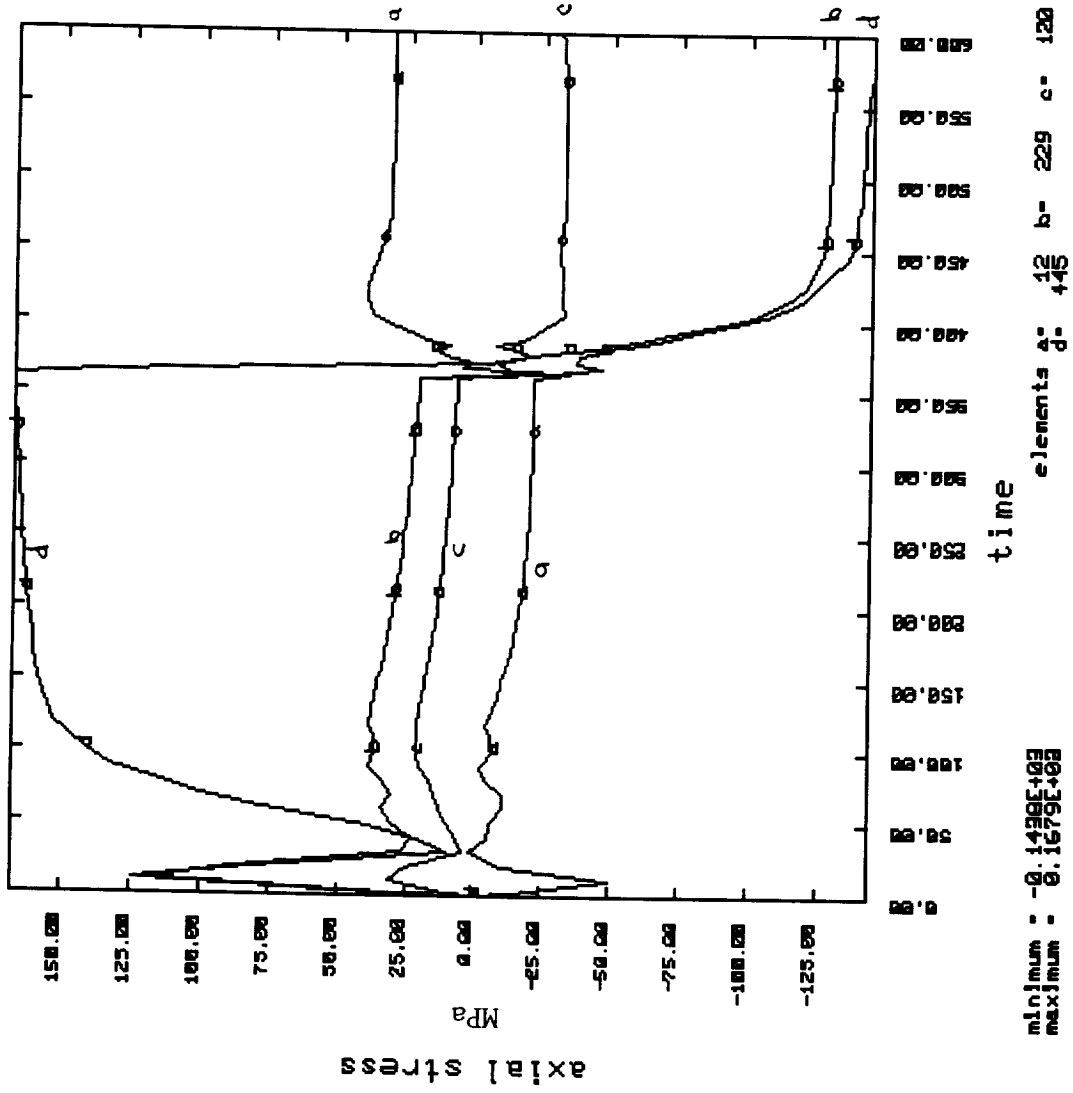
- a= 0.15500E-01
- b= 0.17400E-01
- c= 0.19300E-01
- d= 0.21200E-01
- e= 0.23100E-01
- f= 0.25000E-01
- g= 0.26900E-01
- h= 0.28800E-01
- i= 0.30700E-01



SINE\_2 Interface Geometry Model with Base Materials and 1.5x Amplitude  
 Contour Map of Axial Strain at the Bond Coat/Ceramic Interface.

Figure 4.2.2

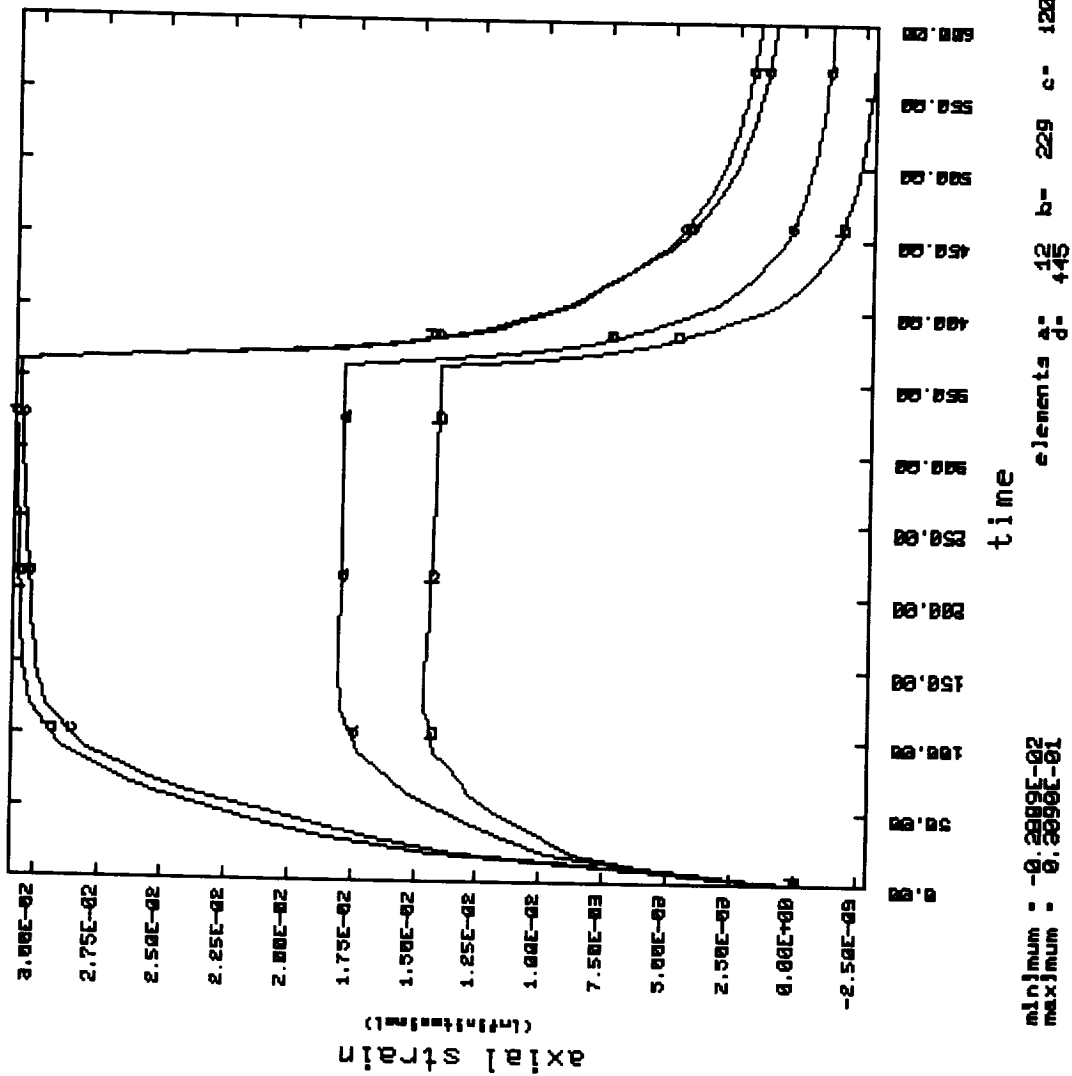
SINE\_2 Interface: Base Materials, 1.5x amplitude



SINE\_2 Interface Model with Base Materials and 1.5x Amplitude - Axial Stress History Plot.

Figure 4.2.3

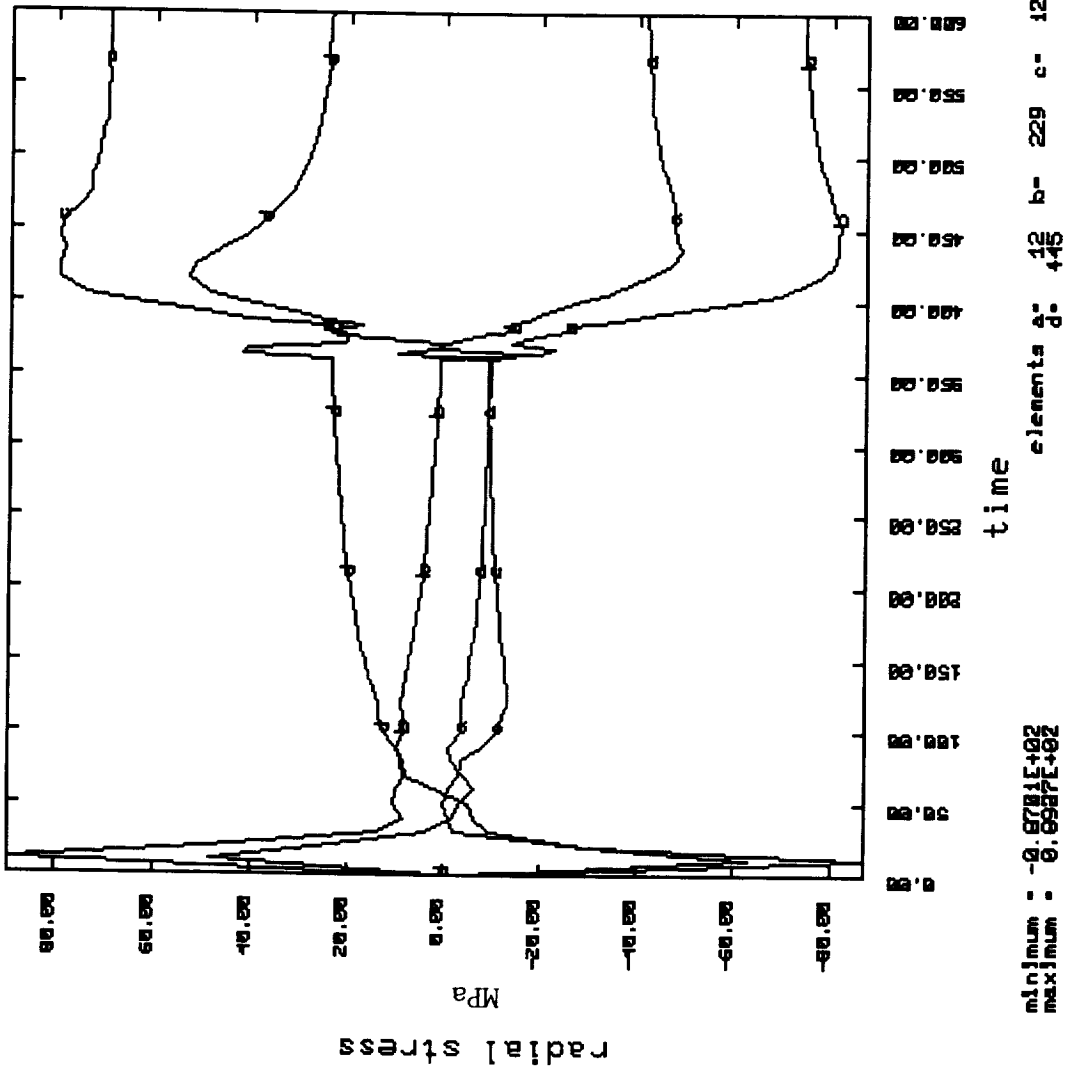
SINE\_2 Interface: Base Materials, 1.5x amplitude



SINE\_2 Interface Model with Base Materials and 1.5x Amplitude - Axial Strain History Plot.

Figure 4.2.4

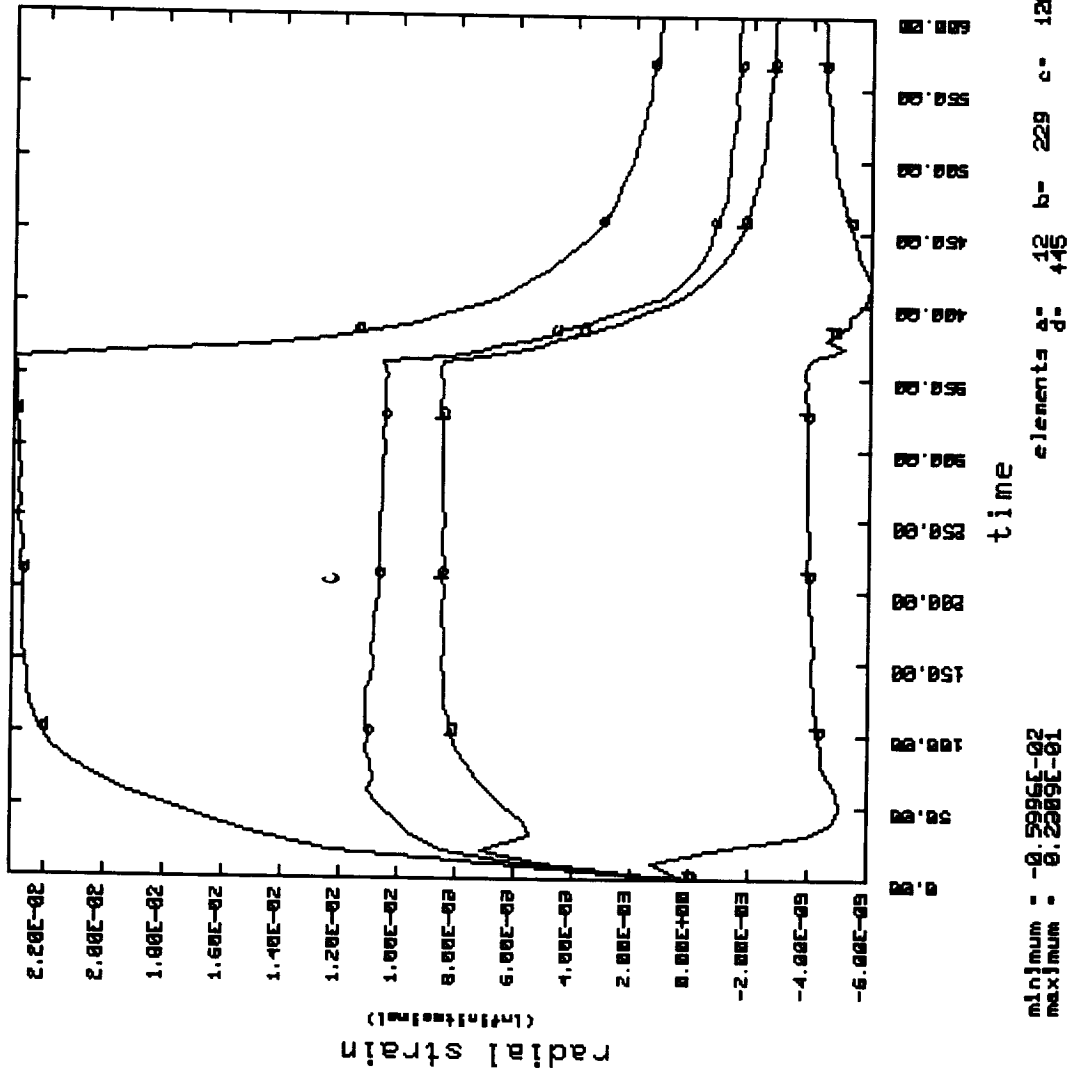
SINE\_2 Interface: Base Materials, 1.5x amplitude



SINE\_2 Interface Model with Base Materials and 1.5x Amplitude -  
Radial Stress History Plot.

Figure 4.2.5

SINE\_2 Interface: Base Materials, 1.5x amplitude



SINE\_2 Interface Model with Base Materials and 1.5x Amplitude -  
Radial Strain History Plot.

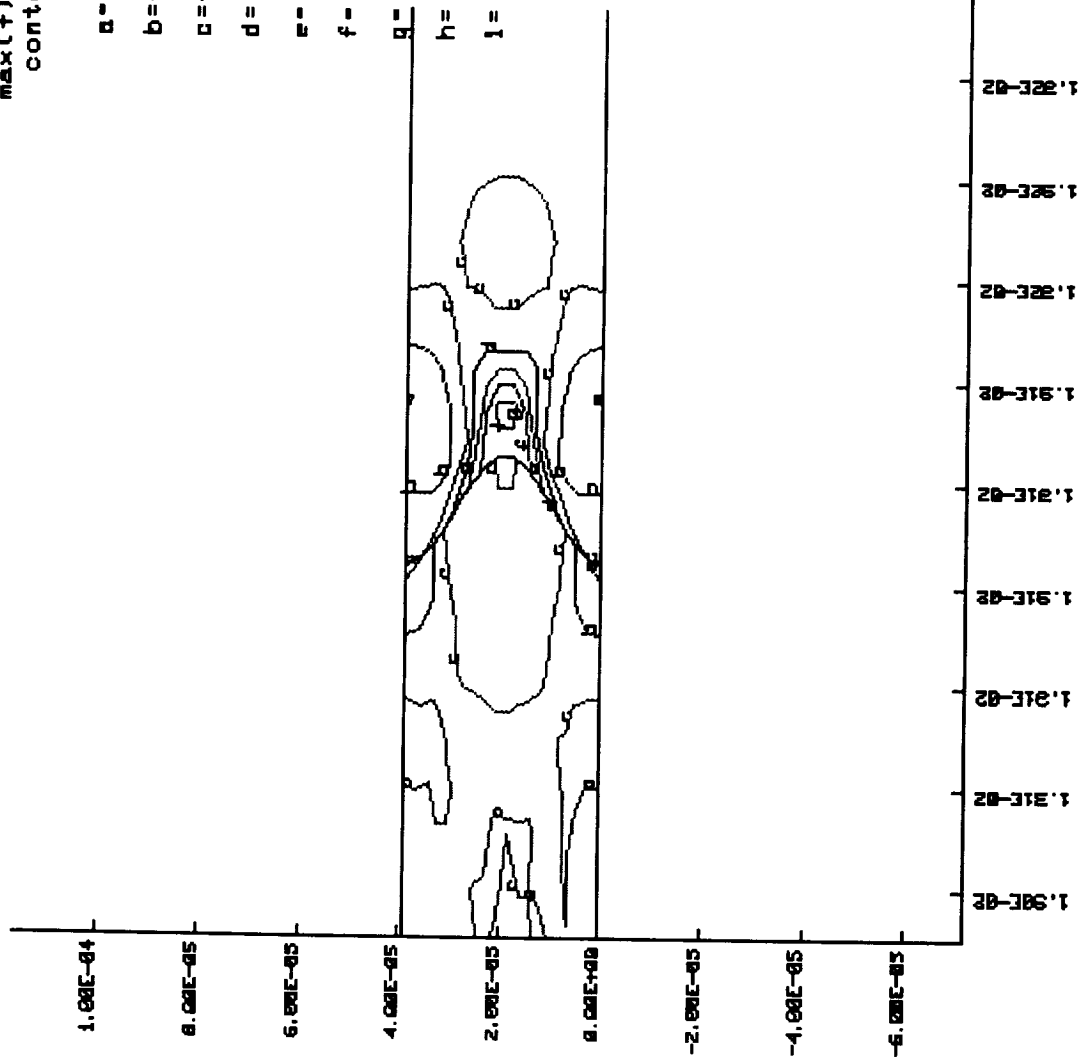
Figure 4.2.6

SINE\_3 Interface: Base Materials, 2x frequency  
 contours of radial stress

time= 0.35000E+03

min(-)=-0.17640E+02  
 max(+)= 0.35581E+02  
 contour levels

- MPa
- a=-0.12320E+02
  - b=-0.70000E+01
  - c=-0.16700E+01
  - d= 0.36500E+01
  - e= 0.89700E+01
  - f= 0.14290E+02
  - g= 0.19610E+02
  - h= 0.24940E+02
  - i= 0.30260E+02



SINE\_3 Interface Geometry with Base Materials and 2x Frequency -  
 Contour Map of Radial Stress at the Bond Coat/Ceramic Interface.

Figure 4.3.1

SINE\_3 Interface: Base Materials, 2x frequency  
 contours of radial strain  
 (infintesimal)

time= 0.35000E+03

min(-)=-0.30326E-02  
 max(+)= 0.22812E-01  
 contour levels

1.00E-04  
 8.00E-05  
 6.00E-05  
 4.00E-05  
 2.00E-05  
 0.00E+00  
 -2.00E-05  
 -4.00E-05  
 -6.00E-05

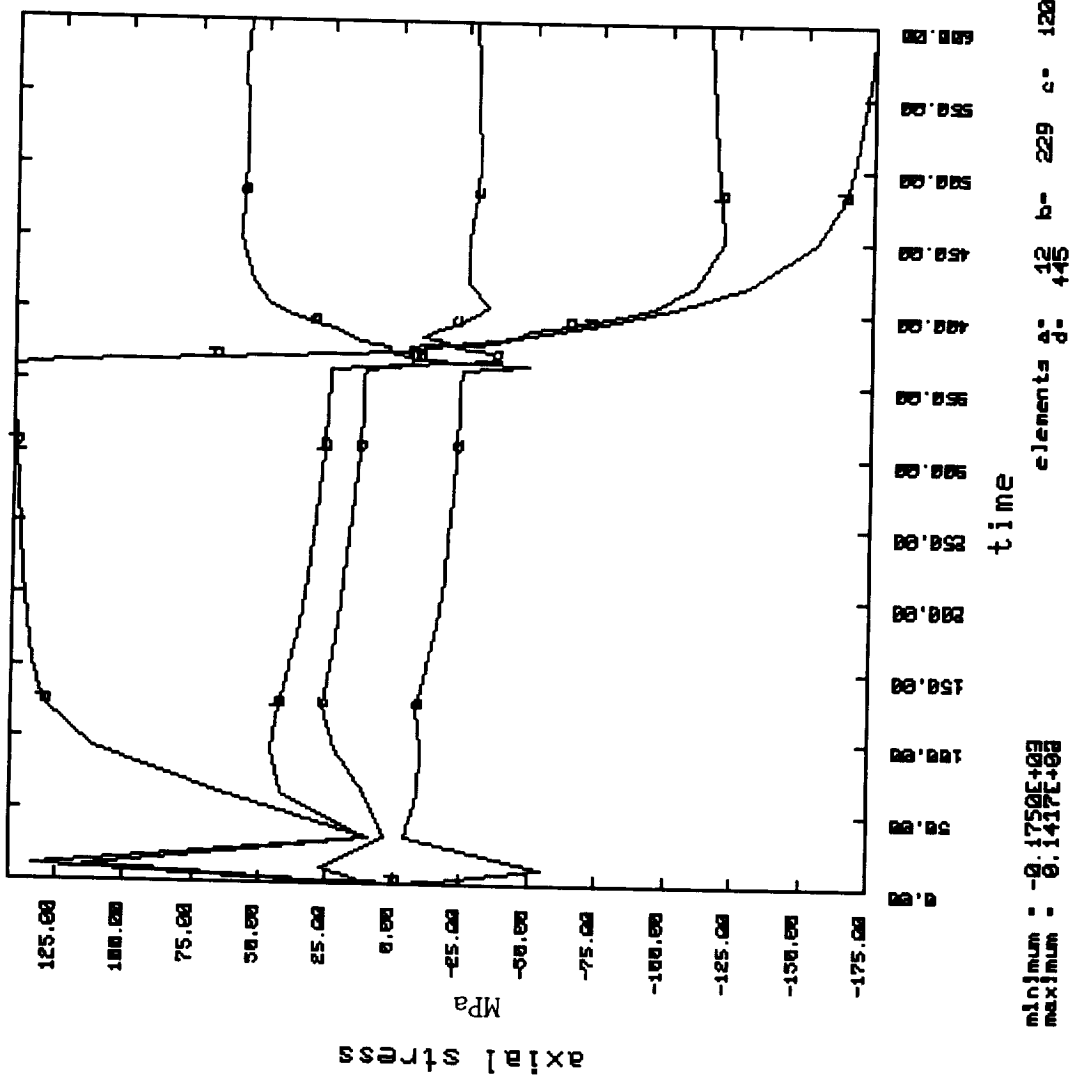
a=-0.44800E-03  
 b= 0.21360E-02  
 c= 0.47210E-02  
 d= 0.73050E-02  
 e= 0.98900E-02  
 f= 0.12500E-01  
 g= 0.15100E-01  
 h= 0.17600E-01  
 i= 0.20200E-01

1.30E-02  
 1.31E-02  
 1.32E-02  
 1.33E-02  
 1.34E-02  
 1.35E-02  
 1.36E-02  
 1.37E-02  
 1.38E-02  
 1.39E-02  
 1.40E-02  
 1.41E-02  
 1.42E-02  
 1.43E-02  
 1.44E-02  
 1.45E-02  
 1.46E-02  
 1.47E-02  
 1.48E-02  
 1.49E-02  
 1.50E-02  
 1.51E-02  
 1.52E-02  
 1.53E-02  
 1.54E-02  
 1.55E-02  
 1.56E-02  
 1.57E-02  
 1.58E-02  
 1.59E-02  
 1.60E-02  
 1.61E-02  
 1.62E-02  
 1.63E-02  
 1.64E-02  
 1.65E-02  
 1.66E-02  
 1.67E-02  
 1.68E-02  
 1.69E-02  
 1.70E-02  
 1.71E-02  
 1.72E-02  
 1.73E-02  
 1.74E-02  
 1.75E-02  
 1.76E-02  
 1.77E-02  
 1.78E-02  
 1.79E-02  
 1.80E-02  
 1.81E-02  
 1.82E-02  
 1.83E-02  
 1.84E-02  
 1.85E-02  
 1.86E-02  
 1.87E-02  
 1.88E-02  
 1.89E-02  
 1.90E-02  
 1.91E-02  
 1.92E-02

SINE\_3 Interface Geometry with Base Materials and 2x Frequency -  
 Contour Map of Radial Strain at the Bond Coat/Ceramic Interface.

Figure 4.3.2

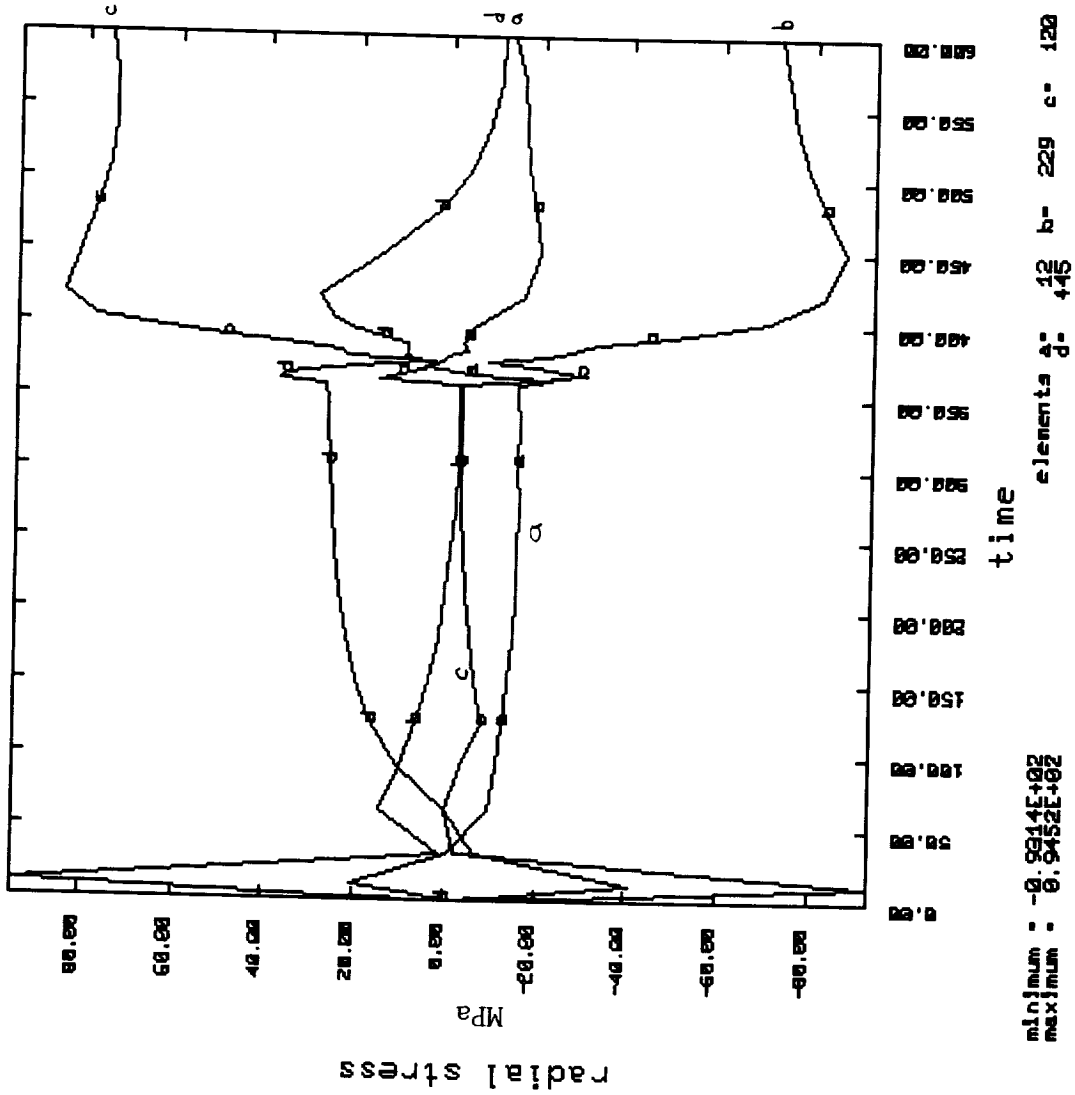
SINE\_3 Interface: Base Materials, 2x frequency



SINE\_3 Interface Geometry with Base Materials and 2x Frequency -  
Axial Stress History Plot.

Figure 4.3.3

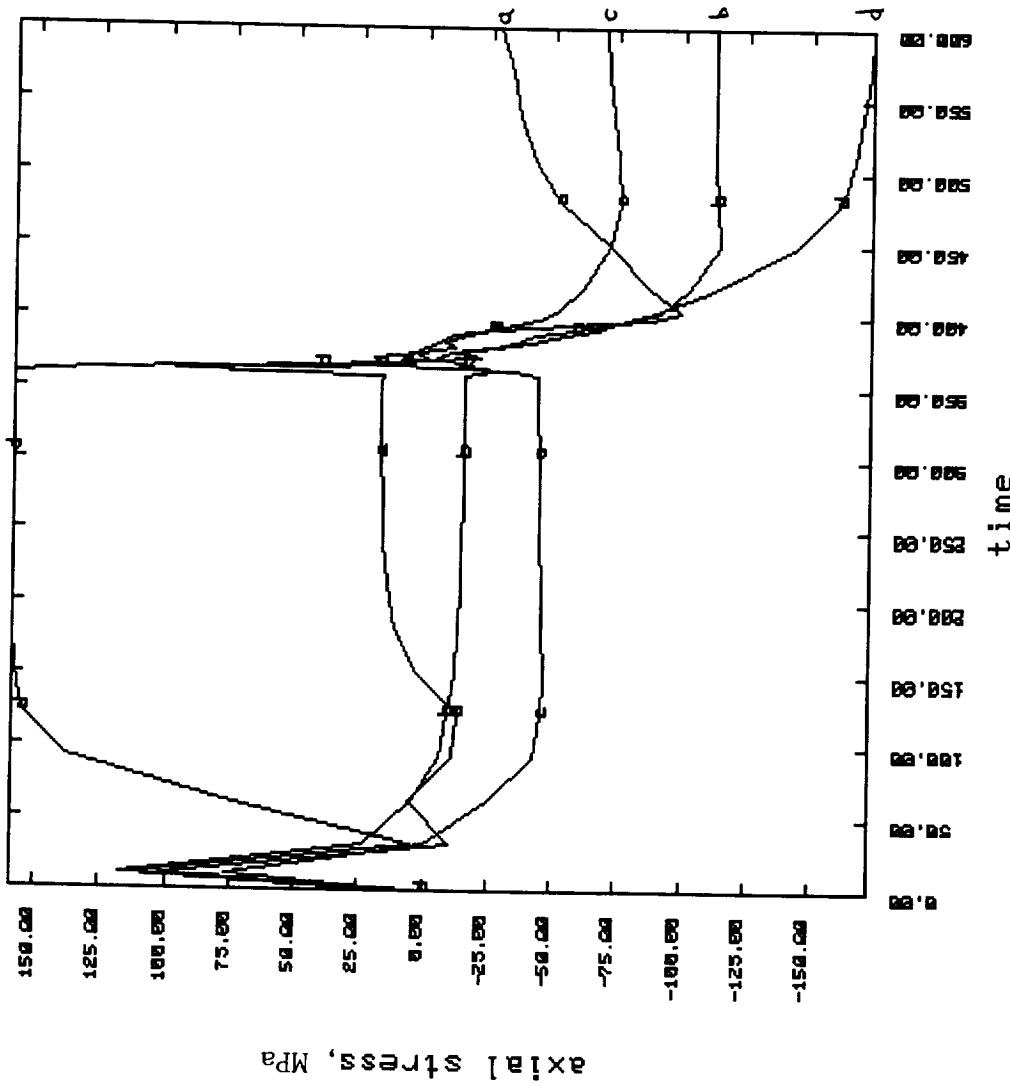
SINE\_3 Interface: Base Materials, 2x frequency



SINE\_3 Interface Geometry with Base Materials and 2x Frequency -  
Radial Stress History Plot.

Figure 4.3.4

SINE\_3 Interface: Higher DC CTE, 2x freq.

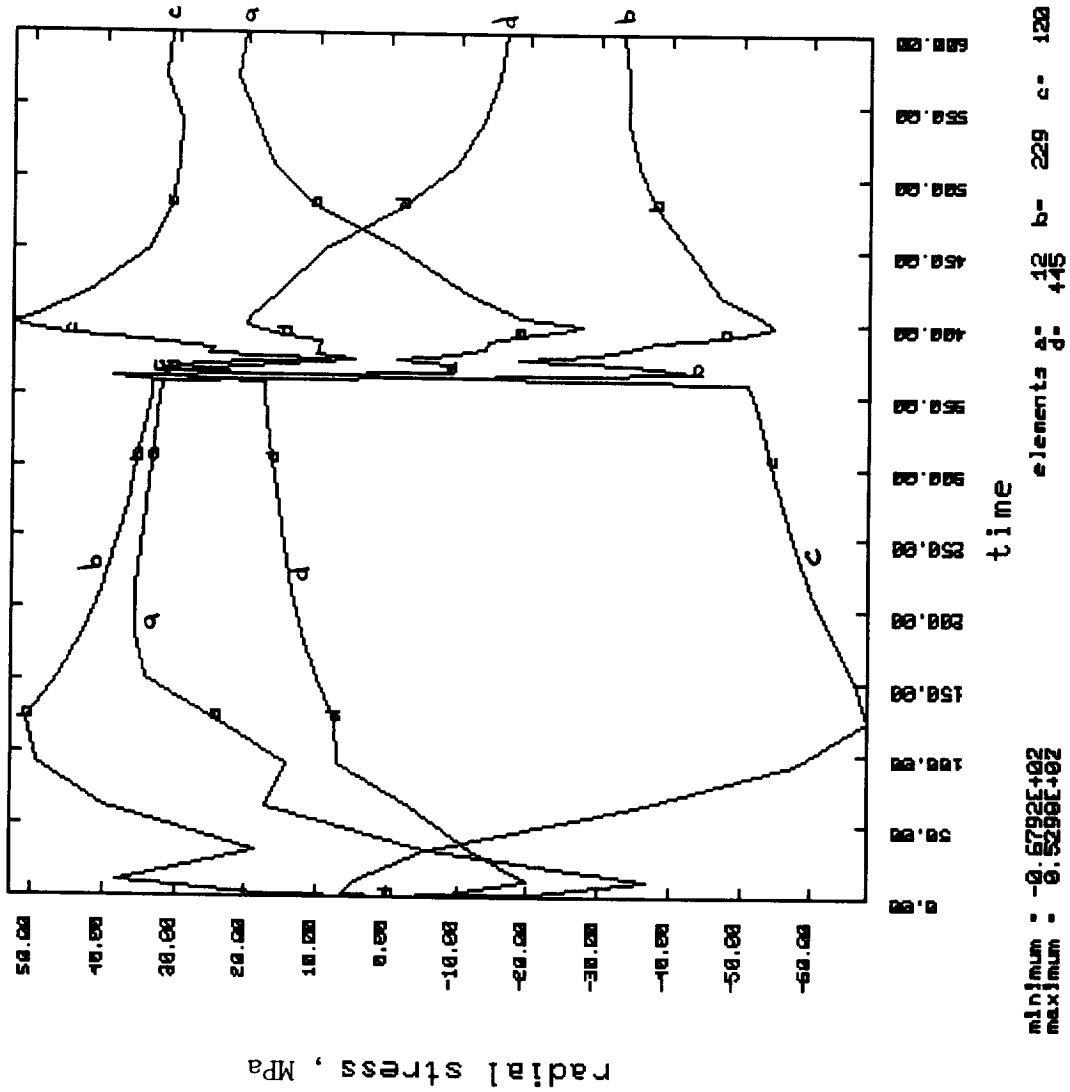


minimum = -0.1722E+03  
 maximum = 0.1592E+03  
 elements a= 12 b= 229 c= 120  
 d= 445

Axial Stress History Plot.

Figure 4.3.5

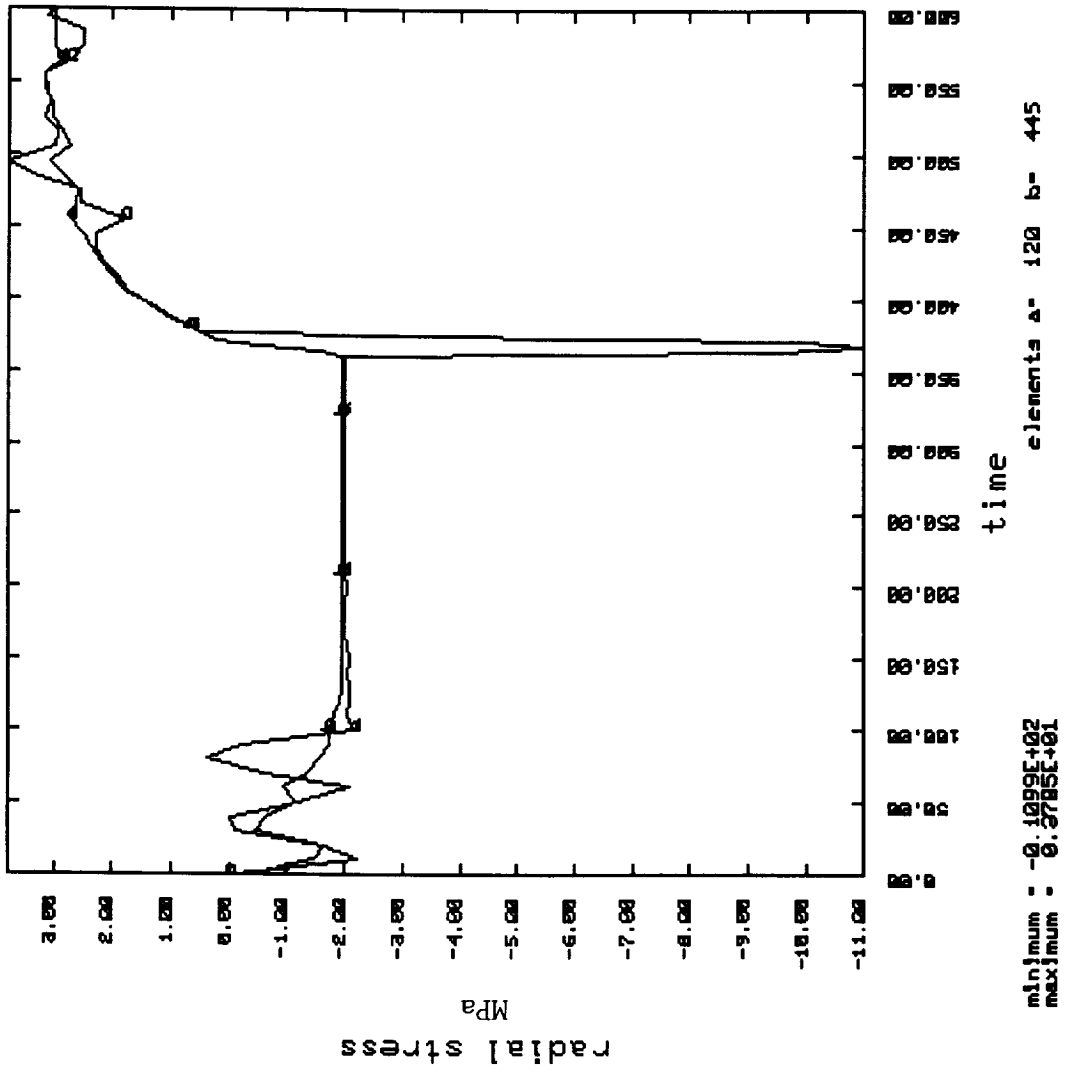
SINE\_3 Interface: Higher BC CTE, 2x freq.



Radial Stress History Plot.

Figure 4.3.6

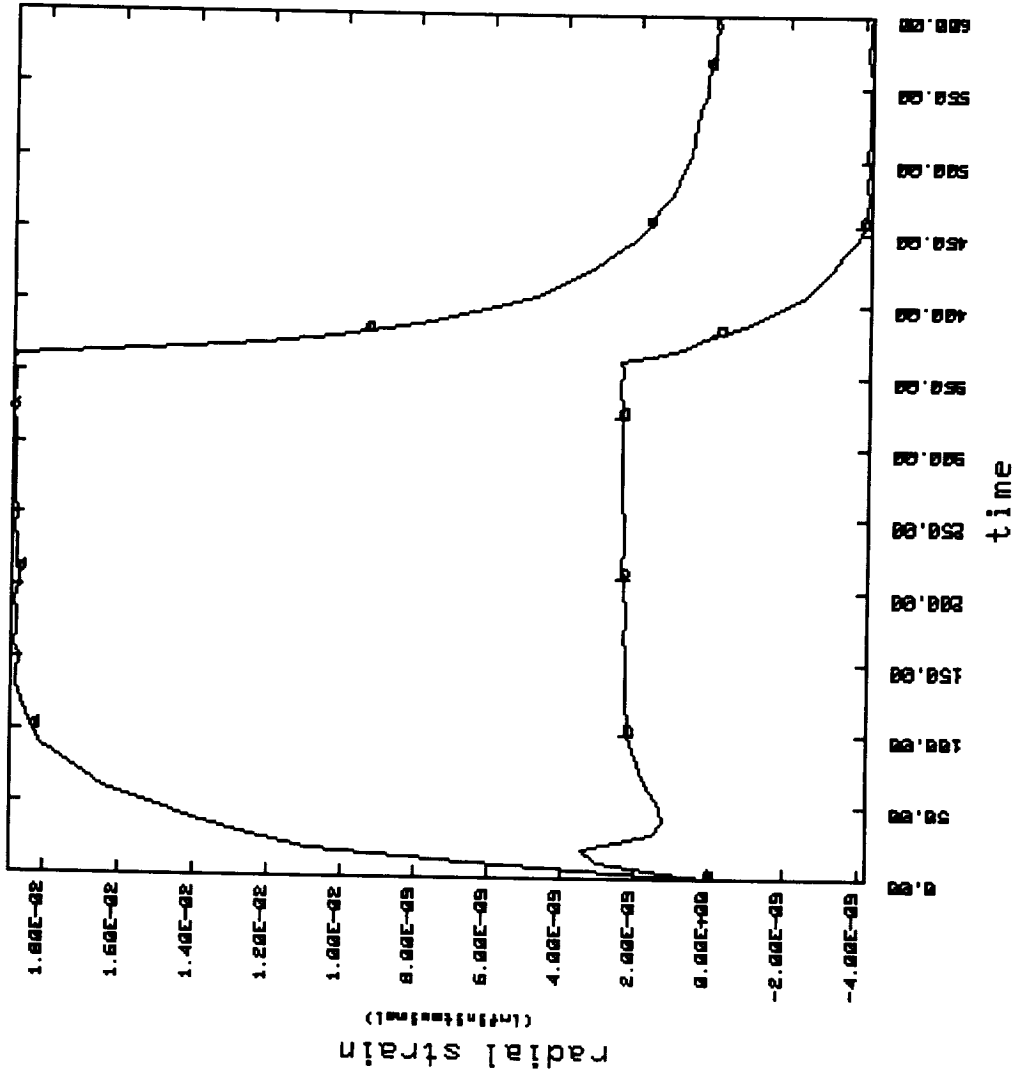
NASA [nB\_0b]



Smooth Interface Model - Radial Stress History Plot.

Figure 4.4.1

NASA [nB\_0b]



minimum : -8.4190E-02  
maximum : 8.1092E-01

Smooth Interface Model - Radial Strain History Plot.

Figure 4.4.2

## Appendix A

### Creep Models Implemented in NIKE2D

#### Model 8 - Thermoelastic-Creep

The material model used in this project and is based on the work of Krieg (1977). The creep rate is given by an equation of the form:

$$\dot{\epsilon} = a|\sigma|^b$$

where  $\dot{\epsilon}$  is the instantaneous creep rate,  
 $\sigma$  is the effective stress, and  
 $a, b$  are temperature dependent material parameters.

Additionally, the shear (G) and bulk (K) moduli are also entered as functions of temperature. Thermal expansion effects are accounted for through the inclusion of temperature dependent secant coefficients of thermal expansion ( $\alpha$ ).

#### Model 11 - Unified Creep Plasticity

Model 11 is a version of a unified creep plasticity model. The model requires a large number of constants and, as implemented, is temperature dependent only the extent that the heat of deformation is taken into consideration. The model has the following form:

$$\sigma = [E / (1 + \nu)] (1 - 2\nu) \text{tr}(\epsilon) + (E / (1 + \nu)) (\epsilon - \epsilon^P),$$

where  $\epsilon^P = f(T) \sinh[(|\dot{\epsilon} - Y(T)| - Y(T)] / V(T)] / |\dot{\epsilon} - Y(T)|$

$$\begin{aligned} \alpha &= k(T) (1 - \beta) \epsilon^P - (g(T) + h(T) |\epsilon^P|) |\alpha| / (1 - \beta) \\ &= k(T) \beta |\epsilon^P| - (g(T) + h(T) |\epsilon^P|)^2 \\ &= s - \alpha \end{aligned}$$

$$V(T) = C_1 \exp(-C_2/T) \quad (\text{rate dependent yield stress})$$

$$Y(T) = C_3 \exp(C_4/T) \quad (\text{rate independent yield stress})$$

$$f(T) = C_5 \exp(-C_6/T) \quad (\text{transition to rate dependency})$$

$$h(T) = C_7 \exp(-C_8/T) \quad (\text{hardening})$$

$$k(T) = C_9 \exp(-C_{10}/T) \quad (\text{dynamic recovery})$$

$$g(T) = C_{11} \exp(-C_{12}/T) \quad (\text{diffusion controlled static or thermal recovery})$$

$$T = (0.95 / C_v) \sigma \epsilon P$$

No attempt has been made to use this model due to the difficulty of locating data for the numerous constants required.

### Model 23 - Primary, Secondary, Tertiary Creep

Model 23, an isothermal primary, secondary, and tertiary creep model has a form of:

$$\epsilon = a \sigma^n t^m$$

where  $\epsilon$  is the effective creep,  
 $\sigma$  is the effective stress,  
 $t$  is effective time, and  
 $a$ ,  $n$ , and  $m$  are material parameters.

The parameter  $m$  dictates which regime the model represents, primary creep for  $m < 1$ , secondary for  $m = 1$ , and tertiary for  $m < 1$ .

A modification to this model provided for the temperature dependence of  $a$ ,  $n$ ,  $Y$ , and  $p_r$ , and the introduction of a temperature dependent coefficient of thermal expansion,  $\alpha$ . This modification was encoded but, to date, the results have not been very satisfactory and further work will be required before the model and its implementation can be considered suitable for non-isothermal creep simulations.

### Model 24 Deformation Mechanism

Model 24 is an implementation of various deformation mechanisms, following Ashby. Four distinct sets of equations are available; only one mechanism is in effect during any one simulation. Initial work using this model in its power law creep mode proved unwieldy due to the number of constants which need to be determined. The equation has the form:

$$\epsilon = T_0/T (a\sigma/sG)^{1/m} \exp(-Q/T)$$

where  $\epsilon$  is the effective creep rate,  
 $\sigma$  is the effective stress,  
 $T$  is temperature,  
 $Q$  is a normalized activation energy,  
 $s$  is a strength parameter,  
 $a$ ,  $T_0$ , and  $m$  are material parameters.

The change in the strength parameter,  $s$ , is defined in terms of the strain rate and current strength:

$$s = k_1 \dot{\epsilon}^{n_1} + k_2 \dot{\epsilon}^{n_2} s^{n_3}$$

where  $k_i$ ,  $n_i$  are material dependent parameters.

## Appendix B

### ISLAND - Adaptive Solution Control for NIKE2D

ISLAND (Interactive Solution Language for an Adaptive NIKE Driver) is a control language built into the NIKE2D code. This language provides for the specification of a dynamic solution strategy, allowing calculation of time step size, iteration limits, convergence tolerances, and solution method based on the current state of the model. Backtracking and restarting from earlier states with new solution parameters is also allowed. This feature of NIKE2D provides a superior level of control and adaptivity.

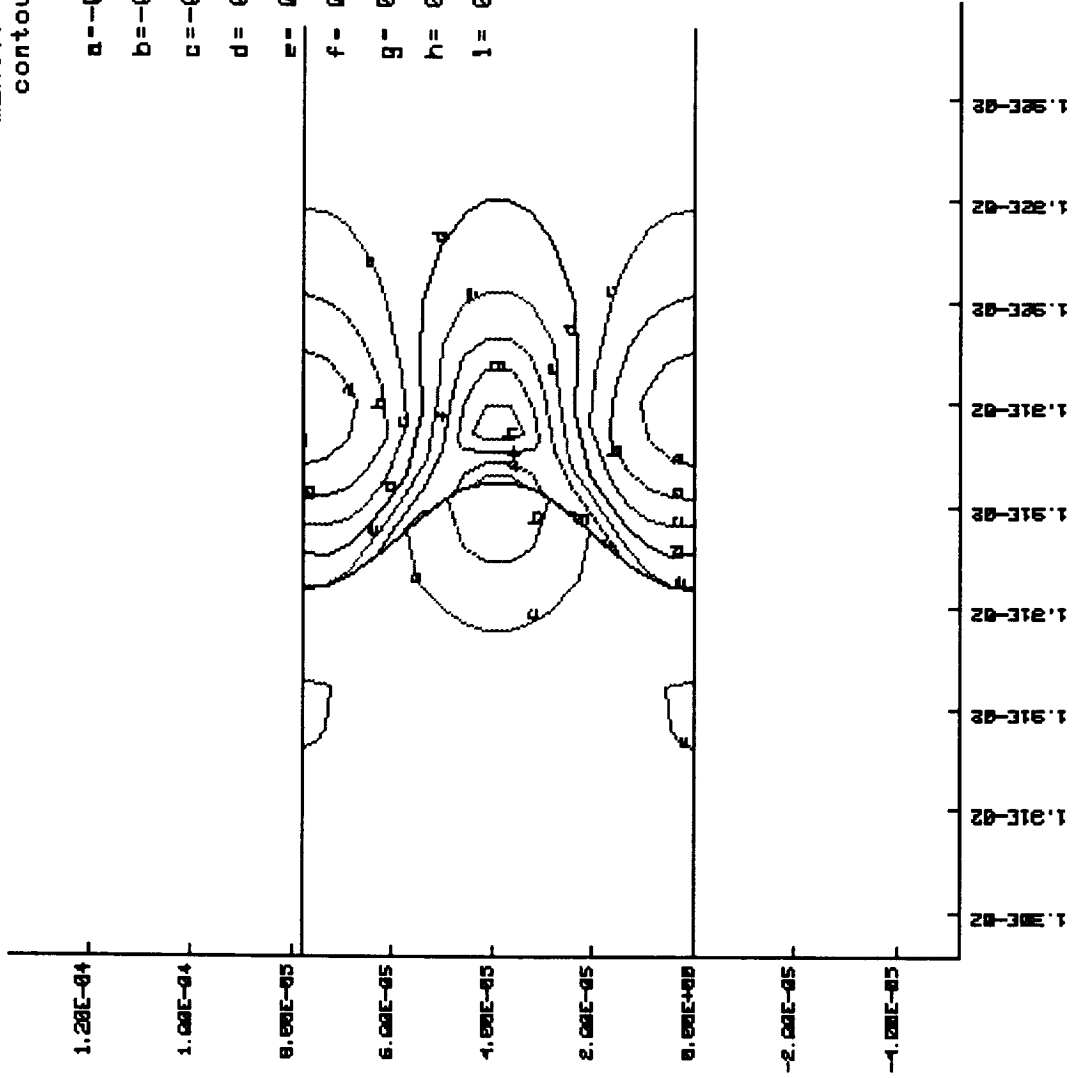
Appendix C

Auxiliary FEA Model Results

SINE\_1 Interface: Base Bond Materials, Elastic TBC & Core  
 contours of radial stress

time= 0.350000E+03  
 min(-) = -0.27710E+02  
 max(+) = 0.41892E+02  
 contour levels

- MPa
- a = -0.20750E+02
  - b = -0.13790E+02
  - c = -0.68300E+01
  - d = 0.13050E+00
  - e = 0.70900E+01
  - f = 0.14050E+02
  - g = 0.21010E+02
  - h = 0.27970E+02
  - i = 0.34930E+02



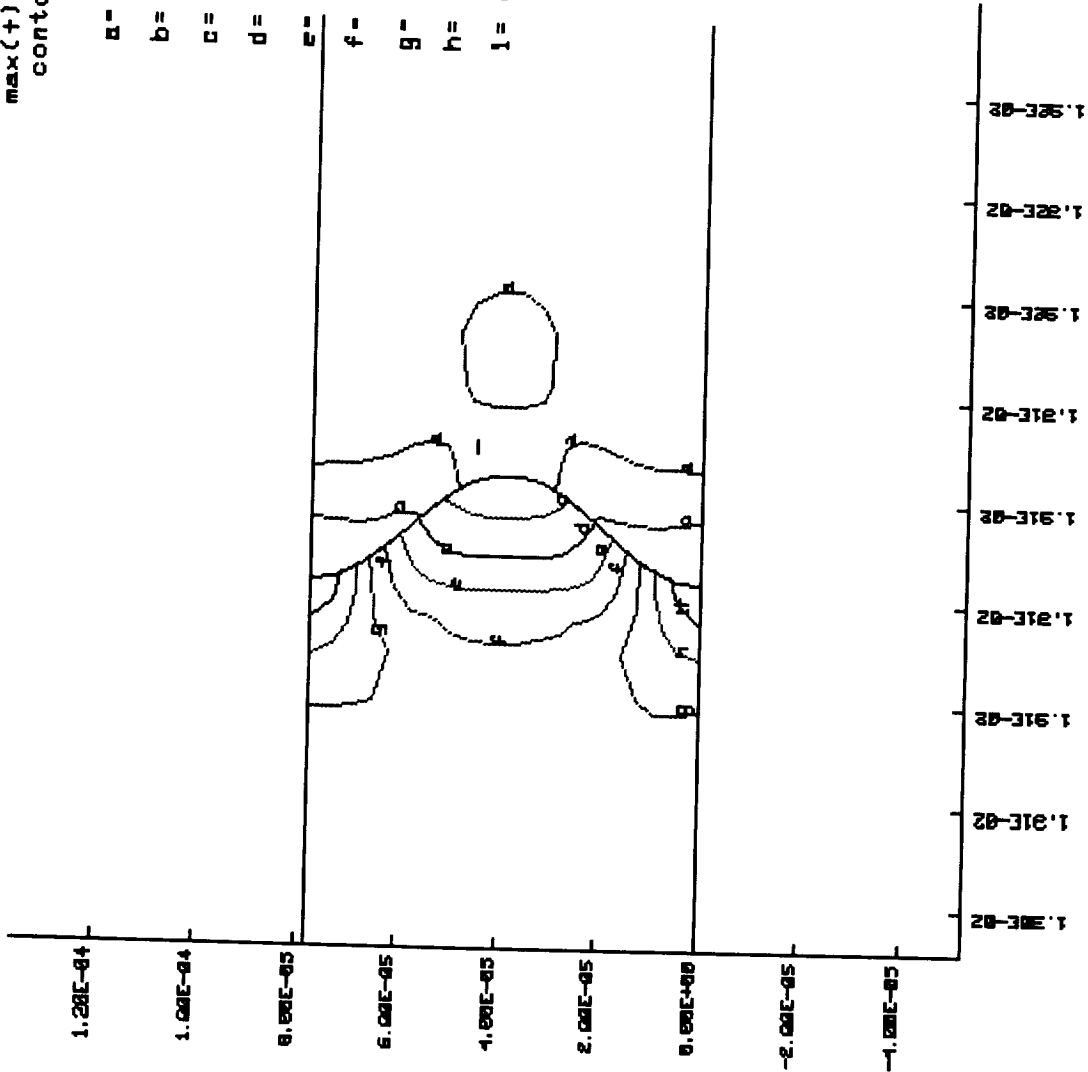
SINE\_1 Geometry with Base Case Bond Material, Elastic TBC and Core.  
 Contour Map of Radial Stress at the Bond Coat/Ceramic Interface.

SINE\_1 Interface: Base Bond Materials, Elastic TBC & Core  
 contours of radial strain

time= 0.350000E+03

min(-) = 0.60749E-02  
 max(+) = 0.24939E-01  
 contour levels

- a= 0.79610E-02
- b= 0.98460E-02
- c= 0.11700E-01
- d= 0.13600E-01
- e= 0.15500E-01
- f= 0.17400E-01
- g= 0.19300E-01
- h= 0.21200E-01
- i= 0.23000E-01



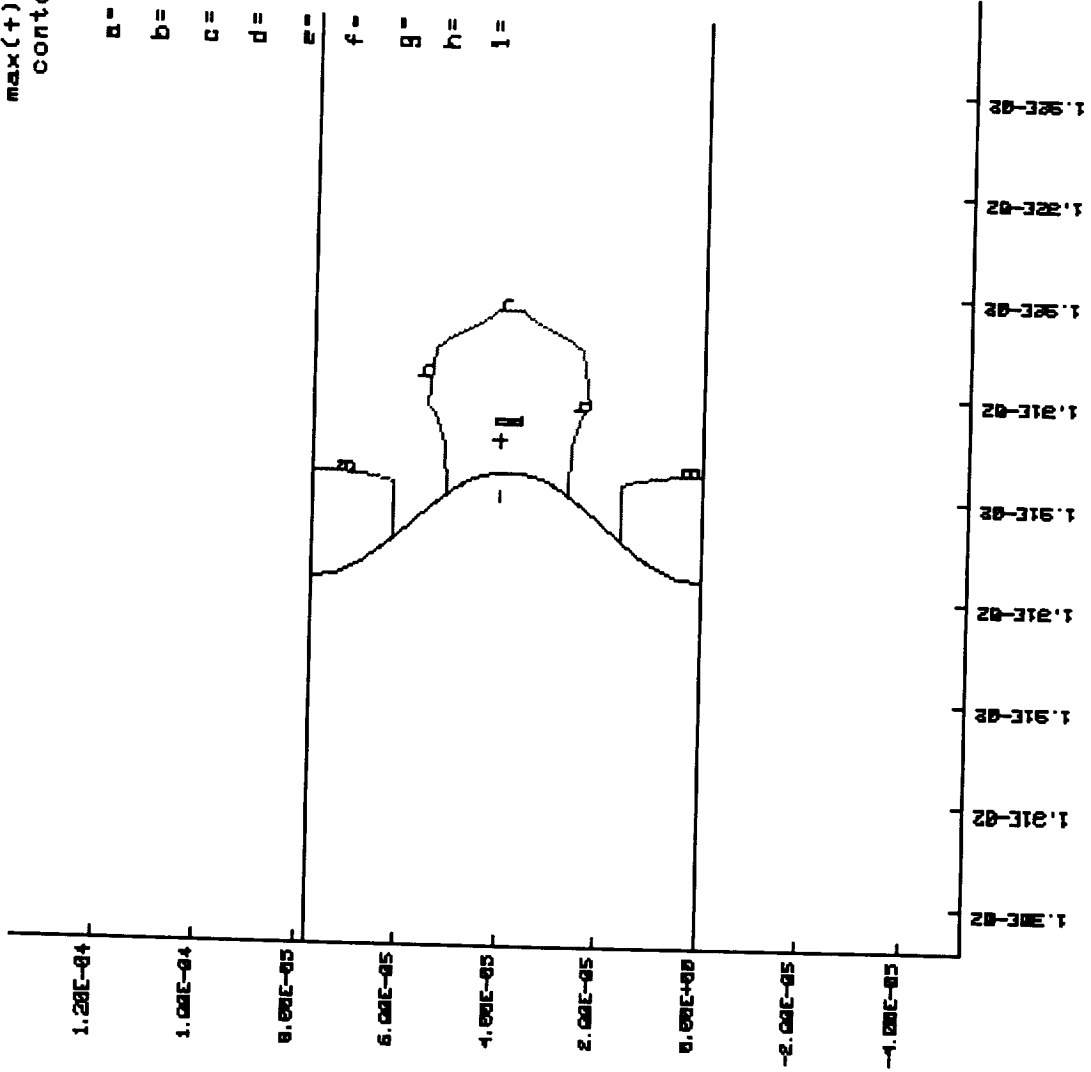
SINE\_1 Interface Geometry with Base Case Bond Material, Elastic TBC and Core -  
 Contour Map of Radial Strain at the Bond Coat/Ceramic Interface.

SINE\_1 Interface: Base Bond Materials, Elastic TBC & Core  
 contours of hoop stress

time= 0.35000E+03  
 min(-)=-0.13139E+02  
 max(+)= 0.28907E+03  
 contour levels

MPa

- a= 0.17000E+02
- b= 0.47300E+02
- c= 0.77520E+02
- d= 0.10800E+03
- e= 0.13800E+03
- f= 0.16800E+03
- g= 0.19800E+03
- h= 0.22900E+03
- i= 0.25900E+03



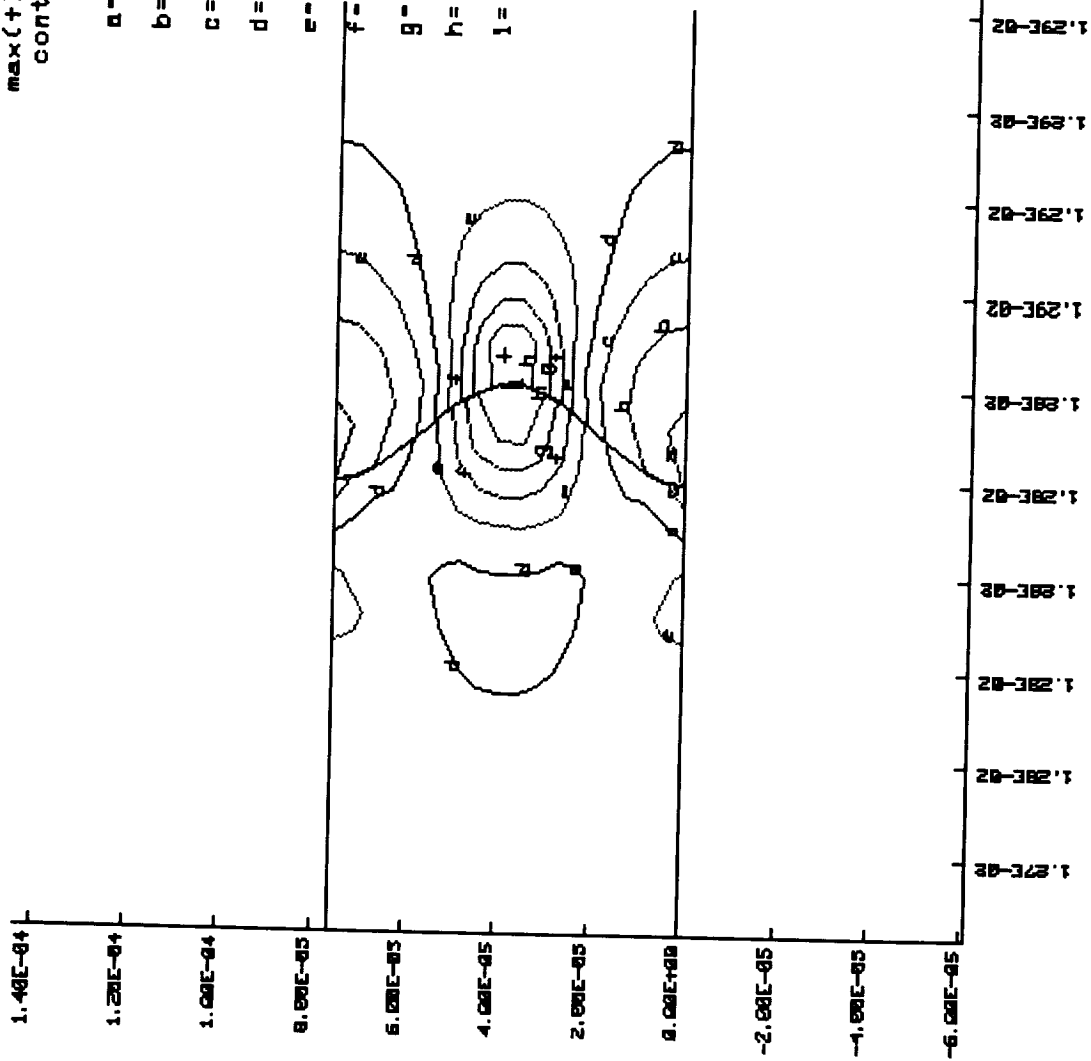
SINE\_1 Interface Geometry with Base Case Bond Material, Elastic TBC and Core -  
 Contour Map of Hoop Stress at the Bond Coat/Ceramic Interface.

SINE\_1 Interface: Base Bond Materials, Elastic TBC & Core  
 Contours of radial stress

time = 0.600000E+03  
 min(-) = -0.81111E+02  
 max(+) = 0.10676E+03  
 contour levels

MPa

- a = -0.62320E+02
- b = -0.43540E+02
- c = -0.24750E+02
- d = -0.59600E+01
- e = 0.12820E+02
- f = 0.31610E+02
- g = 0.50100E+02
- h = 0.69190E+02
- i = 0.87970E+02



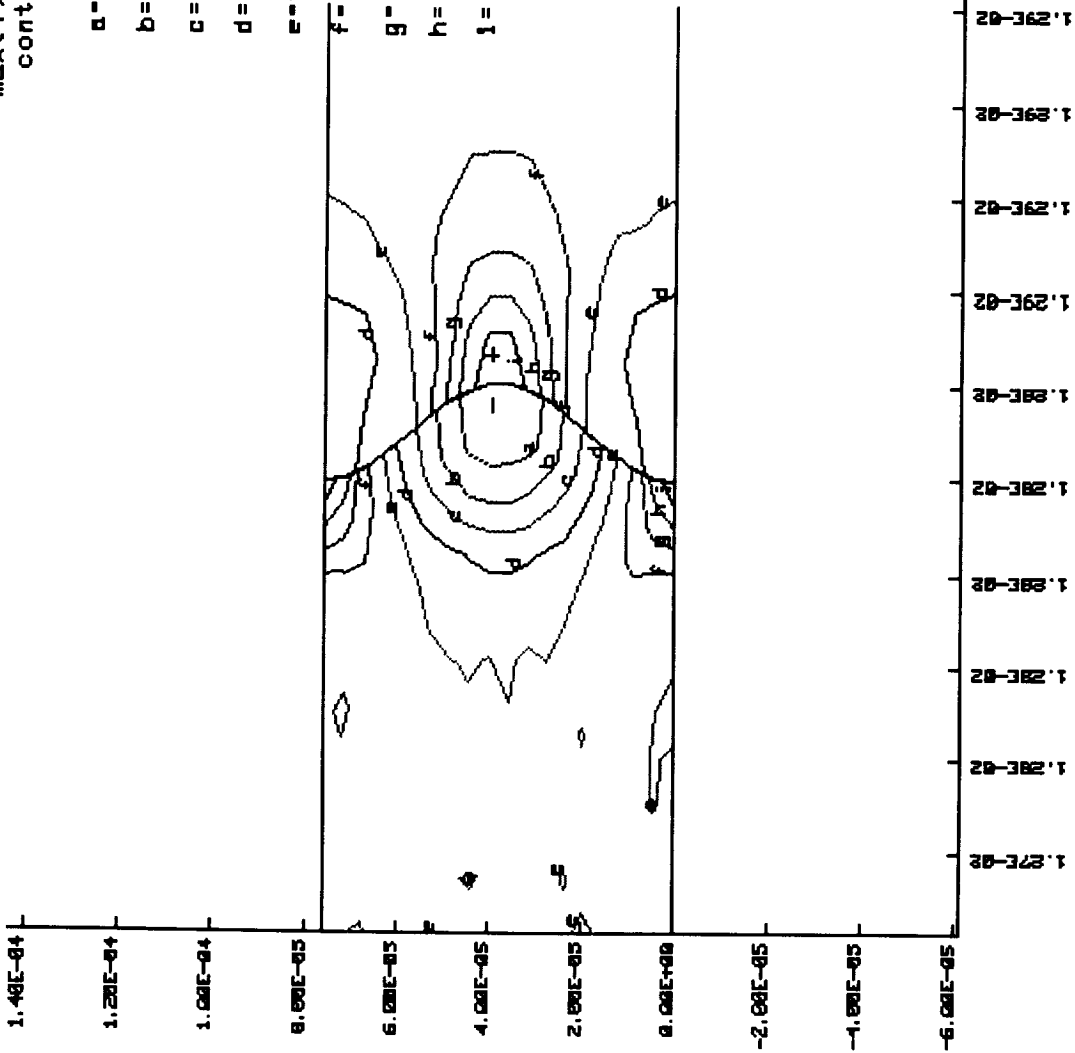
SINE\_1 Interface Geometry with Base Case Bond Material, Elastic TBC and Core -  
 Contour Map of Radial Stress at the Bond Coat/Ceramic Interface.

SINE\_1 Interface: Base Bond Materials, Elastic TBC & Core

contours of radial strain  
( InfIntStrain )

time= 0.60000E+03  
min(-)=-0.23696E-02  
max(+)= 0.23290E-02  
contour levels

- a=-0.19000E-02
- b=-0.14300E-02
- c=-0.96000E-03
- d=-0.49000E-03
- e=-0.20300E-04
- f= 0.45000E-03
- g= 0.91900E-03
- h= 0.13890E-02
- i= 0.18590E-02

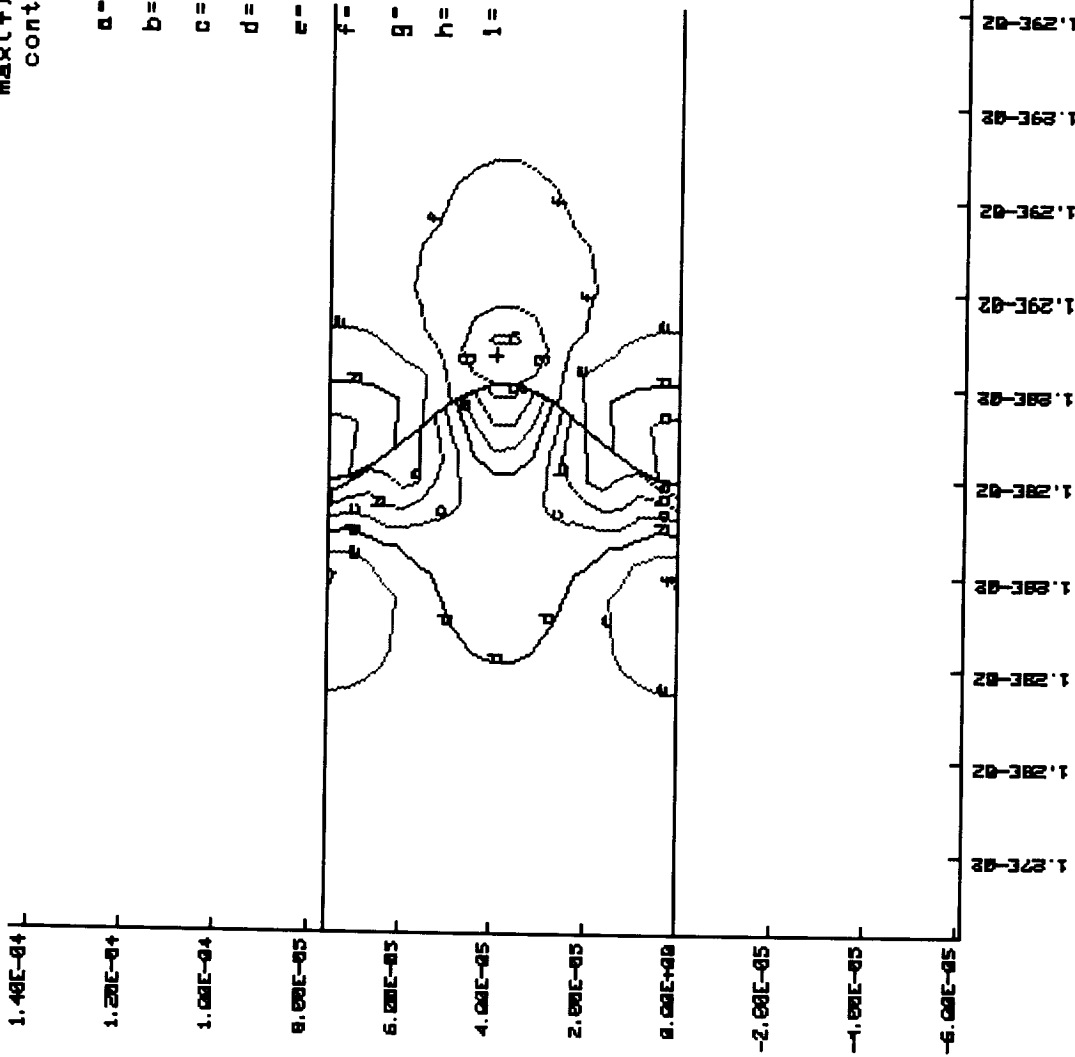


SINE\_1 Interface Geometry with Base Case Bond Material, Elastic TBC and Core -  
Contour Map of Radial Strain at the Bond Coat/Ceramic Interface.

SINE\_1 Interface: Base Bond Materials, Elastic TBC & Core  
 contours of hoop stress

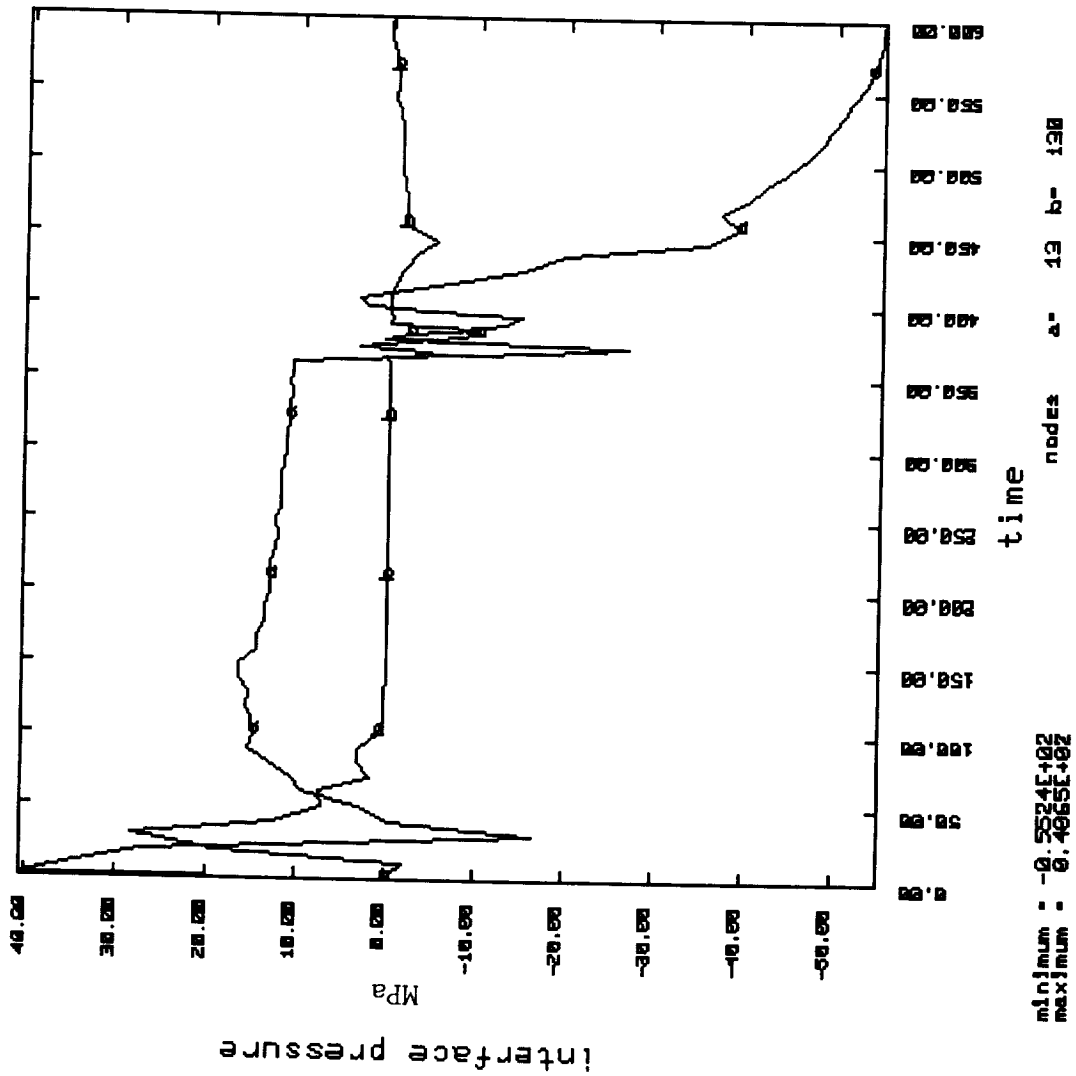
time= 0.60000E+03  
 min(-)=-0.42259E+02  
 max(+)= 0.49526E+02  
 contour levels

- MPa
- a=-0.33000E+02
  - b=-0.23900E+02
  - c=-0.14720E+02
  - d=-0.55400E+01
  - e= 0.36300E+01
  - f= 0.12810E+02
  - g= 0.21990E+02
  - h= 0.31170E+02
  - i= 0.40350E+02



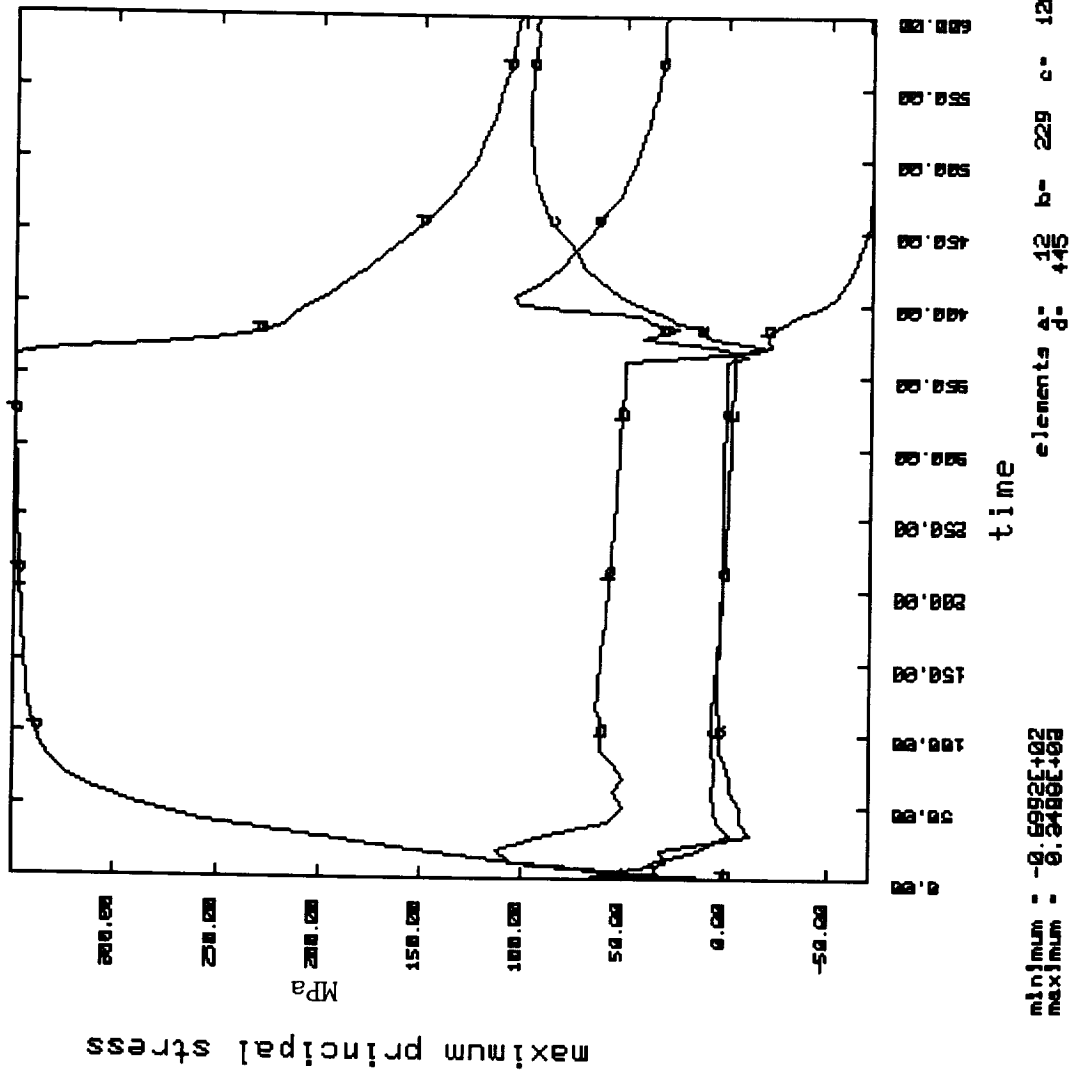
SINE\_1 Interface Geometry with Base Case Bond Material, Elastic TBC and Core -  
 Contour Map of Hoop Stress at the Bond Coat/Ceramic Interface.

SINE\_1 Interface: Base Bond Materials, Elastic TBC & Core



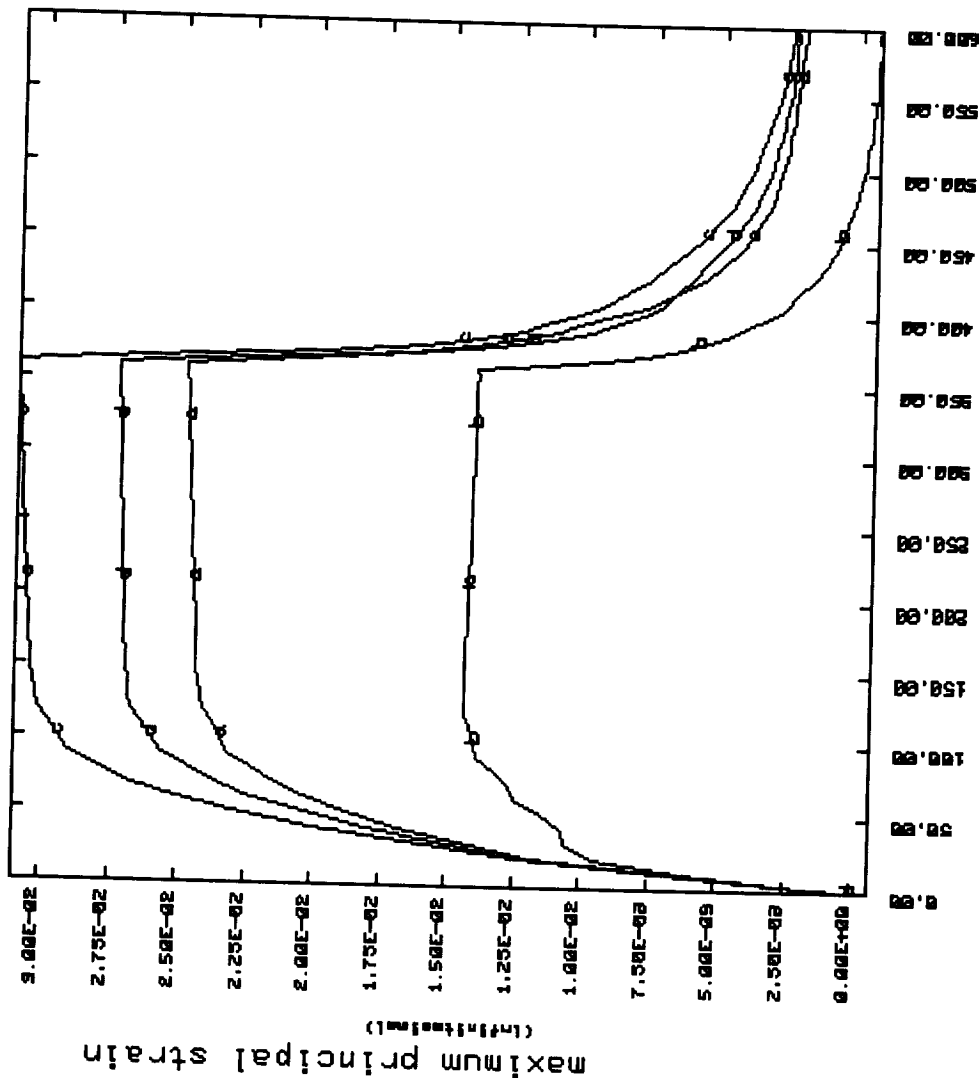
SINE\_1 Interface Geometry with Base Case Bond Material, Elastic TBC and Core - Interface Normal Pressure History Plot.

SINE\_1 Interface: Base Bond Materials, Elastic TBC & Core



SINE\_1 Interface Geometry with Base Case Bond Material, Elastic TBC and Core -  
 Maximum Principal Stress History Plot.

SINE\_1 Interface: Base Bond Materials, Elastic TBC & Core



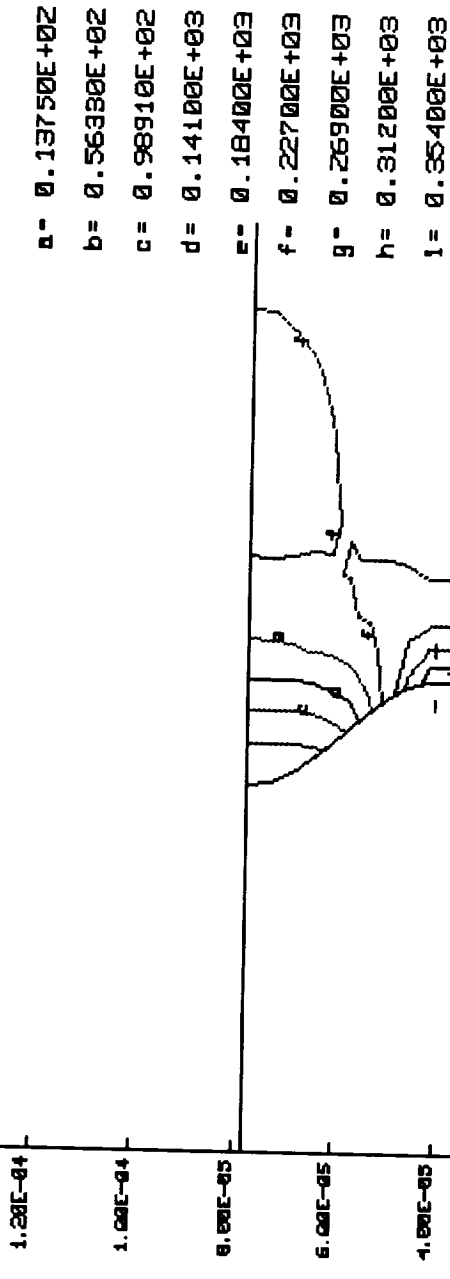
minimum = -0.6529E-03  
maximum = 0.2899E-01

SINE\_1 Interface Geometry with Base Case Bond Material, Elastic TBC and Core -  
Maximum Principal Strain History Plot.

SINE\_1 Interface: Higher Bond Coat CTE, Elastic TBC & Core  
 contours of axial stress

time = 0.350000E+03

min(-) = -0.28834E+02  
 max(+) = 0.39697E+03  
 contour levels

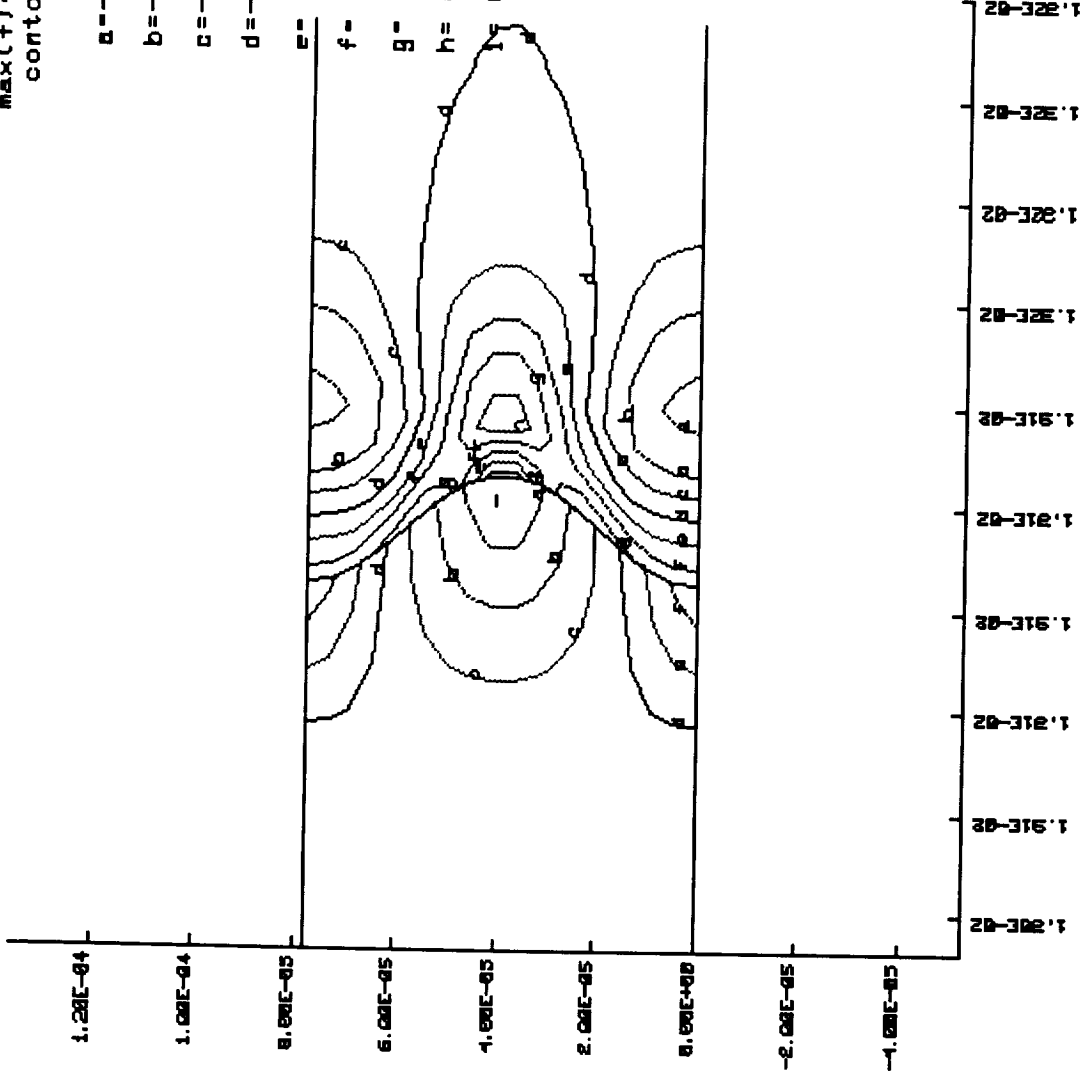


SINE\_1 Interface: Higher Bond Coat CTE, Elastic TBC & Core  
 contours of radial stress

time= 0.35000E+03

min(-)=-0.30738E+02  
 max(+)= 0.40439E+02  
 contour levels

- a=-0.23620E+02
- b=-0.16500E+02
- c=-0.93800E+01
- d=-0.22700E+01
- e= 0.48500E+01
- f= 0.11970E+02
- g= 0.19090E+02
- h= 0.26200E+02
- i= 0.33320E+02

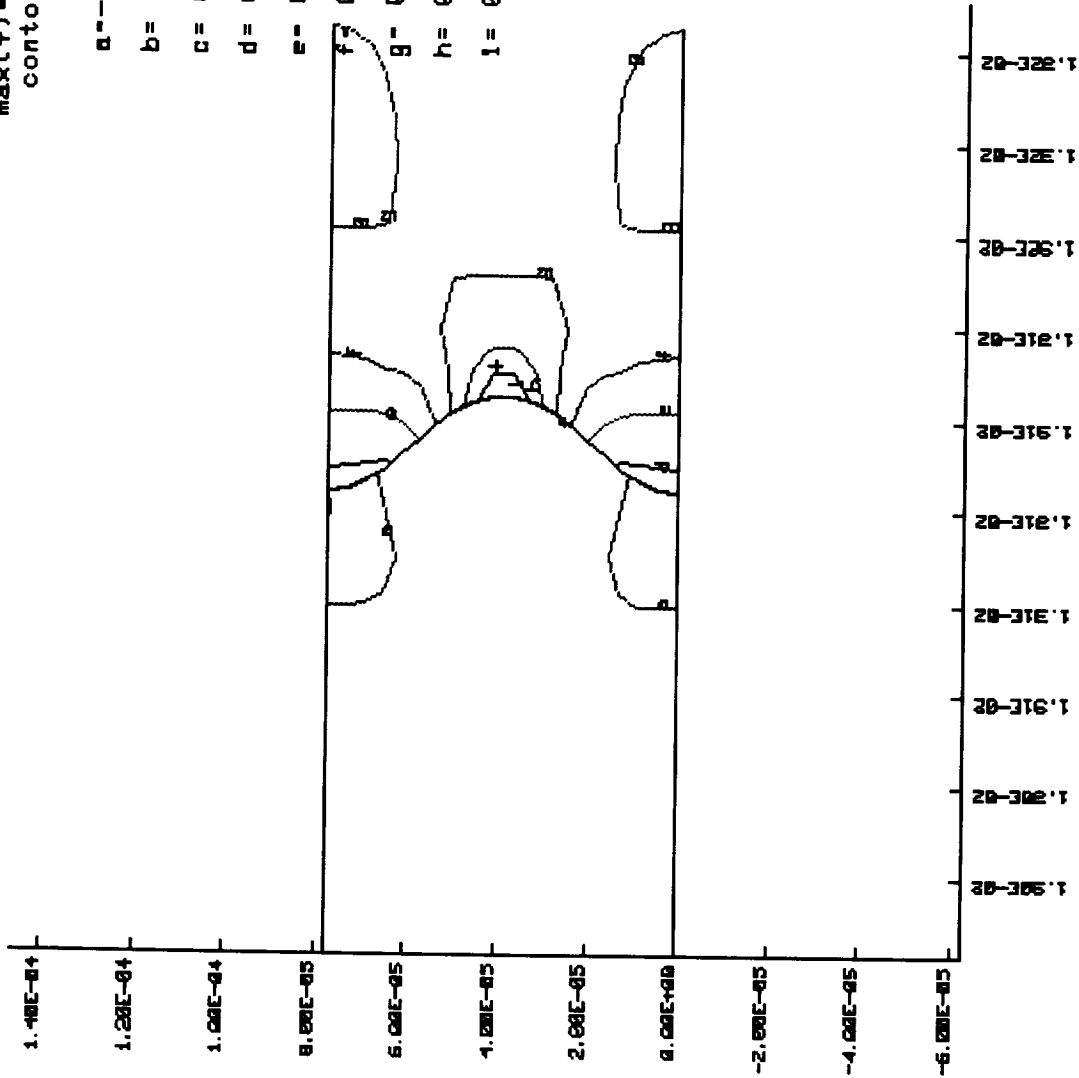


SINE\_1 Interface Geometry  
 contours of axial stress

time= 0.35000E+03

min(-) = -0.21901E+02  
 max(+) = 0.15389E+03  
 contour levels

- MPa
- a = -0.43200E+01
  - b = 0.13260E+02
  - c = 0.32840E+02
  - d = 0.48410E+02
  - e = 0.65990E+02
  - f = 0.83570E+02
  - g = 0.10100E+03
  - h = 0.11900E+03
  - i = 0.13600E+03



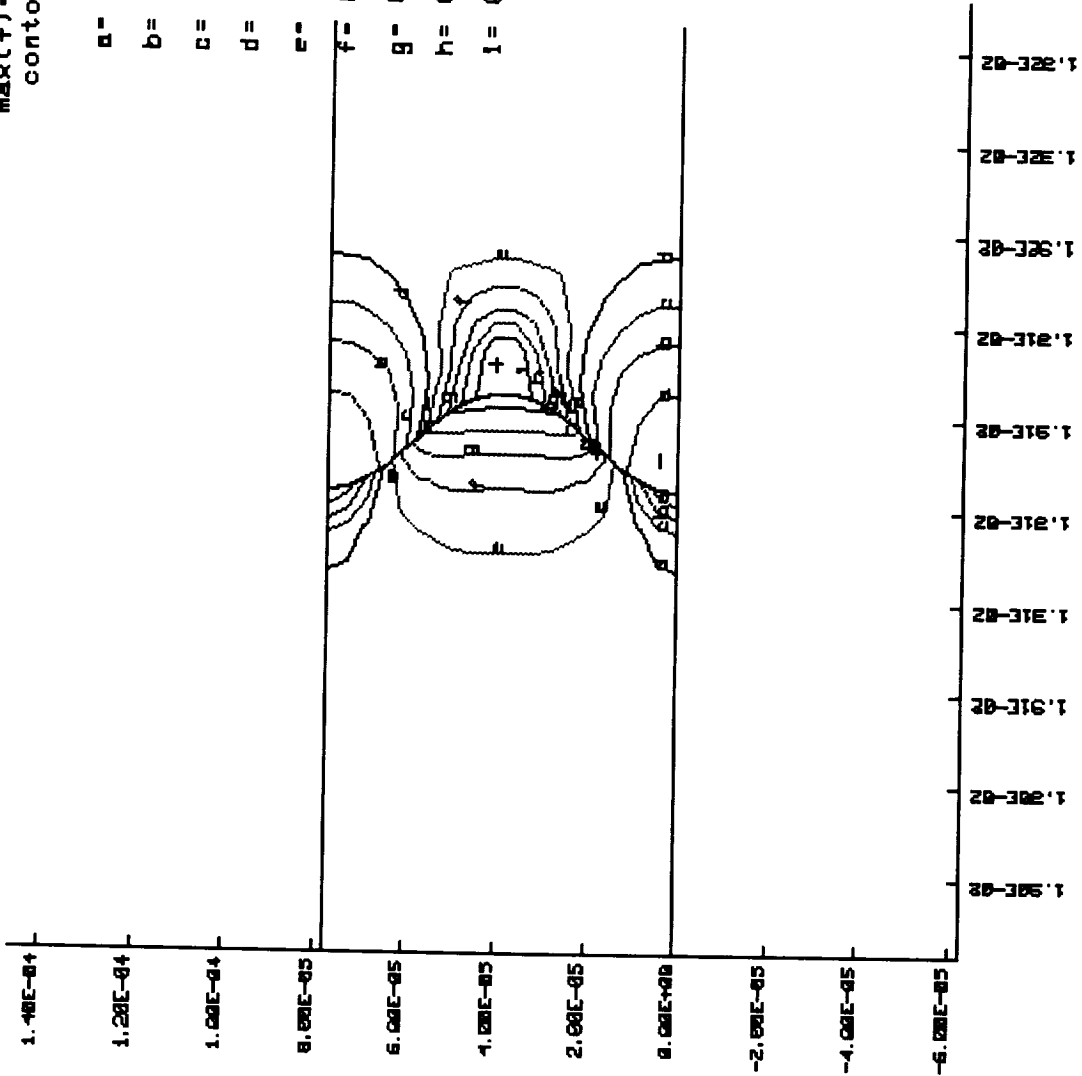
SINE\_1 Interface Baseline Case -  
 Contour Map of Axial Stress at the Bond Coat/Ceramic Interface.

SINE\_1 Interface Geometry contours of axial strain  
 ( infinitesimal )

time= 0.35000E+03

min(-) = 0.16865E-01  
 max(+) = 0.28805E-01  
 contour levels

- a = 0.18100E-01
- b = 0.19300E-01
- c = 0.20400E-01
- d = 0.21600E-01
- e = 0.22800E-01
- f = 0.24000E-01
- g = 0.25200E-01
- h = 0.26400E-01
- i = 0.27600E-01



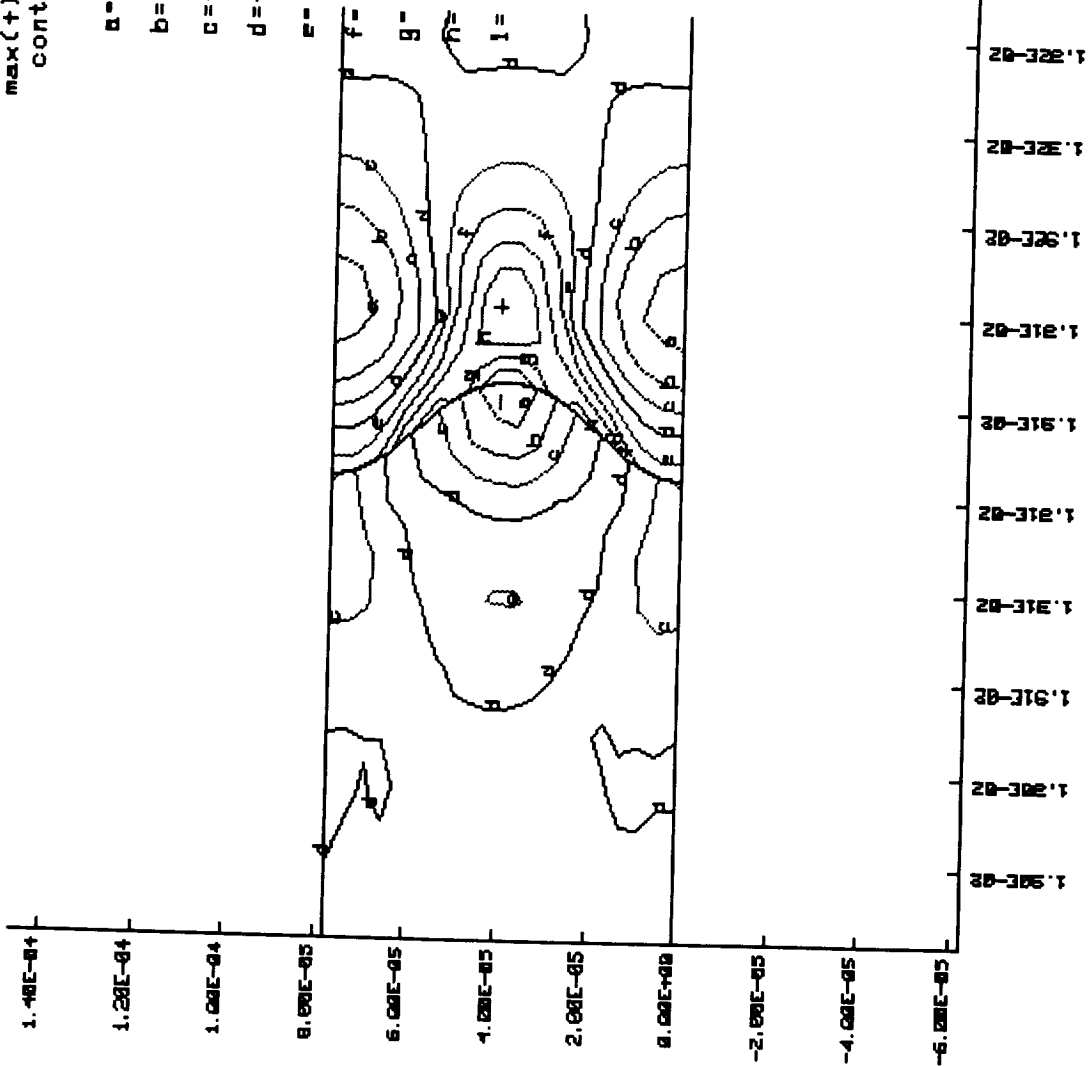
SINE\_1 Interface Baseline Case -  
 Contour Map of Axial Strain at the Bond Coat/Ceramic Interface.

SINE\_1 Interface Geometry  
 contours of radial stress

time= 0.35000E+03

min(-)=-0.15087E+02  
 max(+)= 0.19045E+02  
 contour levels

- MPa
- a=-0.11670E+02
  - b=-0.82600E+01
  - c=-0.48500E+01
  - d=-0.14300E+01
  - e= 0.19800E+01
  - f= 0.53900E+01
  - g= 0.88100E+01
  - h= 0.12220E+02
  - i= 0.15630E+02



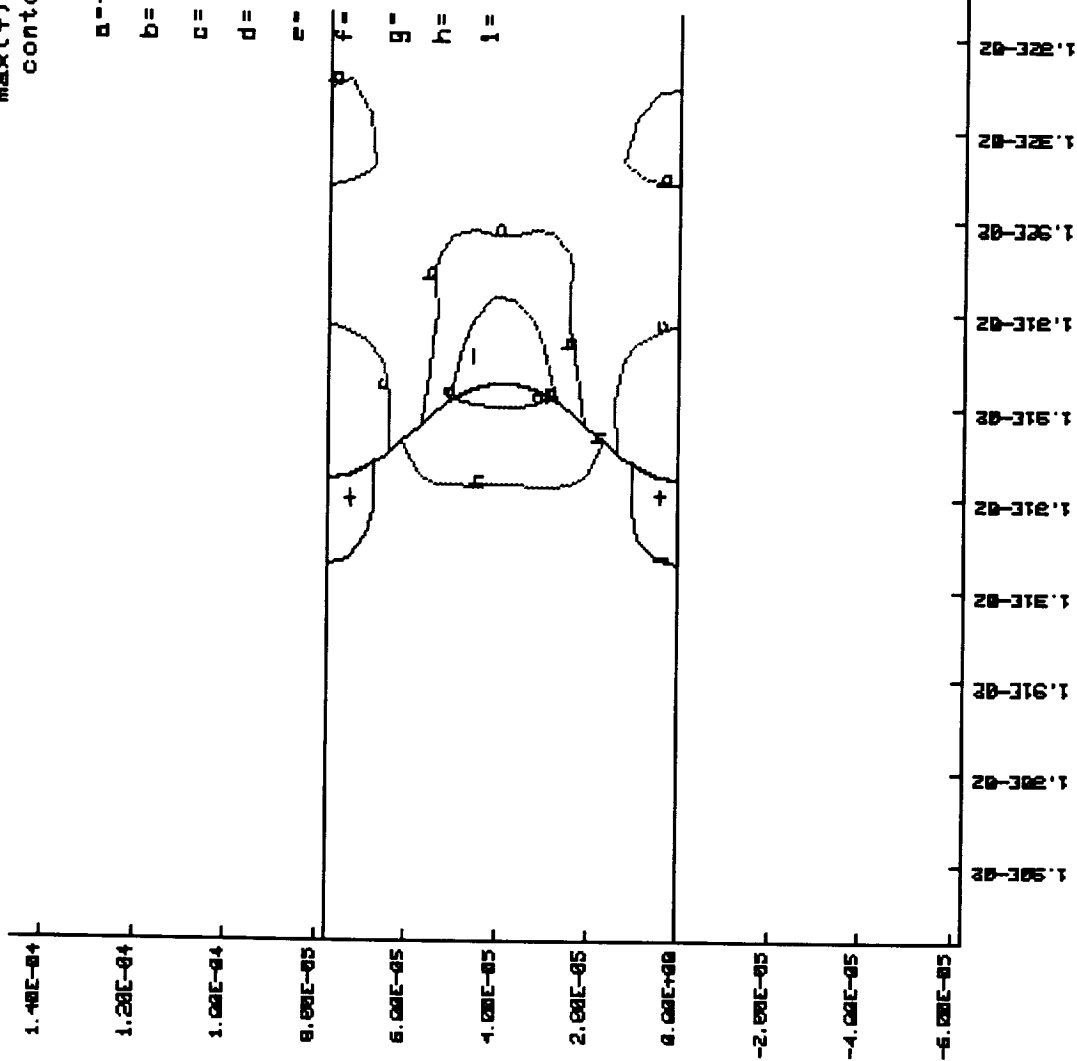
SINE\_1 Interface Baseline Case -  
 Contour Map of Radial Stress at the Bond Coat/Ceramic Interface.

SINE\_1 Interface Geometry  
 contours of radial strain  
 ( Infinitesimal )

time= 0.35000E+03

min(-)=-0.30007E-02  
 max(+)= 0.22160E-01  
 contour levels

- a=-0.55700E-03
- b= 0.19670E-02
- c= 0.44910E-02
- d= 0.70150E-02
- e= 0.95400E-02
- f= 0.12100E-01
- g= 0.14600E-01
- h= 0.17100E-01
- i= 0.19600E-01



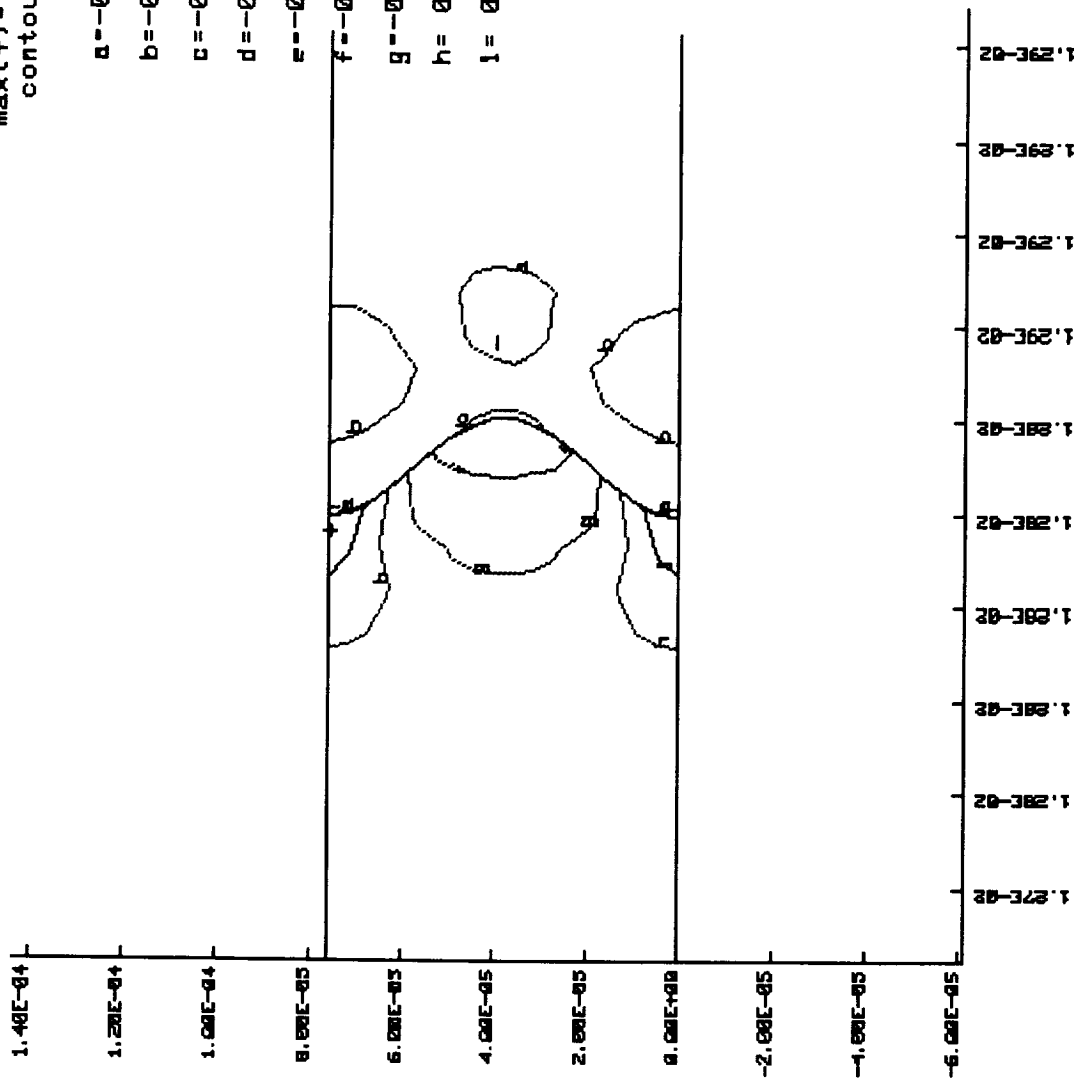
SINE\_1 Interface Baseline Case -  
 Contour Map of Radial Strain at the Bond Coat/Ceramic Interface.

SINE\_1 Interface Geometry  
 contours of axial stress

time= 0.60000E+03

min(-) = -0.12110E+03  
 max(+) = 0.49522E+02  
 contour levels

- MPa
- a = -0.14900E+03
  - b = -0.12700E+03
  - c = -0.10500E+03
  - d = -0.82850E+02
  - e = -0.60790E+02
  - f = -0.38730E+02
  - g = -0.16660E+02
  - h = 0.54000E+01
  - i = 0.27460E+02



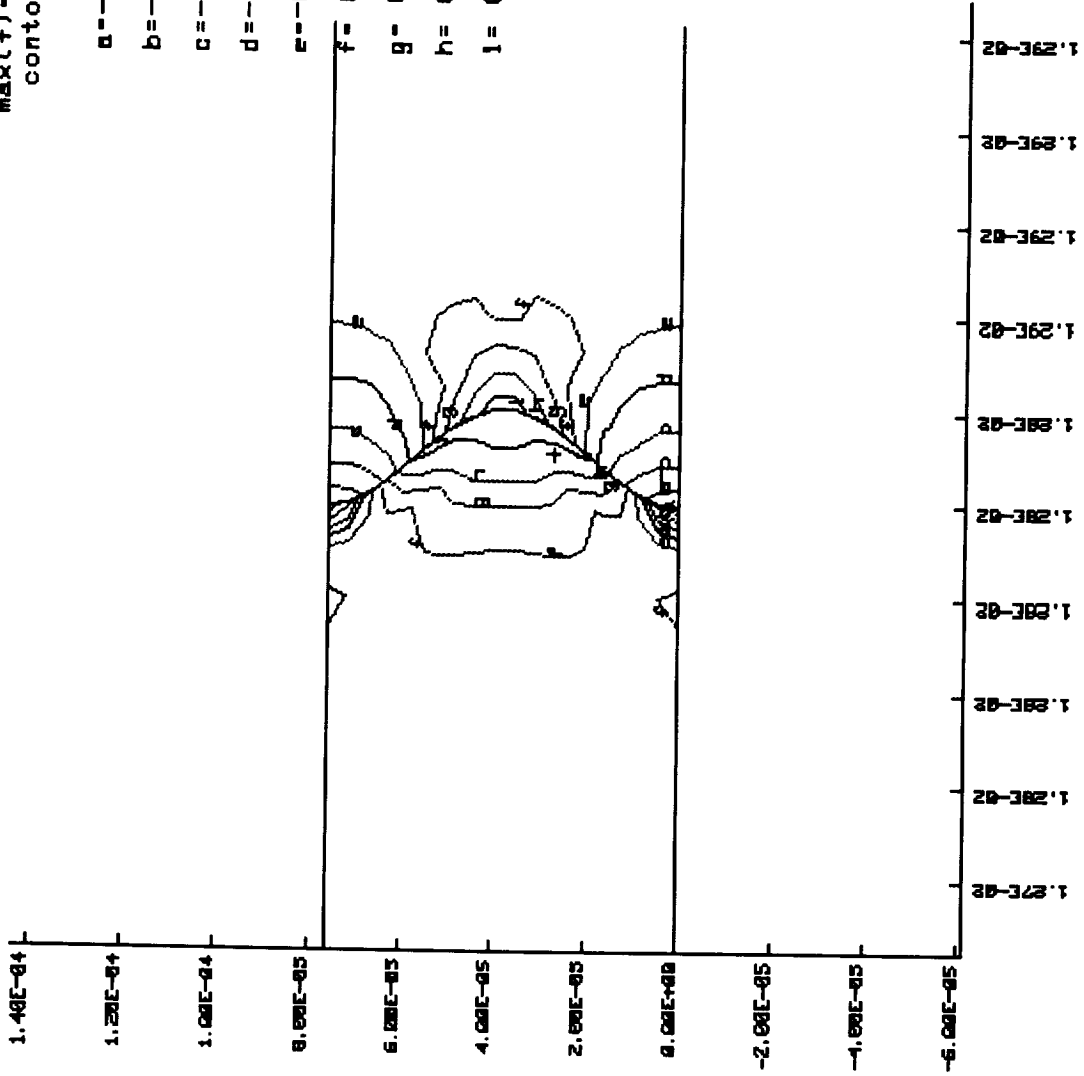
SINE\_1 Interface Baseline Case -  
 Contour Map of Axial Stress at the Bond Coat/Ceramic Interface.

SINE\_1 Interface Geometry  
 contours of axial strain  
 ( Infinitesimal )

time = 0.60000E+03

min(-) = -0.25595E-02  
 max(+) = 0.19736E-02  
 contour levels

- a = -0.21060E-02
- b = -0.16530E-02
- c = -0.12000E-02
- d = -0.74600E-03
- e = -0.29300E-03
- f = 0.16000E-03
- g = 0.61100E-03
- h = 0.10670E-02
- i = 0.15200E-02



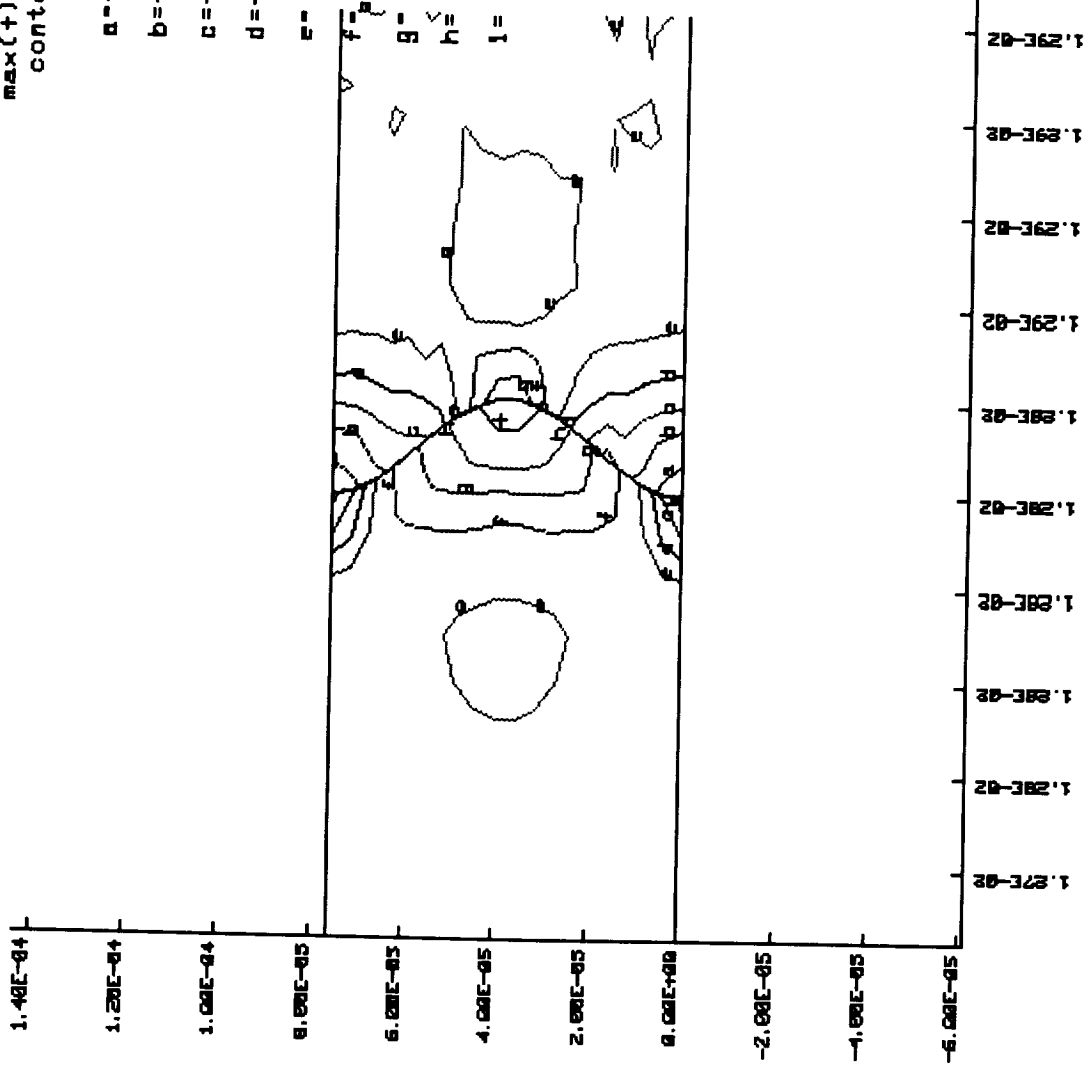
SINE\_1 Interface Baseline Case -  
 Contour Map of Axial Strain at the Bond Coat/Ceramic Interface.

SINE\_1 Interface Geometry  
 contours of radial stress

time= 0.60000E+03

min(-) = -0.60964E+02  
 max(+) = 0.61343E+02  
 contour levels

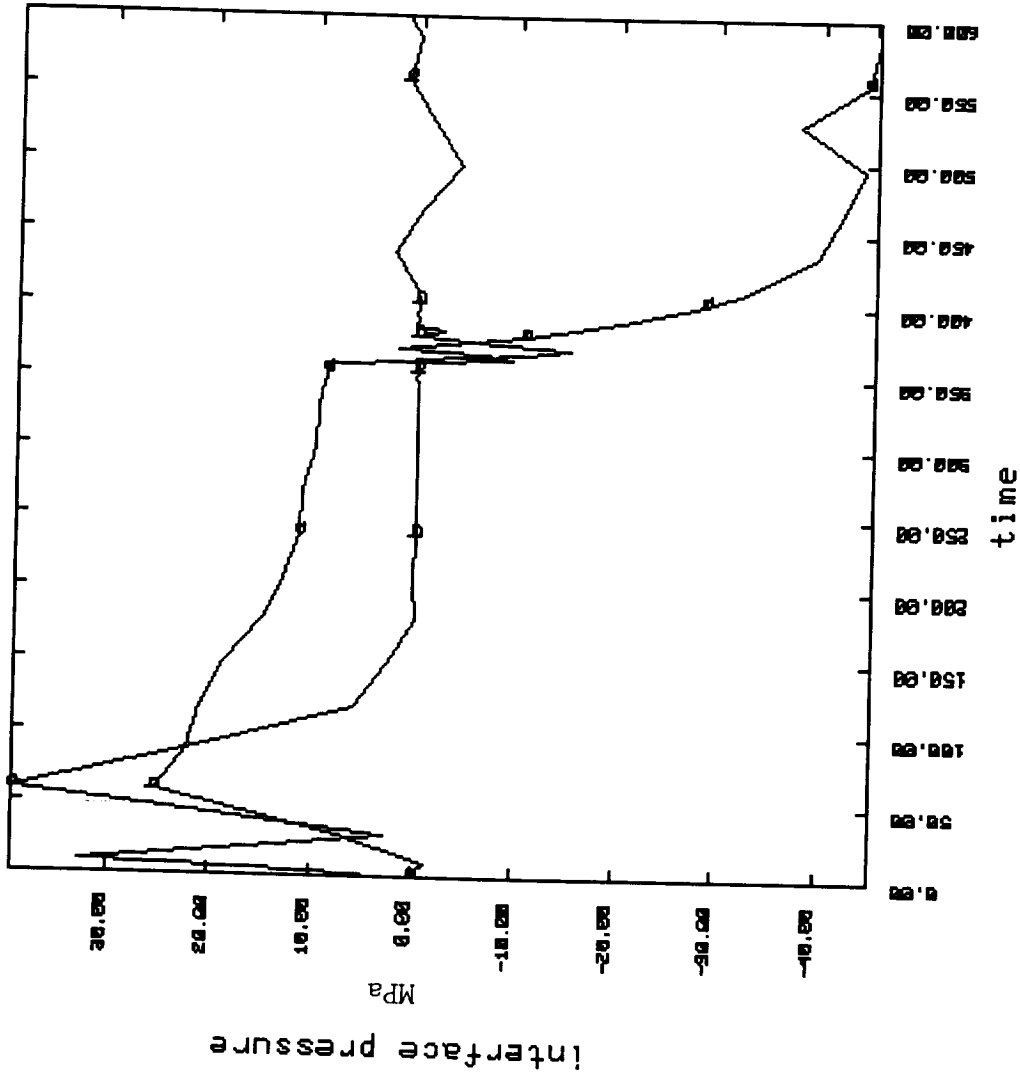
- MPa
- a = -0.48730E+02
  - b = -0.36500E+02
  - c = -0.24270E+02
  - d = -0.12040E+02
  - e = 0.18930E+00
  - f = 0.12420E+02
  - g = 0.24650E+02
  - h = 0.36880E+02
  - i = 0.49110E+02



SINE\_1 Interface Baseline Case -  
 Contour Map of Radial Stress at the Bond Coat/Ceramic Interface/



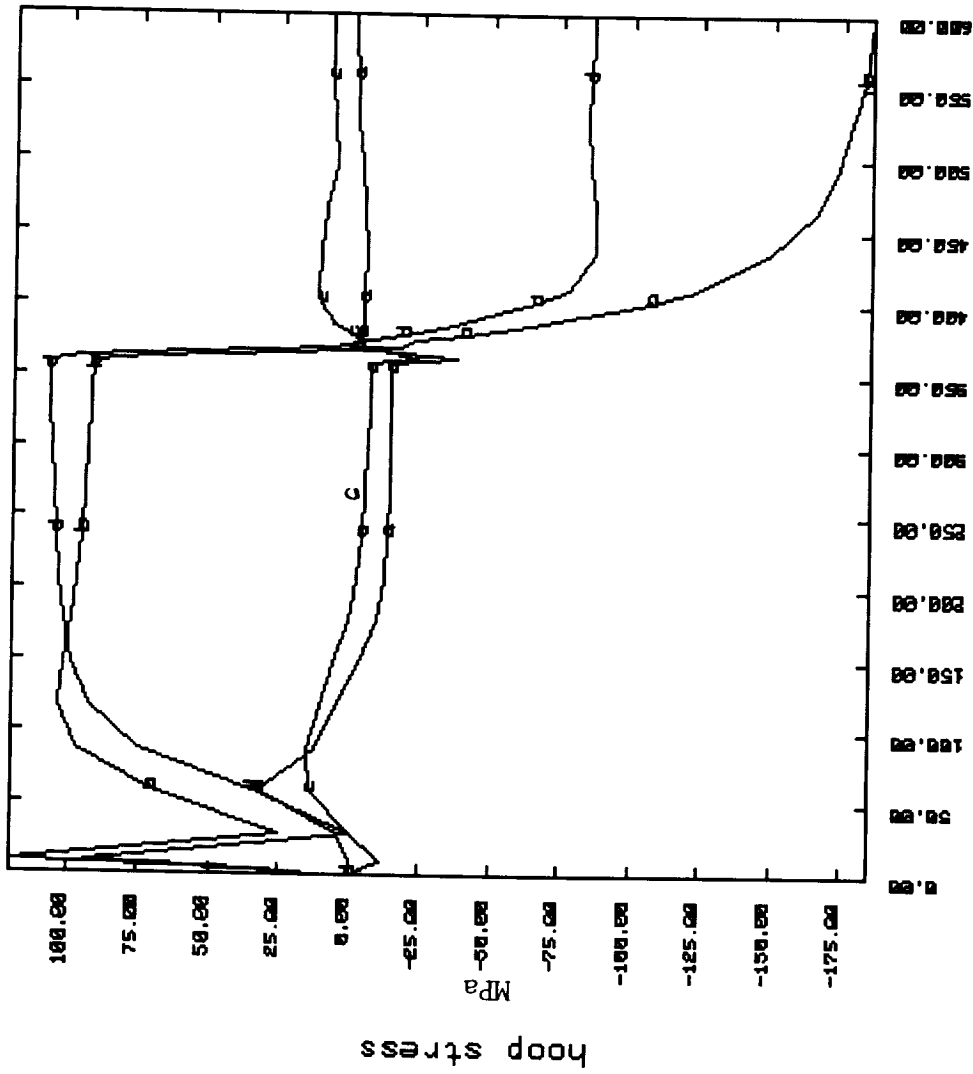
SINE\_1 Interface Geometry



minimum = -0.4541E+02  
 maximum = 0.3925E+02  
 nodes a= 13 b= 13

SINE\_1 Interface Baseline Case -  
 Interface Normal Pressure History Plot.

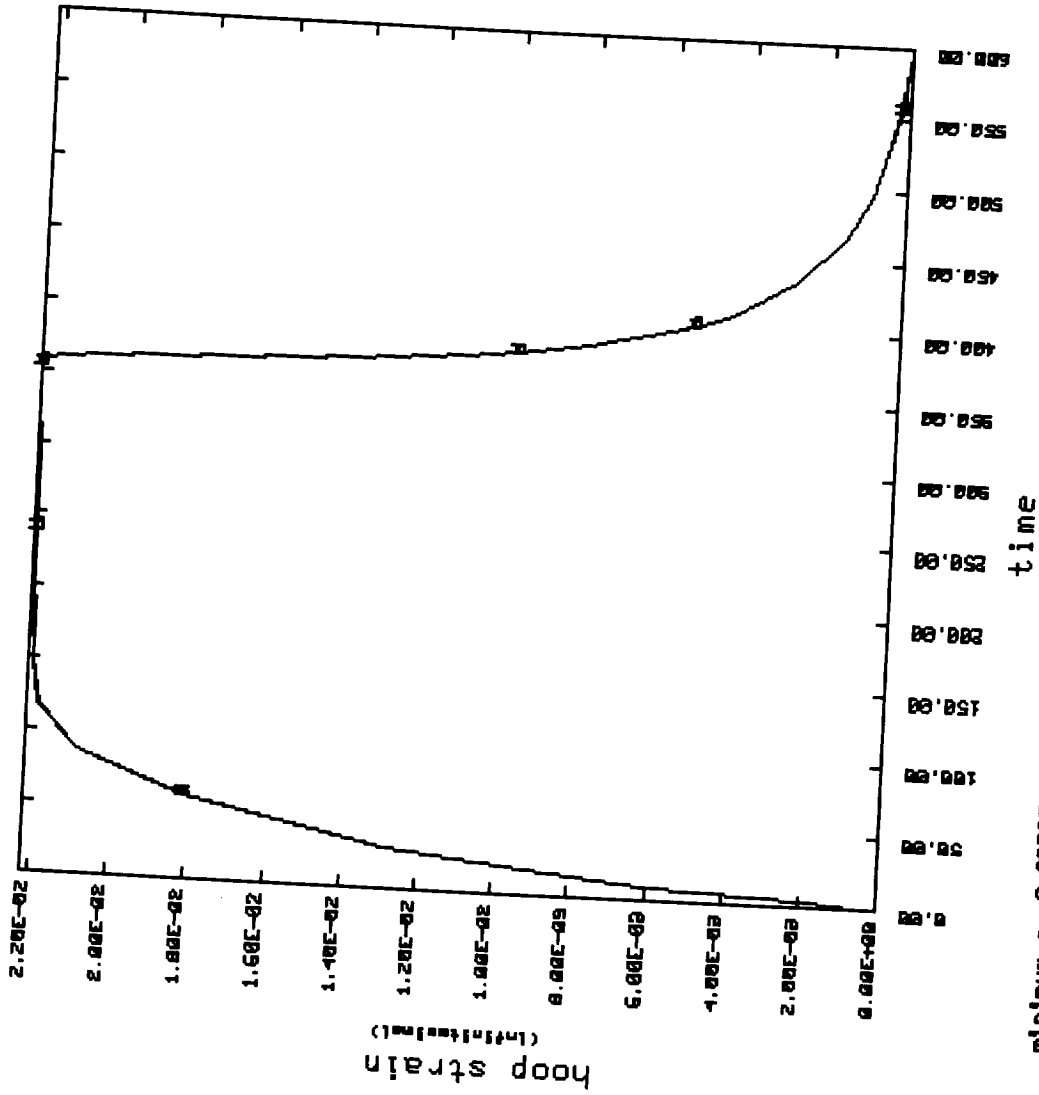
SINE\_1 Interface Geometry



minimum = -0.1949E+03  
 maximum = 0.1197E+08  
 elements a= 12 b= 229 c= 120  
 d= 445

SINE\_1 Interface Baseline Case -  
 Hoop Stress History Plot.

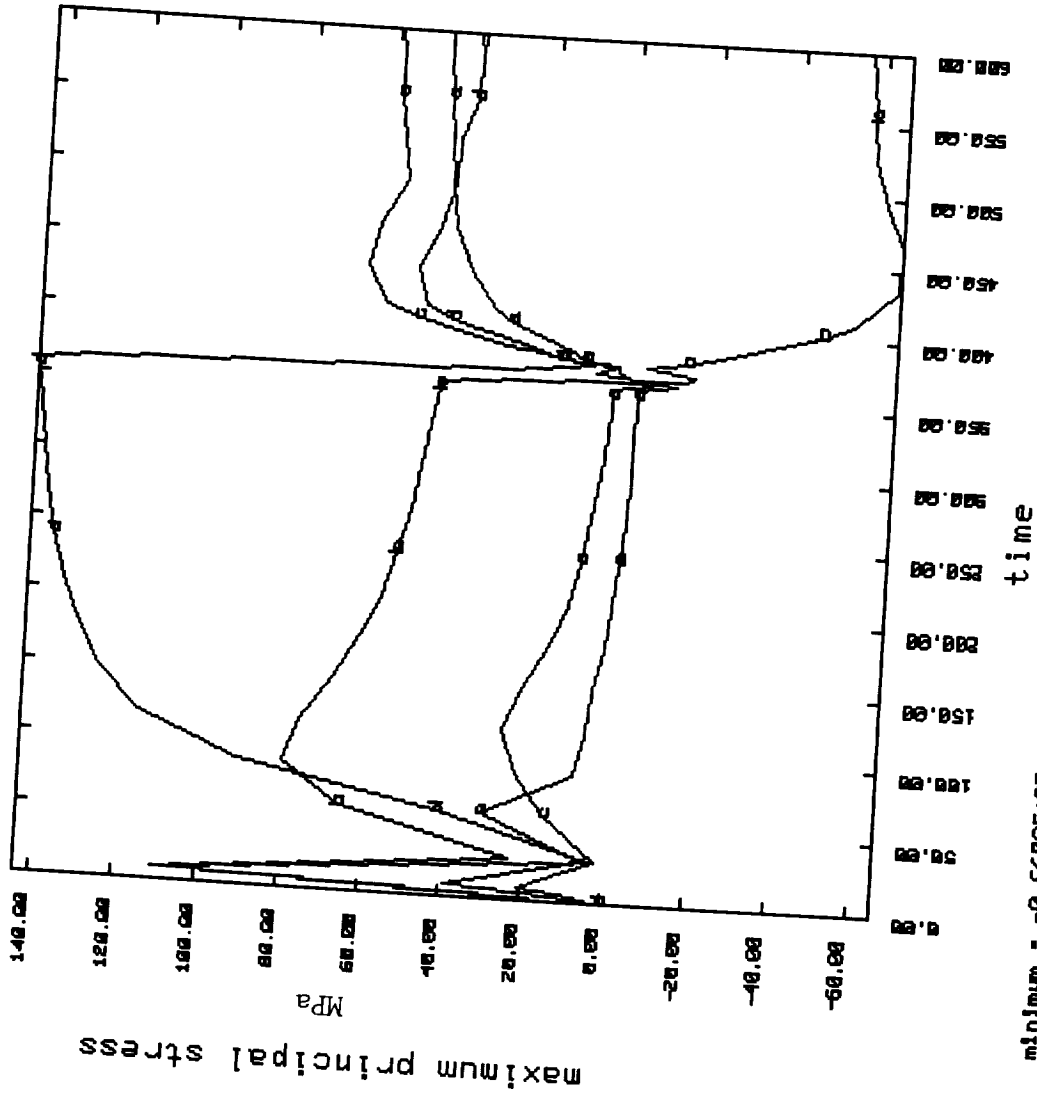
SINE\_1 Interface Geometry



minimum = 0.0000E+00  
 maximum = 0.2220E-01  
 elements a= 12 b= 229 c= 120

SINE\_1 Interface Baseline Case -  
 Hoop Strain History Plot.

SINE\_1 Interface Geometry

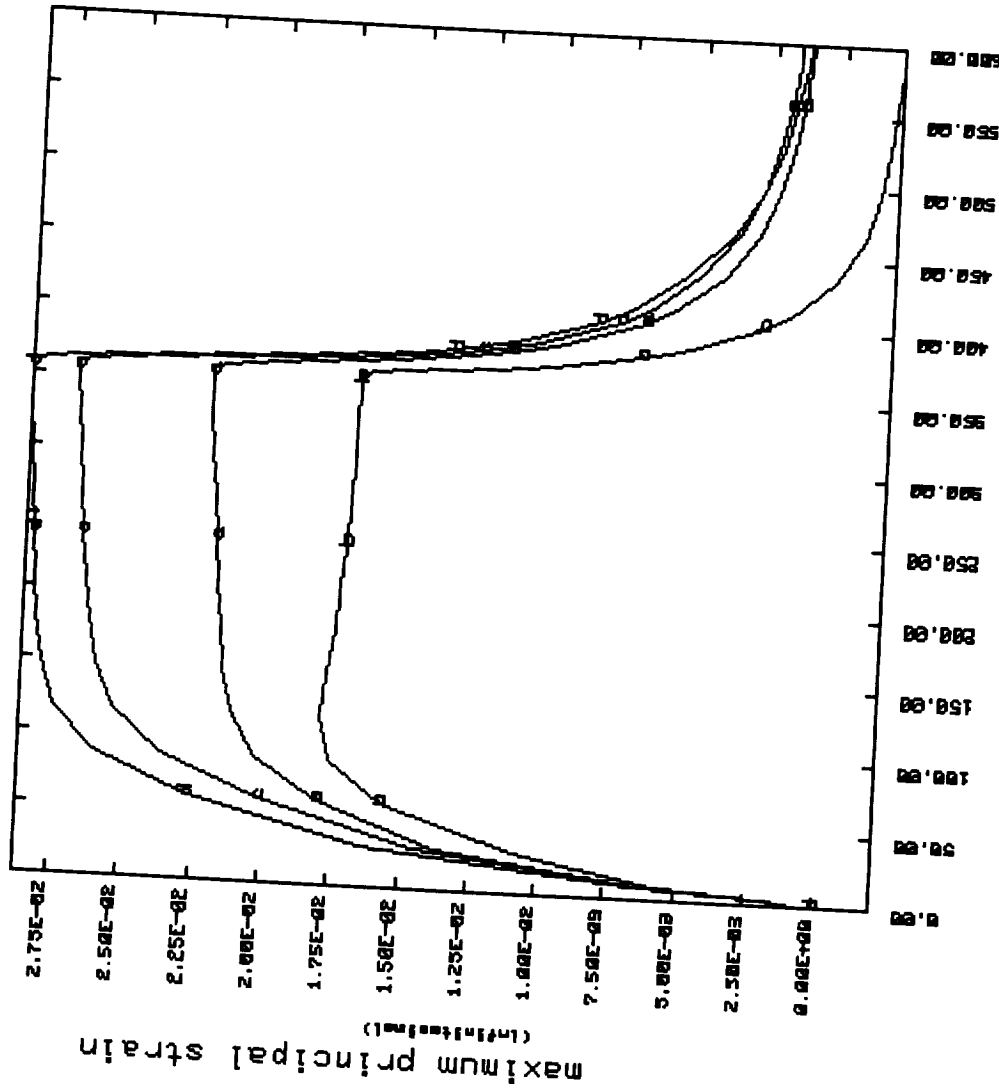


minimum = -0.6483E+02  
 maximum = 0.1441E+03

elements a= 12 b= 229 c= 120

SINE\_1 Interface Baseline Case -  
 Maximum Principal Stress History Plot.

SINE\_1 Interface Geometry



minimum = -0.1984E-02  
 maximum = 0.2669E-01

elements a= 42 b= 229 c= 120

SINE\_1 Interface Baseline Case -  
 Maximum Principal Strain History Plot.

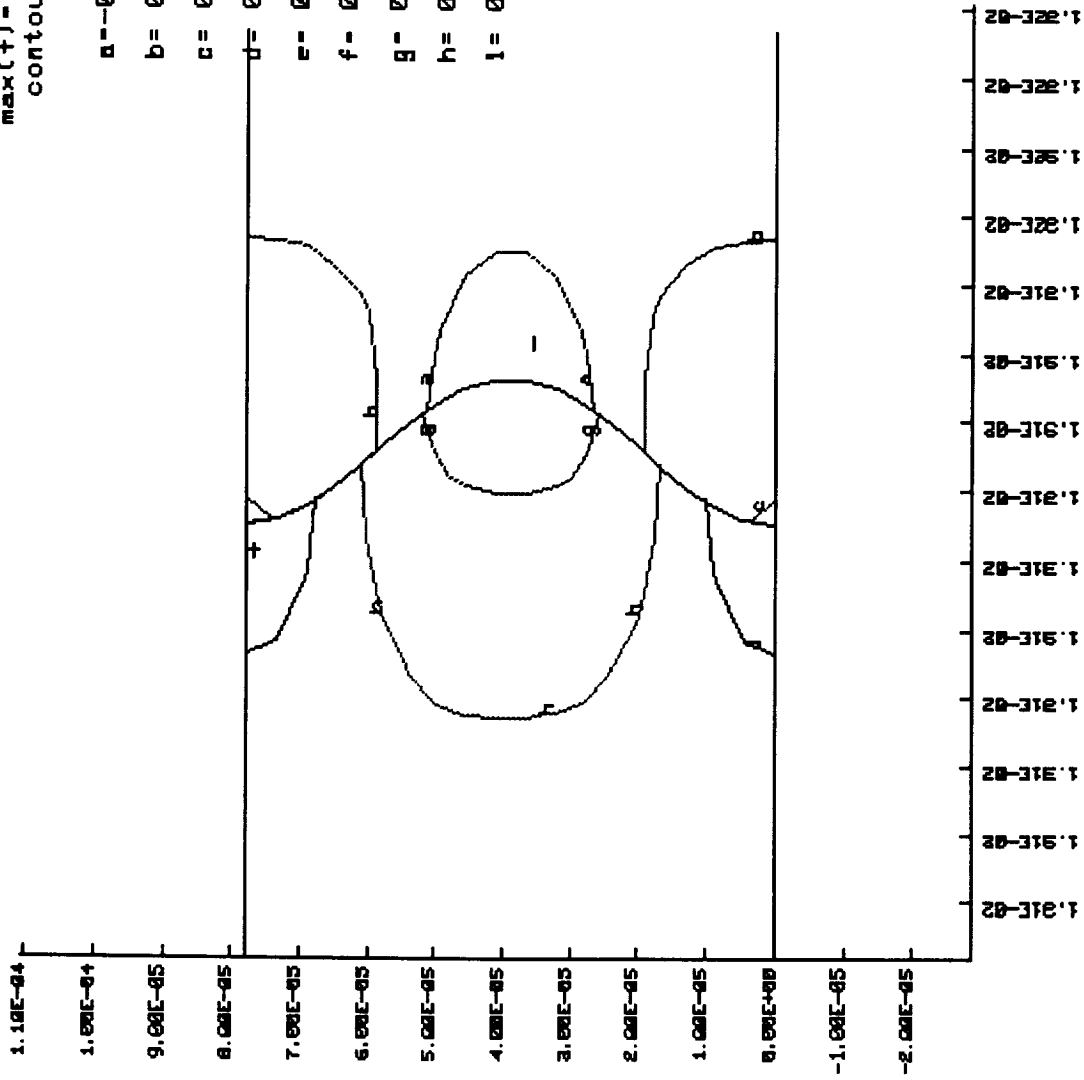


SINE\_1 Geometry, Higher CTE in Bond Coat  
 contours of radial strain  
 ( infinitesimal )

time= 0.35000E+03

min(-) = -0.46117E-02  
 max(+) = 0.35367E-01  
 contour levels

- a = -0.61400E-03
- b = 0.33840E-02
- c = 0.73820E-02
- d = 0.11400E-01
- e = 0.15400E-01
- f = 0.19400E-01
- g = 0.23400E-01
- h = 0.27400E-01
- i = 0.31400E-01



SINE\_1 Interface Model with Higher CTE in Bond Coat -  
 Contour Map of Radial Strain at the Bond Coat/Ceramic Interface.



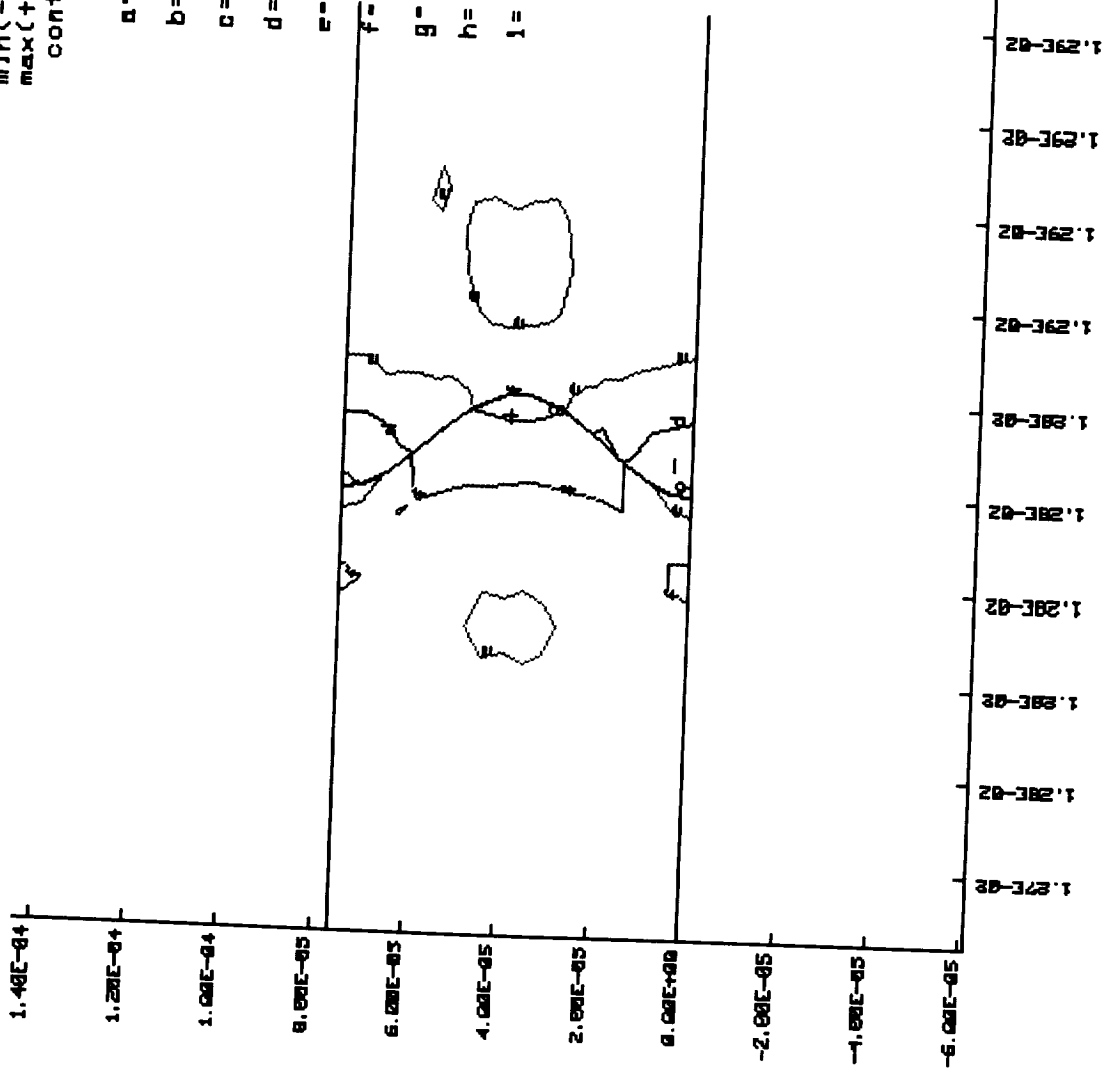
SINE\_1 Geometry, Higher CTE in Bond Coat  
contours of radial stress

time= 0.60000E+03

min(-)=-0.26619E+02  
max(+)= 0.30919E+02  
contour levels

MPa

- a=-0.48730E+02
- b=-0.36500E+02
- c=-0.24270E+02
- d=-0.12040E+02
- e= 0.19000E+00
- f= 0.12420E+02
- g= 0.24650E+02
- h= 0.36880E+02
- i= 0.49110E+02



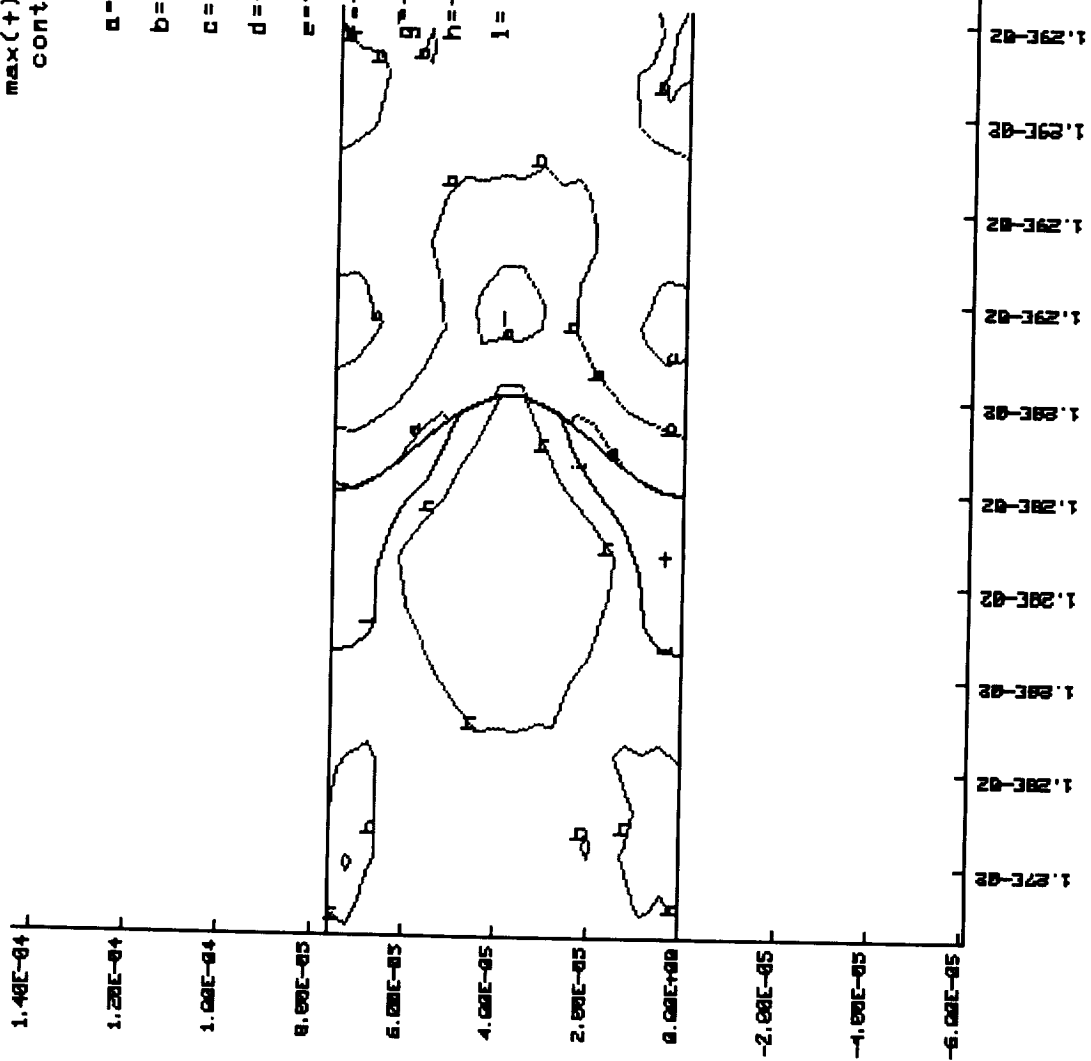
SINE\_1 Interface Model with Higher CTE in Bond Coat -  
Contour Map of Radial Stress at the Bond Coat/Ceramic Interface.

SINE\_1 Geometry, Higher CTE in Bond Coat  
 Contours of radial strain  
 ( infintimass )

time= 0.60000E+03

min(-)=-0.53255E-02  
 max(+)= 0.09989E-03  
 contour levels

- a=-0.48840E-02
- b=-0.42420E-02
- c=-0.36000E-02
- d=-0.29580E-02
- e=-0.23160E-02
- f=-0.16740E-02
- g=-0.10320E-02
- h=-0.39000E-03
- i= 0.00000E+00



SINE\_1 Interface Model with Higher CTE in Bond Coat -  
 Contour Map of Radial Strain at the Bond Coat/Ceramic Interface.

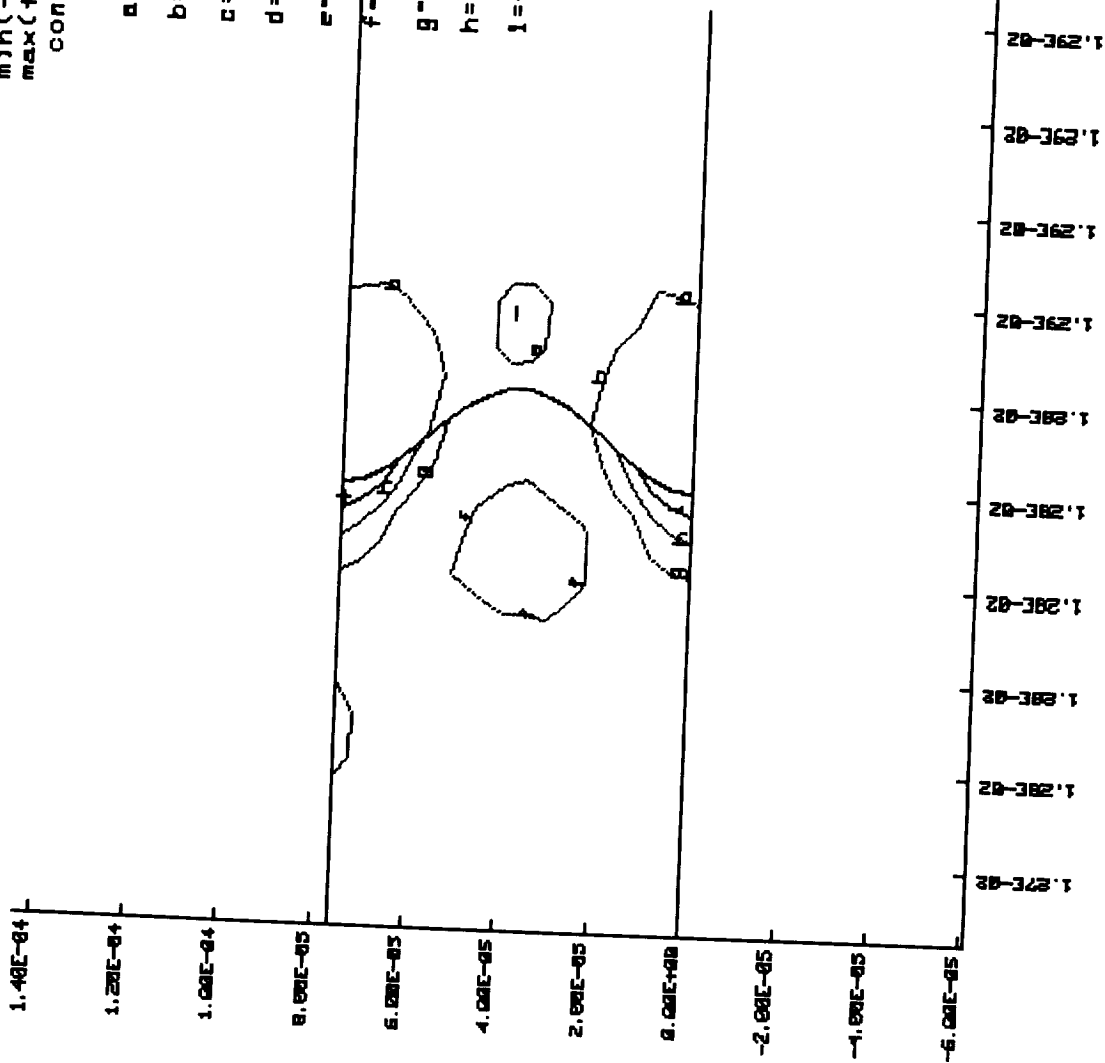
SINE\_1 Geometry, Higher CTE in Bond Coat  
 contours of axial stress

time= 0.600000E+03

m)n(-)=-0.16254E+03  
 max(+)--0.25623E+02  
 contour levels

MPa

- a--0.14900E+03
- b--0.13500E+03
- c--0.12100E+03
- d--0.10800E+03
- e--0.94080E+02
- f--0.80390E+02
- g--0.66700E+02
- h--0.53010E+02
- i--0.39310E+02

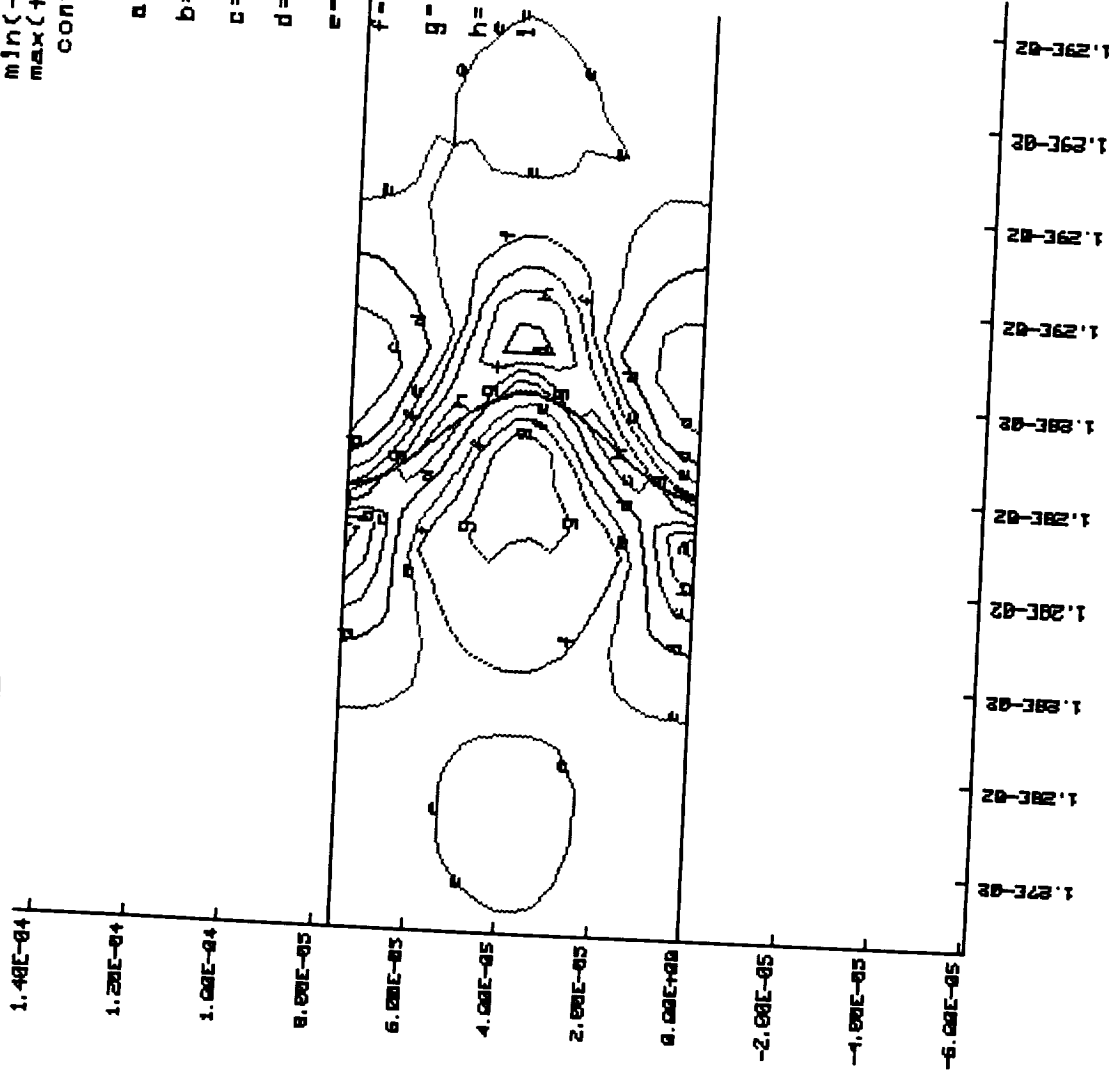


SINE\_1 Interface Model with Higher CTE in Bond Coat -  
 Contour Map of Axial Stress at the Bond Coat/Ceramic Interface.

SINE\_1 Geometry, Higher CTE in Bond Coat  
 Contours of axial strain  
 ( Infinitesimal )  
 time= 0.60000E+03

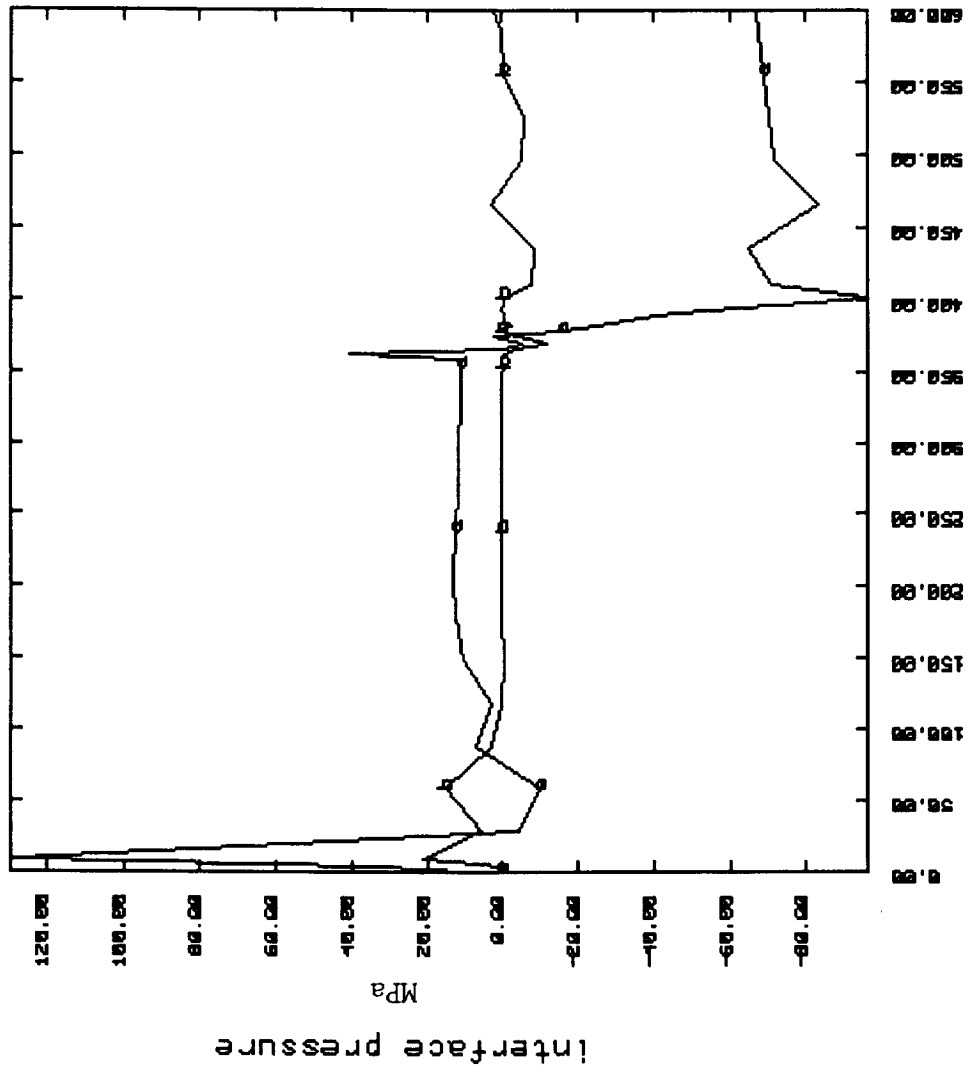
min(-)=-0.12045E-02  
 max(+)= 0.11289E-02  
 contour levels

- a=-0.97100E-03
- b=-0.73800E-03
- c=-0.50400E-03
- d=-0.27100E-03
- e= 0.00000E+00
- f= 0.19600E-03
- g= 0.42900E-03
- h= 0.66200E-03
- i= 0.89600E-03



SINE\_1 Interface Model with Higher CTE in Bond Coat -  
 Contour Map of Axial Strain at the Bond Coat/Ceramic Interface.

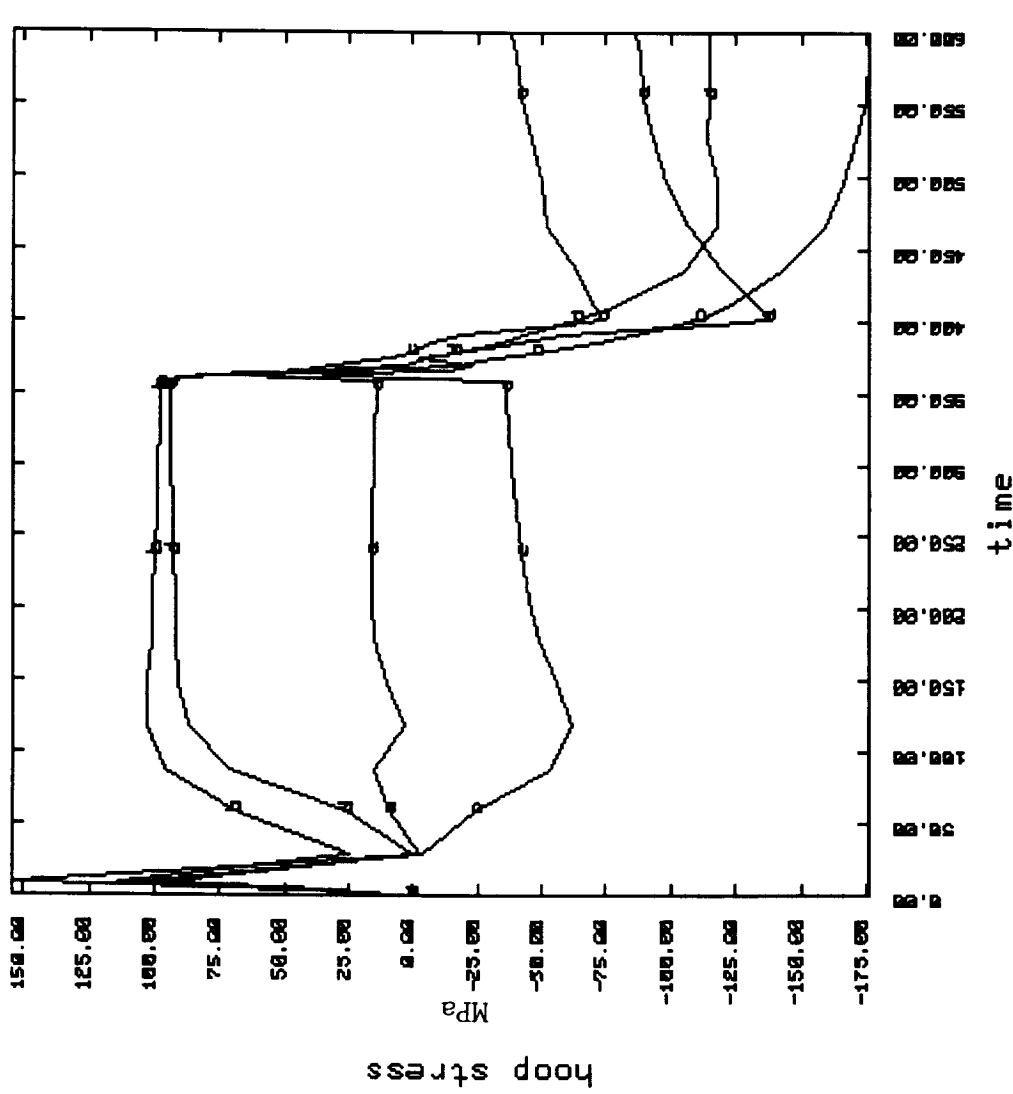
SINE\_1 Geometry, Higher CTE in Bond Coat



minimum : -0.9597E+02  
 maximum : 0.1294E+03  
 time nodes a= 13 b= 130

SINE\_1 Interface Model with Higher CTE in Bond Coat -  
 Interface Normal Pressure History Plot.

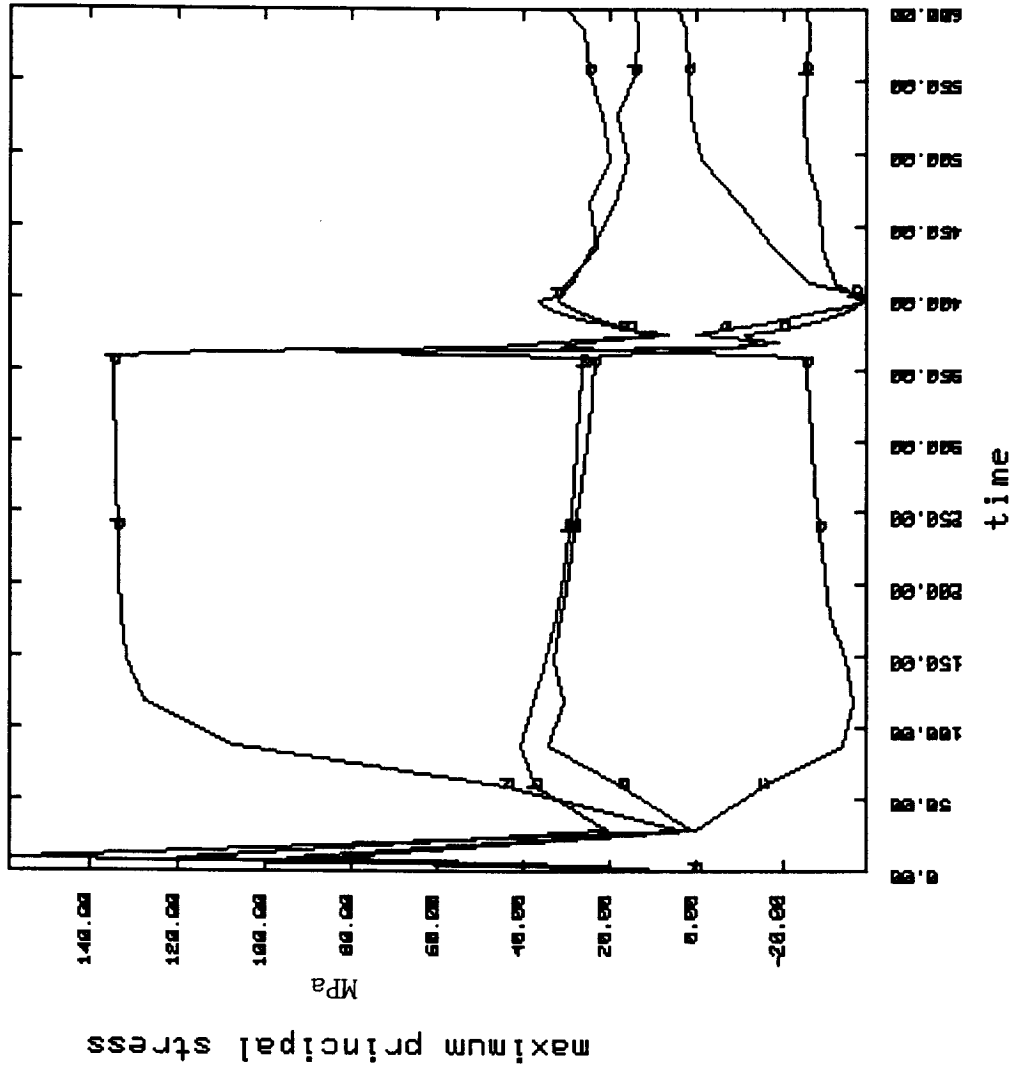
SINE\_1 Geometry, Higher CTE in Bond Coat



minimum = -0.1762E+03  
 maximum = 0.1542E+03  
 elements a= 12 b= 229 c= 120  
 d= 445

SINE\_1 Interface Model with Higher CTE in Bond Coat -  
 Hoop Stress History Plot.

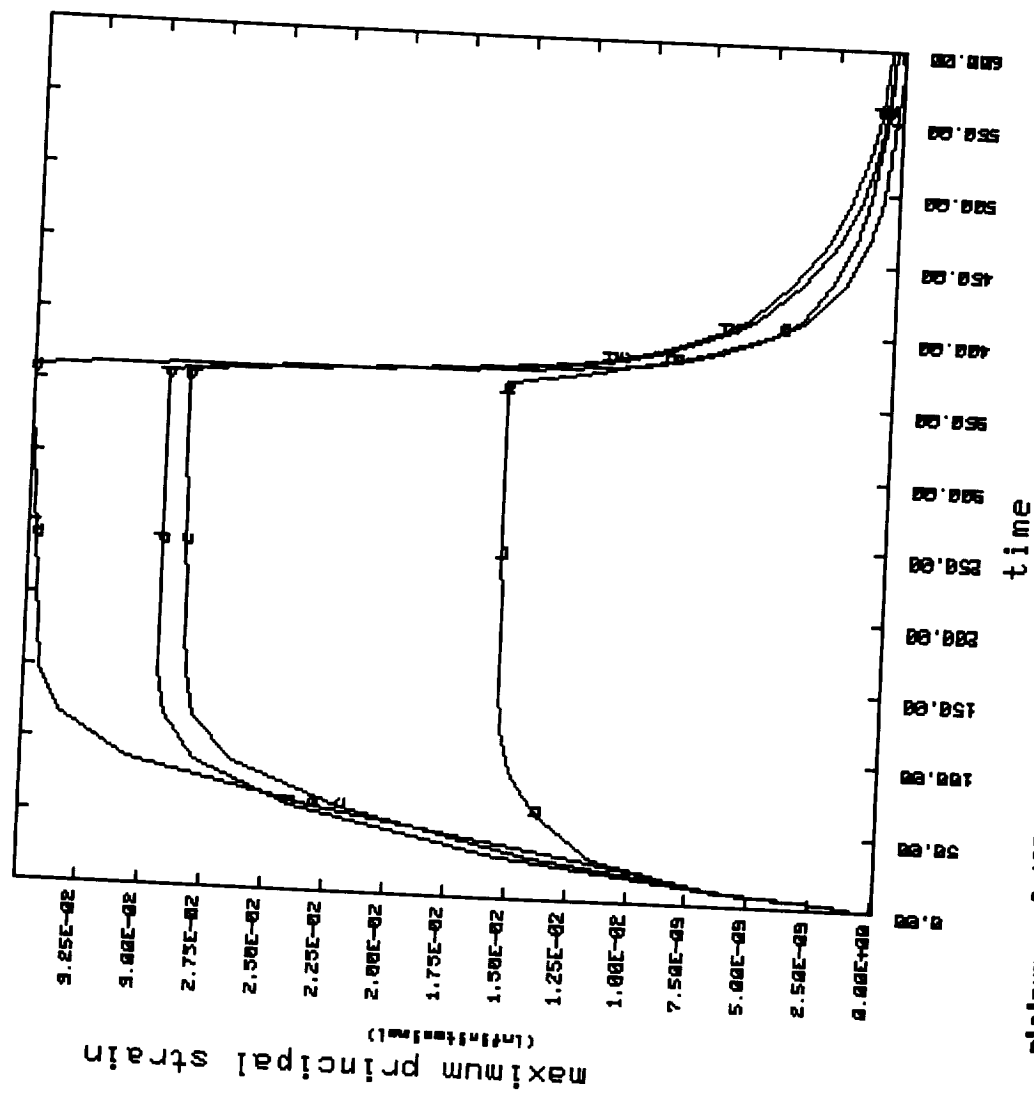
SINE\_1 Geometry, Higher CTE in Bond Coat



minimum : -0.3922E+02  
 maximum : 0.1586E+03  
 elements a: 12 b: 229 c: 120  
 d: 445

SINE\_1 Interface Model with Higher CTE in Bond Coat -  
 Maximum Principal Stress History Plot.

SINE\_1 Geometry, Higher CTE in Bond Coat



minimum = -0.1057E-03  
 maximum = 0.3494E-01  
 elements a= 42 b= 229 c= 120

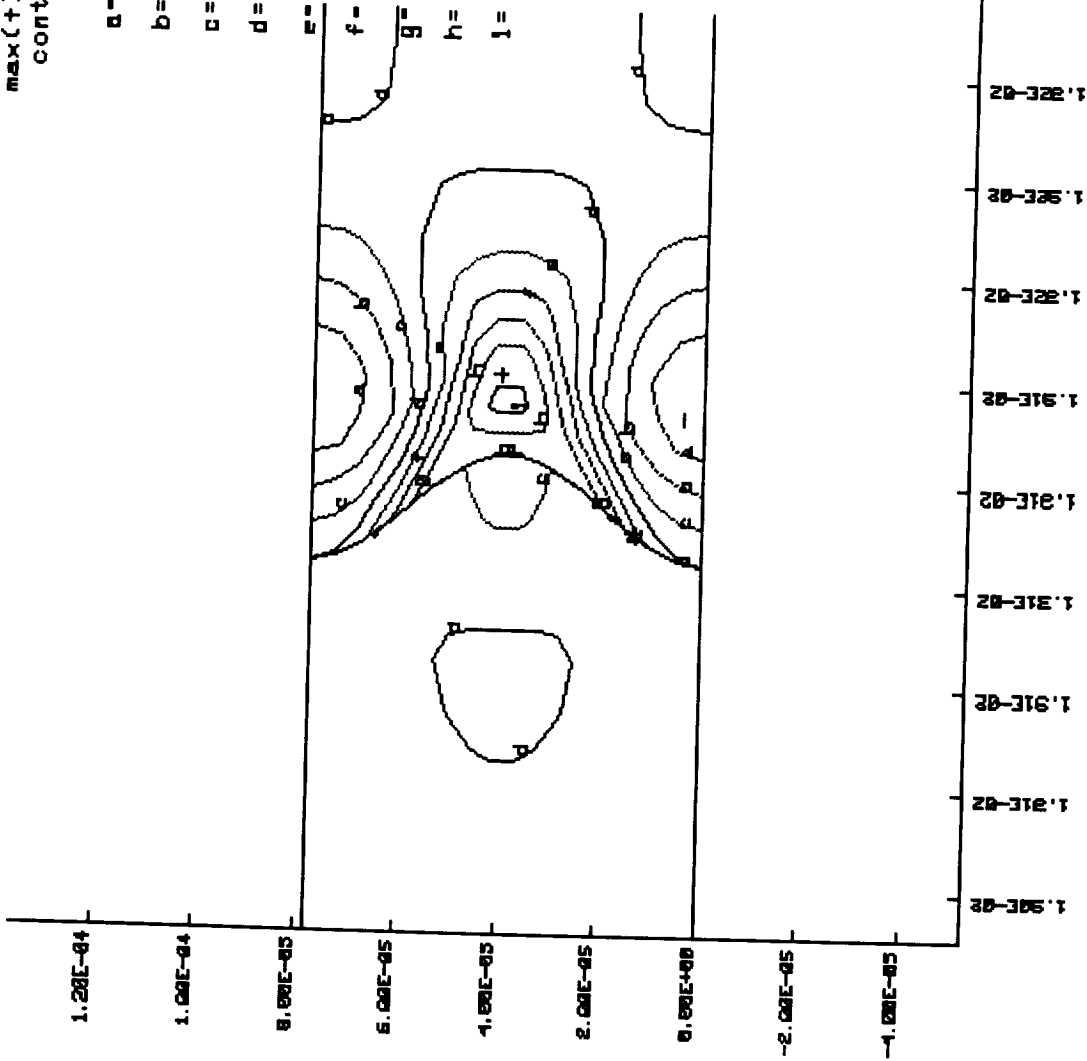
SINE\_1 Interface Model with Higher CTE in Bond Coat -  
 Maximum Principal Strain History Plot.

SINE\_1 Interface: Higher Creep Coefficient  
Contours of radial stress

time= 0.35000E+03

min(-)=-0.18853E+02  
max(+)= 0.25790E+02  
contour levels

- MPa
- a=-0.14390E+02
  - b=-0.99200E+01
  - c=-0.54600E+01
  - d=-0.99600E+00
  - e= 0.34700E+01
  - f= 0.79300E+01
  - g= 0.12400E+02
  - h= 0.16860E+02
  - i= 0.21330E+02



SINE\_1 Interface Model with Higher Creep Coefficients -  
Contour Map of Radial Stress at the Bond Coat/Ceramic Interface.

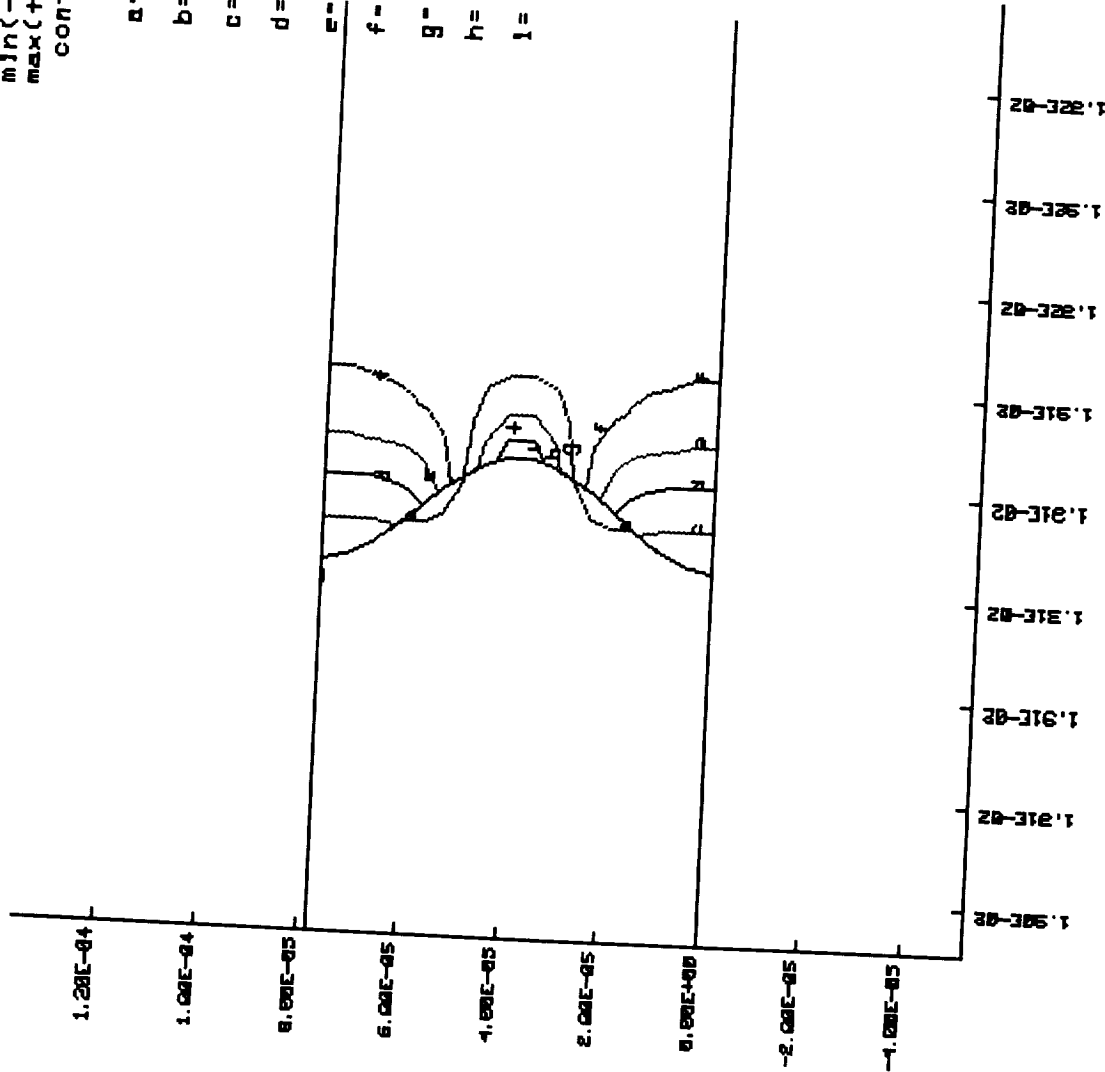
SINE\_1 Interface: Higher Creep Coefficient  
 contours of axial stress

time = 0.35000E+03

min(-) = -0.11338E+02  
 max(+) = 0.17487E+03  
 contour levels

MPa

- a = 0.00000E+00
- b = 0.19500E+02
- c = 0.39000E+02
- d = 0.58500E+02
- e = 0.78000E+02
- f = 0.97500E+02
- g = 0.11700E+03
- h = 0.13650E+03
- i = 0.15600E+03



SINE\_1 Interface Model with Higher Creep Coefficients -  
 Contour Map of Axial Stress at the Bond Coat/Ceramic Interface.

SINE\_1 Interface: Higher Creep Coefficient  
 contours of axial strain  
 ( Infinitesimal )

time= 0.60000E+03

min(-)=-0.40909E-02  
 max(+)= 0.32330E-02  
 contour levels

a=-0.33050E-02

b=-0.25780E-02

c=-0.18520E-02

d=-0.11250E-02

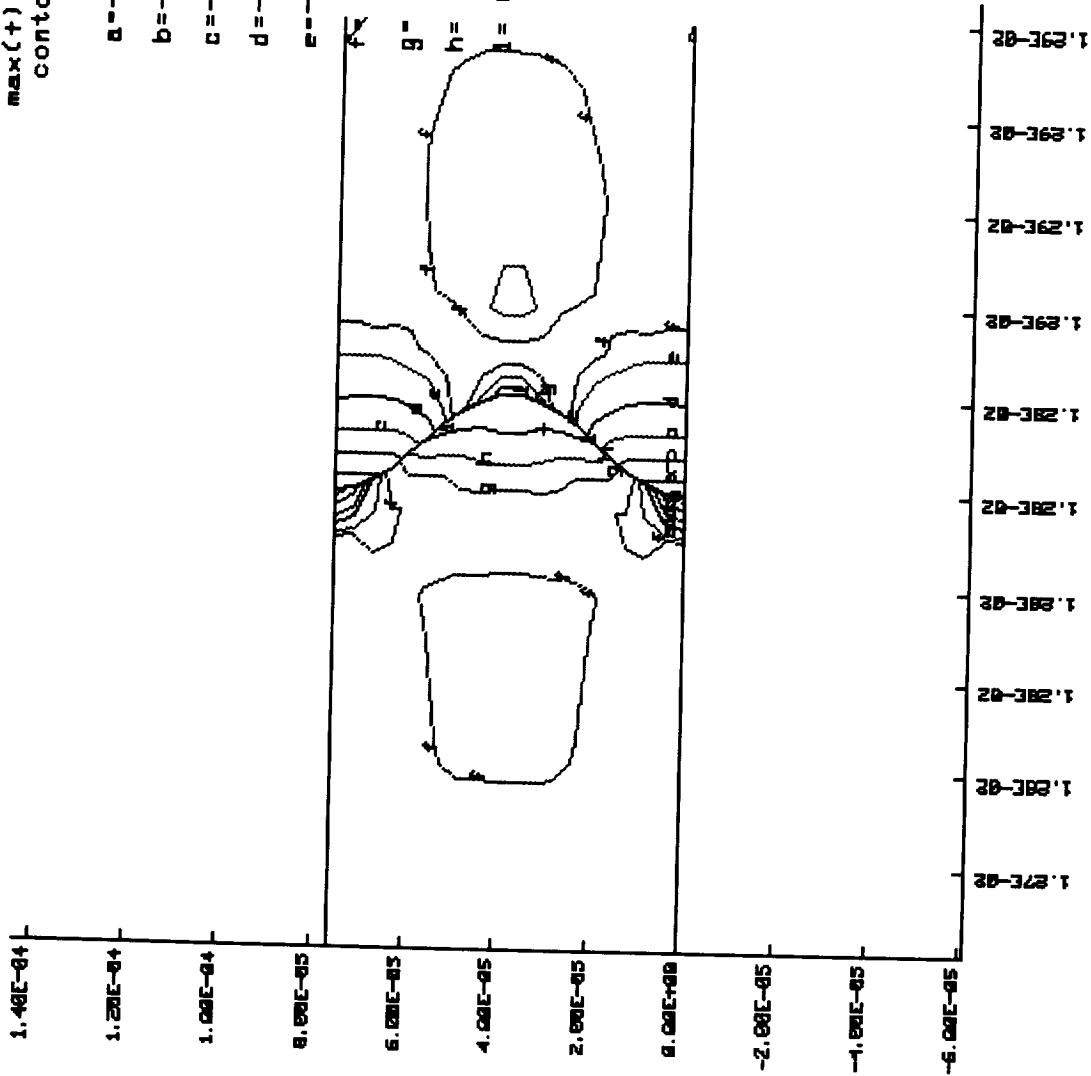
e=-0.39900E-03

f= 0.00000E+00

g= 0.10540E-02

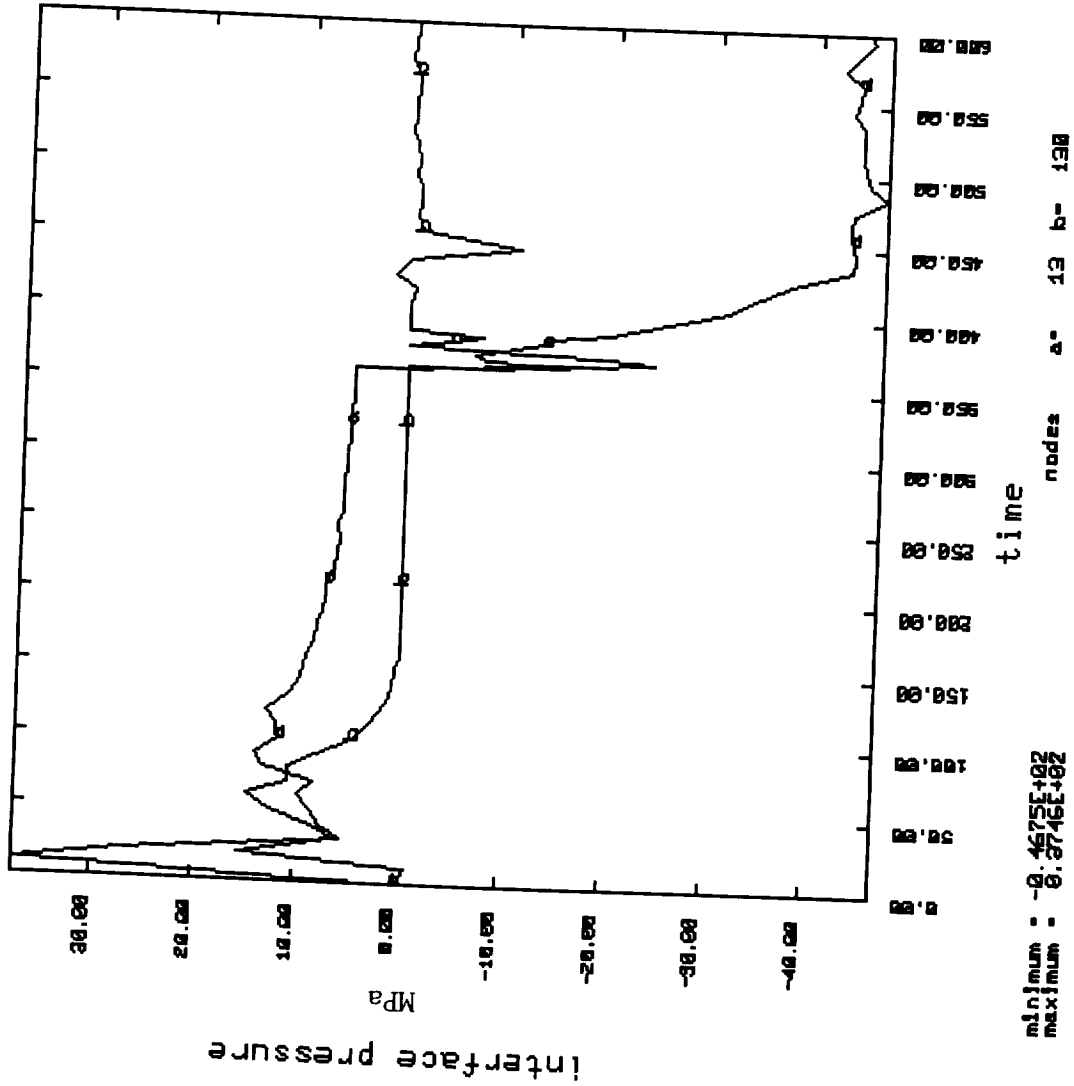
h= 0.17800E-02

i= 0.25070E-02



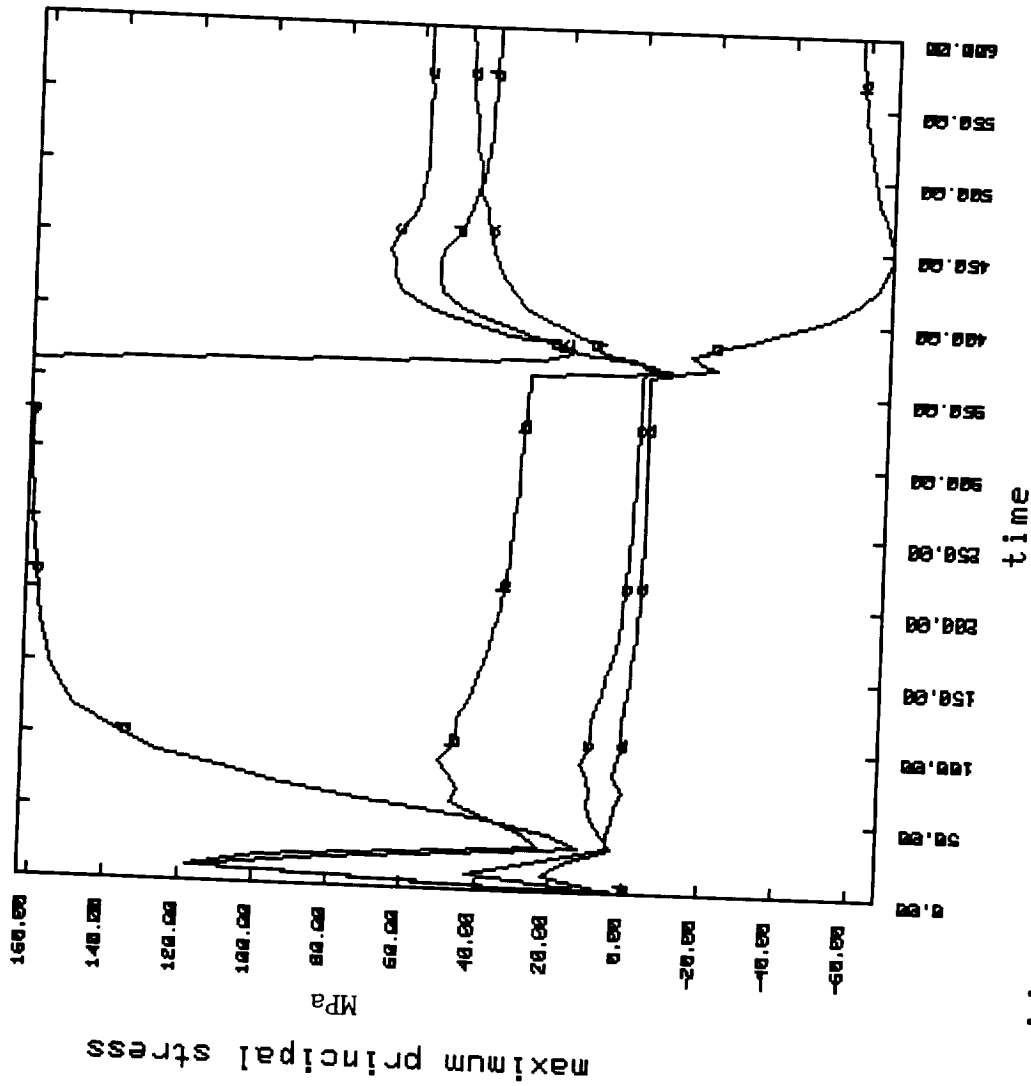
SINE\_1 Interface Model with Higher Creep Coefficients -  
 Contour Map of AxialStrain at the Bond Coat/ Ceramic Interface.

SINE\_1 Interface: Higher Creep Coefficient



SINE\_1 Interface Model with Higher Creep Coefficients -  
Interface Normal Pressure History Plot.

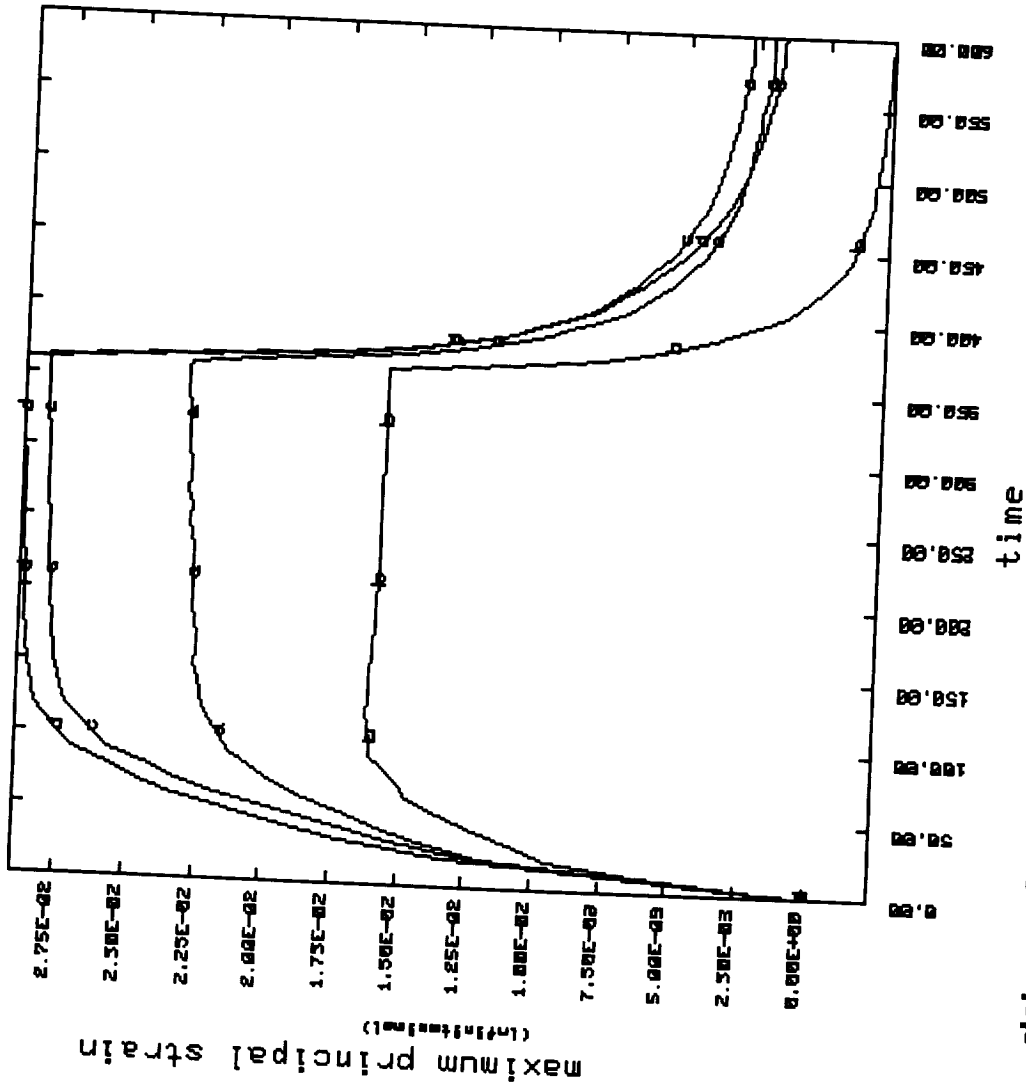
SINE\_1 Interface: Higher Creep Coefficient



minimum = -0.6774E+02  
 maximum = 0.1620E+03  
 elements a= 12 b= 229 c= 120  
 d= 445

SINE\_1 Interface Model with Higher Creep Coefficients -  
 Maximum Principal Stress History Plot.

SINE\_1 Interface: Higher Creep Coefficient



minimum : -0.2385E-02  
 maximum : 0.2985E-01  
 elements a: 12 b: 229 c: 120  
 d: 445

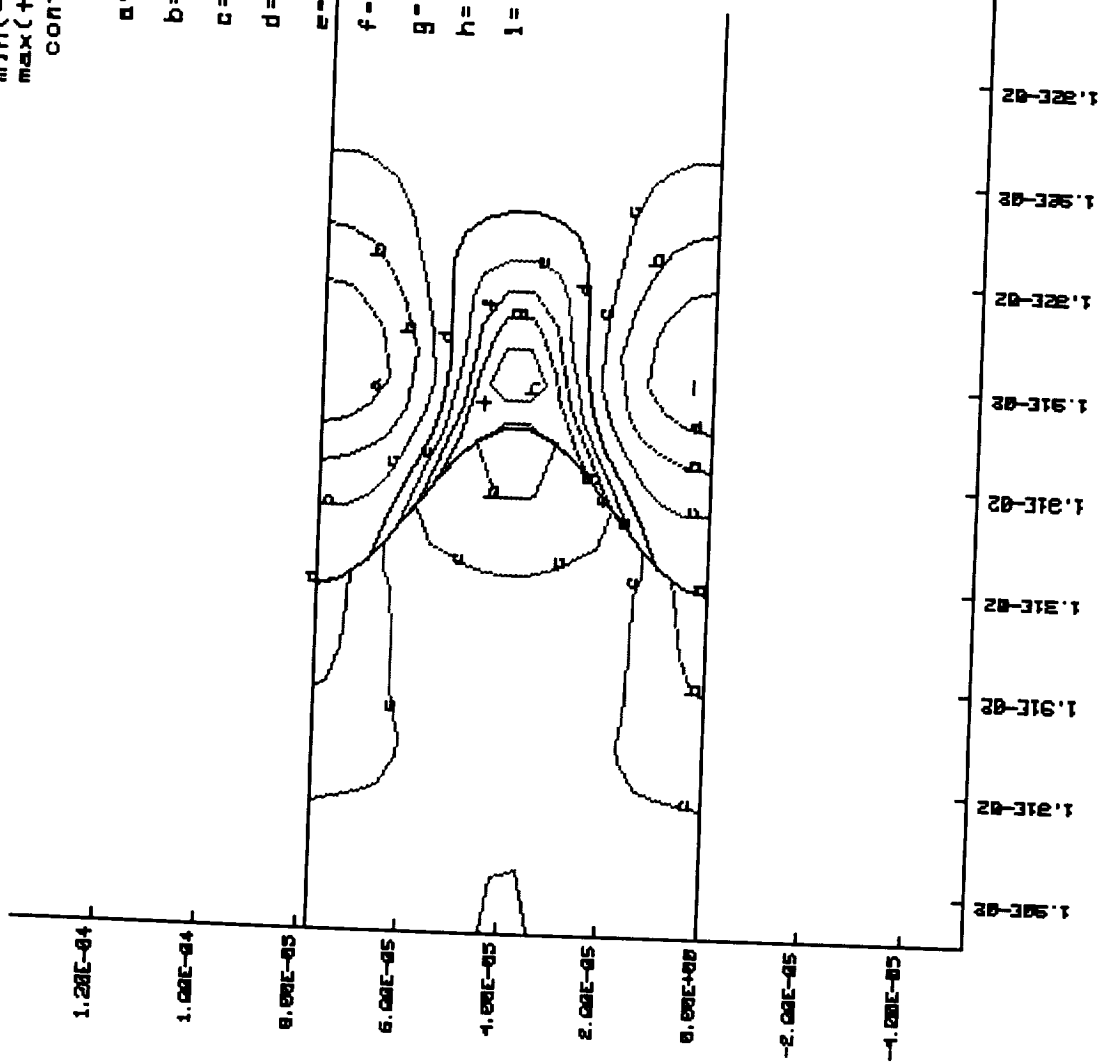
SINE\_1 Interface Model with Higher Creep Coefficients -  
 Maximum Principal Strain History Plot.

SINE\_2 Interface: Base Materials, 1.5x amplitude  
 contours of radial stress

time= 0.35000E+03

min(-) = -0.16858E+02  
 max(+) = 0.30923E+02  
 contour levels

- a = -0.12080E+02
- b = -0.73000E+01
- c = -0.25200E+01
- d = 0.22500E+01
- e = 0.70300E+01
- f = 0.11810E+02
- g = 0.16590E+02
- h = 0.21370E+02
- i = 0.26140E+02



SINE\_2 Interface Geometry Model with Base Materials and 1.5x Amplitude -  
 Contour Map of Radial Stress at the Bond Coat/Ceramic Interface.

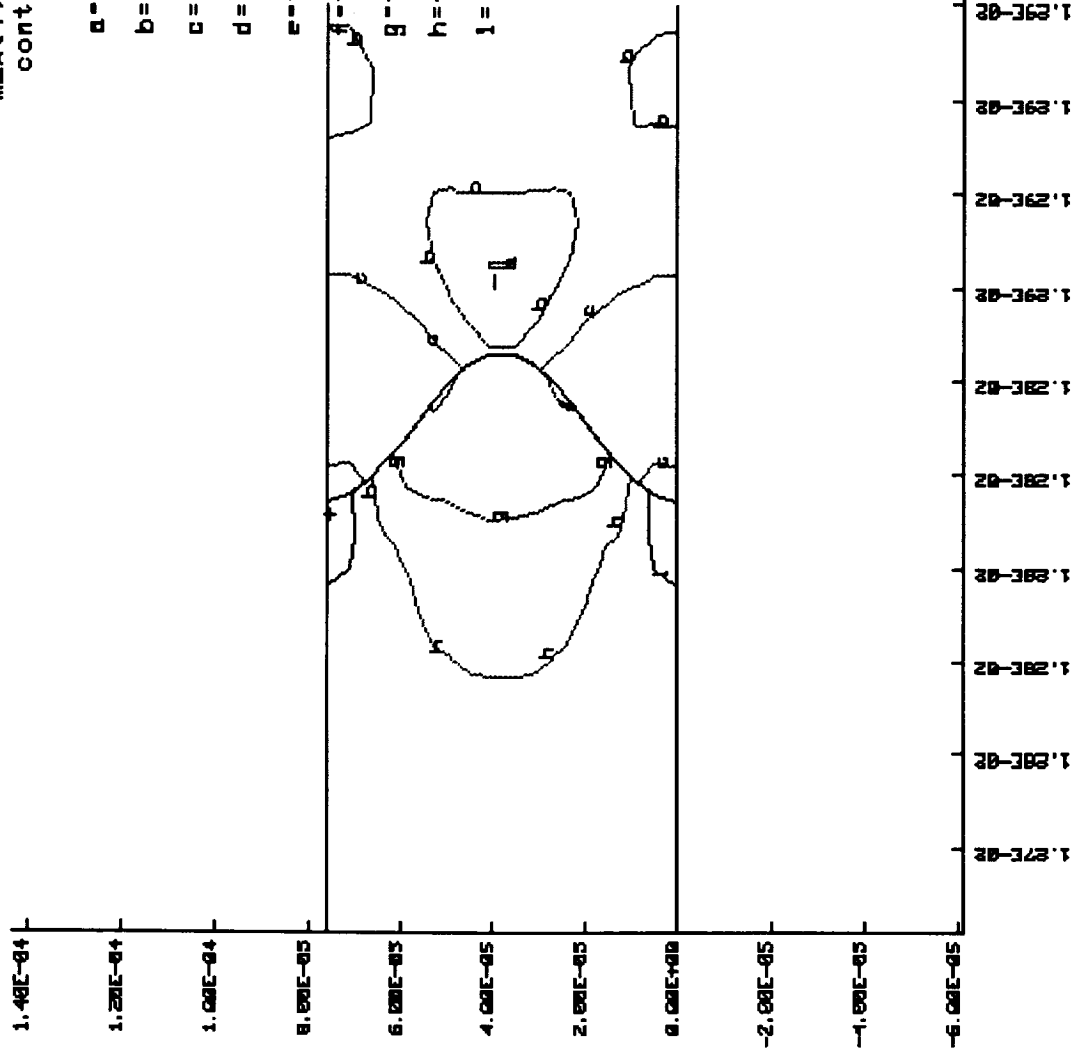


SINE\_2 Interface: Base Materials, 1.5x amplitude  
 contours of axial stress

time= 0.60000E+03  
 min(-)=-0.18867E+03  
 max(+)= 0.41440E+02  
 contour levels

MPa

- a=-0.16600E+03
- b=-0.14300E+03
- c=-0.12000E+03
- d=-0.96620E+02
- e=-0.73610E+02
- f=-0.50600E+02
- g=-0.27590E+02
- h=-0.45800E+01
- i= 0.18430E+02



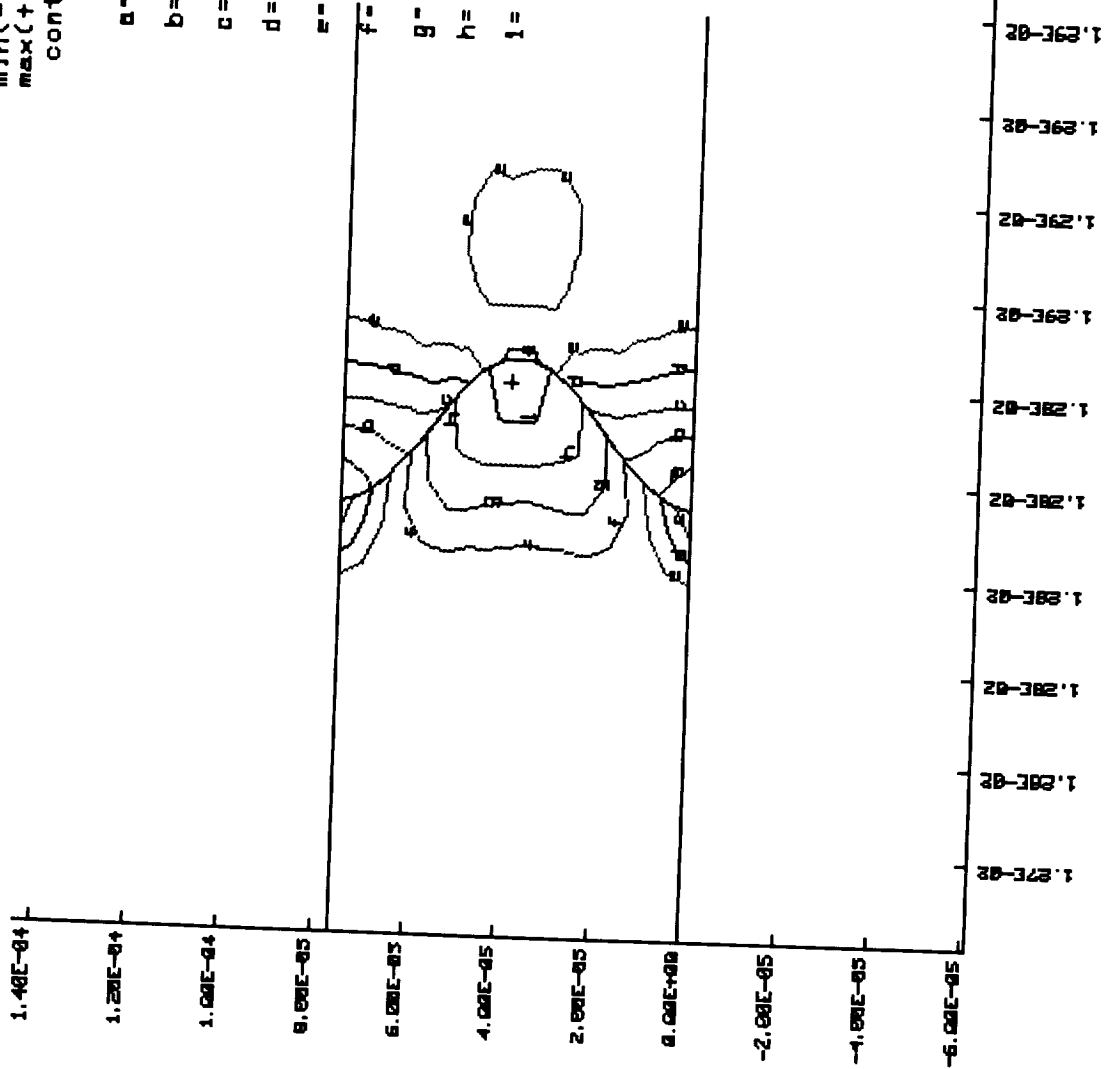
SINE\_2 Interface Model with Base Materials and 1.5x Amplitude -  
 Contour Map of Axial Stress at the Bond Coat/Ceramic Interface.

SINE\_2 Interface: Base Materials, 1.5x amplitude  
 contours of radial stress

time= 0.600000E+03

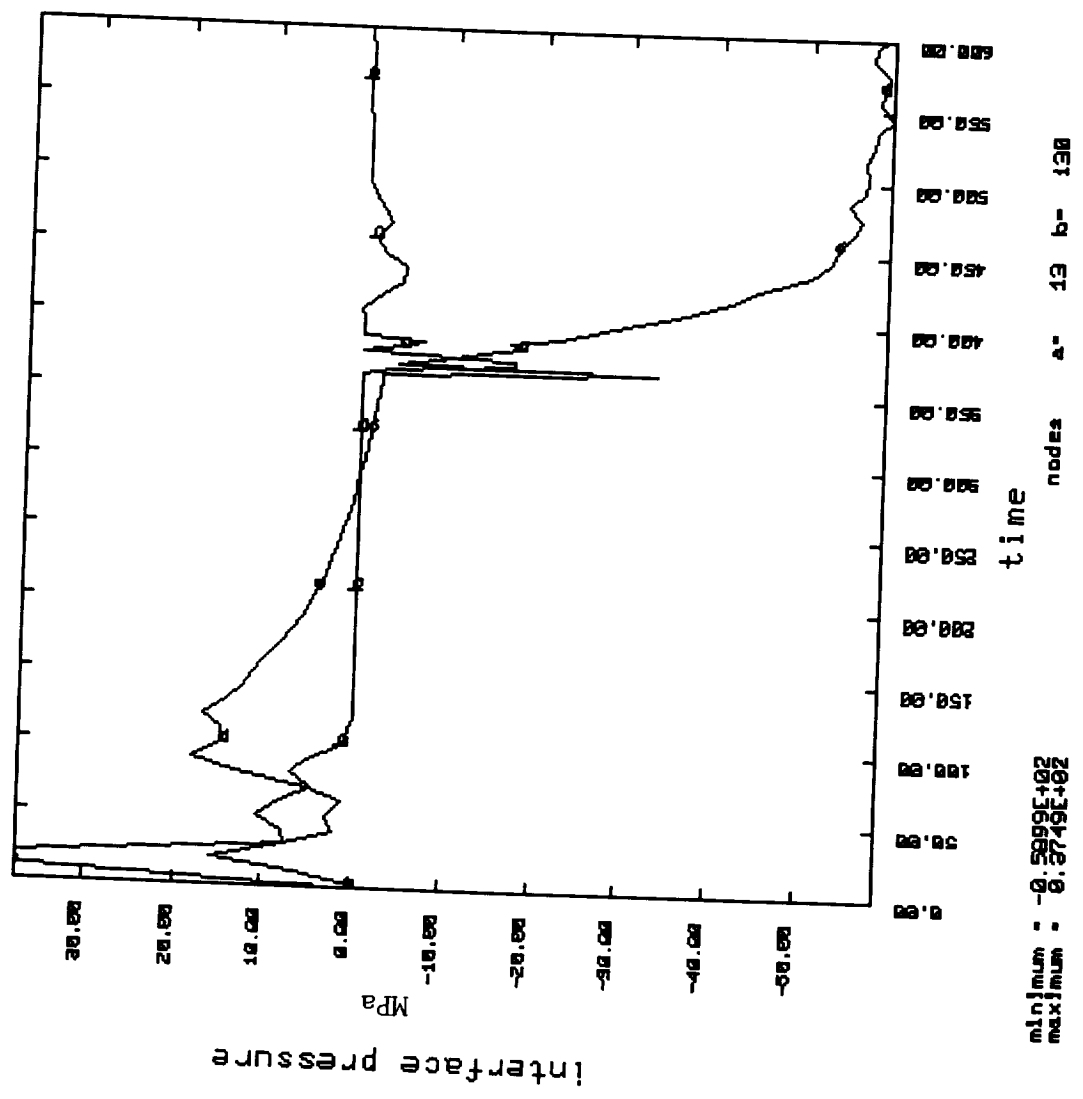
min(-)=-0.77336E+02  
 max(+)= 0.71720E+02  
 contour levels

- MPa
- a=-0.62430E+02
  - b=-0.47520E+02
  - c=-0.32620E+02
  - d=-0.17710E+02
  - e=-0.28100E+01
  - f= 0.12100E+02
  - g= 0.27000E+02
  - h= 0.41910E+02
  - i= 0.56810E+02



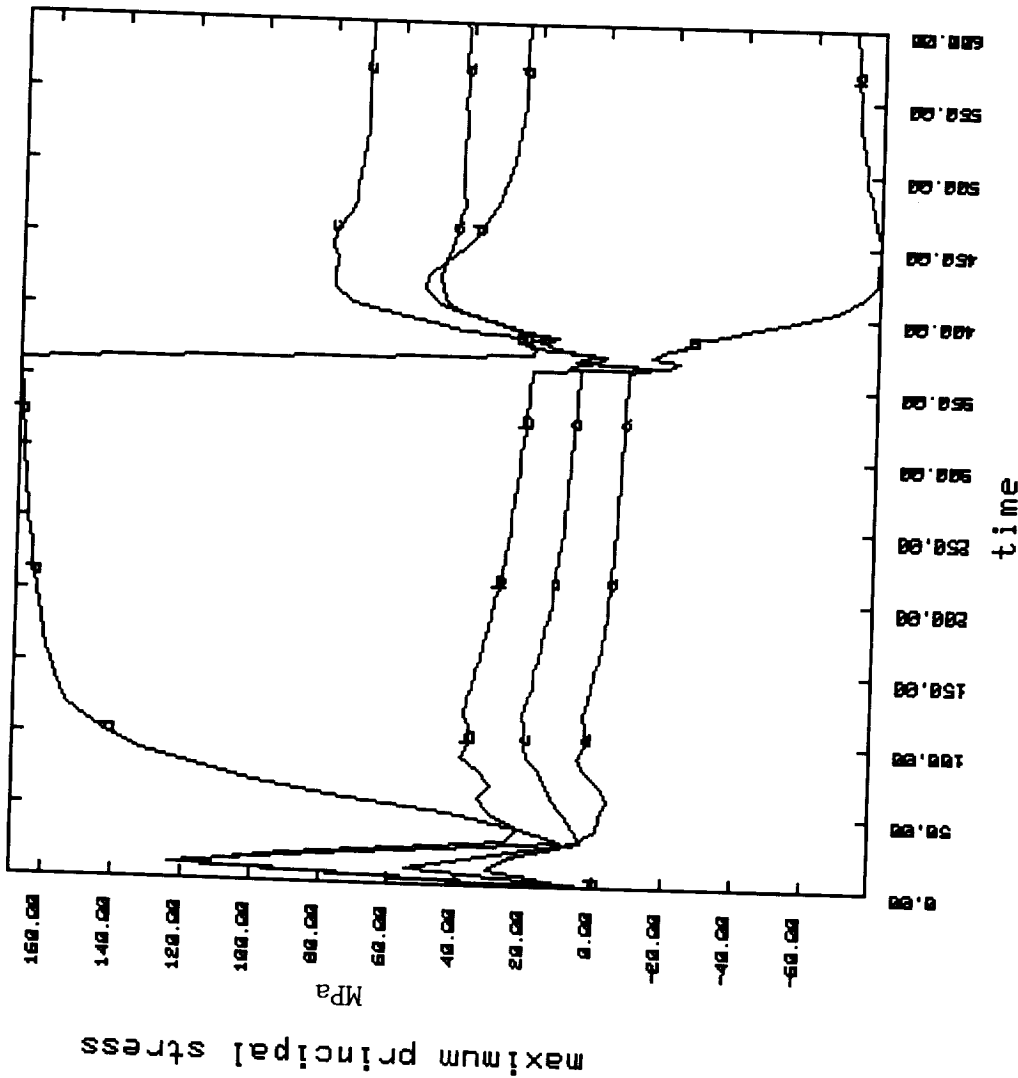
SINE\_2 Interface Geometry Model with Base Materials and 1.5x Amplitude -  
 Contour Map of Radial Stress at the Bond Coat/Ceramic Interface.

SINE\_2 Interface: Base Materials, 1.5x amplitude



SINE\_2 Interface Model with Base Materials and 1.5x Amplitude - Interface Normal Pressure History Plot.

SINE\_2 Interface: Base Materials, 1.5x amplitude

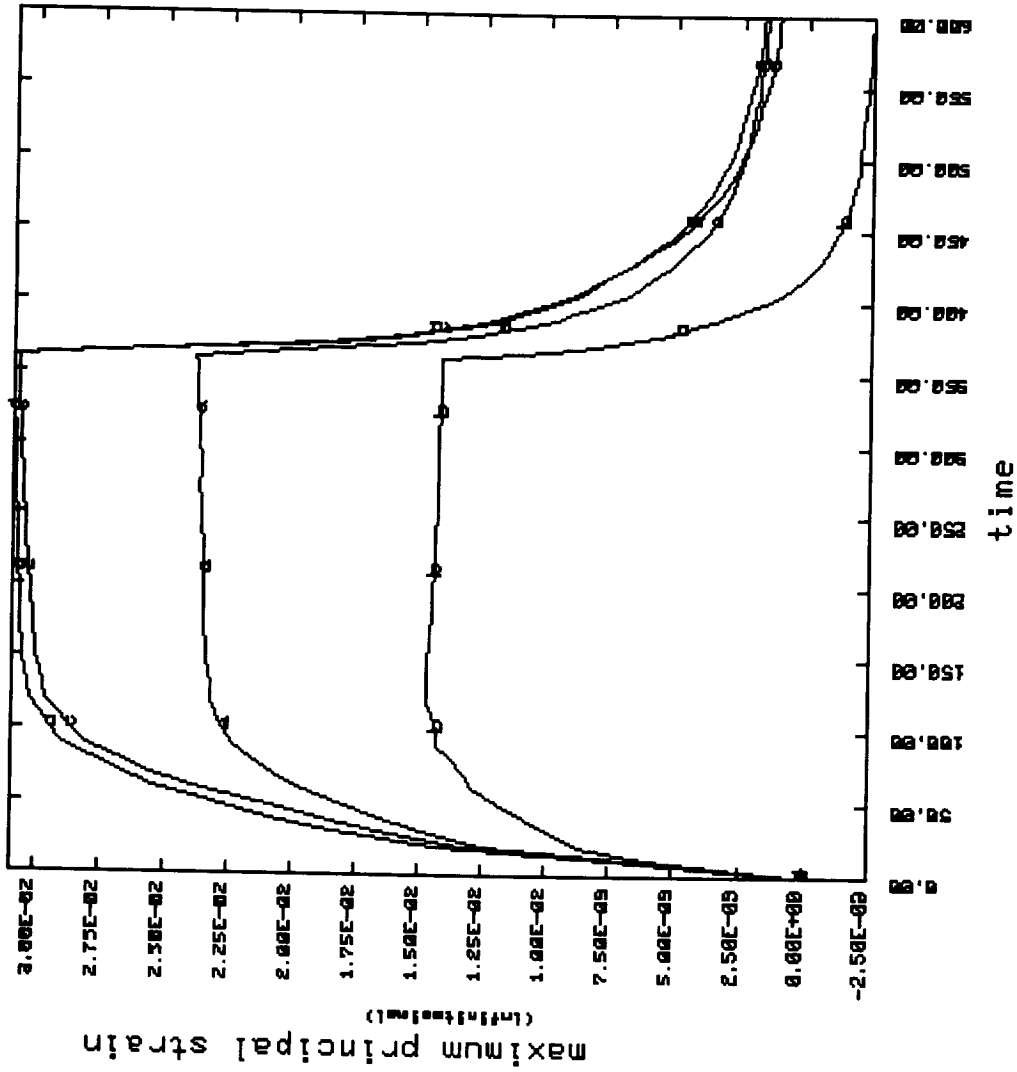


minimum : -0.7916E+02  
 maximum : 0.1691E+03

elements a: 12 b: 229 c: 120

SINE\_2 Interface Model with Base Materials and 1.5x Amplitude -  
 Maximum Principal Stress History Plot.

SINE\_2 Interface: Base Materials, 1.5x amplitude



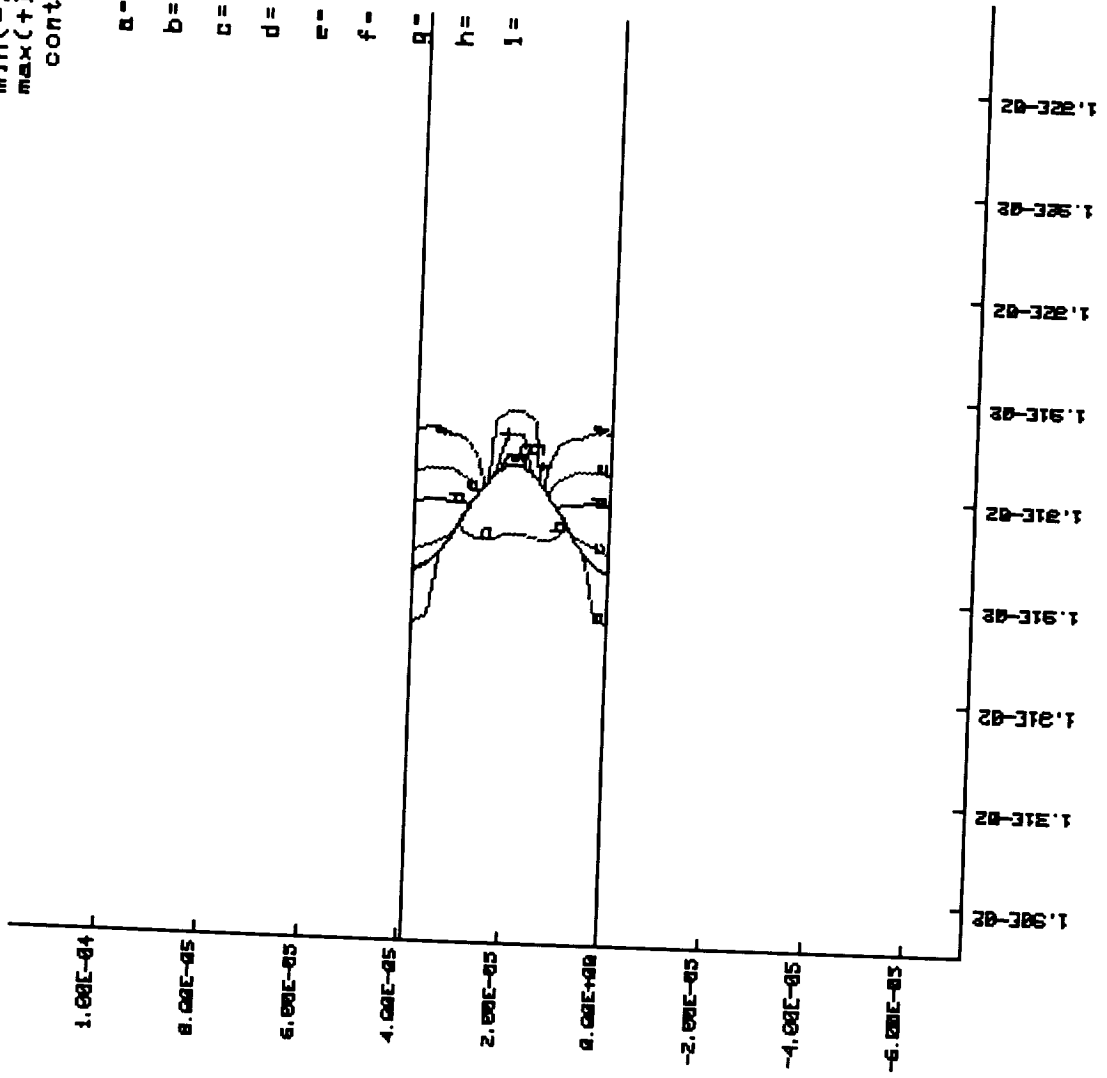
minimum : -0.2557E-02  
 maximum : 0.2691E-01

SINE\_2 Interface Model with Base Materials and 1.5x Amplitude -  
 Maximum Principal Strain History Plot.

SINE\_3 Interface: Base Materials, 2x frequency  
 Contours of axial stress  
 time= 0.35000E+03

min(-)=-0.27420E+02  
 max(+)= 0.15977E+03  
 contour levels  
 MPa

- a=-0.87000E+01
- b= 0.10020E+02
- c= 0.28740E+02
- d= 0.47460E+02
- e= 0.66170E+02
- f= 0.84890E+02
- g= 0.10400E+03
- h= 0.12200E+03
- i= 0.14100E+03

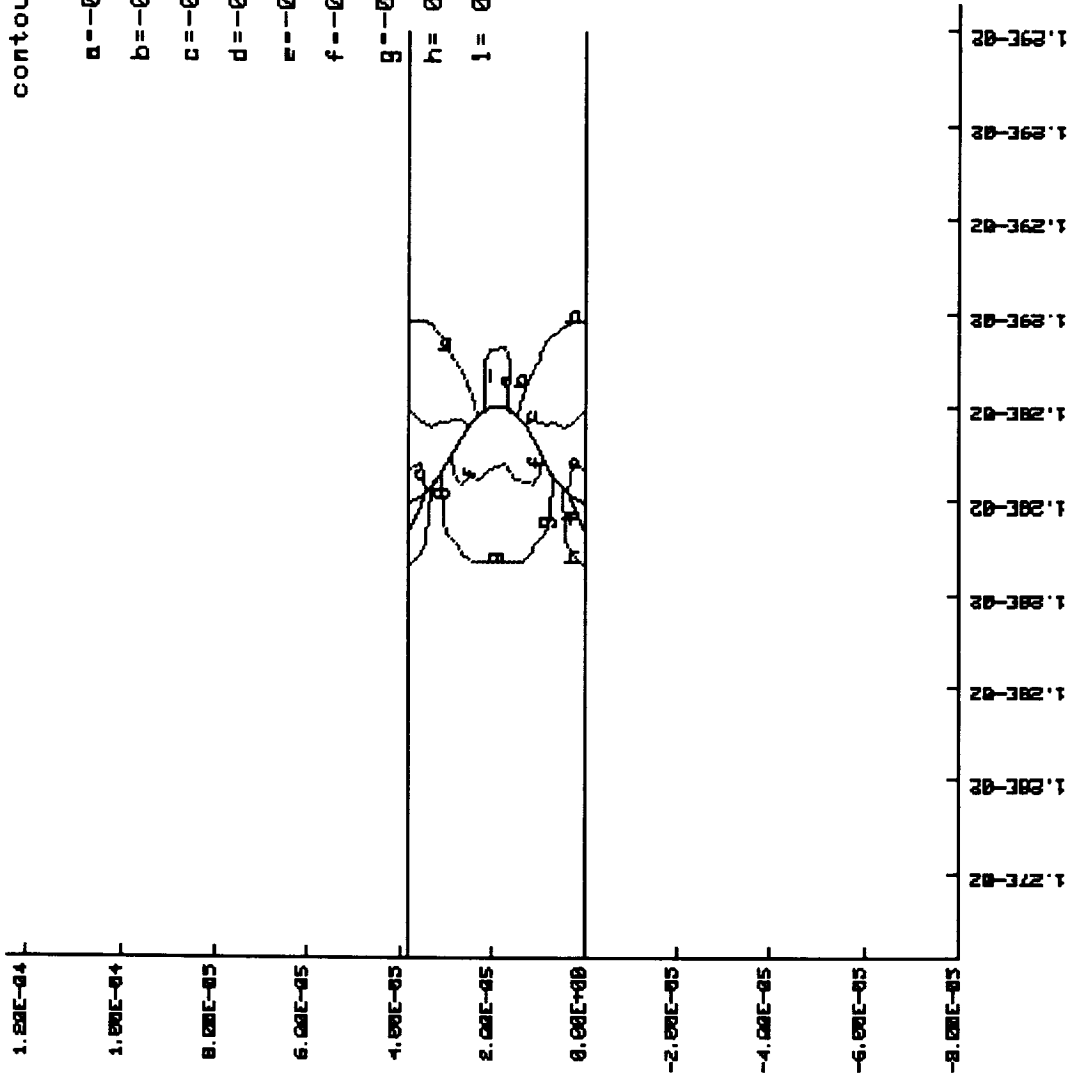


SINE\_3 Interface Geometry with Base Materials and 2x Frequency -  
 Contour Map of Axial Stress at the Bond Coat/Ceramic Interface.

SINE\_3 Interface: Base Materials, 2x frequency  
 contours of axial stress

time = 0.60000E+03  
 min(-) = -0.18294E+03  
 max(+) = 0.66452E+02  
 contour levels

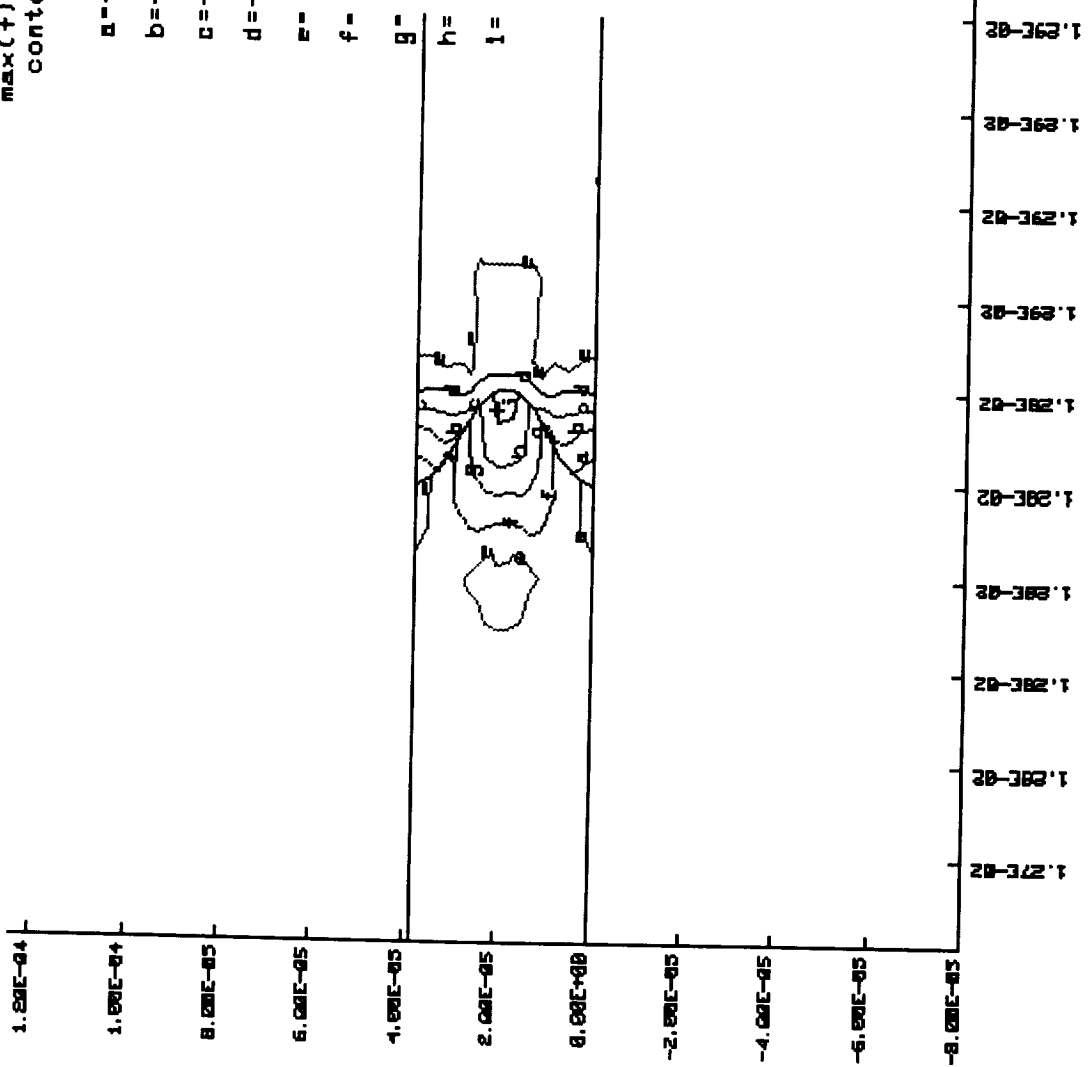
- MPa
- a = -0.15800E+03
  - b = -0.13300E+03
  - c = -0.10800E+03
  - d = -0.83190E+02
  - e = -0.58250E+02
  - f = -0.33310E+02
  - g = -0.83700E+01
  - h = 0.16570E+02
  - i = 0.41510E+02



SINE\_3 Interface Geometry with Base Materials and 2x Frequency -  
 Contour Map of Axial Stress at the Bond Coat/Ceramic Interface.

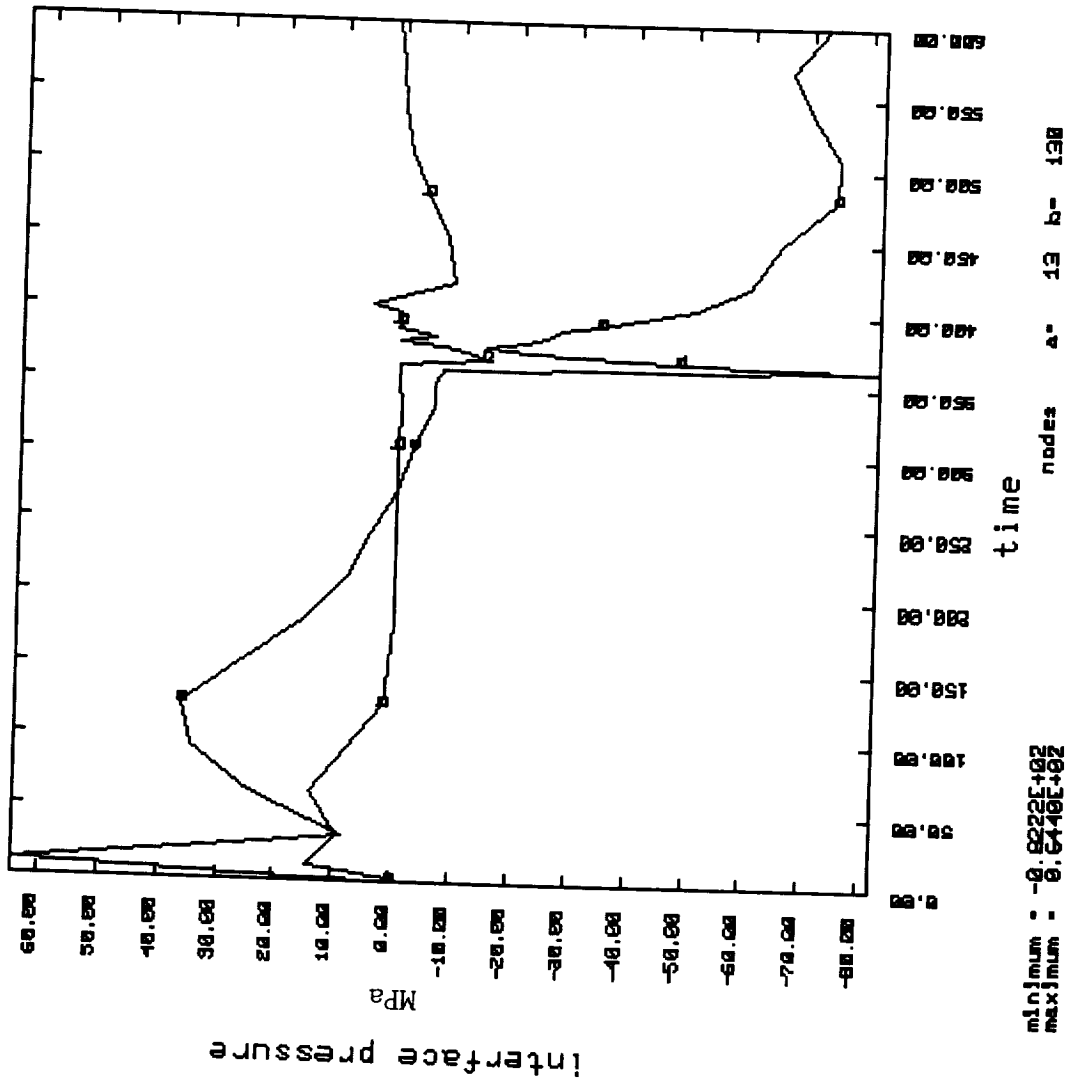
SINE\_3 Interface: Base Materials, 2x frequency  
 contours of radial stress

time= 0.60000E+03  
 min(-)=-0.75496E+02  
 max(+)= 0.75842E+02  
 contour levels  
 MPa  
 a=-0.60336E+02  
 b=-0.45230E+02  
 c=-0.30090E+02  
 d=-0.14960E+02  
 e= 0.17300E+00  
 f= 0.15310E+02  
 g= 0.30140E+02  
 h= 0.45570E+02  
 i= 0.60710E+02



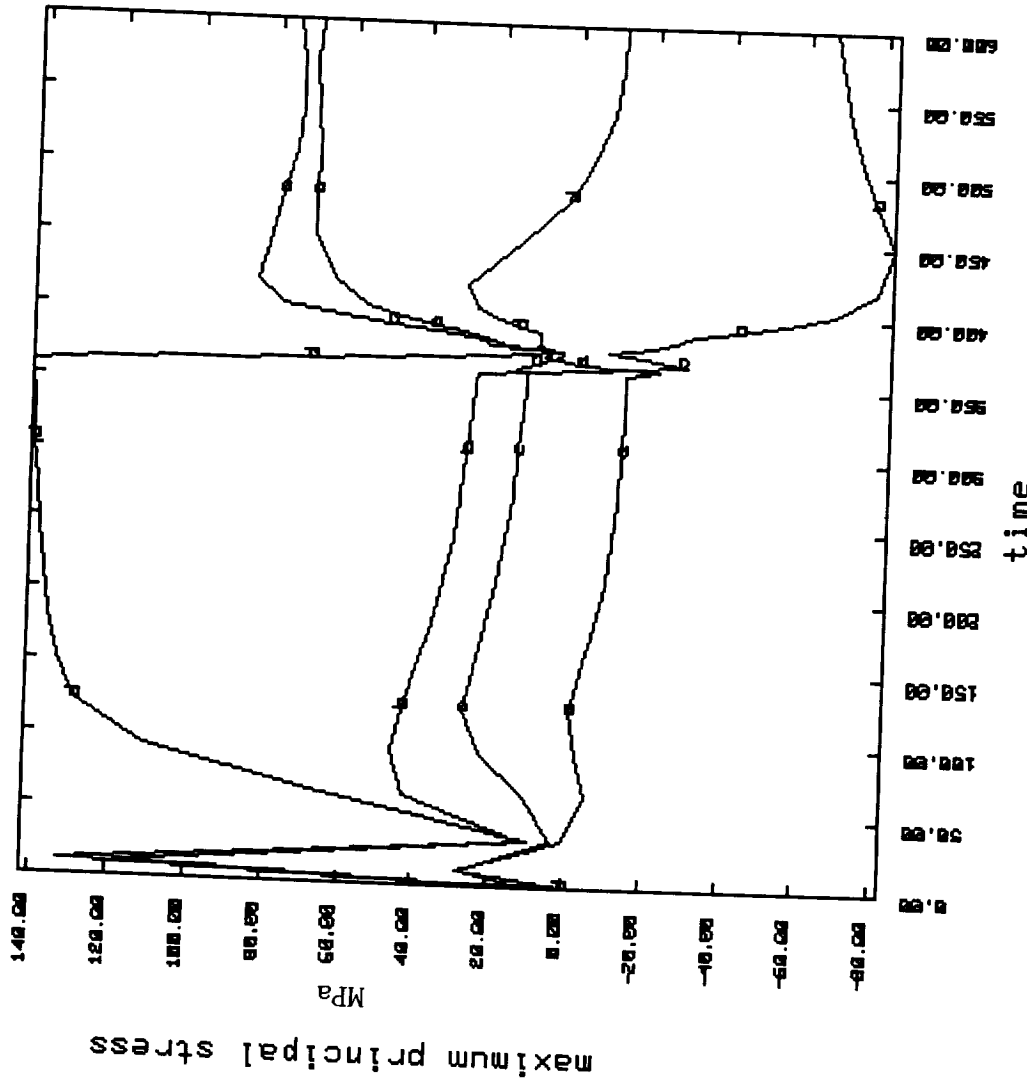
SINE\_3 Interface Geometry with Base Materials and 2x Frequency -  
 Contour Map of Radial Stress at the Bond Coat/Ceramic Interface.

SINE\_3 Interface: Base Materials, 2x frequency



SINE\_3 Interface Geometry with Base Materials and 2x Frequency -  
Interface Normal Pressure History Plot.

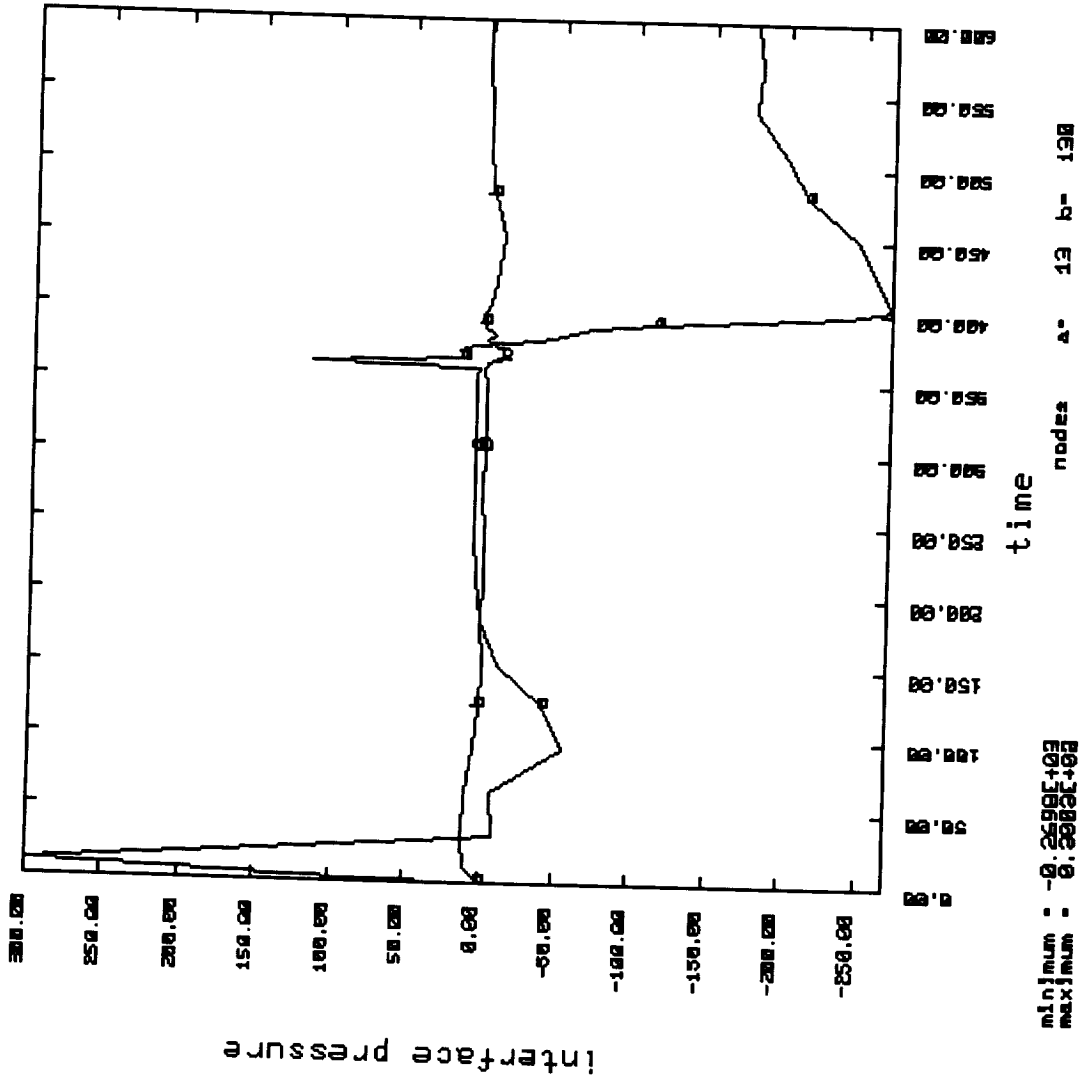
SINE\_3 Interface: Base Materials, 2x frequency



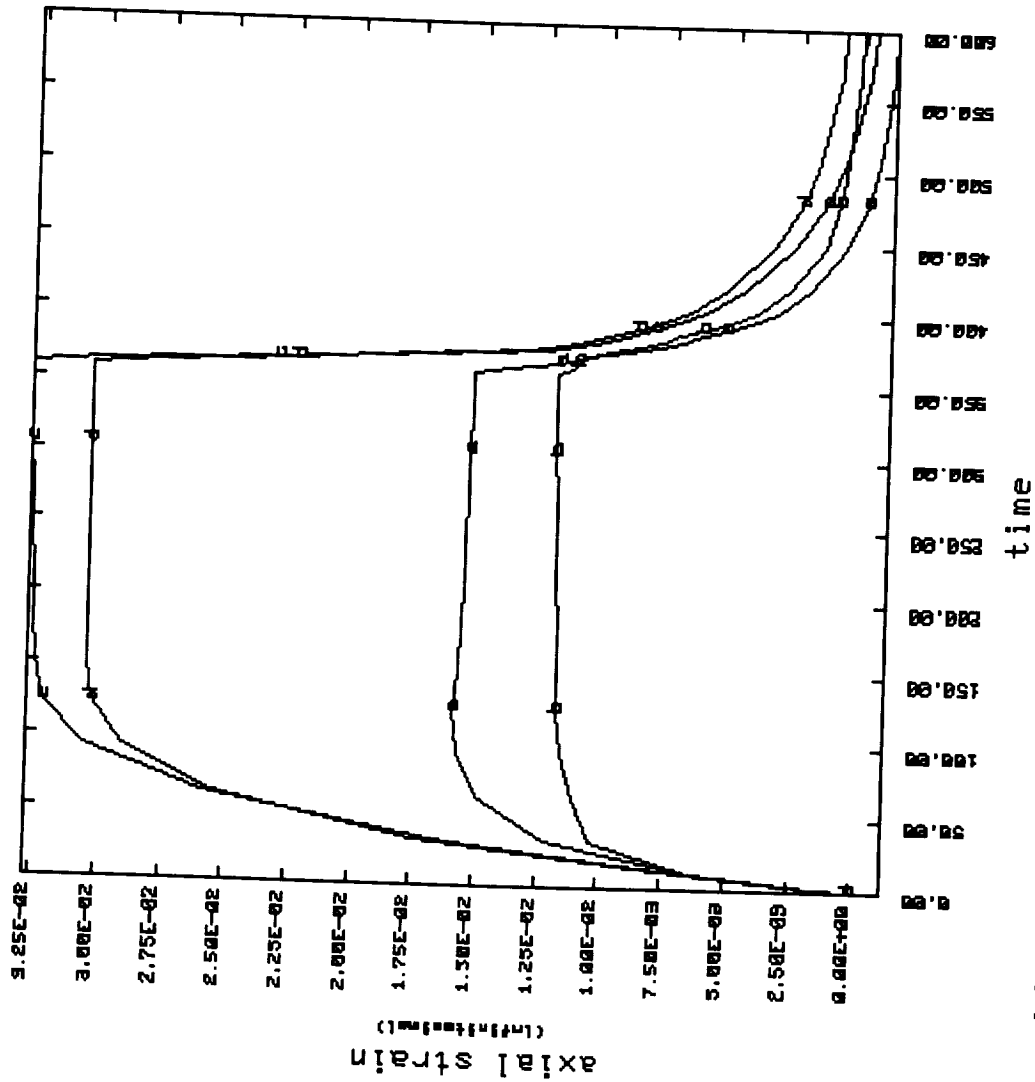
minimum = -0.0262E+02  
 maximum = 0.1424E+03  
 elements a= 12 b= 229 c= 120  
 d= 445

SINE\_3 Interface Geometry with Base Materials and 2x Frequency -  
 Maximum Principal Stress History Plot.

SINE\_3 Interface: Higher BC CTE, 2x freq.

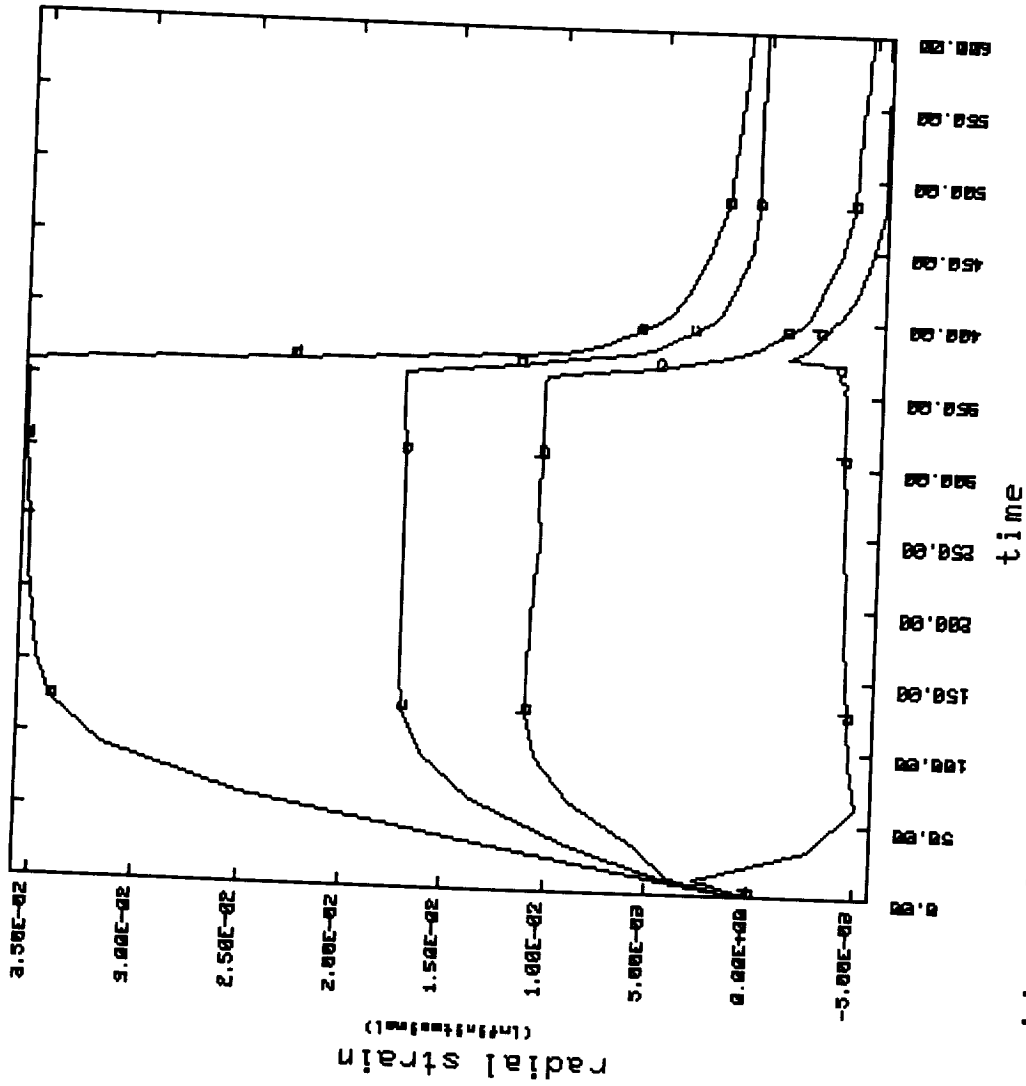


SINE\_3 Interface: Higher BC CTE, 2x freq.



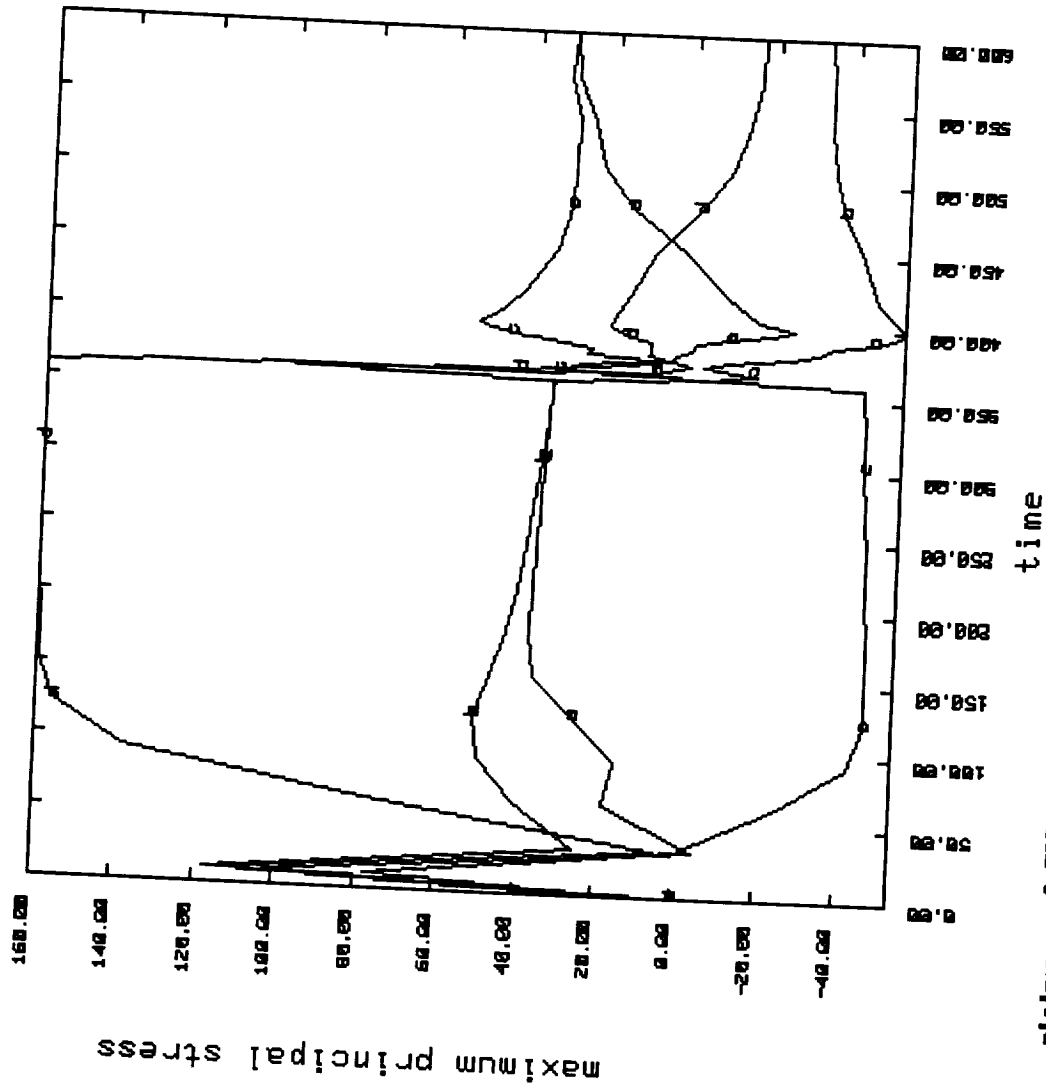
minimum = -0.1219E-02  
 maximum = 0.2278E-01  
 elements a= 12 b= 229 c= 120  
 d= 445

SINE\_3 Interface: Higher BC CTE, 2x freq.



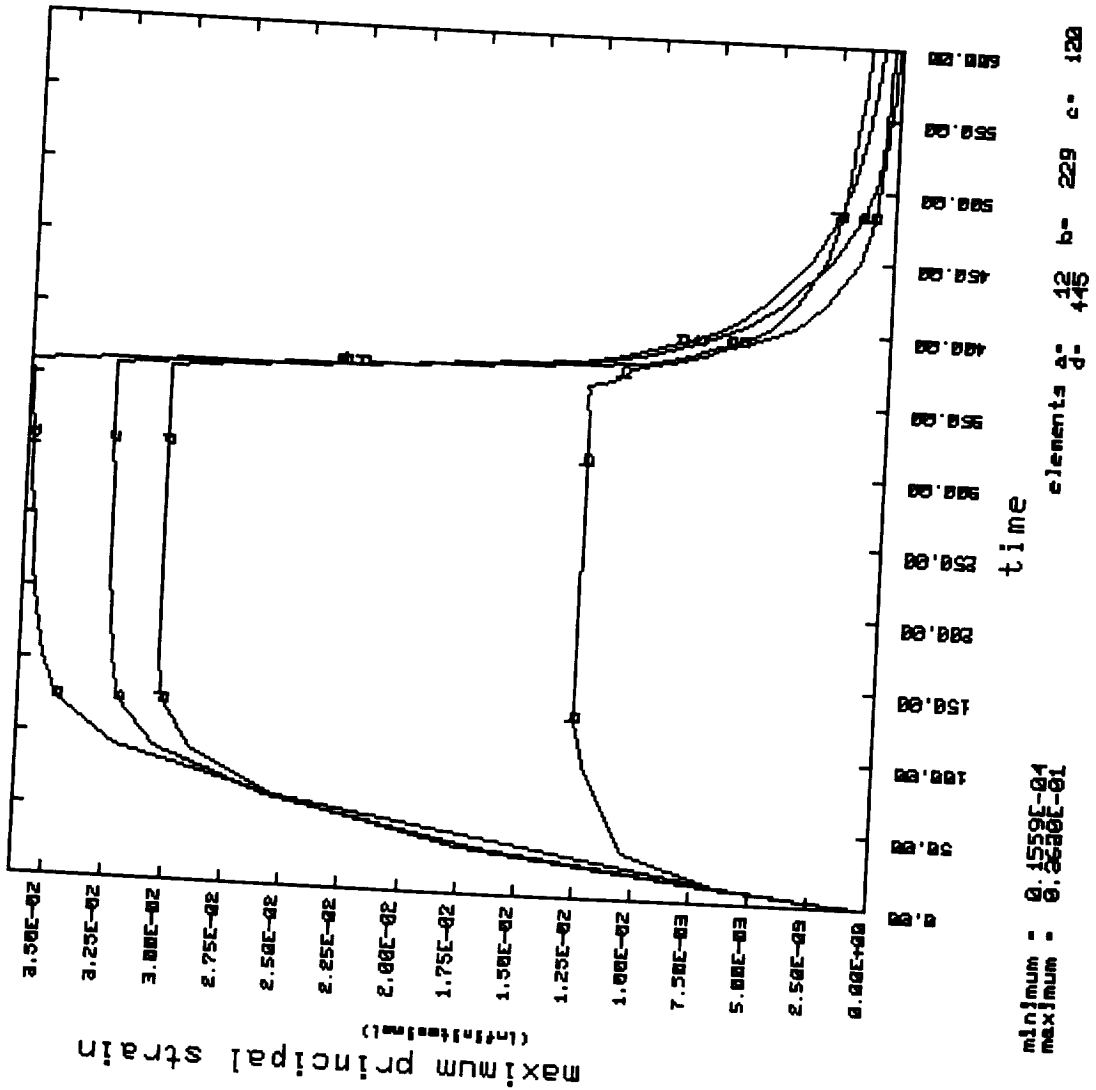
minimum =  $-0.5089 \times 10^{-2}$   
 maximum =  $0.2573 \times 10^{-1}$   
 elements a= 12 b= 229 c= 120  
 time

SINE\_3 Interface: Higher BC CTE, 2x freq.



minimum : -0.5329E+02  
maximum : 0.1681E+03  
elements a= 12 b= 229 c= 128  
d= 445

SINE\_3 Interface: Higher BC CTE, 2x freq.



**REPORT DOCUMENTATION PAGE**Form Approved  
OMB No. 0704-0188

Public reporting burden for this collection of information is estimated to average 1 hour per response, including the time for reviewing instructions, searching existing data sources, gathering and maintaining the data needed, and completing and reviewing the collection of information. Send comments regarding this burden estimate or any other aspect of this collection of information, including suggestions for reducing this burden, to Washington Headquarters Services, Directorate for Information Operations and Reports, 1215 Jefferson Davis Highway, Suite 1204, Arlington, VA 22202-4302, and to the Office of Management and Budget, Paperwork Reduction Project (0704-0188), Washington, DC 20503.

<b>1. AGENCY USE ONLY (Leave blank)</b>		<b>2. REPORT DATE</b> November 1992	<b>3. REPORT TYPE AND DATES COVERED</b> Final Contractor Report	
<b>4. TITLE AND SUBTITLE</b> Modeling of Thermal Barrier Coatings			<b>5. FUNDING NUMBERS</b> WU-505-63-5A C-NAS3-26664	
<b>6. AUTHOR(S)</b> B.L. Ferguson, G.J. Petrus, and T.M. Krauss				
<b>7. PERFORMING ORGANIZATION NAME(S) AND ADDRESS(ES)</b> Deformation Control Technology, Inc. Plaza South II, Suite 105 7261 Engle Rd. Cleveland, Ohio 44130			<b>8. PERFORMING ORGANIZATION REPORT NUMBER</b> E-9033	
<b>9. SPONSORING/MONITORING AGENCY NAME(S) AND ADDRESS(ES)</b> National Aeronautics and Space Administration Lewis Research Center Cleveland, Ohio 44135-3191			<b>10. SPONSORING/MONITORING AGENCY REPORT NUMBER</b> NASA CR-195365	
<b>11. SUPPLEMENTARY NOTES</b> Project Manager, A.D. Freed, Materials Division, NASA Lewis Research Center, organization code 5110, (216) 433-8747.				
<b>12a. DISTRIBUTION/AVAILABILITY STATEMENT</b> Unclassified - Unlimited Subject Category 39			<b>12b. DISTRIBUTION CODE</b>	
<b>13. ABSTRACT (Maximum 200 words)</b> This project examined the effectiveness of studying the creep behavior of a thermal barrier coating system through the use of a general purpose, large strain finite element program, NIKE2D. Constitutive models to simulate thermal-elastic and creep behavior were applied. Four separate ceramic-bond coat interface geometries were examined in combination with a variety of constitutive models and material properties. The model conditions examined include: i) two bond coat coefficient of thermal expansion curves; ii) the creep coefficient and creep exponent of the bond coat for steady state creep; iii) the interface geometry; and iv) the material model employed to represent the bond coat, ceramic, and superalloy base.				
<b>14. SUBJECT TERMS</b> Thermal barrier coating; Creep modeling			<b>15. NUMBER OF PAGES</b> 147	
			<b>16. PRICE CODE</b> A07	
<b>17. SECURITY CLASSIFICATION OF REPORT</b> Unclassified	<b>18. SECURITY CLASSIFICATION OF THIS PAGE</b> Unclassified	<b>19. SECURITY CLASSIFICATION OF ABSTRACT</b> Unclassified	<b>20. LIMITATION OF ABSTRACT</b>	